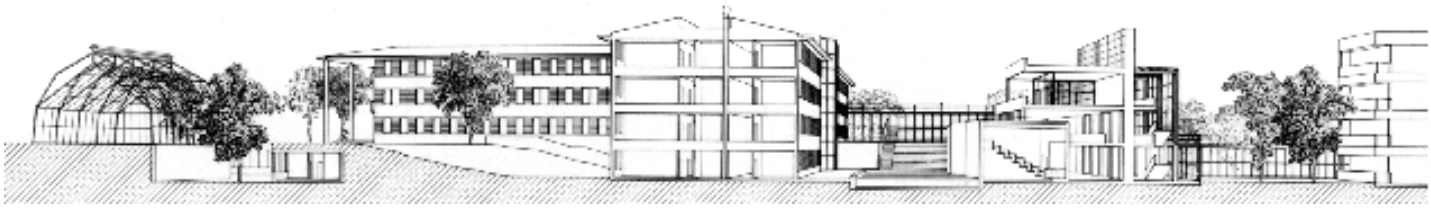

Biochemical and Biophysical Characterization of Extrinsic and Intrinsic Modulators of the Antigen Transporter TAP

Dissertation
zur Erlangung des Doktorgrades
der Naturwissenschaften

vorgelegt beim Fachbereich
Biochemie, Chemie und Pharmazie
der Goethe-Universität in Frankfurt am Main

von
Gabriele Plewnia
aus Reutlingen

Frankfurt am Main, 2008

Vom Fachbereich Biochemie, Chemie und Pharmazie der Goethe-Universität als Dissertation angenommen.

Dekan: Prof. Dr. Harald Schwalbe

1. Gutachter: Prof. Dr. Robert Tampé
2. Gutachter: Prof. Dr. Bernd Ludwig

In der Wissenschaft gleichen wir alle nur den Kindern, die am Rande des Wissens hier und da einen Kiesel aufheben, während sich der weite Ozean des Unbekannten vor unseren Augen erstreckt.

Isaac Newton
(1643-1727)

INDEX

1. Deutsche Zusammenfassung

MHC (*major histocompatibility complex class*)-Klasse I-Moleküle präsentieren den $CD8^+$-T-Lymphozyten intrazellulär prozessierte Antigene. Die Präsentation wird durch den makromolekularen Peptidbeladungskomplex (PLC) vermittelt. Dabei spielen das Glykoprotein Tapasin als auch TAP (*transporter associated with antigen processing*) eine essentielle Rolle in der Peptidbeladung der MHC-Klasse I-Moleküle. Die durch das Proteasom produzierten Peptide werden von TAP aus dem Zytoplasma in das Lumen des Endoplasmatischen Retikulums (ER) transportiert. Anschließend werden diese Peptide auf MHC-Klasse I-Moleküle geladen und über den Golgi-Apparat an die Zelloberfläche transportiert. Dabei spielt das ER-ständige Glykoprotein Tapasin eine wichtige Rolle: Tapasin fördert die optimale Faltung und Assemblierung der MHC-Klasse I-Peptid-Komplexe. Außerdem reguliert Tapasin das Expressionsniveau von TAP, indem es diesen stabilisiert. Sowohl die strukturelle Organisation des PLCs, einschließlich des antigenen TAP-Komplexes, als auch die Funktion von Tapasin auf die Peptidbeladung von MHC-Klasse I-Molekülen ist Gegenstand intensiver Forschung.

In der vorliegenden Arbeit wurden rekombinante Fv, scFv und Fab Antikörperfragmente ausgehend von einer Hybridomzelllinie, die einen TAP1-spezifischen monoklonalen Antikörper mAb148.3 exprimiert, generiert. Wie bereits durch Epitopkartierung identifiziert, besteht das Epitop aus den letzten fünf C-terminalen Aminosäuren von TAP1. Die rekombinanten Antikörper wurden zunächst heterolog in *E. coli* sowie in Insektenzellen exprimiert und mittels Affinitätschromatographie zur Homogenität gereinigt. Sowohl der monoklonale als auch die rekombinanten Antikörper zeigen eine Affinität im nanomolaren Bereich bezüglich der letzten fünf C-terminalen Aminosäuren von TAP1 wie in *enzyme linked immunosorbent assay* (ELISA) und mittels Oberflächen-Plasmonen-Resonanz-Spektroskopie (SPR) gezeigt. Überraschenderweise stabilisieren die rekombinanten Antikörper den heterodimeren TAP-Komplex bei erhöhter Temperatur. Gleichzeitig wird, in Anwesenheit der rekombinanten Antkörper, die Peptid-Translokation durch TAP drastisch inhibiert. Dabei wird die ATP- und Peptid-Bindung an TAP nicht

beeinträchtigt. Die rekombinanten Antikörper wurden ebenfalls bei der Reinigung des Peptidbeladungskomplexes aus einer humanen B-lymphoblastoiden Zelllinie erfolgreich angewendet. Hierbei konnte mittels Matrix-assistierter Laserdesorptionsionisations-Massenspektrometrie (MALDI-MS) eine neue Komponente des PLCs, die Proteindisulfidisomerase (PDI), identifiziert werden.

Ein weiterer Aspekt dieser Arbeit war die Etablierung eines *in vitro* Systems für die Untersuchung der Tapasin-MHC-Klasse I-Interaktion. Dazu wurde ein Verfahren zur heterologen Expression und Reinigung von funktionalen, löslichen *single chain* MHC-Klasse I-Molekülen aus Insektenzellen aufgestellt. Neben einem tapasin-abhängigem MHC-Klasse I-Allel, HLA-B4402, wurde auch ein tapasin-unabhängiges HLA-B4405 als *single chain* Konstrukt generiert. Im Gegensatz zu dem tapasin-abhängigem scB4402-β_2m, wurde das tapasin-unabhängige scB4405-β_2m ins Medium sezerniert und konnte zur Homogenität gereinigt werden. In Peptid-Bindungsstudien, sowie in Anisotropie-Messungen wurde die Funktionalität des scB4405-β_2m nachgewiesen. Bei Untersuchungen der Wechselwirkung zwischen Tapasin und scB4405-β_2m-Molekülen konnte mittels SPR eine direkte Interaktion nachgewiesen werden, wobei Hintergrund-Interaktion der scB4405-β_2m mit der Sensor-Oberfläche und die transiente, niederaffine Interaktion eine kinetische Auswertung schwierig machten. Um detaillierte Untersuchungen zur Rolle von Tapasin als Peptid-Editor durchzuführen, wurden Tapasin und scB4405-β_2m-Peptid-Komplexe auf einer Chelator-Lipid-Oberfläche co-immobilisiert. Die Verwendung einer Lipid-Doppelschicht ermöglichte laterale Mobilität. Mittels TIRFS (Totalinterne Reflektions-Fluoreszenz-Spektroskopie) wurde nun der Einfluß von Tapasin auf die Peptid-Dissoziation beobachtet. Dabei stellte sich heraus, dass die Peptid-Dissoziation des tapasin-unabhängigen scB4405-β_2m in An- bzw. Abwesenheit von Tapasin unverändert blieb.

Mit dem in dieser Arbeit etablierten *in vitro* Untersuchungssystem ist die Grundlage zu detaillierten Studien der Funktion von Tapasin, sowie weiteren Chaperonen des Peptidbeladungskomplexes wie z.B. ERp57 bei der Peptidbeladung von MHC-Klasse I-Molekülen geschaffen.

2. Summary

Presentation of intracellular processed antigens by major histocompatibility (MHC) class I molecules to $CD8^+$ cytotoxic T lymphocytes is mediated by the macromolecular peptide loading complex (PLC). In particular accessory proteins, including the transporter associated with antigen processing (TAP) and tapasin, play a pivotal role in the MHC class I mediated antigen presentation pathway. TAP belongs to the ATP-binding cassette (ABC) superfamily and consists of TAP1 (ABCB2) and TAP2 (ABCB3), each of which possesses a transmembrane and a nucleotide-binding domain (NBD). The ER-resident glycoprotein tapasin promotes the optimal folding and assembly of MHC-peptide complexes, and independently stabilizes the steady state expression level of TAP.

In the present thesis recombinant Fv, scFv and Fab antibody fragments to human TAP from a hybridoma cell line expressing the TAP1-specific monoclonal antibody mAb148.3, were generated. The epitope of the mAb148.3 was mapped to the very last five C-terminal amino acid residues of TAP1 on solid-supported peptide arrays. The recombinant antibody fragments were heterologously expressed in *E. coli* and insect cells, and purified to homogeneity by affinity chromatography. The monoclonal and recombinant antibodies display nanomolar affinity to the last five C-terminal amino acid residues of TAP1 as demonstrated by enzyme linked immunosorbent assay (ELISA) and surface plasmon resonance (SPR). Surprisingly, the recombinant antibody fragments confer thermal stability to the heterodimeric TAP complex in insect cells when incubated at elevated temperature. At the same time, TAP is arrested in a peptide transport incompetent conformation, although ATP and peptide binding to TAP are not affected. Furthermore, the recombinant antibodies were successfully used in the purification of the PLC from a human B-lymphoblastoid cell line and a novel factor, protein disulfide isomerase (PDI), was identified by matrix assisted laser desorption/ionisation-mass spectrometry (MALDI-MS).

In the second part of this thesis the tapasin-MHC class I interaction was investigated. It is for this reason, that an *in vitro* assay had been established for

direct measuring tapasin-MHC class I interactions. First, soluble single chain MHC class I molecules were engineered, choosing two MHC class I alleles: HLA-B4402 representing a highly tapasin-dependent allele and with HLA-B4405, a tapasin-independent allele was chosen. Tapasin as well as the two single chain MHC class I constructs, scB4402-β_2m and scB4405-β_2m, were expressed in insect cells and purified from insect cell supernatants by affinity chromatography. In contrast to the HLA-B4405 allele, which was expressed and secreted at moderate yield, the HLA-B4402 allele was expressed and trapped inside the insect cells instead of secreted into the medium. Peptide-binding and anisotropy measurements with fluorescein-labeled peptides verified the functionality of the scB4405-β_2m. For further investigation of the tapasin-MHC class I interaction an *in vitro* assay was established using surface plasmon resonance spectroscopy. Due to the transient nature of the interaction including the decreased affinity of both interaction partners, kinetic data acquisition was difficult to evaluate. Furthermore, interaction of the scB4405-β_2m with the sensor surface itself contributed to the measured interaction. Additionally, to investigate tapasin editing function, tapasin as well as the scB4405-β_2m-peptide complex were tethered on fluid chelator lipid bilayers and monitored by reflectance interference (RIf) and total internal reflection fluorescence spectroscopy (TIRFS). Stable immobilization of scB4405-β_2m-peptide complex as well as of tapasin was observed, unfortunately no changes in peptide dissociation kinetics monitored in the TIRFS channel were detected. Presumably, the tapasin-independent HLA-B4405 already loaded with a high affinity peptide is not influenced by the peptide-editing function of tapasin. Here, for the first time an *in vitro* assay was established for direct probing interactions within the various proteins of the PLC.

3. Introduction

3.1. The immune system and the quest against invaders

A major task of the immune system in higher vertebrates is the defense against invaders. Pathogenic microorganisms like bacteria, viruses and fungi, which differ greatly in their lifestyles and structures, have evolved manifold mechanisms to escape the immune system surveillance and to invade through external or internal epithelial surfaces: the respiratory tract mucosa provides a route of entry for airborne microorganisms, the gastrointestinal mucosa for microorganisms in food and water, insect bites and wounds allow microorganisms to penetrate the skin, and direct contact between individuals offers opportunities for infection of the skin, the gut, and the mucosa of the reproductive tract. Once a pathogenic agent succeeds in evading the immune system, unbiased defense mechanisms are alerted generally based on activation of tissue macrophages equipped with surface receptors that can bind and phagocytose many different types of pathogens. This leads to an inflammatory response, which causes the accumulation of phagocytic neutrophils and macrophages at the site of infection, the so-called innate immune response. In addition to the cellular innate immune response, plasma proteins accumulate at the site of infection, including the complement components that provide circulating or humoral innate immunity. Innate immunity provides a front line of host defense through effector mechanisms that engage the pathogen directly, act immediately on contact with it, and are unaltered in their ability to resist a subsequent challenge with either the same or a different pathogen. Since the innate responses often fail to clear the infection, dendritic cells, macrophages, and other cells activated in the early innate immune response help to initiate the development of an adaptive immune response. Generally, the reaction taking part in the adaptive immune response is initiated by ligand-receptor interactions. Pathogens displayed as antigenic peptides are recognized by receptors of certain immune cells, known as B- and

T lymphocytes, the main protagonists of the adaptive immune system (Janeway *et al.,* "Immunbiology" 6th edition. Garland Science Publishing, 2005).

The cell-mediated immune response of the adaptive immunity begins with the activation of antigen-specific T cells by antigen-presenting cells (APCs) in the lymphoid tissues and organs (Dustin, 2003). The activation induces the proliferation and the differentiation of T cells into armed effector T cells: $CD8^+$ cytotoxic T cells, T_H1 and T_H2 cells. The process is mediated by the cytokine T cell growth factor IL-2, which binds to a high affinity receptor on the activated T cell. $CD8^+$ cytotoxic T cells target MHC class I-peptide complexes on the cell surface, which are recognized by their T cell receptors and activate the apoptotic pathway. Hence, preformed cytotoxins stored in specialized $CD8^+$ cytotoxic T cells lytic granules are released upon direct contact with an infected cell. The cytotoxins consist of the perforins, which polymerize in target-cell membranes to form transmembrane pores, the granzymes belonging to the serin proteases family and the granulysins, which induce apoptosis in target cells and have an antimicrobial activity. Another mechanism to induce apoptosis in the target cell is the interaction between Fas in the target-cell membrane and the Fas ligand, which is present in the membranes of activated cytotoxic T cells, T_H1 and some T_H2 cells. Ligation of Fas leads to the activation of caspases, which induce apoptosis in the target cell (Medana *et al.*, 2000). Cytotoxic T cells also act by releasing cytokines IFN-γ, TNF-α, and TNF-β. IFN-γ inhibits viral replication but also induces the increased expression of MHC class I as well as other proteins involved in the peptide loading of MHC class I molecules (see 3.2 for details). IFN-γ also activates macrophages by recruiting them to sites of infection both as effector and as antigen-presenting cells. IFN-γ also lowers the tryptophan concentration with cells carrying an IFN-γ receptor and thus can kill intracellular pathogens by starvation. TNF-α and TNF-β can synergize with IFN-γ in macrophage activation and in killing of some target cells (Tseng & Dustin, 2002).

Taken together, $CD8^+$ T cells recognize antigens derived from intracellular pathogens (viruses, intracellular bacteria) and malignantly transformed cells (tumors), which are then proteolytically degraded by the cytosolic proteasom and presented by the MHC class I molecules. In contrast, the T_H1 and the T_H2

cells, both expressing the $CD4^+$ co-receptor, recognize fragments of antigens degraded within intracellular vesicles and displayed at the cell surface by MHC class II molecules. T_H1 cells activate macrophages by releasing IFN-γ as well as by docking to CD40 on macrophages via their CD40 ligand. T_H2 cells are inefficient macrophage activators because they produce IL-10, a cytokine that can deactivate macrophages; they do not produce IFN-γ. They do express CD40 ligand, however, and can deliver the contact-dependent signal required to activate macrophages to respond to IFN-γ. Together with TNF-α produced by the activated macrophage and IFN-γ produced by T_H1 effector cells the reactive nitrogen metabolite NO is induced, which has broad antimicrobial activity. Furthermore, by producing the hematopoietic growth factors IL-3 and GM-CSF, which in turn stimulate the production of new phagocytic cells in the bone marrow, T_H1 cells recruit macrophages to the site of infection. Also, TNF-α and TNF-β, which are secreted by T_H1 cells in case of an infection, change the surface properties of endothelial cells enabling phagocytes to adhere to them. Chemokines such as the macrophage chemotactic protein CCL2, which is produced by T_H1 cells in the inflammatory response, direct these phagocytic cells through the vascular endothelium and to the site of infection (Underhill *et al.*, 1999).

The B lymphocytes are initiators of the humoral immune response, which is responsible for the protection of the extracellular spaces along which pathogens spread by moving from cell to cell. B cells internalize the antigens bound by their surface immunoglobulin receptors and then display peptide fragments of antigen as MHC class II-peptide complexes. The activation of B cells and their differentiation into antibody-secreting plasma cells and memory B cells is triggered by antigen and usually requires the T_H2 class of $CD4^+$ T cells but also a subset of T_H1 cells. B-cell activation takes place first when the B-cell antigen receptor cross-linked to an antigen transmits signals directly to the cell interior and at the same time the antigen is internalized and processed into peptides, which are subsequently presented by MHC class II molecules. In the case of thymus-dependent antigens, the second signal represents helper T cells recognizing the MHC class II-peptide complex, which then transmits activating signals to the B cell. This activation is essentially driven by the interaction of the CD40 ligand on the T cell and CD40 on the B cell. For thymus-independent

antigens, the second signal is delivered solely by the antigen itself. T_H2 cells secrete the B cell stimulating cytokines IL-4 and IL-6 which promote the proliferation and differentiation of the B cell to antibody producing plasma cells (Liu *et al.*, 1991). Binding of bacterial toxins by IgG antibodies or the binding of viruses by IgG and IgA antibodies neutralizes the toxins and protects the cell against toxic effects (Mandel, 1976). Antibodies that coat pathogens are recognized by Fc receptors on phagocytes, which are thereby triggered to engulf and destroy the pathogen. Antibodies can also initiate the destruction of pathogens by activating the complement system (opsonization) (Cooper, 1985). Furthermore, antibody-coated pathogens are also recognized by Fc receptors on NK cells (antibody-dependent cell-mediated cytotoxicity (ADCC)). The destruction of those antibody-coated pathogens is mediated by the release of cytoplasmic granules containing perforin and granzymes (Lanier *et al.*, 1986).

The antigens recognized by $CD4^+$ T cells derive from extracellular bacteria or toxins, which are endocytosed and are proteolytically digested in the endosomes. Thus MHC class II molecules display peptides derived from pathogens, which live in macrophage vesicles or which have been internalized by phagocytic cells and B cells. MHC class II molecules assemble in the endoplasmic reticulum (ER) with the invariant chain. The invariant chain inhibits peptide-binding in the ER as well as during the translocation to the endosomes. In the late endosomes the invariant chain is cleaved by various proteases leaving the remaining CLIP (class II-associated invariant-chain peptide) fragment bound to the MHC class II molecule. HLA-DM/HLA-2M interacts with the MHC class II-CLIP complex and catalyzes the exchange of CLIP for exogenous antigenic peptides (Rocha & Neefjes, 2008). The MHC class II-peptide complex is transported via the Golgi to the cell surface for screening by $CD4^+$-T-cells (Figure 3-1).

Effector cells (B and T cells) have a limited life span. After the elimination of the antigen, part of the clonaly expanded cells differentiate to memory cells, which are circulating awaiting new confrontation with a pathogen. The other effector cells go through apoptosis.

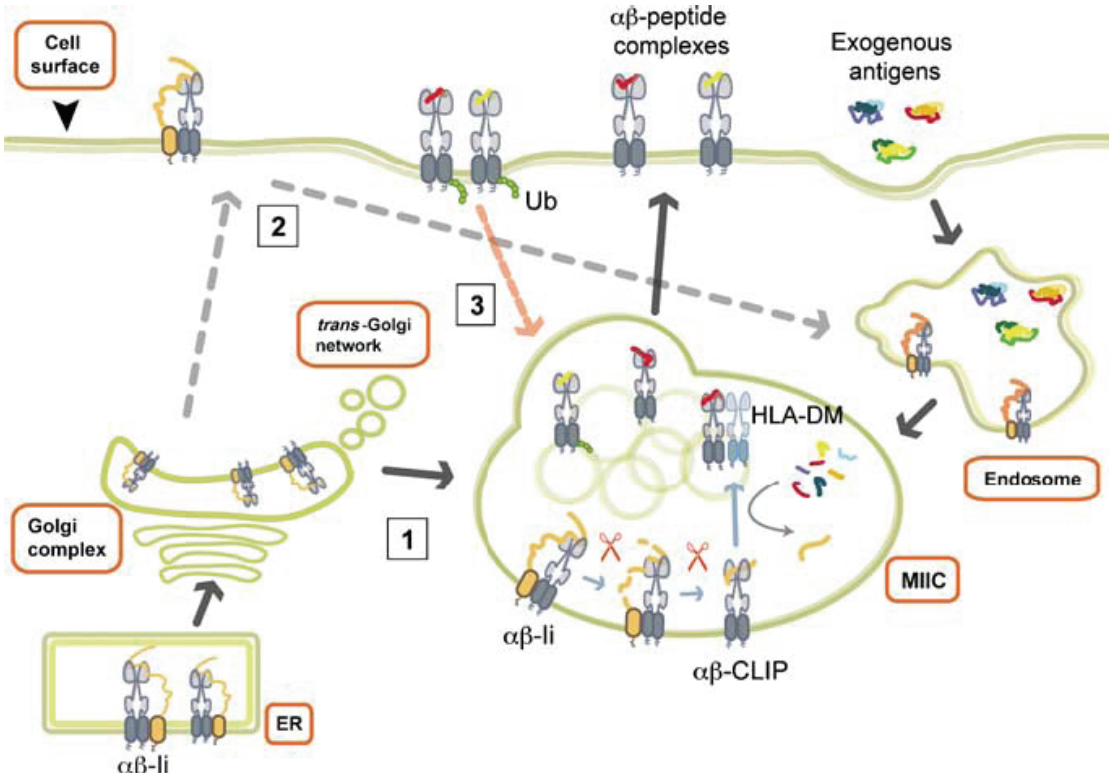

Figure 3-1. The MHC class II processing pathway. MHC class II αβ heterodimers assemble in the endoplasmic reticulum with Ii, which occupies the peptide-binding groove and contains an endosomal targeting signal. Ii chaperones MHC II either directly (route 1; black solid arrow) or indirectly after internalization from the cell surface (route 2; gray dashed arrows) into MHC class II-containing compartment (MIIC). In the MIIC, Ii is finally degraded by a series of endosomal proteases leaving the remaining CLIP fragment (orange). HLA-DM assists the exchange of CLIP for relevant exogenous antigenic fragments (red and yellow) in subdomains of MIIC (the internal vesicles) prior to transport for stable intergration in the plasma membrane (blue arrows in MIIC) unless internalization is induced by a process like ubiquitination (Ub) of the MHC II β-chain cytoplasmic tail (route 3; pink dashed arrow) (Rocha & Neefjes, 2008).

3.2. MHC class I antigen processing and presentation pathway

3.2.1. The major histocompatibility complex (MHC)

The main function of MHC molecules is the presentation of protein fragments derived from pathogens at the cell surface to the appropriate T cells. In order to respond to the multitude of different and rapidly evolving pathogens, the immune system possess as a prerequisite polygenic and polymorphic MHC. The MHC gene locus is subdivided into several different MHC class I and MHC class II genes. This polygenic architecture of the MHC gene provides every individual with a set of MHC molecules with different ranges of peptide-binding specificities. Furthermore, every individual holds additionally multiple variants of each gene within the population as a whole, meaning the MHC gene locus is highly polymorphic.

3.2.1.1. Genomic organization

The major histocompatibility complex is located on chromosome 6 in humans and chromosome 17 in the mouse genome and spans at least 4×10^6 base pairs. Since the MHC genes were first discovered through antigenic differences between white blood cells from different individuals they are also called human leukocyte antigen or HLA genes. In humans there are three MHC class I α-chains, namely HLA-A, -B, and -C, and three pairs of MHC class II α- and β-chain genes, called HLA-DR, -DP, and -DQ (Figure 3-2). All nucleated cells express MHC class I molecules, whereas MHC class II molecules are expressed in epithelial thymus cells and in APCs. The HLA-DR cluster contains an extra β-chain gene whose product can pair with the DRα chain, meaning that the three sets of genes can give rise to four types of MHC class II molecules. Differences between the MHC class I and class II subtypes are found in the presentation of a different range of peptide repertoire, including different peptide specificities, which are unique for every individual. Within the MHC gene cluster, the MHC genes are closely linked to genes involved in the degradation of proteins into peptides, formation of MHC-peptide complexes and the transport of these complexes to the cell surface.

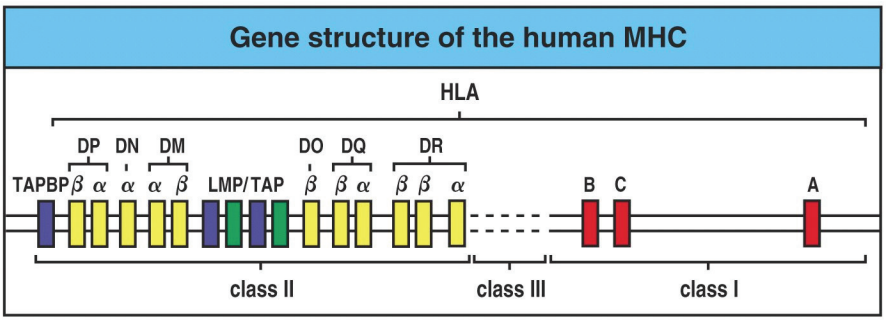

Figure 3-2. Genomic organization of the human major histocompatibility complex (MHC) on chromosome 6. The MHC, also called HLA, is organized in clusters of MHC class I genes (red) and MHC class II genes (yellow). The MHC class I gene cluster is subdivided into three main class I genes, namely HLA-A, -B, and -C. The gene for β_2-microglobulin is located on chromosome 15 in humans. The MHC class II region consists of the α and β chains of the antigen-presenting MHC class II molecules HLA-DR, -DP, and -DQ, the genes for the TAP1/TAP2 complex, the LMP genes encoding proteasome subunits, the genes encoding the DMα and DMβ chains, the genes encoding the α and β chains of the DO molecule (DNα and DOβ, respectively), and the gene encoding tapasin (TAPBP). The class III genes encode proteins of the complement including cytokines (after Janeway *et al.*, "Immunobiology" 6th edition. Garland Science Publishing, 2005).

3.2.1.2. Structural organization

MHC class I molecules consist of the membrane-spanning α heavy chain (45 kDa) encoded in the MHC gene locus and a noncovalently associated invariant β_2-microglobulin chain (12 kDa), which is not polymorphic and is encoded on chromosome 15 in humans. Since both of them derive their origin from the duplication of an original immunoglobulin fold, they belong to the immunoglobulin gene family. The heavy chain is composed of the α_1, α_2 and α_3 domains and includes intramolecular disulfide bridges as well as a membrane-spanning region and a short cytoplasmic tail not resolved in the crystal structure (Figure 3-3). Together the α_1 and α_2 domains of the heavy chain consisting of two α helices atop an extended eight antiparallel β strands form the peptide-binding cleft. The folded structure of the α_3 domain and β_2-microglobulin resembles an immunoglobulin fold. The α_1 domain of human MHC class I molecules is N-glycosylated at position 86, in close proximity to the C-terminus of the bound peptide.

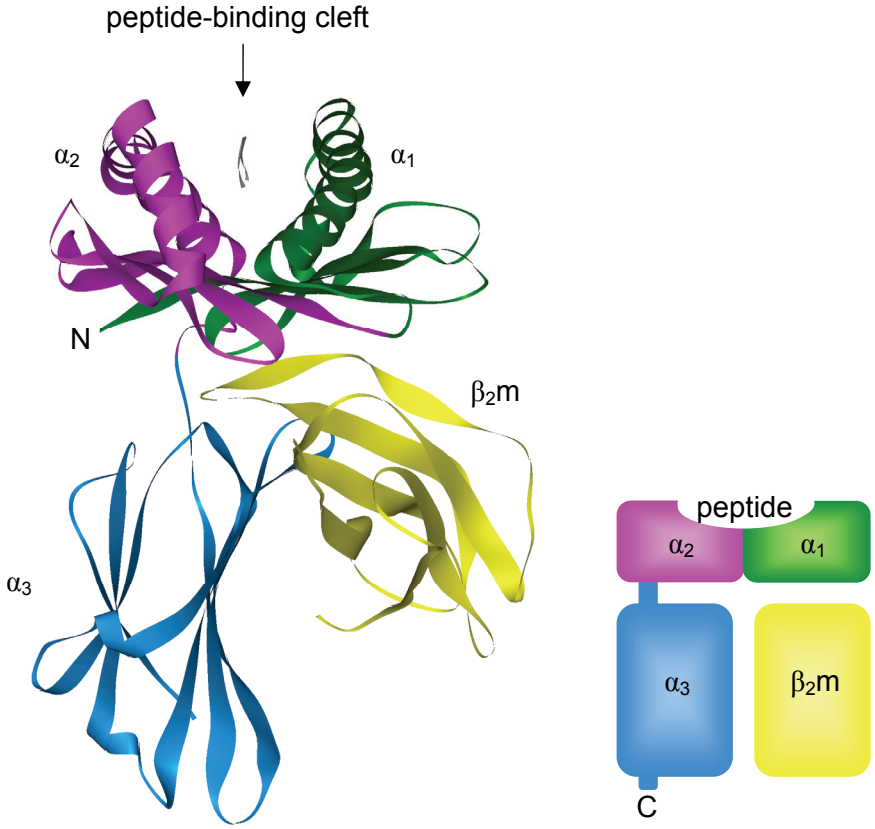

Figure 3-3. Structure of soluble MHC class I HLA-B44. Structure of soluble HLA-B44 produced in *E. coli* and refolded in the presence of epitope peptide EEFGRAYGF was solved by Zernich and colleagues (Zernich *et al.,* 2004; PDB ID 1SYV). Ribbon diagram of the structure consisting of the α chain folded into three domains: α_1 (green), α_2 (magenta) and α_3 (blue). The α_3 domain and β_2-microglobulin (yellow) show similarities in amino acid sequence to immunoglobulin C domains and have similar folded structures, whereas the α_1 and α_2 domains fold together into a single structure consisting of two segmented α helices lying on a sheet of eight antiparallel β strands. The α_1 and α_2 domains create a cleft, which is the site where antigenic peptides bind to MHC class I molecules. Right side at the bottom: a schematic representation of the soluble MHC class I molecule.

3.2.1.3. Peptide-binding cleft

Resolving the crystal structure of a meanwhile abundant number of MHC class I molecules helped incredibly in the characterization of the MHC class I-peptide complexes. Prior to loading, MHC class I molecules associate with β_2-microglobulin in the endoplasmic reticulum and are subsequently loaded with

antigenic peptides of approximately 8-14 amino acids in length (Bouvier, 2003; Ellgaard & Helenius, 2003; Wright *et al.,* 2004). Peptide-binding to MHC class I molecules takes place in a cleft formed by two α-helices, α_1 and α_2, on top of an extended antiparallel β-sheet at the α_1/α_2 domain, site of the highest polymorphism (Madden, 1995) (Figure 3-4, b and c). The N- and C-terminus of the peptide backbone is deeply anchored in the peptide-binding cleft by a network of hydrogen bonds as well as by ionic interactions with conserved residues within the peptide-binding cleft (Figure 3-4, a). Side chains of specific residues point directly toward the β-sheet at the bottom of the α_1/α_2 domain forming hydrogen bonds with residues within the β-sheet as well as the surrounding α-helices. The main differences between the allelic MHC variants are found in the peptide binding cleft resulting in altered amino acid residues located at main positions of the peptide interaction sites in the different MHC alleles. Thus every MHC allele displays a different subset of peptide specificity. One can divide the different peptide-binding clefts into six subgroups (A, B, C, D, E and F). For instance, the HLA-B44 molecule holds a relatively deep peptide-binding groove of the F type, enabling binding of peptides with aromatic amino acids present at the C-terminus (DiBrino *et al.,* 1995) (Figure 3-4). MHC class I molecules are highly polymorphic. The polymorphic residues are located at the bottom and sideways of the peptide-binding cleft (Zhang *et al.,* 1998). One example of the polymorhism of MHC class I molecules is demonstrated by the HLA-B44 allele: Only one amino acid substitution at position 116 turns a highly tapasin-dependent HLA-B4402 (D116) into a completely tapasin-independent HLA-B4405 (Y116) (Figure 3-4, b and c). These various, polymorphic side chains determine the properties of the binding pockets in the peptide-binding cleft, which interacts with the peptide side chain. Further analysis of the peptide repertoire of different MHC class I alleles revealed the positioning of anchor residues specific for every MHC class I allele. These anchor positions lie at the C-terminus as well as at position 2 of the peptide. For HLA-B4402 the peptide-binding specificity is determined by the position 2 and 9, with glutamic acid and phenylalanine respectively, anchoring the N- and C-terminus of the peptide deeply in the peptide-binding cleft (Figure 3-4, a-c). Furthermore, not only the amino acid composition but also the structure of the bound peptide defines decisively the lifetime of the

MHC class I-peptide complexes. The structure of the MHC class I domain interacting with the N-terminus of the peptide is rather rigid in the absence of a peptide (Zacharias & Springer, 2004). Peptide-binding induces a rearrangement of the amino groups of the N-terminus of the peptide facing towards the bottom of the β-sheet and the formation of hydrogen bonds (Madden, 1995). Unlike the rigid N-terminal domain of the peptide-binding cleft, the peptide-binding cleft at the C-terminus of the peptide is rather flexible in the absence of a peptide (Zacharias & Springer, 2004). By the time of peptide-binding, the side chain of the peptide last C-terminal amino acid is anchored in a deep pocket (F-pocket). The terminal carboxyl group is facing outward and the hydrogen bonds are located on the surface of the MHC class I-peptide complex. As a result of the flexibility of the peptide-binding cleft at the C-terminus, peptides with an elongated C-terminus are able to bind more stably to the MHC class I binding cleft. Longer peptides are bound by kinking or looping out of the peptide backbone. Since the part of the α_2 helix anchoring the C-terminus of the peptide, is very flexible and is located close to the tapasin interaction site, it is assumed that tapasin induces a conformational change in this region (Wright *et al.,* 2004). The interaction of tapasin with the exposed α_2 loop could cause an outward positioning of the α_2-1 helix (Figure 3-2 (b)) (completely opened form of the MHC class I-peptide-binding cleft) resulting in the loss of the hydrogen bonds to the C-terminus of the peptide thus allowing peptide exchange (Elliott *et al.,* 1997; Wright *et al.,* 2004). Only high affinity peptides with a slow dissociation rate would be able to induce a mature conformation (closed form) and a stable ternary complex upon which tapasin is excluded and is not able to interact. Amino acid side chains, which do not interact but rather protrude out of the peptide-binding cleft, form together with the accessible elements of the α_1- and α_2- helices the epitope for the MHC class I-peptide-specific binding by the appropriate T cell receptor.

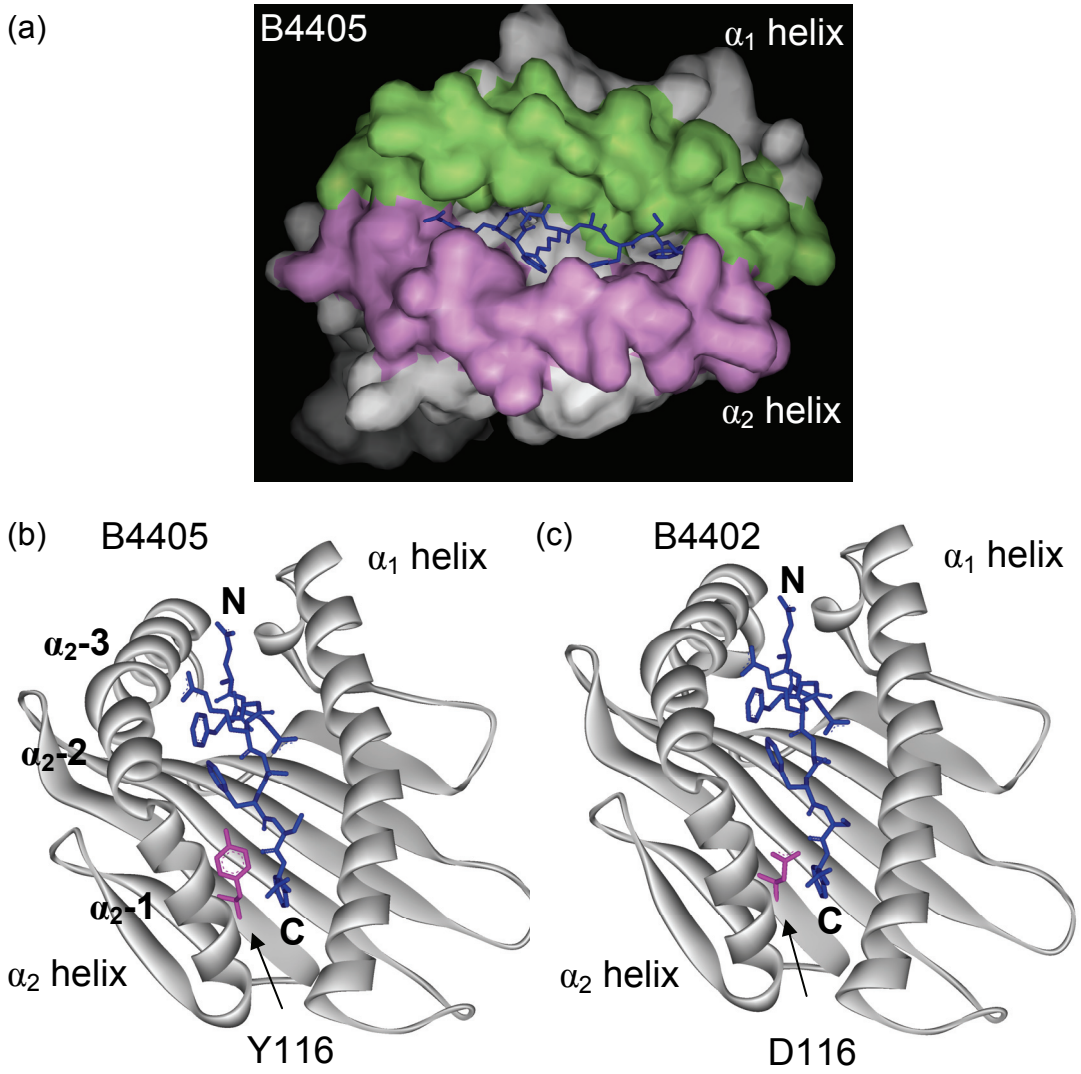

Figure 3-4. The peptide-binding cleft of MHC class I molecules anchors peptides tightly via their N- and C-terminal ends. Surface of the peptide-binding cleft of HLA-B4405 in complex with the epitope peptide EEFGRAYGF according to the α_1 helix (green) and α_2 helix (purple) is shown in (a). Looking down on the peptide-binding cleft from above, the sides of the cleft are formed from the inner faces of the two α helices. The antiparallel β strands building up the β sheet create the floor of the cleft. HLA-B4405 and HLA-B4402 differ only in one amino acid at position 116 as indicated in (b) and (c). From the crystal structure no prediction can be made about structural differences between those two alleles. Tyr as well as Asp do neither interact with the peptide nor do they have any other obvious function or interaction bonding.

3.2.2. The antigen transporter TAP

Supply of peptides in the ER and subsequent binding to MHC class I molecules is a crucial step in the assembly of stable MHC class I molecules. Studies of various mutant cell lines deficient in cell surface expression of MHC class I molecules, but proficient in normal MHC class I heavy chain and β_2m expression, indicated for the first time the presence of peptide transporters (DeMars *et al.,* 1992). Lacking peptides, the MHC class I molecules are held in a partly folded state in the ER. The genes responsible for this defective phenotype, *tap1* and *tap2*, are located in the MHC class II gene locus of human chromosome 6 both comprising 11 exons (Trowsdale *et al.,* 1991). Transfection of these cell lines with cDNA of TAP1 and TAP2 could restore cell surface expression of the MHC class I molecules (Attaya *et al.,* 1992; Powis *et al.,* 1991; Spies *et al.,* 1992; Spies & DeMars, 1991). Subsequent heterologous expression of TAP1 and TAP2 in insect cells and yeast showed a functional peptide translocation in the absence of factors of the adaptive immune system (Meyer *et al.,* 1994; Urlinger *et al.,* 1997). Immunoelectron and immunofluorescence studies showed the localization of TAP1 and TAP2 in the ER or *cis*-Golgi membranes (Kleijmeer *et al.,* 1992; Meyer *et al.,* 1994).

The functional peptide transporter is organized as a heterodimer consisting of TAP1 (ABCB2) and TAP2 (ABCB3), and belongs to the ATP-binding cassette (ABC) transporter superfamily (Kelly *et al.,* 1992; Spies *et al.,* 1992). As predicted by hydrophobicity analysis and sequence alignments with other known ABC transporters TAP1 and TAP2, the so-called half-size transporters, are composed of ten and nine hydrophobic transmembrane helices, respectively, followed by a highly conserved nucleotide-binding domain (NBD). The sequence identity within the NBDs resembles 60%, whereas for the TMDs of TAP only 30% are reached. The predicted topology of TAP1 was confirmed by applying cysteine scanning mutagenesis (Schrodt *et al.,* 2006) (Figure 3-5). Single cysteines were introduced into putative loops between transmembrane segments following the analysis of hydrophobicity algorithms and sequence alignments of TAP from different species and other members of the ABC-B subfamily. The accessibility of single residues facing the cytosol or endoplasmic reticulum lumen was probed with membrane-impermeable, thiol-specific

fluorophores in semipermeabilized cells. Based on the results the authors conclude that the transporter core is formed by 6+6 TMs, which is common for most ABC transporters. In addition to the 6+6 TM core, TAP1 and TAP2 comprise an extra N-terminal domain, consisting of four well predicted TMs, that is essential for the assembly of the peptide-loading complex (PLC), mediated by the adapter protein tapasin (Figure 3-5). Deletion of the N-terminal four (TAP1) or three (TAP2) putative TMHs, as predicted by the topological model (Figure 3-5), does not affect peptide transport. Instead they were proven to be essential for tapasin recruitment (Koch *et al.,* 2004; 2005; 2006). Both transmembrane domains of human TAP1 and TAP2 contribute to the peptide-binding site (Androlewicz *et al.,* 1993; 1994). Photo-crosslinking experiments mapped the peptide-binding site between the cytosolic loops of TM4 and TM5 and a C-terminal stretch of approximately 15 amino acids after TM6 (Nijenhuis & Hämmerling, 1996). Additionally, two further peptide sensing sites were mapped in TAP1 by modifying epitope peptides with a chemical iron-dependent chemical protease and subsequent mass spectrometry and cysteine cross-linking experiments (Herget *et al.,* 2007). One contact site was mapped to a stretch following TM6 of TAP1 and extends over the already identified peptide-binding pocket obtained by photo-crosslinking studies. The second peptide sensing site was identified in the cytosolic core loop 1 between TMH 2 and TMH 3 of TAP1. Mechanistic questions regarding ATP binding to the non-equivalent NBDs of TAP1 and TAP2 as well as ATP hydrolysis and subsequent translocation of the peptides across the hydrophobic lipid bilayer are heavily discussed. To date, proposed models of the transport cycle are based on biochemical studies as well as on high-resolution structures of isolated NBDs in various conformations (Janas *et al.,* 2003; Smith *et al.,* 2002). Based on these models, the key aspect of the transport cycle is the ATP-induced dimer formation and subsequent ATP hydrolysis by the head-to-tail sandwich dimer of the NBDs, following the dissociation of the NBDs dimer.

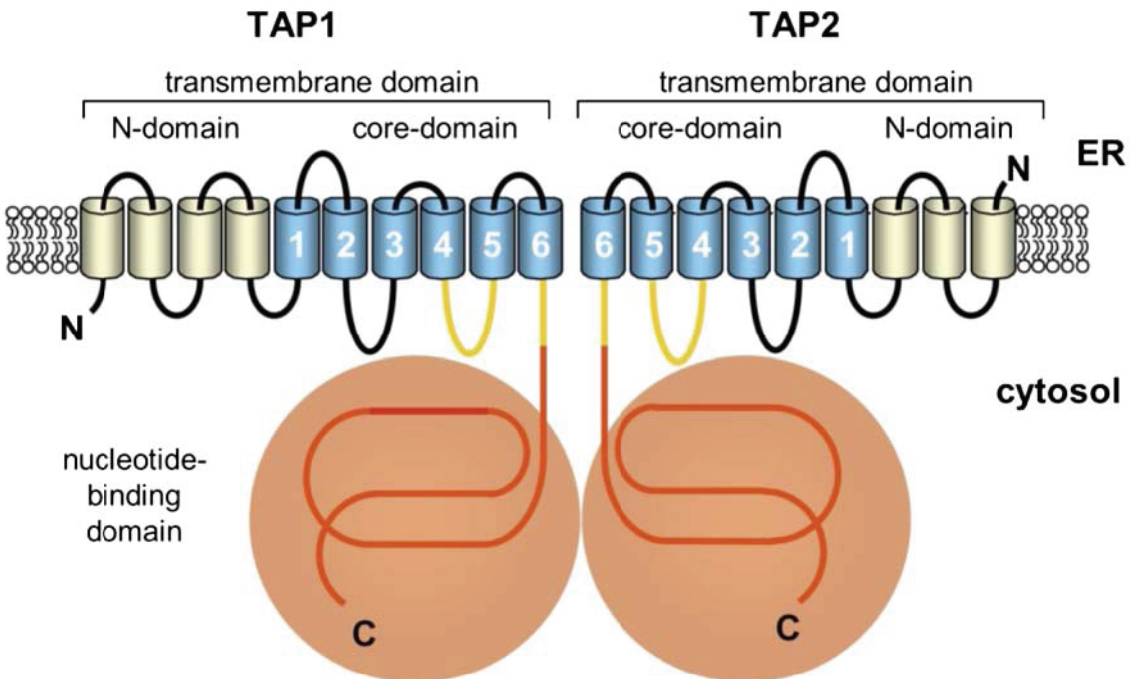

Figure 3-5. Schematic model of the TAP complex. TAP is a heterodimer consisting of TAP1 and TAP2. Each subunit is subdiveded into a N-terminal transmembrane domain (TMD) and a C-terminal cytosolic nucleotide binding domain (NBD). The TMDs can be subdivided into a core-domain of six helices and an N-terminal extension of four and three helices for TAP1 and TAP2, respectively. The peptide binding region is depicted in yellow (Abele and Tampé, 2005; Schrodt *et al.,* 2006).

3.2.3. Tapasin

In 1994 Ortmann and colleagues discribed for the first time a 48 kDa protein which was co-immunoprecipitated with the peptide transporter TAP from digitonin-solubilized B-lymphoblastoid cells (Ortmann *et al.,* 1994). This type I glycoprotein called TAP-associated protein tapasin was found to bridge MHC class I molecules, awaiting a suitable peptide, and TAP, the peptide transporter. High mRNA levels of tapasin are found in T cells, bone marrow, thymus, gut, lung and kidney. In carcinoma and melanoma cell lines the tapasin expression is often reduced, however it can be restored by treatment with IFN-γ or a combination of IFN-β and TNF-α (Ritz *et al.,* 2001; Seliger *et al.,* 2001 a/b/c). The gene for human tapasin is encoded on chromosome 6 in the so-called extended MHC II domain (Herberg *et al.,* 1998). The 8 exons encode a 448 amino acids long type I transmembrane protein. Tapasin is structurally divided into an ER-luminal domain (residues 1-392),

followed by a transmembrane helix (residues 393-417), and a short cytosolic tail (residues 418-428) bearing an ER retention signal (consensus sequence KKxx) (Figure 3-6).

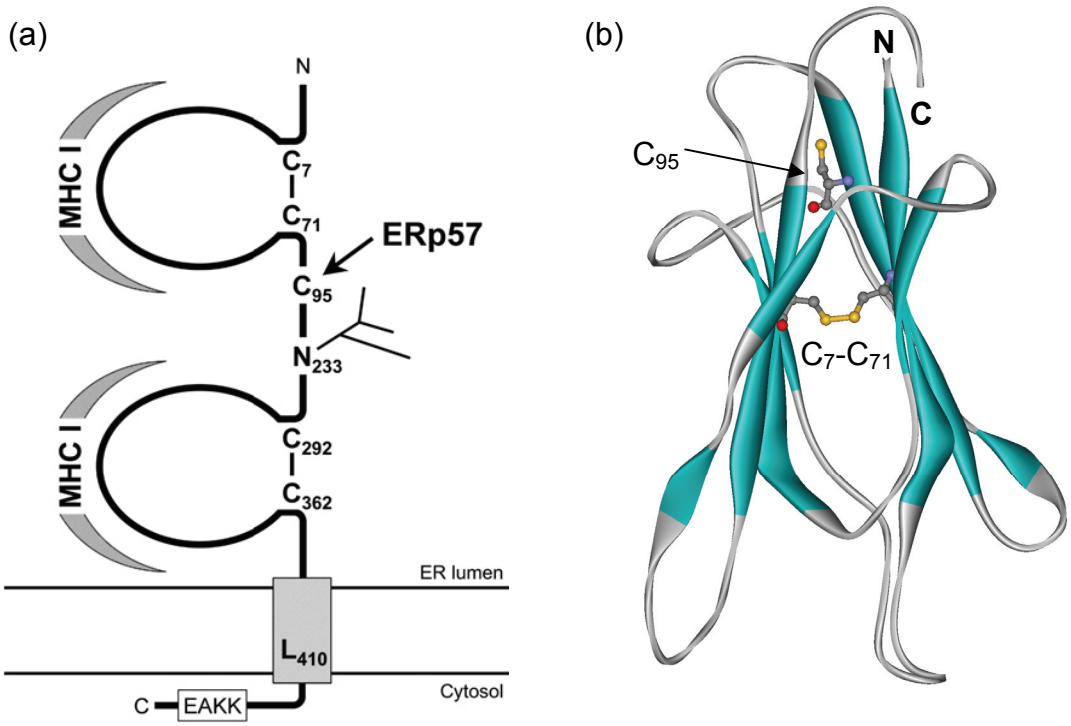

Figure 3-6. Structural organization of the type I transmembrane protein tapasin. (a) Schematic model of tapasin including interaction sites with MHC class I and ERp 57 as well as N-glycosylation site are indicated (Koch and Tampé, 2005). (b) Modeled structure of the N-terminal Ig-fold domain of tapasin (residues 1-128). N and C-terminus indicated in bold. The amino acid Cys 95 and the disulfide bridge Cys_7-Cys_{71} are indicated (structure modelled by Janusz Bujnicki, http://genesilico.pl/).

The ER-luminal domain can be subdivided into at least two immunoglobulin (Ig) fold domains. Each domain is stabilized by a disulfide bond (Cys_7-Cys_{71} and Cys_{292}-Cys_{362}). The cysteine at position 95 is essential for the disulfide formation to ERp57, thus recruiting tapasin into the PLC (Dick *et al.,* 2002; Peaper *et al.,* 2005; Bangia *et al.,* 2005). The asparagine residue at position 233 (Asn_{233}) is the site of N-core glycosylation with the consequence of slower electrophoretic mobility in SDS-PAGE (Li *et al.,* 1997; Turnquist *et al.,* 2001) (Figure 3-6). Mutagenesis studies have shown that the N-terminal 50amino acids of tapasin as well as the two Ig folds are important for the recruitment of MHC class I molecules (Bangia *et al.,* 1999;

Turnquist *et al.,* 2001; Harris *et al.,* 2001). Indications were provided that tapasin is associated with coat-protein complex (COP) I vesicles operating as a cargo receptor to transport incorrectly folded MHC class I molecules from the *cis*-Golgi network back to the ER lumen (Paulsson *et al.,* 2002). The transport of peptide loaded MHC class I molecules from the ER to *cis*-Golgi network in COP II vesicles is regulated presumably by the B cell associated protein (Bap) cargo receptor 31 (Spiliotis *et al.,* 2000; Paquet *et al.,* 2004). Bap 31 interacts, independently of MHC class I molecules with tapasin and recruits MHC class I molecules to the ER exit site. Already in the PLC, Bap 31 is screening for potential cargo (Paquet *et al.,* 2004).

Tapasin plays an important role in the loading of MHC class I molecules with high-affinity peptides. It was shown that tapasin associates independently with TAP and MHC class I molecules respectively (Sadasivan *et al.,* 1996). Transfection of a tapasin-deficient B-lymphoblastoid cell line 721.220 (.220) with human tapasin restored the MHC class I association with TAP as well as the MHC class I cell surface expression (Ortmann *et al.,* 1997; Lewis *et al.,* 1998; Tan *et al.,* 2002). Thus tapasin bridges MHC class I molecules awaiting the appropriate peptides and the peptide supplier TAP. Investigating the stoichiometry of the PLC by blue native-PAGE in combination with antibody (Ab)-shift assays, Rufer and colleagues postulated very recently that the fully assembled PLC comprises two tapasin, two ERp57, but only one MHC class I and calreticulin, associated with the heterodimeric peptide transporter TAP (Rufer *et al.,* 2007). Peptide photo-crosslinking experiments showed that tapasin interacts only with one MHC class I molecule (Bangia & Cresswell, 2005). Both in .220 cells and in tapasin knockout mice a reduced MHC class I cell surface expression as well as MHC class I stability was observed (Sadasivan *et al.,* 1996; Ortmann *et al.,* 1997; Tan *et al.,* 2002; Greenwood *et al.,* 1994; Barnden *et al.,* 2000; Purcell *et al.,* 2001; Williams *et al.,* 2002; Garbi *et al.,* 2000; Grandea *et al.,* 2000). These MHC class I molecules are either empty or loaded with suboptimal peptides, rapidly fall apart on the cell surface, and are degraded. It was shown that tapasin also promotes the retention of MHC class I molecules in the ER, potentially increasing the efficiency of peptide loading (Schoenhals *et al.,* 1999; Barnden *et al.,* 2000; Grandea *et al.,* 2000). Furthermore, it was suggested that

tapasin optimizes peptide-binding to MHC class I molecules, thus stabilizing the MHC class I complexes (Lewis & Elliott, 1998; Garbi *et al.,* 2000; Purcell *et al.,* 2001; Tan *et al.,* 2002; Zarling *et al.,* 2003; Howarth *et al.,* 2004). It was suggested that tapasin would edit the repertoire of bound peptide to MHC class I molecules by exchanging low against high affinity peptides (Howarth *et al.,* 2004). Binding of a high affinity peptide may stabilize the MHC class I molecule and induce a conformational change. This conformational change would probably cause the dissociation of the loading complex and the translocation of the MHC class I-peptide complexes to the cell surface. So far it is not apparent, which of the above mentioned functions of tapasin require, if at all, other components of the PLC. Recently, Wearsch and colleagues reported in a cell-free system, that although recombinant soluble tapasin (residues 1-392) was ineffective in recruiting MHC class I molecules and facilitating peptide binding, recombinant tapasin-ERp57 conjugates accomplished both of those functions and also edited the repertoire of bound peptides to increase their affinity (Wearsch and Cresswell, 2007).

N-terminal tapasin deletion mutants lacking 50 to 300 amino acids still interact with TAP. But they are deficient in the association with HLA-B8 leading to reduced cell surface expression of HLA-B8 (Bangia *et al.,* 1999). Additionally, no association of calreticulin with tapasin or the heavy chain of MHC class I was observed (Bangia *et al.,* 1999). Deletion of N-terminal 19 amino acids resulted in loss of up-regulation of HLA-B8 molecules in .220 cells (Momburg & Tan, 2002). These results suggest the presence of structural elements located in the N-terminal domain of tapasin which are crucial for tapasin-MHC class I interactions. Mutation of Cys_7 or Cys_{71}, cysteine residues crucial for the formation of one of the two disulfide bridges, destabilizes tapasin and therefore impaires tapasin function (Dick *et al.,* 2002). The surface exposed amino acids (residues 334-342) in the membrane proximal Ig-like domain of tapasin, are also involved in the interaction with MHC class I molecules (Turnquist *et al.,* 2001; 2004). This region possibly interacts with an exposed loop (residues 222-229) with the acidic amino acids Asp_{227} and Glu_{229}) in the α_3 domain of the MHC class I (this loop also interacts with CD8) (Carreno *et al.,* 1995; Wright *et al.,* 2004). An exposed loop of the MHC class I-α_2 domain (residues 128-137) interacts with the N-terminal domain of tapasin (Yu *et al.,* 1999).

Additionally, residues Gln_{115} and Asp_{122}, which are located at the bottom of the peptide-binding cleft and contact β_2m, participate in the interaction with the N-terminal domain of tapasin (these residues also interact with CD8) (Beissbarth *et al.,* 2000).

Murine MHC class I molecules are tapasin-dependent in respect to their cell surface expression and intrinsic stability, whereas allelic HLA molecules show discrete differences upon tapasin dependency. Interaction of the side group of the C-terminal amino acid of the peptide with the peptide-binding cleft is defined by the polymorphic MHC class I residues 114 and 116, which point from the bottom of the F-pocket towards the peptide (Bjorkman *et al.,* 1987). Peptide-binding by HLA-B4402 is highly tapasin-dependent, whereas peptide-binding by HLA-B8 is moderately and HLA-B2705 barely dependent on tapasin (Peh *et al.,* 1998). Mutation of the residue Glu_{114} to His_{114} in the highly tapasin-dependent HLA-B4402 leads to loading with high affinity peptide and restoration of the cell surface expression even in the absence of tapasin. Substitution of His_{114} to Glu_{114} is sufficient to turn the otherwise tapasin-independent HLA-B2705 into a tapasin-dependent one (Park *et al.,* 2003). Also, it was shown that the presence of Ser_{116} (rather than Phe_{116} and Tyr_{116}) in HLA-B subtypes goes along with an inefficient association with the PLC as well as a reduced MHC class I cell surface expression (Neisig *et al.,* 1996; Turnquist *et al.,* 2000). Albeit, tapasin-independent MHC class I alleles efficiently bind and present peptides in the absence of tapasin, the bound peptide repertoire is edited, and the MHC class I maturation as well as intrinsic stability improves in the presence of tapasin (Peh *et al.,* 1998; Purcell *et al.,* 2001; Zernich *et al.,* 2004).

The herpes simplex virus (HSV) type 1 and 2 encoding immediate early protein ICP47 blocks release of MHC class I molecules from the ER (Hill *et al.,* 1994; York *et al.,* 1994). ICP47 inhibits binding and translocation of peptides from the cytosol into the ER lumen without interfering with ATP binding (Früh *et al.,* 1995). Interaction of ICP47 and TAP is species-specific, since murine TAP is not efficiently inhibited by ICP47 from human simplex virus (Ahn *et al.,* 1996; Früh *et al.,* 1995). Interestingly, the cell surface expression of the tapasin-independent allele HLA-B4405 (Tyr_{116}), which is barely incorporated

into the PLC, was less affected by the viral TAP inhibitor ICP47 than the tapasin-dependent HLA-B4402 (Asn_{116}) (Zernich *et al.,* 2004). This indicates that tapasin-independent alleles have developed during the evolution to sustain the antigen presentation in case the PLC is attacked by viruses.

Tapasin interacts with MHC class I molecules as well as with TAP. A soluble tapasin variant lacking the TMD and the cytoplasmic tail fails to associate with TAP but displays normal association with HLA-B8 (Lehner *et al.,* 1998). This illustrates the necessity of the TMD and the cytoplasmic domain on the interaction of tapasin with TAP. Furthermore, tapasin upregulates the expression level of TAP (Lehner *et al.,* 1998; Li *et al.,* 2000; Tan *et al.,* 2002; Garbi *et al.,* 2003).

3.2.4. Auxiliary factors

3.2.4.1. ERp57

The co-chaperone ERp57 (57 kDa) is a thiol-dependent oxidoreductase belonging to the protein disulfide isomerase (PDI) family, promoting proper disulfide bond formation during the folding of newly synthesized glycoproteins (Garbi *et al.,* 2007; Ellgaard & Ruddock, 2005). ERp57 consists of four thioredoxin-like domains (abb'a'), with the a and a' domains each having a canonical CxxC motif (x is any amino acid) within the active redox site including catalytic activity. The Lys-rich C-terminal domain of ERp57 is basic and bears a QDEL ER retention signal sequence. It was shown that the basic C-terminal b' and a' domains of ERp57 play a crucial role in the interaction with the acidic end of the P-domain of calnexin and calreticulin (Pollock *et al.,* 2004). Transient disulfide bonds are formed between the substrate and the amino-terminal cysteine residue within the motif and are resolved by an intramolecular attack of the carboxyl-terminal cysteine residue on the amino-terminal cysteine residue. Tapasin has been recognized as a unique substrate for ERp57 because it does not disengage from the oxidoreductase, trapping ERp57 in a stable intermolecular disulfide (Peaper *et al.,* 2005). The disulfide linkage includes the Cys_{57} residue of ERp57 (amino-terminal cysteine residue of the a-domain active

site) and the Cys_{95} residue of tapasin. In ERp57-deficient mouse B cells as well as in human cells, replacement of Cys_{95} in tapasin and consequent inhibition of disulfide bonding with ERp57, resulted in a decrease of MHC class I-recruitment into the PLC as well as lower thermostability of MHC class I-β_2m dimers (Dick *et al.,* 2002; Garbi *et al.,* 2006; Wearsch & Cresswell, 2007). It was shown that heavy chains which associate with tapasin Cys_{95} to Ala_{95} mutant devoid of ERp57 interaction site, are reduced in the α_2 peptide-binding domain (Dick *et al.,* 2002). This indicates that the ERp57-tapasin conjugate might be involved in maintaining the oxidized redox state of the α_2 peptide-binding domain during peptide loading. Kienast and colleagues reported an explanation for the formation of the ERp57-tapasin conjugate (Kienast *et al.,* 2007). They found that in the absence of tapasin, MHC class I molecules were sensitive to disulfide bond reduction in the peptide-binding cleft. Tapasin, by forming the disulfide conjugate with ERp57, protected the empty peptide-binding groove against α_2 disulfide reduction until ligand peptide was bound. A tapasin-dependent allele (HLA-B4402) was sensitive to α_2 disulfide reduction, whereas a tapasin-independent allele (HLA-B4405) was insensitive to α_2 disulfide reduction. Furthermore, they showed that when not conjugated to tapasin, ERp57 was able to act directly on the α_2 disulfide bond in the peptide-binding groove. Recently, Wearsch and Cresswell showed *in vitro* the necessity of the ERp57-tapasin conjugate, unlike soluble tapasin alone, on the reassembly of the subcomplex (Wearsch & Cresswell, 2007). Furthermore, they verified functionality of the ERp57-tapasin heterodimer in respect to stabilization of empty MHC class I molecules, to catalysis of peptide binding and to selection of high-affinity peptides.

3.2.4.2. Calnexin and calreticulin

Calnexin and calreticulin are homologous ER resident glycoproteins which assist in the folding of newly synthesized glycoproteins. Calnexin (65 kDa; apparent molecular mass 90 kDa (Ortmann *et al.,* 1997)) is a type I transmembrane protein, whereas calreticulin (46 kDa) is a soluble protein in the ER lumen. Both lectins possess an N-terminal domain, a globular β sandwich structure, followed by a proline rich arm domain (P domain) (Schrag *et al.,* 2001;

Leach *et al.,* 2002). The C-terminal domain of calnexin and calreticulin is rich in acidic amino acids. The C-terminal domain of calnexin ends with an KxRRx ER retention signal sequence, whereas in the case of calreticulin a KDEL ER retention signal sequence is found (Bergeron *et al.,* 1994; Helenius & Aebi, 2004). Both, the P domain as well as the C-terminal domain represent calcium binding sites.

Calnexin and calreticulin form complexes with ERp57 and play a crucial role in the ER glycoprotein quality control (Hebert *et al.,* 2005). Nascent polypeptide chains are co-translationally translocated into the ER and subsequently N-core glycosylated ($Glc_3Man_9GlcNAc_2$). After trimming of the core oligosaccharide to the monoglycosylated form ($Glc_1Man_9GlcNAc_2$), calnexin and calreticulin interact via their N-terminal domains with the sugar moieties of the polypeptide chain (Hammond *et al.,* 1994). The chaperones calnexin and calreticulin prevent aggregation, followed by degradation and export of incompletely or incorrectly folded nascent polypeptide chains. Furthermore, calnexin and calreticulin recruit ERp57, which forms transient intermolecular disulfide bonds with the newly synthesized glycoproteins and interacts with the P domain of the chaperones, to the complex (Frickel *et al.,* 2002; Oliver *et al.,* 1999; Morrice & Powis, 1998). Following correct folding of the nascent polypeptide chain, the third glucose moiety is removed by glucosidase II leading to dissociation of calnexin/calreticulin. The released, correctly folded glycoprotein, is trimmed by mannosidase I and II and recognized by the mannose-binding lectin ER-Golgi intermediate compartiment (ERGIC)-53, following packaging into COP II vesicles and transported from the ER to the Golgi. The transport receptor ERGIC-53 recycles between the ER and Golgi. Partially folded substrates are reglycosylated by the UDP-glucose:glycoprotein-glucosyltransferase and rebound by calnexin and calreticulin. Incorrectly folded proteins lose a mannose residue by action of mannosidase I resulting in the dissociation of calnexin and calreticulin and subsequent binding by the lectin ER degradation enhancing α-mannosidase like protein (EDEM) (Jakob *et al.,* 2001; Hosokawa *et al.,* 2001). EDEM bound substrates are transported via the Sec61 complex from the ER to the cytosol for degradation.

Calnexin interacts via its N-terminus and P domain with the heavy chain of MHC class I molecules (Zhang *et al.,* 1995; Leach *et al.,* 2002; Leach & Williams, 2004). However, calnexin seems to be dispensable for the early folding, peptide loading as well as the ER export of MHC class I molecules. In calnexin-deficient cell lines, MHC class I folding, as well as peptide loading and peptide presentation were not disturbed (Sadasivan *et al.,* 1995; Scott & Dawson, 1995). However, in glucosidase II deficient cells binding of calnexin to the heavy chain of MHC class I was abolished. At the same time an increased interaction of BiP was observed leading to the assumption that BiP takes over the role of calnexin (Balow *et al.,* 1995). In the early calnexin-associated state ERp57 is recruited and interacts with the incompletely oxidized heavy chain of MHC class I (Farmery *et al.,* 2000). Association of β_2m with the fully oxidized heavy chain induces the exchange of calnexin by calreticulin. In mice and humans calreticulin binding occurs at Asn_{86}-linked carbohydrate present in the α_1 helix of the heavy chain (Sadasivan *et al.,* 1996). In tapasin deficient .220 cells or in the presence of tapasin variants lacking N- or C-terminal domains, interaction between MHC class I and calreticulin was significantly diminished (Lewis & Elliott, 1998; Harris *et al.,* 2001; Bangia *et al.,* 1999; Tan *et al.,* 2002). Thus tapasin promotes the recruitment of calreticulin. The interaction of TAP-tapasin complexes with MHC class I variants, lacking the docking site Asn_{86} for calreticulin, was drastically decreased (Sadasivan *et al.,* 1996; Yu *et al.,* 1999; Harris *et al.,* 2001). Hence, it is assumed that the recruitment of heavy chain/β_2m dimer by tapasin into the TAP-tapasin complex is calreticulin dependent. Analysis of calreticulin deficient murine cells revealed that calreticulin plays an important role in peptide loading (Gao *et al.,* 2002). The cell surface expression of MHC class I was 70-75% reduced in the absence of calreticulin. Furthermore, the presentation of certain T cell epitopes was drastically affected, although at the same time the ER export of MHC class I molecules was up regulated, indicating the crucial role of calreticulin and tapasin onto ER retention of empty or suboptimal loaded heavy chain/β_2m dimers.

3.2.4.3. The immunoglobulin binding protein (BiP)

BiP is a member of the heat shock protein family 70. Its function is to stabilize synthesized polypeptide chains during folding processes as well as to mediate their ER retention, to prevent aggregate formation and to avoid non-native disulfide bonds formation (Gething & Sambrook, 1992). Furthermore, BiP is involved in the translocation of newly synthesized proteins to the ER and in the degradation of misfolded proteins.

3.2.5. Peptide translocation to the ER

Peptide translocation from the cytosol to the ER lumen by TAP is divided into several steps. Analysis of peptide transport in the presence of the viral protein ICP47, which inhibits peptide binding to TAP, proved that peptide binding is not a prerequisite for ATP binding (Tomazin *et al.,* 1996). Peptides and nucleotides bind independently of each other to TAP. Peptide translocation is energized by ATP hydrolysis in the NBDs. The NBDs are L-shaped with the long arm I formed by α-β-structures and include Walker A and B motifs, as well as the highly conserved D- and H-loop (also called switch region). The shorter arm II consists of an α-helical domain including Q- and C-loop. ATP binding induces the formation of the NBD sandwich dimer (Smith *et al.,* 2002), a prerequisite for ATP hydrolysis and subsequent peptide translocation (Hopfner *et al.,* 2000; Smith *et al.,* 2002). Kinetic data provided a two step mechanism for peptide binding to TAP: a fast association step followed by slow isomerization of the TAP complex (Neumann & Tampé, 1999). The isomerization step includes a conformational change in TAP (Neumann *et al.,* 2002). It is proposed that the molecular switch, which basically induces ATP hydrolysis, is a consequence of structural rearrangement. Stimulation of ATP hydrolysis was shown to be correlated with peptide binding (Gorbulev *et al.,* 2001). Sterically unfavoured peptides bound to TAP do not stimulate ATP hydrolysis (Gorbulev *et al.,* 2001).
During a translocation cycle ATP hydrolysis takes place in both NBDs (Chen *et al.,* 2003). The non-equivalence of both subunits was determined by mutagenesis studies. Mutation of the highly conserved Lys residue at Walker A motif of TAP2 resulted in the loss of peptide transport activity, while the same mutation in TAP1 led to a minor reduction of peptide transport

(Karttunen *et al.,* 2001; Lapinski *et al.,* 2001). Peptide transport by TAP requires ATP hydrolysis, however also GTP, CTP and UTP can energize the transporter (Müller *et al.,* 1994). The non-equivalence of both NBDs is reflected in sequence alignments of highly conserved regions of ABC transporters. Sequence alignments of the ATP-binding regions of NBD1 and NBD2 with other NBDs revealed major differences in the ATP-binding region of TAP1. In TAP1 sequences, the conserved Glu following directly the Walker B motif, is exchanged to Asp. This Asp residue is thought to be involed in ATP hydrolysis as the catalytic base. Furthermore, the TAP1 sequence contains a Gln residue instead of a His residue in the H-loop. This His residue contacts the γ-phosphate of ATP and is essential for the substrate transport in different ABC transporters (Shyamala *et al.,* 1991; Hung *et al.,* 1998). The C-loop sequences in TAP2 of humans and gorillas are LAAGQ in comparison to LSGGQ in other species. Two critical residues (Leu and Gly) are highly conserved and are often substituted by other amino acids forming an irregular sequence xSxGQ. Therefore, this type of C-signature motif is usually called “degenerated C-loop”. Based on this, it was proposed that one NBD in the complex hydrolyzes ATP to provide the energy for translocation, while the other one only binds ATP as a regulatory domain (Yang *et al.,* 2003).

Peptides of 8-12 amino acids were observed to be transported most efficiently by TAP (Koopmann *et al.,* 1996), however the optimal length for peptide binding is 8-16 amino acids (Van Endert *et al.,* 1994). Nevertheless, peptides of 6 or 40 amino acids in length are also transported by TAP, however with considerable lower efficiency (Koopmann *et al.,* 1996). Since the optimal length of peptides for loading onto MHC class I is 8-10 amino acids and TAP transports peptides with slightly larger length, the ER-resident aminopeptidase associated with antigen processing (ERAAP) is essential for further peptide trimming (Falk & Rotzschke, 2002; Saric *et al.,* 2002; Serwold *et al.,* 2002; York *et al.,* 2002). The sequence specificity of TAP was determined by screening combinatorial peptide libraries (Uebel *et al.,* 1997). The first three N-terminal and the last C-terminal residues were found as determinants for peptide-binding specificity. At the N-terminus, human TAP generally displays preferences for peptides with Lys, Asn and Arg in the first, Arg in the second, and Trp and Tyr in the third position. In the case of human TAP the C-terminal

residue is preferred to be a hydrophobic or basic residue. The peptide-binding spectrum of TAP and MHC class I molecules overlap in their C-terminal residue, suggesting that the binding principle of TAP and MHC class I molecules coevolved. Furthermore, it was shown that the substrate recognition by TAP is also strictly stereospecific. Interestingly, the introduction of D-amino acids at the termini of peptides causes complete abrogation of peptide transport (Gromme *et al.,* 1997; Uebel *et al.,* 1997). Acetylation or methylation of the N-terminus or conversion of the C-terminal carboxyl group of a peptide to an amide decreases its translocation efficiency considerably (Momburg *et al.,* 1994; Schumacher *et al.,* 1994). Circular peptides, which lack free termini generally, do not represent a substrate for TAP. Indicated by the structure of MHC class I molecules, the hydrogen bonds between the two termini and MHC class I molecules contribute largely to the free energy of binding. Therefore, TAP was expected to apply an analogous strategy for peptide binding. The residues in the center of the peptide have only little or no effect on the substrate specificity of TAP. Interestingly, these residues are responsible for the detection of the MHC class I-peptide complex by the T cell receptor which interacts mainly with the residues 5-8 of MHC class I bound peptide. In conclusion, TAP binds peptides through the N- and C-termini and transports them with maximal diversity in the center of the peptide for T cell recognition.

MHC class I molecules are unstable in the absence of peptides. Hence, TAP1-deficient mice exhibit approximately 90-fold reduced MHC class I cell-surface expression as well as a 20-fold reduced $CD8^+$ T cell number, in comparison to TAP1-proficient mice (Garbi *et al.,* 2005). The $CD8^+$ cytotoxic T cell response is as well reduced similar to the $CD8^+$ T cell number (Van Kaer *et al.,* 1992; Garbi *et al.,* 2000). Also the $CD8^+$ T cell repertoire is impaired in TAP1-deficient mice. These data demonstrate that peptides translocated by TAP are important for a positive influence on the selection in the thymus. Since even in TAP1-deficient mice an altered $CD8^+$ T cell repertoire as well as a reduced $CD8^+$ cytotoxic T cell response is found, indicates the existence of TAP-independent pathways. However, these pathways play a minor role in the MHC class I antigen presentation. Secreted proteins including their ER signal sequences are translocated to the ER via the Sec61 complex, and the signal sequences are

cleaved off by an ER-resident endopeptidase. This leads to the TAP-independent release of hydrophobic peptides in the ER lumen and subsequent loading onto HLA-A2 molecules in a human TAP-deficient cell line (T2; Wei & Cresswell, 1992). Another TAP-independent peptide source is the degradation of antigens by endosomal proteases in dendritic cells. These peptides are loaded onto recycled MHC class I molecules in vesicular compartments (Ackermann *et al.* 2005).

3.2.6 Assembly of the peptide loading complex

A prerequisite for the assembly of the ternary MHC class I complex, consisting of the MHC class I heavy chain, β_2-microglobulin and the peptide, is the effective interplay between multiple ER-resident proteins and chaperones of the peptide loading complex (PLC) (Figure 3-7). The MHC class I heavy chain and β_2-microglobulin are synthesized at the rough ER and are subsequently co-translationally translocated into the ER via the Sec61 complex. During the translocation, the ER signal sequence is cleaved off and the heavy chain is co-translationally N-core glycosylated. Then, the newly synthesized and unfolded heavy chain assembles with the ER-resident folding chaperone BiP and the lectin chaperone calnexin (Paulsson & Wang, 2003). Calnexin assists in the folding of the heavy chain as well as its assembly with β_2m. The thiol-dependent oxidoreductase ERp57 interacts with the incompletely oxidized β_2m-free MHC class I heavy chain and is together with tapasin involved in the correct folding as well as in the formation of proper intramolecular disulfide bridges (Dick *et al.,* 2002). Binding of ERp57 induces the dissociation of BiP. After the pre-assembly of the MHC class I molecule, calnexin is exchanged by another lectin calreticulin. Subsequently, tapasin recruits the pre-assembled MHC class I molecules into the proximity of the TAP complex, where MHC class I molecules await their loading with high affinity peptides. The TAP complex translocates peptides of 8-16 amino acids in length across the ER membrane energized by ATP hydrolysis. Several N-terminally elongated precursor peptides display even a higher affinity for TAP than the final epitope (Neisig *et al.,* 1995; Lauvau *et al.,* 1999). Peptides with a Pro residue at position 2 or 3 are transported less efficiently by TAP but are often ligands of human and

murine MHC class I molecules (Rammensee *et al.,* 1993). Since longer peptides than are presented by MHC class I, are translocated in the ER lumen, ER resident exopeptidases are needed for subsequent trimming. Experiments in TAP-deficient cells with minigene-encoded N-terminally elongated precursor peptides bearing an ER signal sequence are imported to the ER and confirm N-terminal trimming (Powis *et al.,* 1996; Serwold *et al.,* 2001). However, carboxypeptidase activity in the ER could not be detected (Lobigs *et al.,* 2000). An aminopeptidase was independently identified by two groups but named differently, ER-aminopeptidase 1 (ERAP1; Saric *et al.,* 2002) and ER-associated aminopeptidase (ERAAP; Serwold *et al.,* 2002). The IFN-γ induced zinc-dependent aminopeptidase ERAP1 has a broad tissue distribution and exhibits a special characteristic by preferring peptides with 9-16 amino acids in length and a hydrophobic C-terminal residue (Serwold *et al.,* 2002; Chang *et al.,* 2005). The preference corresponds to the substrate length and sequence preference of TAP. The blockage of ERAP1 function leads to reduced antigen presentation (Serwold *et al.,* 2002; York *et al.,* 2002). A second ER-localized aminopeptidase, ER-aminopeptidase 2 (ERAP2) a homolog of ERAP1, also seems to be involved in peptide processing (Tanioka *et al.,* 2003). ERAP2 is cleaving preferentially units of basic dipeptides (Lys and Arg) (Tanioka *et al.,* 2003). The molecular mechanism of tapasin as a peptide editor is still under debate, and it is speculated how peptide binding to MHC class I molecules occurs. It was shown by conformation-specific antibodies that immature, peptide-receptive MHC class I molecules are prevalent in the peptide-loading complex (Carreno *et al.,* 1995; Yu *et al.,* 1999). Presumably tapasin interacts with MHC class I molecules in a conformation where the α_2 loop (residues 128-123) as well as the contact site to β_2m are involved. Upon optimal loading, the peptide-MHC class I molecules are released from the tapasin-TAP complex. The highly sophisticated molecular complex consisting of the TAP complex, MHC class I molecules, tapasin, ERp57 and calreticulin is known as the PLC. The fully assembled PLC is essential for the loading of high affinity peptides, thus generating kinetically stable MHC class I complexes with increased half lifes. These MHC class I complexes display an increased stability on the cell surface, avoiding the loss of antigenic peptides before encounter with effector cells. The optimally loaded MHC class I molecules are further

translocated to the cell surface via the Golgi for presentation to effector cells of the immune system.

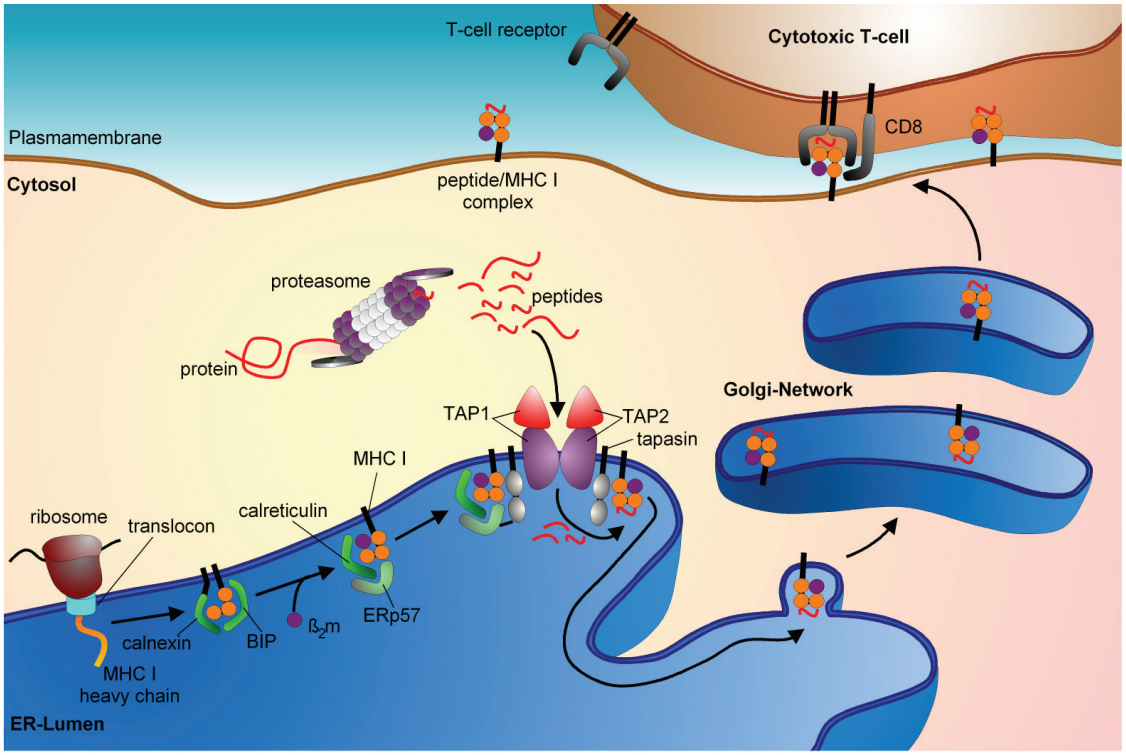

Figure 3-7. The MHC class I antigen presentation pathway. The MHC class I heavy chain and β_2-microglobulin are co-translationally translocated into the ER. Following folding and assembly of MHC class I heavy chain and β_2-microglobulin which are assisted by calnexin and immunoglobulin binding protein (BiP), the MHC class I molecules are recruited into a macromolecular peptide-loading complex (PLC) consisting of calreticulin, ERp57, tapasin, TAP1 and TAP2. Cytosolic peptides are translocated by TAP into the ER lumen, where they are loaded onto pre-assembled MHC class I molecules. MHC class I-peptide complexes dissociate from the PLC and are then transported via the Golgi to the cell surface where cytotoxic T cells screen the cell surface for infected or malignantly transformed cells. Once identified as foreign, T cell receptor and CD8 co-receptor bind to the MHC class I-peptide complex and trigger the killing of the target cell (Schölz & Tampé, 2005).

3.3. Objectives

An optimal immune surveillance is a prerequisite for the survival of higher vertebrates. However, herpes- and adenoviruses have evolved sophisticated strategies to circumvent the immune surveillance by interacting and at the same time modulating especially proteins of the macromolecular PLC. Predominantly TAP, tapasin and MHC class I molecules, represent a major target for viral effector proteins (Loch *et al.*, 2008; Loch & Tampé, 2005; McCluskey *et al.,* 2004). Besides the manifold strategies of viral evasion, synthetic or protein engineered modulators have not been described so far. In the current work the production and purification of TAP-specific recombinant antibodies such as Fv, scFv and Fab fragments (Figure 3-8, a) in pro- and eukaryotic expression systems has to be established and evaluated. Furthermore, cell-based assays were applied for functional characterization of the generated recombinant antibody fragments.

The X-ray crystal structures of soluble MHC class I molecules as well as of the soluble TAP1 NBD have been solved. However, no structural information about the organization of the macromolecular PLC is available so far. Here, the generated recombinant antibody fragments were used for the purification of the endogenous PLC from a human B-lymphoblastoid Raji cell line. Subsequently, the composition of the PLC was investigated using electrophoretic methods in combination with mass spectrometry as well as single particle analysis.

To get a better mechanistic understanding of the transient assembly and disassembly of the PLC as well as the highly sophisticated interplay of the diverse components of the PLC and their defined functions, it was necessary to establish an *in vitro* platform for measuring single interaction and their immediate interplay with other proteins of the PLC as well as their modulating function on those. The following questions are heavily discussed in the field: how is peptide translocation, peptide loading and dissociation of the trimeric MHC class I-peptide complex synchronized? And what is the precise function of the chaperone tapasin and the oxidoreductase ERp57 in the peptide transfer onto MHC class I molecules? Since the molecular events during peptide loading onto MHC class I molecules are not well defined, it was necessary to establish an *in vitro* method for direct measuring interaction between the single

components of the PLC as well as changes in peptide kinetics in the presence or absence of certain PLC components, which provide a more detailed mechanistic understanding of the transient assembly and disassembly of the PLC. My aim was to engineer single chain MHC class I molecules (Figure 3-8, b), precisely two different alleles, the HLA-B4405 a tapasin-independent, and HLA-B4402 highly tapasin-dependent allele, and to functionally produce those in insect cells. For the analysis of individual interactions between MHC class I molecules and tapasin, soluble tapasin as well was expressed and purified from insect cell supernatants. The tapasin-MHC class I interaction was first investigated by surface plasmon resonance (SPR) spectroscopy. To investigate the differences in peptide kinetics in presence and absence of tapasin, both MHC class I molecules and tapasin were co-immobilized on a solid-supported lipid bilayer mimicking the lateral mobility of the cell membrane. The proteins were tethered via their C-terminal His_6-tags onto a lipid functionalized with a multivalent chelator head group. The co-immobilization of both proteins in combination with surface-sensitive fluorescence detection allowed the investigation of changes in peptide kinetics. Thus reconstitution of the interaction partners *in vitro* should help to narrow the functions of tapasin in regard to the interaction with MHC class I molecules and peptide kinetics.

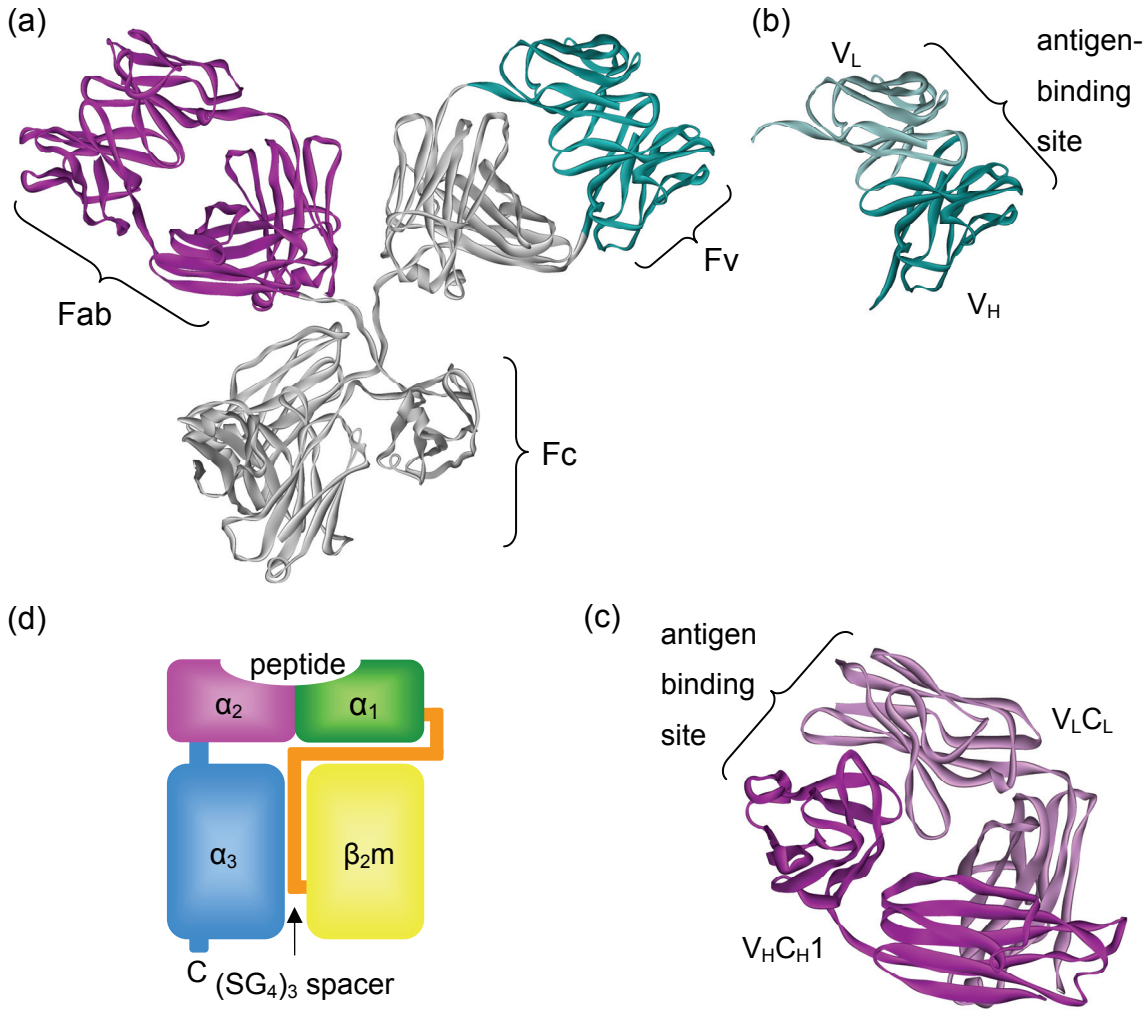

Figure 3-8. Structure of an antibody and schematic model of soluble single chain MHC class I molecule. Ribbon diagram based on the X-ray crystallographic structure of an IgG1 antibody is shown in (a). Three globular regions form a Y shape. The two antigen-binding sites are at the tips of the arms, which are tethered to the trunk (=Fc domain) of the Y by a flexible hinge region. The protease papain cleaves antibody molecules into two Fab and one Fc fragment. (c) The Fab (Fragment antigen binding) fragment contain the antigen-binding site and consists of a complete light chain (V_LC_L, light magenta) paired with the V_H and C_H1 domains of the heavy chain. (b) Genetic engineering technique permits the construction of a truncated Fab comprising only the V domain of the heavy chain (V_H in blue) and light chain (V_L light blue), named Fv (fragment variable). By tethering the V_H and V_L by a $(SG_4)_3$ spacer produces a single chain Fv (scFv) fragment (not shown). The Fc (fragment crystallizable) fragment consists of the paired C_H2 and C_H3 domains and is the part of the antibody interacting with effector molecules and cells. (d) Schematic representation of an engineered soluble MHC class I molecule. Heavy chain MHC class I, lacking the membrane-spanning domain as well the short cytosolic domain, is linked via a $(SG_4)_3$ spacer to β_2m and expressed as a single polypeptide chain.

4. Material

4.1. Microorganisms

Strain	Genetic markers	Source
DH5α	F$^-$ *gyrA96* (Nal^r) *recA1 endA1 thi-1 hsdR17* ($r_k^-m_k^+$) *glnV44 deoR Δ(lacZYA-argF)U169* [Φ80d Δ(*lacZ*)*M15*]	Hanahan, 1983 Invitrogen
XL1-Blue	F'Tn *10* (Tet^r) *proA$^+$B$^+$ lacI^q* Δ(*lacZ*)*M15 I rec A1 endA1 gyrA96* (Nal^r) *thi-1 hsdR17* ($r_k^-m_k^-$) *glnV44 relA 1 lac*	Stratagene
JM83	F$^-$ *ara* Δ*(lac-proAB) rpsL* (Str^r) *thi* [Φ80d Δ(*lacZ*)*M15*]	Vieira & Messing, 1982; 35607 (ATCC number)
DH10Bac	F$^-$ mcrA D(mrr-hsdRMS-mcrBC) φ80*lacZM15* Δ*lacX*74 deoR recA1 endA1 araD139 Δ(ara,leu)7697 galU galK λ$^-$rpsL nupG / bMON14272 / pMON7124	Invitrogen

4.2. Plasmids

Plasmid	Provider/Company
pCRScript	Stratagene
pSL1180	Pharmacia
pASK68	Arne Skerra / IBA
pASK85	Arne Skerra / IBA
pFastBac1	Invitrogen
pFastBacDual	Invitrogen
pGAMZ – B4402	Sebastian Springer (Jacobs University Bremen)
pGAMZ – B4405	Sebastian Springer (Jacobs University Bremen)

4.3. Eukaryotic cell lines

Cell lines	Provider/Company
Raji (Human Burkitt Lymphoma)	CCL-86 (ATCC number)
*Sf*9 (*Spodoptera frugiperda*)	CRL-1711 (ATCC number)
*Tn*5 (High Five, BTI-Tn-5B1-4, *Trichoplusia ni*)	Invitrogen
.720	kindly provided by Kajsa Paulsson (Panum Institute, Copenhagen)
.721	kindly provided by Kajsa Paulsson (Panum Institute, Copenhagen)

4.4. Antibodies

Antibodies	Type	Specificity
148.3	monoclonal (mouse)	TAP1
429.3	monoclonal (mouse)	TAP2
435.4	monoclonal (mouse)	TAP2
7F6	monoclonal (rat)	tapasin
HC10	monoclonal (mouse)	MHC class I
9E10	monoclonal (mouse)	*c-myc*-epitope

Commercially available antibodies		
Specificity	Type	Company
ERp57	monoclonal (mouse)	Abcam
calreticulin	polyclonal	Sigma-Aldrich
β_2m	polyclonal (rabbit)	Sigma-Aldrich
α-His_6	monoclonal (mouse)	Novagen
Streptactin-HRP	HRP conjugate	IBA
goat-α-mouse-HRP	HRP conjugate	Sigma-Aldrich
goat-α-rat-HRP	HRP conjugate	Sigma-Aldrich
goat-α-rabbit-HRP	HRP conjugate	Sigma-Aldrich

4.5. Oligonucleotides

Primers for pASK68 and pASK85	5‘ – sequence – 3’ (restriction site highlighted)
forVH148 (PstI)	AGGTGAAGCTGCAGGAGACTG
revVH (BstEII)	GGAGACGGTGACCGAGGTTCCTTGAC
forVL148 (SacI)	TTGAGCTCACTCAGGCTGCACCCTCTG
pASK68/85 for (sequencing primer)	TCTAGATAACGAGGGCAAAA
pASK68/85 rev (sequencing primer)	TCACTTCACAGGTCAAGCTTA
dT15 (cDNA synthesis)	TTTTTTTTTTTTTTT

Primers for pFB1 and pFBD	5‘ – sequence – 3’ (restriction site highlighted)
PH forward primer (BamHI) (melittin signal sequence)	CCGGATCCTAAAAAACCGCCACCATGA AATTCTTAGTCAACGTTGCCCTTGTTTT TATGGTCG
PH reverse primer (SacI) (melittin signal sequence)	CCGAGCTCGATGTCGGCCGCATAGATG TAAGAAATGTATACGACCATAAAAACAA GGGC
p10 forward primer (melittin signal sequence)	TAATCCCGGGTAAAAAACCGCCACCAT GAAATTCTTAGTCAACGTTGCCCTTGTT TTTATGGTCG
p10 reverse primer (melittin signal sequence)	TTCTGCAGTTTAACTTCGGCCGCATAG ATGTAAGAAATGTATACGACCATAAAAA CAAGGGC
$(SG_4)_3$ linker forward (SacI, XhoI)	AAGAGCTCGAATTCCTCGAGATCAAAC GGTCTGGTGGCGGTGGCTCGGGTGGC GGCGGTTCGGGCGG
$(SG_4)_3$ linker reverse (HindIII, NcoI, PstI)	ATTAAGCTTCCATGGGTGACCCTGCAG TTTAACTTCAGAACCGCCACCGCCCGA ACCGCCGCC

Primers for MHC I in pFB1	5‘ – sequence – 3’ (restriction site highlighted)
NgoMIVstrepfor	TTAATTGCCGGCTGGAGTCATCCACAGTTTG
NgoMIV$\beta_2$mfor	TTAATTGCCGGCATCCAGCGTACTCCAAAG
tevhisrev	TAATTAACCGGTAAGCTTTCATTAGTGATGG TGATGGTGATGAGACTGGAAGTACAGGTTC TCGTCGACCGGCTCCCATC

Sequencing primers	5‘ – sequence – 3’
pFBD_PH_REV	GTAACCATTATAAGCTGC
pFBD_PH_FOR	AAATGATAACCATCTCGC
pFBD_p10_REV	GTATTGTCTCCTTCCGTG
pFBD_p10_FOR	CCTTTAATTCAACCCAAC
M13_FOR	GTAAAACGACGGCCAGT
M13_REV	CAGGAAACAGCTATGAC

4.6. Peptides

Peptides	Sequence
C4F	RRY(C)^{Fluorescein}KSTEL
NSTCL	RRYQNST(C)^{Fluorescein}L
NSTEL	RRYQNSTEL
R9LQK	RRYQKSTEL
ICP47 (2-34)	SWALEMADTFLDTMRVGPRTYADVRDEINKRGR
EEFGRAFSF	EEFGRAFSF
CAFSF	EEFG(C)^{Fluorescein}AFSF
CFSF	EEFGR(C)^{Fluorescein}FSF
CSF	EEFGRA(C)^{Fluorescein}SF
CF	EEFGRAF(C)^{Fluorescein}F

4.7. Chemicals

Chemicals	Company
Acetic acid (99%)	Carl Roth
Acrylamide 30% (w/v)	Carl Roth
Agar	Carl Roth
Agarose	Carl Roth
Ampicillin	Carl Roth
APS (Ammonium persulfate)	Carl Roth
Ammonium sulfate	Carl Roth
Anhydrotetracycline	IBA
Avidin	IBA
Benzonase Nuclease	Merck
Bromophenol Blue	Sigma-Aldrich
BSA (Bovine Serum Albumin)	Carl Roth
Chloramine T	Riedel de Haen
Coomassie Brilliant Blue R	Sigma-Aldrich
Desthiobiotin	Sigma-Aldrich
Disodium hydrogenphosphate	Carl Roth
DMF (N,N-Dimethylformamide)	Fluka Chemie
DMSO (Dimethylsulfoxide)	Merck
dNTP-Mix	MBI Fermentas
DTT (Dithiothreitol)	Merck
EDTA (Ethylenediaminetetraacetic acid)	Carl Roth
Ethanol, p.a.	Carl Roth
Ethanol, denatured	Carl Roth
Ethidium bromide	Merck
Formaldehyde	Carl Roth
Glycerol	Carl Roth
Glycine	Carl Roth
Guanidine hydrochloride	Carl Roth
Hydrochloric acid, 37%	Carl Roth
HABA (2-(4-Hydroxyphenylazo)benzoic acid)	Sigma-Aldrich
Imidazole	Carl Roth
IPTG (Isopropyl-β-D-1-thiogalactopyranoside)	MBI Fermentas

Methanol	Carl Roth
Ponceau S red	Sigma-Aldrich
Potassium chloride	Carl Roth
Sodium carbonate	Carl Roth
Sodium chloride	Carl Roth
Sodium dihydrogen phosphate	Carl Roth
SDS (Sodium dodecyl sulfate)	Carl Roth
Sodium hydroxide	Carl Roth
Sodium thiosulfate	Carl Roth
Strep-Tactin-HRP conjugate	IBA
Streptomycine	Sigma
TEMED (N,N,N,N-Tetramethylethylenediamine)	Carl Roth
TRIS (Tris(hydroxymethyl)aminomethane)	Carl Roth
Triton X-100	Sigma-Aldrich
Tryptone	Carl Roth
Tween 20	Sigma
Yeast-Extract	Carl Roth
X-Gal (5-Bromo-4-chloro-3-indolyl β-D-galactopyranoside)	MBI Fermentas
Xylene cyanole	Sigma-Aldrich

4.8. Enzymes

Enzymes	Company
Cfr9I (isoschizomer of XmaI)	MBI Fermentas
DpnI	MBI Fermentas
Eco9I (isoschizomer of BstEII)	MBI Fermentas
EcoRI	MBI Fermentas
HindIII	MBI Fermentas
Mph1103I (isoschizomer of NsiI)	MBI Fermentas
NsiI	NEB Biolabs
NgoMIV	NEB Biolabs
Pfu polymerase	Promega
PowerScript DNA polymerase	PAN Biotech
PstI	NEB Biolabs
Reverse Transcriptase SuperScript II	Invitrogen

SacI	MBI Fermentas
Taq polymerase	MBI-Fermentas
T4 DNA ligase	NEB Biolabs
T4-Polynucleotide kinase	MBI Fermentas
XbaI	MBI Fermentas
XhoI	NEB Biolabs

Kits	Company
Maus-Hybridoma-Subtyping Kit	Roche
RNeasy Kit	Qiagen
QIAquick PCR Purification Kit	Qiagen
QIAquick Gel Extraction Kit	Qiagen
Nucleospin Plasmid	Macherey & Nagel
PCR-Purification Kit	Macherey & Nagel
Gel-Extraction Kit	Macherey & Nagel
QIAprep Spin Miniprep Kit	Qiagen
QIAGEN PCR Cloning Kit	Qiagen
QuikChange Multi site-directed Mutagenesis Kit	Stratagene

4.9. Equipment

Apparatus	Company
Autoclave 5075 ELVC	Systec
BIAcore T100	GE Healthcare
Cary 50 Bio UV Vis spectrophotometer	Varian
Douncer (30 mL)	Braun Melsungen
Eppendorf centrifuge 5417R	Eppendorf
Fluorescence spectrometer	Instruments S.A., France
Gilson pipettes: P-2, -10, -20, -200, -1000	Abimed
Incubator Kelvitron	Heraeus
Incubator Innova 4330	New Brunswick Scientific
Ino Lab pH-meter	WTW
Lumi Imager F1	Roche

Milli Q-Plus water system	Millipore
Multipipette	Eppendorf
Multiscreen filtration system	Millipore
Polarstar Galaxy (ELISA reader)	BMG
Rotors for ultracentrifugation (SW 28, Ti60, Ti70, TLA100, TLA110, TLA55)	Beckmann Instruments
Semidry blotting apparatus	BioRad
SDS-PAGE gel apparatus	BioRad
Sepatec Megafuge	Heraeus
Speed Vac evaporator	Buchofer
Sorvall centrifuge RC 3C Plus	Kendro
Sorvall centrifuge RC 5B Plus	Kendro
Thermomixer	Eppendorf
Thermocyler T-personal	Whatman Biometra
Ultracentrifuge Beckmann L-50	Beckmann Instruments
Ultracentrifuge Beckmann TLX 100	Beckmann Instruments
UV-Vis spectrometer, nanodrop	PEQlab
Vortexer	Scientific Industries

4.10. Chromatography material

Material	Company
Aekta Explorer	GE Healthcare
Activated CH-Sepharose 4B	GE Healthcare
ATP-Agarose ((A2767))	Sigma
ETTAN	GE Healthcare
HiTrap Chelating (1 mL)	GE Healthcare
Ni-NTA Agarose	Qiagen
SMART Chromatography System	GE Healthcare
Superdex 200 PC 3.2/30	GE Healthcare
Superdex 75 PC 3.2/30	GE Healthcare

4.11. Supplementary material

Material	Company
Cuvette (plastic)	Fischer Scientific
Cuvette (quartz glass)	Hellma
Eppendorf tubes	Greiner
Filter paper	Whatman
Microliter syringe	Hamilton
Multiwellplates	Greiner
Multiwellplates MaxiSorb	Nunc
Spin Concentrator (Amicon)	Millipore
Spin Columns	BioRad
Sterile filter	Millipore
CM5 chip	Biacore
SA chip	Biacore

5. Methods

5.1. Molecular biology

5.1.1. Mini preparation of plasmid DNA

A 2 mL culture of *E. coli* containing the plasmid and the appropriate antibiotic were incubated for 8-12 h at 37°C with sufficient aeration following centrifugation for 1 min at 14,000 g to form a pellet. For the isolation and purification of pure and low salt DNA, the alkaline denaturation method was applied using Nucleospin Plasmid Kit (Macherey & Nagel) following the manufacturer's instructions. The cell pellet was resuspended in 300 µL TE buffer, resulting in a homogenous suspension. 300 µL of alkaline lysis buffer was added and the capped tube was inverted several times and subsequently incubated for 5 min at RT. The solution was then mixed with 300 µL of low acidic neutralization buffer and incubated for 5 min on ice. The coagulated white mass of detergent and denatured genomic DNA which coprecipitates was centrifuged for 10 min at 14,000 g and 4°C. The supernatant was transferred to a microfuge tube and mixed with 800 µL of isopropanol. After centrifugation for 15 min at 14,000 g and 4°C the DNA pellet was washed with 80% EtOH and dried at RT. The pellet was finally resuspended in 20-50 µL autoclaved dH_2O.

5.1.2. Restriction enzyme digestion

Restriction analysis was performed following standard protocols and using restriction endonucleases from New England Biolabs or MBI Fermentas. The reaction was preformed in 20 µL volume containing the appropriate 1 x restriction endonuclease buffer, the restriction endonuclease itself (1 U/µg DNA) and the plasmid DNA. The digestion was performed for 1 h at 37°C and terminated by incubation for 20 min at 65-80°C if needed for subsequent

reaction. The digestion was analyzed by agarose gel electrophoresis (see 5.1.4).

5.1.3. Ligation

The ligation reaction was performed in a volume of 10 µL using T4 DNA ligase (New England Biolabs) for 12 h at 16°C. 50 - 100 ng DNA and 10 U T4 DNA ligase were used in the ligation reaction. For the transformation of *E. coli* DH5α 10 µL of the ligation reaction was used.

5.1.4. Nucleic acid electrophoresis and DNA recovery

Nucleic acids are separated and visualized in agarose gels after electrophoresis. Electrophoresis is defined as the movement of ions and charged macromolecules through a medium when an electric current is applied. Agarose and polyacrylamide are the primary stabilizing media used in the electrophoresis of macromolecules. Macromolecules are separated through the matrix based on their size, charge distribution, and structure. In general, nucleic acids migrate through a gel based on size, with no influence from base composition or sequence. The appropriate amount of agarose powder was weighed, resuspended in 1 x TAE buffer and heated in a microwave. The agarose solution was thouroughly mixed and while cooling, the gel casting tray was assembled. Subsequently the agarose solution was poured into the gel tray, the comb was inserted and the agarose was left to gel at room temperature. The 0.8 – 2% agarose gels were then transferred into an electrophoresis chamber filled with 1 x TAE buffer. Prior to loading, the DNA was resuspended in 6 x DNA loading buffer and electrophoresed at 20-150 mA. After separation of the DNA, the agarose gel was removed from the electrophoresis chamber and submerged for 20 min in the ethidium bromide solution and visualized subsequently by UV radiation (312 nm). The ethidium bromide intercalates between the bases of DNA, resulting in an increase in fluorescence yield when the DNA/ethidium bromide complex is exposed to UV radiation.

For further purpose DNA was recovered from an agarose gel by cutting the DNA out with a steril scalpel. The DNA was recovered using QIAquick Gel Extraction Kit (Qiagen) following manufacturer's instructions.

TAE (50 x)	DNA loading buffer (6 x)	Ethidium bromide solution
2 M TrisAc, pH 8.0	60% glycerol	5 µg/mL in dH_2O
50 mM EDTA	60 mM EDTA	
	0.09% bromophenol blue	
	0.09% xylene cyanole	

5.1.5. Photometric concentration determination of nucleic acids

The concentration of nucleic acids was determined by measuring the absorbance of UV light at 260 nm. An OD unit corresponds to the amount of nucleic acid in µg in 1 mL volume using 1 cm length quartz cuvette resulting in $OD_{260\,nm}$ = 1 = 50µg / mL. For the concentration determination the DNA solution was diluted 1:100 and the OD was measured in a spectrophotometer.

$$concentration\,[{}^{ng}\!/_{\mu L}] = 50 \times absorption_{260\,nm} \times dilution\ \ factor$$

5.1.6. Amplification of V_H and V_L genes of mAb 148.3

The variable heavy (V_H) and variable light (V_L) genes were amplified from a hybridoma cell line 148.3 (Meyer *et al.*, 1994).

5.1.6.1. Poly-mRNA isolation

In general there are two strategies to isolate mRNA: 1) isolation of total RNA, 2) isolation of messenger RNA (mRNA). Almost all eukaryotic mRNA are monocystronic and contain a post-transcriptionally added, poly-adenylic acid (poly A) at their 3' terminal. This poly-A tail permits separation and isolation of mRNA from the total pool of RNA. Hybridoma cells 148.3 (1-2 x 10^8 cells) were harvested at 500 g for 5 min at 4°C and the supernatant was discarded. Cell pellet was washed twice with ice-cold PBS and the RNA isolation was continued by using RNeasy Mini Kit (Qiagen) following the manufacturer's instructions.

Usually 1 to 3% of the total RNA pool represent the mRNA level. The purification of mRNA is based on the hybridization of poly-A^+-RNA tail to oligo-dT-nucleotides immobilised on a matrix under high salt concentration. The poly-A-mRNA was isolated by using Oligotex Direct mRNA Mini Kit (Qiagen) following the manufacturer's instructions.

5.1.6.2. cDNA synthesis

For the synthesis of single stranded DNA the enzyme SuperScript II Reverse Transcriptase (from *E. coli*) (Invitrogen) was used following the manufacturer's instructions. The following reaction mixture was prepared:

4 µL	first strand buffer (5x)
1 µL	RNasin (20 U/µL), RNase inhibitor
1 µL	dNTP (10 mM)
1 µL	DTT (0.1 M)
4 µL	dT15 primer (10 pmol/µL)
1-5 µg	RNA
ad 19 µL	RNase-free dH_2O

The reaction mixture was incubated for 1 min at 42°C. 1 µL of the reverse transcriptase was added and the reaction was continued for 1 hour at 42°C, followed by a 15 min incubation at 70°C to terminate the reaction. The reaction mixture was transferred on ice and centrifuged for 5 min at 18,000 g and 4°C. Supernatant was transferred to a fresh 1.5 mL tube and stored at -80°C.

5.1.6.3. Polymerase chain reaction (PCR)

DNA fragments are amplified sequence specifically by using polymerase chain reaction (PCR) (Saiki *et al.,* 1985; Mullis *et al.,* 1986). DNA templates flanked by two oligonucleotides hybridized to opposite strands of the template are synthesized by DNA polymerase starting from the 3' end of each oligonucleotide. Following repeating cycles of heat denaturation of the template, annealing of the primers and extension of the annealed primers by DNA polymerase, the DNA fragment is synthesized and amplified. These newly

synthesized DNA strands are used again as DNA templates in a new cycle. To amplify the V_H and V_L chain genes cDNA (see 3.1.1.2) template and degenerate primers (Hunte & Müncke 2004) specific for antibody genes were used in the following reaction mixture of 100 µL:

1 µL	cDNA (10 ng)
10 µL	Polymerase buffer (10 x)
3 µL	$MgCl_2$ (50 mM)
20 µL	Optizym enhancer (5 x)
2 µL	*forward* primer (10 pmol/µL)
2 µL	*reverse* primer (10 pmol/µL)
2 µL	dNTPs (10 mM)
1 µL	PowerScript DNA polymerase
59 µL	dH_2O

The thermal cycling profile looked as follows:

94°C	1 min	
94°C	1 min	┐
50°C	90 sec	┘ 30 x
72°C	2 min	
72°C	10 min	
4°C	break	

The resulting PCR products were cloned into pDrive vector (Invitrogen) following the manufacturer's instructions and sequenced.

To introduce restriction sites into the antibody and HLA-B44 genes, *Pfu* DNA polymerase (Lundberg *et al.,* 1991) with 3' → 5' exonuclease activity (proofreading) was used. The following reaction components in a volume of 50 µL were used in a standard PCR:

1 µL	DNA (10 ng)
5 µL	Pfu buffer (10 x)
2.5 µL	*forward* primer
2.5 µL	*reverse* primer
5 µL	dNTPs (2 mM)
0.5 µL	Pfu polymerase (2.5 U/µL)
33.5 µL	dH_2O

The following thermal cycling profile was used for the antibody genes:

95°C	3 min	
95°C	30 sec	30 x
60°C	30 sec	
72°C	2 min	
72°C	10 min	
4°C	break	

To introduce restriction sites into the HLA-B44 genes the following reaction mixture in a total volume of 100 µL was prepared:

1 µL	DNA (10 ng)
20 µL	*Phusion* buffer (5 x)
2.5 µL	*forward* primer
2.5 µL	*reverse* primer
10 µL	dNTPs (2 mM)
1 µL	*Phusion* polymerase (2.5 U/µL)
5 µL	DMSO
58 µL	dH_2O

The following thermal cycling profile was used for the HLA-B44 genes:

95°C	3 min	
95°C	1 min	30 x
55°C	1 min	
72°C	45 sec	
72°C	10 min	
4°C	break	

The PCR products were analyzed by agarose gel electrophoresis.

5.1.6.4. Colony PCR

Instead of plasmid preparation and subsequent restriction analysis, colony PCR was used to screen *E. coli* colonies directly from LB plates for their DNA with insert specific primers. *E. coli* colony was resuspended in 50 µL sterile water and incubated for 10 min at 95°C following centrifugation for 2 min at 20,000 g. 10 µL of the supernatant was transferred into an appropriate PCR tube and following reaction components were added:

5 µL	Taq buffer (10 x)
5 µL	$MgCl_2$ (50 mM)
0.25 µL	*forward* primer (10 pmol/µL)
0.25 µL	*reverse* primer (10 pmol/µL)
5 µL	dNTPs (2 mM)
0.25 µL	Taq polymerase (5 U/µL)
34.25 µL	dH_2O

The following thermal cycling program was used:

95°C	4 min	
95°C	4 min	┐
55°C	30 sec	├ 30 x
72°C	90 sec	┘
72°C	10 min	
4°C	break	

5.1.6.5. Bacmid PCR

To proof the transposition of the pFB1 or pFBD in DH10Bac cells, a PCR with sequence specific and M13 standard primers was performed. DH10Bac colony was resuspended in 50 µL sterile water and incubated for 10 min at 95°C following centrifugation for 2 min at 20,000 g. 10 µL of the supernatant were transferred to a PCR tube and following reaction components were added:

5 µL	Taq buffer (10 x)
5 µL	$MgCl_2$ (50 mM)
0.5 µL	DMSO
0.25 µL	*forward* primer (10 pmol/µL)
0.25 µL	*reverse* primer (10 pmol/µL)
5 µL	dNTPs (2 mM)
0.25 µL	Taq polymerase (5 U/µL)
33.75 µL	dH_2O

95°C	3 min	
95°C	30 sec	30 x
50°C	30 sec	
72°C	4 min	
72°C	10 min	
4°C	break	

5.1.7. Construction of expression plasmids

5.1.7.1. Bacterial expression plasmids for recombinant antibodies

The isolated and sequenced V_H and V_L chain genes were PCR amplified to introduce restriction sites PstI (NsiI) and BstEII into the V_H gene and SacI and XhoI into the V_L chain gene (Kleymann *et al.,* 1995). Following PCR, PCR products and the plasmids pASK68 (Fv expression) and pASK85 (Fab Expression) were cut with the appropriate set of restriction endonucleases (see also 5.1.2) and ligated (see also 5.1.3). The genes inserted into the expression vectors were verified by sequencing.

5.1.7.2. Insect cell expression plasmids for recombinant antibodies

For the expression of scFv148.3 and Fab148.3 in insect cells, a pro-melittin signal sequence from honeybee (www.expasy.ch, UniProt data base, accession number P01501) together with a $(SG_4)_3$ spacer sequence was synthesized by GenScript (GenScript Corporation, New Yersey, U.S.A.) and cloned into pUC57. The antibody heavy (V_HC_{H1}) and light (V_LC_L) chains of the Fab fragment in pASK85 were cut with SacI, HindIII and PstI, NcoI respectively and cloned into

the pUC57 including the melittin signal sequence. The light chain (V_LC_L) of the Fab fragment including the melittin signal sequence was subsequently cloned into pFasBacDual with BamHI and HindIII. Afterwards the heavy chain (V_HC_{H1}) of the Fab fragment including the melittin signal sequence was cloned into pFastBacDual using XmaI and NcoI. The variable heavy (V_H) and variable light (V_L) chains in the pASK68 were cut with PstI, NcoI and SacI, XhoI, respectively, and ligated into pUC57 including the melittin signal sequence and the $(SG_4)_3$ linker. The antibody genes including the melittin signal sequence were cut from the pUC57 and ligated into pFastBac1 (scFv) via BamHI and HindIII restriction sites.

5.1.7.3. Insect cell expression plasmids for HLA-B4402 and HLA-B4405

The single chain MHC class I B4402-β_2m (scB4402-β_2m) and single chain MHC class I B4405-β_2m (scB4405-β_2m) genes were PCR-amplified from the pGAPZ plasmid (kindly provided by Sebastian Springer, Jacobs University Bremen) with NgoMIVstrepfor, with a N-terminal strep tag, or with NgoMIV$\beta_2$mfor, without N-terminal strep tag and tevhisrev, introducing a TEV cleavage site and a His_6-tag. PCR products were cut with NgoMIV and HindIII, following ligation into pFastBac1 already bearing the melittin signal sequence gene. Ligation products were checked via restriction analysis and verified by DNA sequencing (Scientific Research & Development GmbH, Germany).

5.2. Microbiology

5.2.1. Preparation of competent *E. coli* cells

An overnight culture of *E. coli* DH5α cells was diluted 1:200 in 200 mL of LB medium and grown at 37°C to an OD_{550} of 0.5. The culture was incubated on ice for 10 min and harvested at 2,000 × g for 10 min at 4°C. The cell pellet was carefully resuspended in 35 mL of sterile, ice-cold TFB I buffer and incubated on ice for 1 h. After centrifugation at 3,000 × g for 10 min at 4°C, the cell pellet was resuspended in 6 mL of ice-cold TFB II buffer. Cell aliquots of 100 µL were

frozen in liquid nitrogen and stored at -80°C. To make *E.coli* DH10Bac competent cells, the same procedure was applied except for LB medium containing 50 µg/mL kanamycin and 10 µg/mL tetracycline.

TFB I solution	TFB II solution
30 mM KAc	10 mM MOPS
10 mM $CaCl_2$	10 mM $RbCl_2$
50 mM $MnCl_2$	75 mM $CaCl_2$
100 mM $RbCl_2$	15% (v/v) glycerol
15% (v/v) glycerol	adjusted pH 6.8 with 1 M KOH
adjusted pH 5.8 with 1 M acetic acid	

5.2.2. Transformation of competent *E. coli* cells

100 µL of *E. coli* BL21, DH5α or JM83 competent cells were incubated with 1 µL plasmid DNA on ice for 30 min. Heat shock was performed for 1 min at 42°C and subsequently cells were incubated for 1 min on ice. 900 µL of SOC medium were added and regeneration was carried out for 45 min at 37°C in a thermomixer. 100 µL of the regenerated cells were plated on LB-agar plates containing the appropriate antibiotic and incubated overnight at 37°C.

LB-agar	SOC medium
10 g/L peptone/tryptone	20 g/L peptone/tryptone
5 g/L yeast extract	5 g/L yeast extract
5 g/L NaCl	10 mM NaCl
15 g/L agar	2.5 mM KCl
	10 mM $MgCl_2$
	20 mM glucose

5.2.3. Transformation of competent DH10 Bac cells

1 µL of DNA (100 ng) was added to 100 µL of competent DH10Bac cells thawed on ice and the transformation mixture was incubated on ice for 15-20 min. Following a heat shock at 42°C for 1 min and a 2 min incubation on ice, 1 mL of SOC medium was added and the transformed cells were subsequently incubated at 37°C for 4 h. The transformation mixture was then plated onto LB

agar plates containing 50 µg/mL kanamycin, 7 µg/mL gentamicin, 10 µg/mL tetracycline, 100 µg/mL Bluo-Gal and 40 µg/mL IPTG. Plates were incubated at 37°C for at least 36 h. The white colonies were amplified to isolate the recombinant bacmids for transfection of insect cells.

5.3. Cell culture

5.3.1. Expression of recombinant antibodies in *E. coli*

Recombinant antibodies were expressed in *E. coli* (strain JM83) as described by Skerra (Skerra, 1988). An overnight culture, grown at 30°C in 2 x YT medium supplemented with 100 µg/mL ampicillin and 30 µg/mL streptomycin, was diluted 40-fold in 2 L of the same medium without streptomycin and grown at 22.5°C till mid exponential phase ($A_{550\ nm}$=0.5). Protein expression was induced by adding 1 mM IPTG (pASK68) or 0.2 mg/L AHT (pASK85). After 3 h the cells were harvested by centrifugation at 5,000 g for 15 min at 4°C, resuspended in 20 mL of periplasmic extraction buffer, and incubated on ice for 30 min. Spheroblasts were removed at 5,000 g for 45 min at 4°C and the periplasmic fraction was stored at -20°C.

YT medium (2 x)	Periplasmic extraction buffer
16 g/L peptone/tryptone	100 mM Tris/HCl, pH 8.0
10 g/L yeast extract	500 mM sucrose
5 g/L NaCl	1 mM EDTA

5.3.2. Monolayer culture of *Sf*9 insect cells

Monolayer cultures of *Spodoptera frugiperda* (*Sf*9) insect cells were cultured at 27°C in Sf900 II medium (including 10 units/mL penicillin, 0.1 mg/mL streptomycin, 0.2% pluronic acid and 5% fetal calf serum). For passaging, medium and floating cells from a confluent monolayer were discarded and replaced by pre-warmed medium.

5.3.3. Monolayer culture of *Tn*5 insect cells

Monolayer cultures of *Trichoplusia ni* cell line (BTI-Tn-5B1-4), commercially known as High Five insect cells, were cultured in Express Five SFM medium (supplemented with 18 mM L-glutamine and 10 units/mL penicillin, 0.1 mg/mL streptomycin). Before passaging of a confluent culture (T75, 75 cm^2 growth surface) non-adherent, floating cells were removed and pre-warmed medium was added.

5.3.4. Shaker culture of *Sf*9 and *Tn*5 insect cells

Insect cells were subcultured from monolayer cultures at a cell density of 0.4-4 x 10^6 cells/mL to a volume of up to 600 mL under defined shaking conditions (<200 mL at 110 rpm, >200 mL at 60 rpm).

5.3.5. Transfection of *Sf*9 insect cells

2 x 10^6 *Sf*9 cells were seeded onto a 35-mm tissue culture plate and incubated for one hour at 27°C. The cell densitiy should be 50-70% confluent before proceeding with the transfection. The transfection was carried out as described in the Baculogold manual (BD Bioscience Pharmingen) using the Baculogold Transfection Kit (BD Bioscience Pharmingen). After seeding the cells the culture medium was removed and 1 mL of transfection buffer A (BaculoGold) was added. 5 µg bacmid DNA were mixed with 1 mL transfection buffer B and was immediately added dropwise to the transfection mixture. After incubation at 27°C for 4 h the transfection medium was discarded and 3 mL of fresh Sf900 medium were added. The plate was incubated for 5-7 days at 27°C before the recombinant virus (P_0) was harvested.

5.3.6. Amplification of virus

For the amplification of virus P_1 (10 mL), 1.2 x 10^6 cells/mL seeded in a T75 flask and incubated at 27°C for 1 h were infected with 2 mL recombinant virus P_0 (P_0 has typically a titer of 1 x 10^7 pfu (*plaque forming units*)/mL). Recombinant virus P_1 was harvested after 5-7 days. 15 mL P_2 were harvested

from infection of 3 x 10^7 cells with 2 mL of P_1 for 5-7 days. Following 5-7 days infection of 1 x 10^9 cells with 15 mL P_2, recombinant virus P_3 (500 mL) was harvested and stored at 4°C.

5.3.7. Infection of *Sf*9 and *Tn*5 cells for protein production

500 - 700 mL shaker culture of *Sf*9 or *Tn*5 cells were grown at 27°C in a Fernbach flask to a density of 3-3.5 x 10^6 cells/mL. 30-50 mL of virus stock P_3 were added and the culture was incubated until a cell death rate of 30% was achieved (usually after 3 – 4 days). Subsequently cells were harvested by centrifugation at 200 g for 5 min and the supernatant was kept at 4°C until protein purification proceeded.

5.3.8. Raji cells

Human Burkitt lymphoma cells (Raji cells) were propagated in roller bottles at 37°C and 95% humidity in RPMI medium 1640 supplemented with 10% FCS, 1 mM sodium pyruvate, and each 40 units/mL penicillin and streptomycin. The cell density of the culture was generally maintained at 1.5-3 x 10^6 cells/mL.

5.4. Biochemical methods

5.4.1. Preparation of microsomes

For the preparation of microsomes (Ehses, 2005; van Endert, 1994), Raji cell pellets (10^9 cells from 400 mL culture) were thawed and resuspended in 50 mL of cavitation buffer. All steps were performed at 4°C. Cells were then homogenized by a glass douncer and centrifuged at 800 g for 5 min. The pellet was discarded and 25 mL of 1.3 M sucrose buffer were added to the supernatant and another centrifugation step at 800 g, for 10 min was started. The resulting supernatant was then centrifuged at 20,000 g for 30 min. The pellet was carefully resuspended in 4 mL of 0.25 M sucrose buffer and supplemented with 28 mL of 2.5 M sucrose buffer, before dispensing the cell

sucrose suspension on ultracentrifuge tubes. A sucrose gradient containing 3 mL of 2 M sucrose buffer, 3 mL 1.3 M sucrose buffer and 0.8 mL 250 mM sucrose buffer on top was poured and centrifuged at 100,000 g overnight in a SW-28 rotor. The microsomes were harvested from the 2.0 M / 1.3 M sucrose interphase and diluted with 2 volumes of 1 x PBS and centrifuged at 20,000 g for 20 min. The pellet was resuspended in 2 mL of 1 x PBS and aliquots were frozen in liquid nitrogen and stored at -80°C. Protein concentration was determined by BCA (Pierce).

Cavitation buffer	PBS (10 x)
10 mM Tris/HCl, pH 7.5	90 mM Na_2HPO_4
2.5 mM benzamidine	18 mM KH_2PO_4
1 mM PMSF	1.4 M NaCl
	27 mM KCl
	ad pH 6.86

0.25 M sucrose buffer	1.3 M sucrose buffer	2.0 M sucrose buffer	2.5 M sucrose buffer
20 mM HEPES, pH 7.5	20 mM HEPES, pH 7.5	20 mM HEPES, pH 7.5	20 mM HEPES, pH 7.5
25 mM KAc	25 mM KAc	25 mM KAc	25 mM KAc
5 mM MgAc	5 mM MgAc	5 mM MgAc	5 mM MgAc
0.25 M sucrose	1.3 M sucrose	2.0 M sucrose	2.5 M sucrose

5.4.2. Preparation of membranes

For preparation of membranes *Sf*9 cell pellets (10^9 cells) were carefully thawed on ice by adding 3 volumes of cavitation buffer. All steps were performed at 4°C. Using a glas douncer cells were homogenized and cell debris was removed by a two step centrifugation: at 200 g for 4 min, at 700 g for another 8 min. The supernatant was then centrifuged at 20,000 g for 30 min and the pellet was resuspended in 1 x PBS. Aliquots were frozen in liquid nitrogen and stored at -80°C.

5.4.3. SDS-polyacrylamide-gelelectrophoresis

The discontinuous sodium dodecyl sulfate polyacrylamid gel electrophoresis (SDS-PAGE, Lämmli, 1970) is used for the electrophoretic separation of proteins based on their molecular weight. Treatment with SDS, an anionic detergent, disrupts non-covalent interactions in native proteins and gives a denatured protein a large net-negative charge due to the deprotonated sulfate group, which is roughly proportional to the mass of the protein. Reducing agents like DTT or β-Mercaptoethanol (2-thioethanol) are necessary to break disulfide bonds. After assembling the Mini-Protean 3 casting chamber (BioRad) of a mid-size gel 10.1 x 8.2 mm and a gel thickness of 0.75 mm, first the running gel and after 10 min of polymerization the stacking gel was poured and a comb was inserted.

	Stacking gel	Separating gel	
	5%	10%	12%
30% acrylamide	650.00 µL	3.10 mL	3.76 mL
collecting gel buffer	1.10 mL	-	-
separating gel buffer	-	3.95 mL	2.82 mL
dH_2O	2.70 mL	3.95 mL	2.82 mL
10% APS	30.00 µL	40.00 µL	40.00 µL
TEMED	10.00 µL	20.00 µL	20.00 µL

Prior to electrophoresis proteins were denatured in 2 x sample buffer and incubated for 10 min at 95°C. SDS electrophoresis was performed at 25 mA per gel for 1-1.5 h in electrophoresis buffer. *Prestained Protein Marker* (Fermentas) was used as a standard.

Stacking gel buffer	Separating gel buffer	SDS sample buffer (2x)	Running buffer (10x)
0.5 M Tris/HCl, pH 6.8	1.5 M Tris/HCl, pH 8.8	0.1 M Tris/HCl, pH 6.5	0.25 M Tris/HCl, pH 8.8
0.4% SDS (w/v)	0.4% SDS (w/v)	4% SDS (w/v)	2 M glycine
		0.2% bromophenol-blue (w/v)	10% SDS (w/v)
		20% glycerol (v/v)	
		0.9 M β-mercaptoethanol	

5.4.4. Tricine-SDS-polyacrylamide-gelelectrophoresis

Tricine-sodium dodecyl sulfate-polyacrylamide gel electrophoresis (Tricine-SDS-PAGE) is used for the separation of proteins in a broader range from 1 to 100 kDa resulting in a higher resolution of protein complexes (Schägger, 1987). The stacking and separating gel composition as well as the gel and running buffers are listed in the following tables.

	Stacking gel	Separating gel	
	4.5%	12%	16%
30% acrylamide	650 µL	2.92 mL	3.90 mL
3 x gel buffer	1.50 mL	2.50 mL	2.50 mL
dH_2O	2.30 mL	1.18 mL	0.20 mL
10% APS	30.00 µL	25.00 µL	25.00 µL
TEMED	10.00 µL	2.50 µL	2.50 µL

Cathode buffer (5 x)	Anode buffer (5 x)	Gel buffer (3 x)
0.5 M Tris	1 M Tris/HCl, pH 8.9	3 M Tris/HCl, pH 8.5
0.5 M Tricine		0.3% (w/v) SDS
0.5% (w/v) SDS		

5.4.5. Coomassie and silver staining

Proteins separated on an SDS-PAGE were visualized by staining with a solution of Coomassie Blue for 30 min. After staining, the excessive dye was removed by incubating the gel in a destain solution (10% acetic acid, 20% methanol) until

distinct protein bands were visible. The detection limit is approximately 400 ng protein per lane.

Stain solution	Destain solution
40% (v/v) methanol	40% (v/v) methanol
10% (v/v) acetic acid	10% (v/v) acetic acid
0.25% (w/v) Coomassie Blue G250	

Silver staining is far more sensitive than Coomassie and can detect 10 ng protein per lane. For silver staining the SDS gel was incubated for at least 1 h in 50 mL fixation solution and rinsed two times for 10 min with water before incubating the gel for 1 min in thiosulfate buffer. Afterwards the gel was rinsed two times with water for 1 min. For staining it was incubated for 20 min in 50 mL silver nitrate solution. After rinsing the gel two times with water for 1 min, 50 mL of the developing solution was added and the gel was incubated for 20 min. Again, the gel was rinsed two times with water following incubation in developing solution until protein staining became visible.

Fixation solution	Thiosulphate buffer	Silver nitrate solution	Developing solution
40% EtOH (v/v)	0.02% (w/v) NaS_2O_3	0.1% (w/v) $AgNO_3$	2% (w/v) Na_2CO_3
10% HAc (v/v)		0.04% (v/v) form-aldehyde	0.04% (v/v) form-aldehyde

5.4.6. Immunoblotting

After the electrophoretic separation of a protein sample on an SDS-polyacrylamide gel, the proteins were transferred onto a nitrocellulose membrane by electroblotting. The gel was placed on a nitrocellulose membrane and sandwiched by Whatmann paper soaked in blotting buffer in a Semidry blotting apparatus (Bio-Rad Laboratories GmbH, Germany) with the nitrocellulose facing the anode. The transfer ran for 1 h with a current of 75 mA per membrane.

Blotting buffer	Blocking buffer	Wash buffer	TBS (10 x)
25 mM Tris/HCl pH 7.5	1 x TBS, pH 8.0	1 x TBS, pH 8.0	200 mM Tris/HCl, pH 8.0
192 mM glycine	0.05% Tween-20	0.05% Tween-20	2.5 M NaCl
0.03% (w/v) SDS	5% (w/v) skim milk		
20% methanol	**or** 3% (w/v) BSA		

To determine the transfer efficiency, the membrane was stained with Ponceau Red (0.1% Ponceau S red (w/v), 5% (v/v) acetic acid) for 1 min and washed with water until background stain was removed and protein bands became visible. For immunodetection the membrane was incubated with blocking buffer for at least 30 min at room temperature or overnight at 4°C. After blocking, the membrane was incubated at room temperature for 1 h or overnight at 4°C with the primary antibody (dilutions given below), subsequently washed three times for 5 min with washing buffer and finally incubated with horseradish peroxidase conjugated secondary antibody for 1 h at room temperature. Afterwards, the membrane was washed again three times for 5 min and incubated with a mixture of 10 mL each ECL solution 1 and ECL solution 2 for 1 min. The chemiluminescent signal was detected by a LumiImager.

Antibody	Dilution	Directed against
148.3	1:10	TAP1
435.3	1:5	TAP2
429.4	1:5	TAP2
7F6	1:20	tapasin
HC10	1:20	MHC class I
α-His	1:2,000	His-tag
streptactin-HRP	1:20,000	Strep-tag
goat-α-mouse-HRP	1:20,000	mouse-IgG
goat-α-rabbit-HRP	1:20,000	rabbit-IgG

ECL solution 1	ECL solution 2
100 mM Tris/HCl, pH 8.5	100 mM Tris/HCl, pH 8.5
0.4 mM coumaric acid	0.12% (v/v) H_2O_2
2.5 mM luminol sodium salt	

5.4.7. Stripping of immunoblots

To remove antibodies from already developed western blots, membranes were stripped with stripping buffer for 20 min at RT and washed afterwards 3 x with TBS-T for at least 5 min following blocking for at least 1 h and incubation with the next antibody.

Stripping buffer	Washing buffer
0.1 M glycin/HCl, pH 2.7	1 x TBS 0.05% Tween-20

5.4.8. Protein G affinity chromatography

The hybridoma supernatant containing the monoclonal antibody was adjusted to 0.02 M NaH_2PO_4, pH 7.0 with 1.0 M $NaHPO_4$. Protein G column (1 mL bed volume) was equlibrated with 5 column volumes of binding buffer. Hybridoma supernatant was applied to the protein G column which was subsequently washed with 5-10 column volumes of the binding buffer. The antibody was eluted with 5 column volumes of elution buffer and immediately neutralized with 60-200 µL of the neutralization buffer per mL elution fraction. The protein G column was re-equilibrated with 5-10 column volumes of the binding buffer, washed with 5-10 column volumes of dH_2O and finally stored in 20% EtOH at 4°C.

Binding buffer	Elution buffer	Neutralization buffer
20 mM NaH_2PO_4, pH 7.0 150 mM NaCl	0.1 M glycine/HCl, pH 2.7	1.0 M Tris/HCl, pH 9.0

5.4.9. Epitope coupled affinity chromatography

The peptide CYWAMVQAPADAPE corresponding to the C-terminus of human TAP1 was coupled to Ultralink Iodoacetyl Gel (Pierce) *via* the N-terminal cysteine according to the manufacturer's instructions. After equlibration of the column with running buffer, 50 mL of hybridoma supernatant (mAb148.3, adjusted to pH 7.0) or periplasmic fractions or insect cell supernatant of the

recombinant antibodies (Fv, scFv and Fab fragments, dialyzed against running buffer) were loaded. After washing, bound antibodies were eluted with the elution buffer. The antibodies were immediately buffered to neutral pH with the neutralization buffer, concentrated by ultrafiltration (Amicon, Millipore) and quantified by Micro BCA Protein Assay (Pierce).

Running and washing buffer	Elution buffer	Neutralization buffer
50 mM Na-phosphate buffer, pH 7.0 150 mM NaCl	100 mM glycine/HCl, pH 2.7	1 M Tris/HCl, pH 9.0

5.4.10. Streptavidin affinity chromatography

The *Strep*-tag I, an eight amino acid peptide (WRHPQFGG) has been originally selected from a genetic random library (Schmidt & Skerra, 1993), which binds specifically to *core* streptavidin (proteolytically truncated version of the natural bacterial protein). The *Strep*-tag binds reversibly to the same pocket as the natural ligand D-biotin and can be eluted under mild conditions with D-desthiobiotin, which is a derivative of D-biotin with less strong affinity. An optimized *Strep*-tag II exists, which can be placed at the N- or C-terminus whereas the *Strep*-tag I is placed only at the C-terminus. An engineered streptavidin variant, called *Strep*-Tactin, with improved peptide-binding capacity has been developed and is commerically distributed by IBA.

5.4.10.1. Refolding of core streptavidin

Inclusion bodies derived from 1 L cell culture were dissolved in 8 mL ice-cold 6 M guanidium/HCl and dialyzed in 10-fold volume (1:10) for 2 x 4 h against 6 M guanidium/HCl at 4°C to remove biotin. Dialyzate was poured in a steady, nearly dropwise stream in stirring ice-cold PBS at a ratio of 1:25 and incubated at least 3 h or overnight at 4°C without stirring. Non-dissolved protein was sedimented for 30 min at 20,000 g and fractionated ammonium sulfate precipitation was performed to remove protein contaminations. In the first step 0-40% (taken from 25°C table, Arne Skerra), 243 g/L, were dissolved, stirred

further for 10 min and incubated for 3 h without stirring. The precipitated protein was removed by centrifugation for 30 min at 20,000 g and the supernatant was carefully decanted. The ammonium sulfate concentration was increased to 40-70%, 205 g/L, and after dissolving it was incubated overnight without stirring. The precipitated streptavidin was recovered by centrifugation for 1 h at 20,000 g and the pellet was resuspended in 10 mL 2.2 M of ammonium sulfate / L cell culture and incubated for 2-3 h following centrifugation for 30 min at 20,000 g. Again, the protein pellet was resupended in 10 mL 1 x PBS / L cell culture and non dissolved protein was sedimented for 30 min at 20,000 g. The supernatant was sterile filtered (0.22 µm filter) and aliquots were stored at 4°C. If not used for coupling immediately, the filtered supernatant was dialyzed twice 1:100 against 1 x PBS to remove ammonium sulfate and stored in 1 x PBS including 1 mM EDTA and 0.01% NaN_3.

Guanidiumhydrochlorid	PBS (10 x)	Ammoniumsulfate
6 M guanidium/HCl, pH 1.5	40 mM KH_2PO_4 160 mM Na_2HPO_4 1150 mM NaCl pH 7.0	2.2 M ammoniumsulfate in 1 x PBS

To quantify the refolded streptavidin, the sample was diluted in 1 x PBS and absorption at 280 nm was measured. The following equation was used:

$$w = (E_{280\,nm} \times M \;\; x\; dilution \;\; factor) \times \varepsilon^{-1}$$

$E_{280\,nm}$ = measured extinction at 280 nm

M = molar mass (13310 g/mol for monomeric streptavidin)

ε = extinction coefficient at 280 nm (35600 M^{-1} cm^{-1} for monomeric streptavidin)

5.4.10.2. Preparation of streptavidin sepharose

Activated CH Sepharose 4B (GE Healthcare) was suspended in 1 mM HCl following the manufacturer's instructions and washed for 15 min with 1 mM HCl on a sintered glass filter. About 200 mL of 1 mM HCl per gram freeze-dried sepharose powder were used, added in several aliquots. The *core* streptavidin

was dialyzed 12-16 h against coupling buffer in a ratio 1:100. The dialyzed streptavidin solution (10 mg/mL) was mixed with the already washed gel suspension in a stoppered vessel. The mixture was rotated end-over-end for 1-2 h at RT. Excess of ligand was washed out with at least 5 gel volumes of coupling buffer. Remaining active groups were blocked by incubating the gel for 1 h in 0.1 M Tris/HCl, pH 8.0. The gel suspension was washed thoroughly with three cycles of alternating pH. Each cycle consisted of a wash with 0.1 M acetate buffer pH 4.0 containing 0.5 M NaCl followed by a wash with 0.1 M Tris/HCl buffer pH 8.0 containing 0.5 M NaCl. The coupled gel matrix was stored in 0.1 M Tris/HCl, pH 8.0 including 0.01% NaN_3 at 4°C.

Coupling buffer	Blocking buffer	Washing buffer 1	Washing buffer 2
0.1 M $NaHCO_3$, pH 8.0	0.1 M Tris/HCl, pH 8.0	0.1 M Ac, pH 4.0	0.1 M Tris/HCl, pH 8.0
0.5 M NaCl		0.5 M NaCl	0.5 M NaCl

5.4.10.3. Immobilized streptavidin affinity chromatography

A streptavidin sepharose column with a bed volume of 2 mL was prepared and equlibrated with 10 column volumes of binding buffer. The periplasmic extracts were dialyzed for 12-16 h against 100-fold (1:100) binding buffer. After the addition of avidin to a final concentration of 20 µg/mL, the dialyzed periplasmic extracts were applied on the streptavidin column. The column was washed with 5 column volumes of binding buffer and the Fv fragments were eluted with 5 column volumes of elution buffer, concentrated, and stored in 50 mM Tris/HCl, pH 8.0, 150 mM NaCl at 4°C. The streptavidin column was washed with 5 column volumes of regeneration buffer followed by 5 column volumes of binding buffer and stored at 4°C.

Binding buffer	Elution buffer	Regeneration buffer
20 mM Tris/HCl, pH 8.0	20 mM Tris/HCl, pH 8.0	20 mM Tris/HCl, pH 8.0
150 mM NaCl	150 mM NaCl	150 mM NaCl
1 mM EDTA	1 mM EDTA	1 mM EDTA
	2.5 mM desthiobiotin	1 mM HABA

5.4.11. Immobilized metal chelate affinity chromatography

Immobilized metal chelate affinity chromatography (IMAC) was first used to purify proteins in 1975 (Porath *et al.*, 1975) and is based on the chelating ligand iminodiacetic acid (IDA) or nitrilotriacetic acid (NTA). NTA occupies four of the six ligand binding sites in the coordination sphere of the nickel ion, leaving two sites free to interact with His_6-tag. Since insect cell medium contains several ingredients acting as chelators, which are removing metal ions from the IMAC-columns, the supernatants were dialyzed three times against 15 L dialysis buffer given below.

Dialysis and running buffer
20 mM Tris/HCl, pH 8.0
200 mM NaCl

Ni-NTA Agarose (Qiagen) or the IDA-column (1 mL HiTrap Chelating, Amersham Pharmacia) were used for protein purification. The IDA-column was conditioned with 10 mL of stripping buffer, 10 mL of water, 10 mL of $ZnSO_4$ (20 mM) and 10 mL of running buffer. The resin was loaded with a flow rate of 1 mL/min. In the case of Ni-NTA agarose (1 mL bed volume), the resin was equilibrated with 10 mL of running buffer before applying the dialyzed supernatant adjusted to 500 mM NaCl. After loading, the column was washed with 50 mL of buffer A, 50 mL of buffer B, 25 mL of buffer C and finally eluted with the elution buffer. Protein-containing samples were identified by SDS-PAGE, pooled, concentrated in a centricon device (Millipore), and stored at 4°C until size exclusion chromatography.

Stripping buffer	Buffer A	Buffer B	Buffer C	Elution buffer
50 mM EDTA, pH 8.0	20 mM,Tris/HCl, pH 8.0	20 mM,Tris/HCl, pH 8.0	20 mM,Tris/HCl, pH 8.0	20 mM,Tris/HCl, pH 8.0
	200 mM NaCl	200 mM NaCl	200 mM NaCl	200 mM NaCl
	5 mM histidine	10 mM histidine	20 mM histidine	200 mM histidine

5.4.12. Immobilized antibody fragment affinity chromatography

Recombinant antibody fragments are widely used to purify membrane proteins including multisubunit membrane protein complexes. To co-purify the antigenic TAP complex together with associated factors the Fab148.3 expressed in *Tn*5 cells was used as capture agent. Microsomes prepared from 3.2 L Raji cells were centrifuged for 2 min at 14,000 g and the pellet was washed with PBS and centrifuged again for 2 min at 14,000 g. The microsome pellet was resuspended in solubilization buffer adjusting the total protein concentration to 5 mg/mL and digitonin was added to a final concentration of 1% (v/v). The solubilizate was incubated for 45 min on ice and subsequently centrifuged for 30 min at 98,000 g to remove unsoluble cell material. Purified Fab148.3 was added to the supernatant in a stoichiometry of 2:1 (Fab148.3:TAP complex, assuming the expressed TAP level is 1% of the total protein content present) and incubated for 30 min at 4°C. 1 mL of Ni-NTA agarose beads equilibrated with solubilization buffer were added to the solubilizate including Fab148.3 and incubated for 2 h at 4°C. Following washing with each 10 column volumes of wash buffer 1, 2, 3 and 4, the TAP complex including Fab148.3 was either eluted with 5 column volumes of elution buffer or 50 µM of the 5mer epitope peptide Ac-ADAPE-OH in wash buffer 1. The purified protein complex was precipitated by incubating the elution fraction with 10-50 µL of Strataclean beads (Stratagene), centrifuged for 1 min at 1,000 g, and the beads were resuspended in 30 µL of 2 x SDS sample buffer.

Solubilization buffer	Wash buffer 1	Wash buffer 2
20 mM Tris/HCl, pH 7.4	20 mM Tris/HCl, pH 7.4	20 mM Tris/HCl, pH 7.4
100 mM NaCl	100 mM NaCl	100 mM NaCl
1% (v/v) PMSF (0.1 M)	1% (v/v) PMSF (0.1 M)	1% (v/v) PMSF (0.1 M)
1% (v/v) benzamidine (0.3 M)	1% (v/v) benzamidine (0.3 M)	1% (v/v) benzamidine (0.3 M)
15% glycerol (v/v)	15% glycerol (v/v)	15% glycerol (v/v)
1% digitonin	1% digitonin	1% digitonin
	5 mM histidine	10 mM histidine

Wash buffer 3	Wash buffer 4	Elution buffer
20 mM Tris/HCl, pH 7.4	20 mM Tris/HCl, pH 7.4	20 mM Tris/HCl, pH 7.4
100 mM NaCl	100 mM NaCl	100 mM NaCl
1% (v/v) PMSF (0.1 M)	1% (v/v) PMSF (0.1 M)	1% (v/v) PMSF (0.1 M)
1% (v/v) benzamidine (0.3 M)	1% (v/v) benzamidine (0.3 M)	1% (v/v) benzamidine (0.3 M)
15% glycerol (v/v)	15% glycerol (v/v)	15% glycerol (v/v)
1% digitonin	1% digitonin	1% digitonin
20 mM histidine	40 mM histidine	200 mM histidine

5.4.13. Size exclusion chromatography

Size exclusion chromatography (SEC) was performed on a Superdex 200 PC 3.2/30 column (GE Healthcare) in running buffer (20 mM HEPES, pH 8.0, 140 mM NaCl) with a flow rate of 50 µL/min at 4°C.

5.4.14. Generation of proteolytic Fab fragments

Papain cleavage of the mAb148.3 was carried out as described by Parham (Parham, 1986) with some modification. Digestion was performed in 50 µL aliquots with 10 µM mAb in reaction buffer. To activate the protease, 500 ng papain (Sigma) were pre-incubated in reaction buffer supplemented with 100 mM cysteine (Sigma) for 15 min at 20°C. The reaction was started by adding the mAb and continued for 16 h at 35°C. The digest was terminated with 70 mM iodoacetamide for 30 min at 20°C. After the addition of neutralization buffer the mixture was loaded onto Protein G Sepharose (GE Healthcare) pre-equilibrated with ten column volumes of running buffer and subsequently washed with ten column volumes of the same buffer. The Fab fragments were eluted with ten column volumes of the elution buffer, immediately buffered to neutral pH with the neutralization buffer, and concentrated by ultrafiltration (Amicon,Millipore).

Reaction buffer	Neutralization buffer	Running buffer	Elution buffer
100 mM NaOAc, pH 5.5 1 mM EDTA	1 M Tris/HCl, pH 9.0	50 mM Na-phosphate, pH 7.0	100 mM glycine/HCl, pH 2.7

5.4.15. Protein concentration determination

5.4.15.1. UV/Vis spectroscopy

Protein concentration is determined by UV/Vis spectroscopy taking the theoretical extinction coefficients (determined with ProtParam Software, from www.expasy.ch) into account.

$$A_{280} = \varepsilon \times c \times d \times dilution\ factor$$

A_{280} = Absorption at 280 nm

ε = extinction coefficient (M^{-1} cm^{-1})

d = pathway (1 cm)

5.4.15.2. Bicinchonin acid (BCA)

The BCA assay is based on the reduction of Cu^{2+} to Cu^{+} by reducing agents like peptide bonds in proteins. Bicinchonin acid forms specifically a complex with Cu^{+} with an absorption maximum at 562 nm. For protein determination the Micro BCA Protein Assay Kit (Pierce) was used.

5.4.16. Peptide iodination with $Na^{125}I$

For iodination of peptides the chloramin T method was used (Hunter & Greenwood, 1964). 10 µL of the peptide (500 µM) in 40 µL PBS (pH 7.0) together with 10 µL chloramin T (1 mg/mL) and 1 µL (100 µCi) $Na^{125}I$ were incubated for 5 min. The reaction was terminated by adding 120 µL NaS_2O_5 (0.17 mg/mL). Free iodine was removed by anion exchange chromatography using Dowex 1 x 8 material. 10 mg of Dowex were equilibrated in PBS (pH 7.0) containing 0.2% dialyzed BSA and washed twice with PBS without BSA. 220 µL of the Dowex suspension were added to the radio-labeled reaction mix, carefully resuspended and incubated for 5 min at RT. To separate the radiolabeled peptide (2.3 µM) from free iodine, the suspension was applied

to an empty spin column (BioRad) and centrifuged for 30 s at 1,000 g. The radio-labeled peptide containing flow-through was kept at 4°C.

5.4.17. Peptide labeling with iodoacetamidofluorescein

50 mM iodoacetamidofluorescein stock solution was prepared in DMF. Peptides containing one single cysteine were dissolved in PBS, pH 6.5, 20% DMF to a concentration of 10 mM. The labeling reaction was initiated by adding 1.2 molar excess of iodoacetamidofluorescein to the peptide solutions. Following 90 min incubation at RT, the labeling solution was applied onto a C18 column (Vydac-218TP510-C18 protein and peptide, 10 x 250 mm) equlibrated with 0.1% trifluoroacetic acid. Free fluorescein was separated from peptides with an acetonitrile gradient running from 15% - 38% within 30 min (for peptides EEFGRAFCF, EEFGRACSF, EEFGCAFSF) and with an acetonitrile gradient running from 26% - 33% within 28 min at a flow rate of 1 mL/min. The absorption at 455 nm was monitored to localize the fluorescein and peptides. The peak containing fluorescein-labeled peptide was pooled and lyophilized peptides were dissolved in water supplemented with 20% DMF. The peptide concentration was determined by absorption at 492 nm in tricine buffer, pH 9.0 (molar extinction coefficient at pH 9.0 75,000 cm^{-1} M^{-1}). Purity of the fluorescein-labeled peptides was verified by MS spectrometry.

5.4.18. Generation of "empty" MHC class I molecules

To investigate peptide association to recombinant soluble MHC class I molecules it was necessary to remove any bound peptide. To generate "empty" MHC class I molecules the pH shock method was used (Shields, 1998; Sugawara, 1987; van der Burg, 1995). Decreasing pH of purified MHC class I molecules by 0.1 M citric acid to a pH of 2.5 led the bound peptide dissociate and left the MHC class I in an "empty" state. The sample was incubated on ice for 2 min and the reaction was terminated by neutralizing the protein sample with 1 M Tris/HCl, pH 9.0. After neutralization the unbound peptide was removed from the sample by gelfiltration, applying the sample on a pre-equilibrated size ecxlusion chromatography Micro-Spin column (BioRad) with a

cut-off of 30 kDa. The sample was centrifuged at 1,000 g for 4 min and the flow-through containing "empty" MHC class I molecules was immediately used for peptide-binding experiments.

5.4.19. Peptide-binding assay with "empty" MHC class I molecules

"Empty" MHC class I molecules (500 nM) were mixed with fluorescein-labeled peptide EEFGRCAFSF (500 nM) in 50 µL of 20 mM Tris/HCl, pH 7.5, 120 mM NaCl. The protein sample was incubated overnight at 18°C in a shaker. Background binding was determined by adding a 500-fold excess of unlabeled peptide (competitor). To remove unbound peptide the protein mixture was applied on a pre-equilibrated size exclusion chromatography Micro-Spin column (BioRad) and the peptide loaded MHC class I molecules in the flow-through were quantified with a fluorescence plate reader ($\lambda_{ex/em}$=485/520 nm).

5.4.20. Peptide-binding assay

Peptide binding to TAP was measured in filter assays using a multiple filtration manifold (Multiscreen Assay System, Millipore). TAP-containing microsomes (15 µg total protein) were pre-incubated in the absence of ATP, with 3 mM ATP or 5 µM Fv fragment for different periods at 27°C. Subsequently 1 µM radiolabeled peptide RR(^{125}I)YQKSTEL was added to a final volume of 50 µL in AP-buffer. After 15 min on ice the samples were transferred onto a multiscreen filter (Multiscreen Plates with glass fiber filter, pore size 1.0 µm, Millipore), pre-incubated with 100 µL of polyethylene imine, followed by 100 µL of 0.2% dialyzed BSA. Unbound peptide was removed by washing the filter plates three times with 100 µL of 1 x PBS. Peptides bound to the filters were quantified by γ-counting. The data were corrected for background binding determined in the presence of a 100-fold molar excess of unlabeled peptide.

5.4.21. Peptide transport assay with semipermeabilized cells

2.5 x 10^6 *Sf*9 cells were semi-permeabilized in 50 µL of AP-buffer supplemented with 0.05% saponin (w/v) for 1 min at 20°C. After washing with AP-buffer, the

cells were pre-incubated with 10 µM mAb148.3, 10 µM mAb435.3 or different concentrations of the Fv fragment for 20 min at 4°C. After incubation protein samples were mixed with 500 nM fluorescein-labeled peptide RRYQNSTC$^{(F)}$L and 10 mM ATP in 100 µL of AP-buffer. The transport assay was performed for 3 min at 32°C and terminated by adding 1 mL of ice-cold PBS supplemented with 10 mM EDTA. After centrifugation for 8 min at 20,000 g, the cells were solubilized in 1 mL lysis buffer for 15 min at 20°C. Insoluble debris was removed by centrifugation. N-core glycosylated and therefore transported peptides were bound to 60 µL of concanavalin A Sepharose (50% (v/v)) overnight at 4°C. After three times washing of the beads with 1 mL of lysis buffer, peptides were eluted with 200 mM methyl α-D-mannopyranoside for 30 min at 4°C and quantified with a fluorescence plate reader ($\lambda_{ex/em}$=485/520 nm). Background transport activity was determined by replacing ATP with 1 unit of apyrase. Specific inhibition of the Fv fragment was determined in the presence of a 1,000-fold molar excess of 5mer epitope peptide (Ac-ADAPE-OH). ICP47 was used as a control at identical conditions as described for the Fv fragment.

AP-buffer	Lysis buffer
1 x PBS, pH 7.0	50 mM Tris/HCl, pH 7.5
5 mM $MgCl_2$	150 mM NaCl
	5 mM KCl
	1 mM $CaCl_2$
	1 mM $MnCl_2$
	1% (v/v) NP-40

5.4.22. Peptide transport with membranes or microsomes

Membranes or microsomes (100 – 250 µg total protein) were incubated together with 3 mM ATP and 0.5 µM radio-labeled RRY(^{125}I)QNSTEL in 50 µL of AP buffer for 3 min at 32°C. The reaction was stopped by adding 1 mL of ice-cold stop buffer. After centrifugation, the pellets were solubilized in 900 µL of lysis buffer and incubated for 20 min at RT. After removing insoluble material by centrifugation at 20,000 g for 8 min, the supernatant was incubated with 70 µL of concanavalin A Sepharose (50%, v/v) overnight. After three washing steps, the radioactivity associated with the ConA-Sepharose was quantified by γ-counting.

AP buffer	Stop buffer	Lysis buffer
1 x PBS, pH 7.0	1 x PBS, pH 7.0	50 mM Tris/HCl, pH 7.5
5 mM $MgCl_2$	10 mM EDTA	150 mM NaCl
		5 mM KCl
		1 mM $CaCl_2$
		1 mM $MnCl_2$
		1% (v/v) NP-40

5.4.23. Nucleotide-binding assay

The ATP-binding activity of TAP was analyzed based on published procedures (Knittler *et al.,* 1999). All solutions and centrifuges were pre-cooled to 4°C. The ATP-agarose was prepared following the manufacturer's instructions. 400 µL of Raji microsomes (5 mg/mL) were digitonin-solubilized in solubilization buffer for 30 min at 4°C. Insoluble material was removed at 100,000 g for 30 min at 4°C. The supernatant was pre-incubated with 10 µM Fv148.3 following 1 h incubation with pre-equilibrated ATP-agarose beads. The ATP-agarose beads were washed three times with 500 µL of washing buffer. Bound proteins were eluted with MgATP (10 mM) and analyzed by SDS-PAGE and immunoblotting using the TAP1-specific monoclonal antibody 148.3.

Solubilization buffer	Washing buffer	Elution buffer
20 mM HEPES, pH 7.4	20 mM HEPES, pH 7.4	20 mM HEPES, pH 7.4
150 mM NaCl	150 mM NaCl	150 mM NaCl
1 mM KCl	1 mM KCl	1 mM KCl
1.5 mM $MgCl_2$	1.5 mM $MgCl_2$	5 mM $MgCl_2$
2% digitonin	0.2% digitonin	0.2% digitonin
15% glycerol	15% glycerol	15% glycerol
		5 mM ATP

5.4.24. Enzyme-linked immunosorbent assay (ELISA)

96-well plates (MaxiSorb, Nunc) were coated with 1 µg of soluble NBD of TAP1 in coating buffer (100 µL/well) for 16 h at 4°C. After saturation of non-specific binding sites with blocking buffer, the mAb148.3 or the antibody fragments were bound for 1 h at 25°C and detected with a goat anti-mouse HRP-conjugated antibody (Sigma). Bound antibodies were visualized with

3,3',5,5'-tetramethylbenzidine (TMB, Progen) and quantified in an ELISA reader at a wavelength of 450 nm.

Coating buffer	Blocking buffer	Washing buffer
1 M $NaHCO_3$, pH 9.0	3% (w/v) BSA 1 x TBS 0.05% (v/v) Tween-20	1 x TBS 0.05% (v/v) Tween-20

5.4.25. Fluorescence polarization

To investigate rotational diffusion of fluorophores within the fluorescence life time in fluid solution the polarization or anisotropy of the emission is measured. Anisotropy measurements are based on the excitation of fluorophores by polarized light. The absorption is maximal when the transition dipole of the fluorophore is parallel to the electric vector of the light, the so-called photoselection. Since in homogenous solution the ground-state fluorophores are oriented randomly, only those fluorophores, which have their absorption transition moments oriented along the electric vector of the light, are excited upon exposure to polarized light. Measuring the fluorescence intensities of the vertically and horizontally polarized emission of a sample which is excited with vertically polarized light, one can calculate the fluorescence anisotropy (*R*) and polarization (*P*):

$$R = \frac{(I_{VV} - GI_{VH})}{(I_{VV} + 2GI_{\mathrm{VH}})}$$

Equation 3-1: Calculation of the anisotropy. I_{VV} – emission parallel to vertical excitation, I_{VH} – emission orthogonal to vertical excitation

$$P = \frac{(I_{VV} - GI_{VH})}{(I_{VV} + GI_{\mathrm{VH}})}$$

Equation 3-2: Calculation of the polarisation. I_{VV} – emission parallel to vertical excitation, I_{VH} – emission orthogonal to vertical excitation

Anisotropy is dimensionless and independent of the total intensity of the sample. Two methods are used for steady state measurements: the L-format

method, which uses a single emission channel, and the T-format method, which uses two emission channels (parallel and perpendicular). The FLUOLOG-3 uses the single-channel method. Since the monochromator or the emission filter used in these measurements have different transmission efficiency for vertically and horizontally polarized light, rotation of the emission polarizer changes the measured parallel and perpendicular intensities. For this reason it is necessary to determine the G-factor, which is the ratio of the sensitivities of the detection system for vertically and horizontally polarized light:

$$G = \frac{S_V}{S_H}$$

Equation 3-3: Definition of the G-Factor. S_V – sensitivity for vertically polarized light, S_H-sensitivity for horizontally polarized light

The G-factor is dependent on the emission wavelength and also on the bandpass of the monochromator. Filters generally do not have any polarizing effect (G = 1.0). Nonetheless the G-factor should always be determined since the rotation of the emission polarizer can cause the focussed image of the fluorescence to change the position, changing the effective sensitivity. The G-factor is measured using horizontally polarized excitation where both horizontally and vertically polarized components are equal because both polarizer orientations are perpendicular to the polarization of the excitation. Thus any measured differences between I_{HV} and I_{HH} are due to the properties of the detection system.

$$G = \frac{S_V}{S_H} = \frac{I_{HV}}{I_{HH}}$$

Equation 3-4: Determination of the G-factor

The anisotropy measurements were carried out at 20°C with 1 µM peptide-deficient scB4405-β_2m (see 5.4.18) and 20 nM fluorescein-labeled peptide in 200 µL of HBS buffer. The reassociation of the fluorescein-labeled peptides with the peptide-deficient scB4405-β_2m conjugate was investigated by recording the changes in the anisotropy using the FLUOLOG-3 spectrometer (Instruments S.A., France) with an excitation wavelength of 470 nm and an emission wavelength at 515 nm of the fluorophore. The time-dependent changes in the

anisotropy were fitted by a monoexponential function yielding the association and dissociation rate constants, k_a and k_d, based on pseudo first-order reaction.

HBS buffer
20 mM HEPES/HCl, pH 7.5
140 mM NaCl

5.4.26. Fluorescence emission

Fluorescence quenching is the decrease of fluorescence emission which takes place for instance in case of fluorescein, which senses alteration in the polarity or pH of the environment. Time-dependent change of fluorescence emission was analyzed during the binding and dissociation of fluorescein-labeled peptide to TAP in presence or absence of Fab148.3. 80 nM fluorescein-labeled peptide (C4F) were preincubated in 170 µL HBS (pH 7.5) buffer at 10°C. After reaching a stable fluorescence emission signal, 30 µL of purified TAP1/TAP2 heterodimer or purified TAP1/TAP2 heterodimer preincubated with 10 µM Fab148.3, were injected into the cuvette. When binding reached equilibrium as indicated by a stable fluorescent emission signal, a 100-fold molar excess of non-labeled peptide (RRYQKSTEL) was added to induce the dissociation of the peptide. The fluorophore was excited at a wavelength of 470 nm and the emission signal at 515 nm was recorded using the FLUOLOG-3 spectrometer (Instruments S.A., France) equipped with a microstirring device.

HBS buffer
20 mM HEPES/HCl, pH 7.5
140 mM NaCl
0.1% digitonin

5.4.27. Surface plasmon resonance

5.4.27.1. Binding kinetics of recombinant antibodies

Binding kinetics were determined on a CM5 chip using the Biacore T100 (Biacore) surface plasmon spectrometer (GE Healthcare). The peptide epitope

CYWAMVQAPADAPE was coupled to the dextran matrix in citric acid buffer using a thiol coupling kit (GE Healthcare). All experiments were carried out at a flow rate of 30 µL/min using HBS buffer. Different concentrations of recombinant antibody were injected onto the chip and dissociation was followed in a constant flow of HBS buffer without antibody. The surface was regenerated using regeneration buffer with a low pH. The analysis of the binding data was carried out using the BIAevaluation software (Biacore) and Origin (OriginalLab Corporation, Northhampton, U. S. A.) based on a standard model for 1:1 interaction.

Coupling buffer	HBS buffer	Regeneration buffer
0.1 M citric acid, pH 2.5	20 mM HEPES, pH 7.5 150 mM NaCl 0.05% surfactant P20	0.1 M glycine/HCl, pH 2.7

5.4.27. Interaction of soluble tapasin and MHC class I molecules

Interaction studies by SPR were carried out using the Biacore T100 instrument (GE Healthcare). Biacore experiments were carried out in HBS buffer on a streptavidin-functionalized surface (sensor chip SA, GE Healthcare). For functionalization ^{BT}tris-NTA (1 µM) in HBS buffer was injected on a single flow channel for 60 s, following conditioning of the surface with imidazole, EDTA and divalent cations (Ni^{2+}). Subsequently soluble tapasin (100 nM) in HBS buffer with a flow rate of 10 µL/min was immobilized on the ^{BT}tris-NTA-functionalized flow channel. All samples of MHC class I molecules (B2709, B2705, B4405) were injected over this channel and an adjacent flow channel for referencing. Finally the surface was regenerated with imidazol and EDTA. The analysis of the binding data was carried out using the BIAevaluation software (Biacore) and Origin (OriginalLab Corporation, Northhampton, U. S. A.) based on a standard model for 1:1 interaction.

Imidazol	EDTA	$NiSO_4$	HBS buffer
250 mM imidazol	250 mM EDTA	10 mM $NiSO_4$	20 mM Hepes, pH 7.5 140 mM NaCl 0.01% Tween-20

5.4.28. Total internal reflectance fluorescence spectroscopy (TIRFS)

For vesicle preparation, SOPC and Tris-NTA-SOA chelator lipid (75% SOPC, 25% tris-NTA-SOA), resuspended in chloroform, were mixed, dried by a gentle stream of nitrogen and rehydrated with HBS buffer. Subsequently small unilaminar vesicles (SUV) were prepared by sonification (15 min on ice). The transducer surface was incubated for at least 20 min in a freshly prepared mixture of one part of 30% (v/v) hydrogen peroxide and two parts of concentrated sulfuric acid. After extensive washing with water, the transducer was mounted immediately into the flow cell. SUV's at a concentration of 250 µM were injected and bilayer formation was followed by reflectance interference detection (RIf). Vesicle fusion should appear rapidly with a signal intensity corresponding to 5 ng/mm^2. For every measurement the bilayer was conditioned by sequential 50 sec injections of 500 nM imidazole, 200 mM EDTA and 10 mM $NiSO_4$ (in HBS), 270 µL each. Bilayers were used for one day of measurements or until an air bubble destroyed the bilayer.

To investigate the influence of tapasin on peptide dissociation of MHC class I molecules, both proteins were immobilized subsequently on a lipid bilayer to achieve lateral mobility of the individual proteins in plane of the membrane. Protein immobilization was monitored by RIf, and the fluorescence labeled peptide bound to MHC class I molecule was simultaneously detected by TIRFS. After loading of MHC class I molecules with a fluorescein-labeled peptide overnight, 150 nM of the loaded MHC class I molecule (in 250 µL) was injected for 36 s. Proper immobilization of the MHC class I molecule on the surface was checked by washing for 150 s. After probing the surface with 500 nM of soluble tapasin for 36 s, again the surface was washed and finally 100 µM non-labeled peptide was injected for 435 s, following 10 s washing of the surface. After every binding experiment, the surface was conditioned with imidazole, EDTA and $NiSO_4$ as described above.

Imidazole	EDTA	$NiSO_4$	HBS buffer
500 mM imidazole	250 mM EDTA	10 mM $NiSO_4$	20 mM HEPES, pH 7.5 140 mM NaCl

6. Results

6.1. Recombinant antibodies as extrinsic modulators of the antigen peptide transporter TAP

6.1.1. The mAb148.3 binds to the very last five C-terminal amino acid residues of human TAP1

The mAb148.3, which is specific for human TAP1 is an important diagnostic tool to investigate the antigen processing machinery in tumor development and viral escape mechanisms (Kyritsis *et al.*, 2001; Seliger *et al.*, 2001). Moreover, the mAb148.3 has led to the identification and subunit mapping of the macromolecular peptide-loading complex in the ER membrane (Bangia *et al.,* 2005; Ortmann *et al.,* 1997).

The mAb148.3 belongs to the immunoglobulin G1 (IgG1) κ-chain subtype, which I determined by immunological subtyping.

6.1.2. Cloning, expression, and purification of recombinant antibody fragments of mAb148.3 from *E. coli*

In order to convert the TAP1-specific mAb148.3 into Fv and Fab formats, cDNA was prepared from hybridoma cells, and the V_H and V_L chain genes were PCR amplified using a set of degenerate primers. Not all the PCR-amplified gene segments were functional, since part of them accumulated mutations that prevent them from encoding a functional protein. These pseudogenes were excluded by sequencing and the complementarity determining regions (CDRs) and framework regions (FR) of the functional antibody chains were assigned as described by Kabat and colleagues (Kabat *et al.,* 1987) (Figure 6-1).

The genes of the identified V_H and V_L chains were subsequently cloned into the expression vectors pASK68 and pASK85 for periplasmic production of Fv and Fab fragments, respectively. Recombinant Fv and Fab fragments were

produced at different levels in *E. coli* (Figure 6-2). Both antibody fragments were detected after 1 h of induction as shown by SDS-PAGE and immunoblotting with tag-specific antibodies (Figure 6-2).

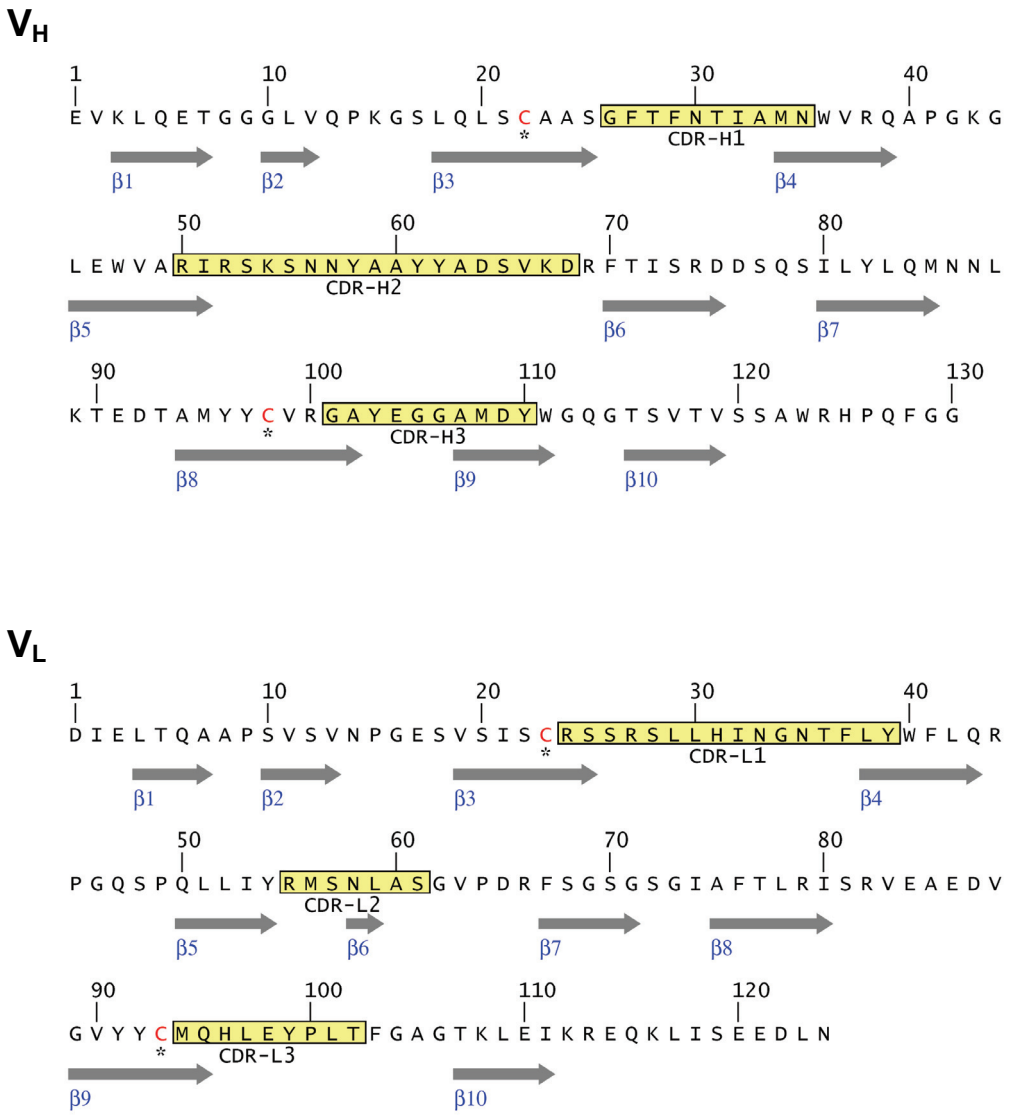

Figure 6-1. Amino acid sequence of the variable heavy and variable light chains of the mAb148.3. The complementarity determining regions (CDRs), which are involved in epitope recognition, are annotated as described (Kabat *et al.,* 1987) (yellow boxes). Interspersed β-sheets, responsible for the stability of the scaffold of the antigen-binding site, are indicated by arrows. The variable region of the heavy (V_H) and light (V_L) chain consists of 130 and 124 amino acid residues, respectively. The intramolecular disulfide bonds between Cys22 and Cys98, and between Cys23 and Cys93, respectively, are indicated with an asterisk.

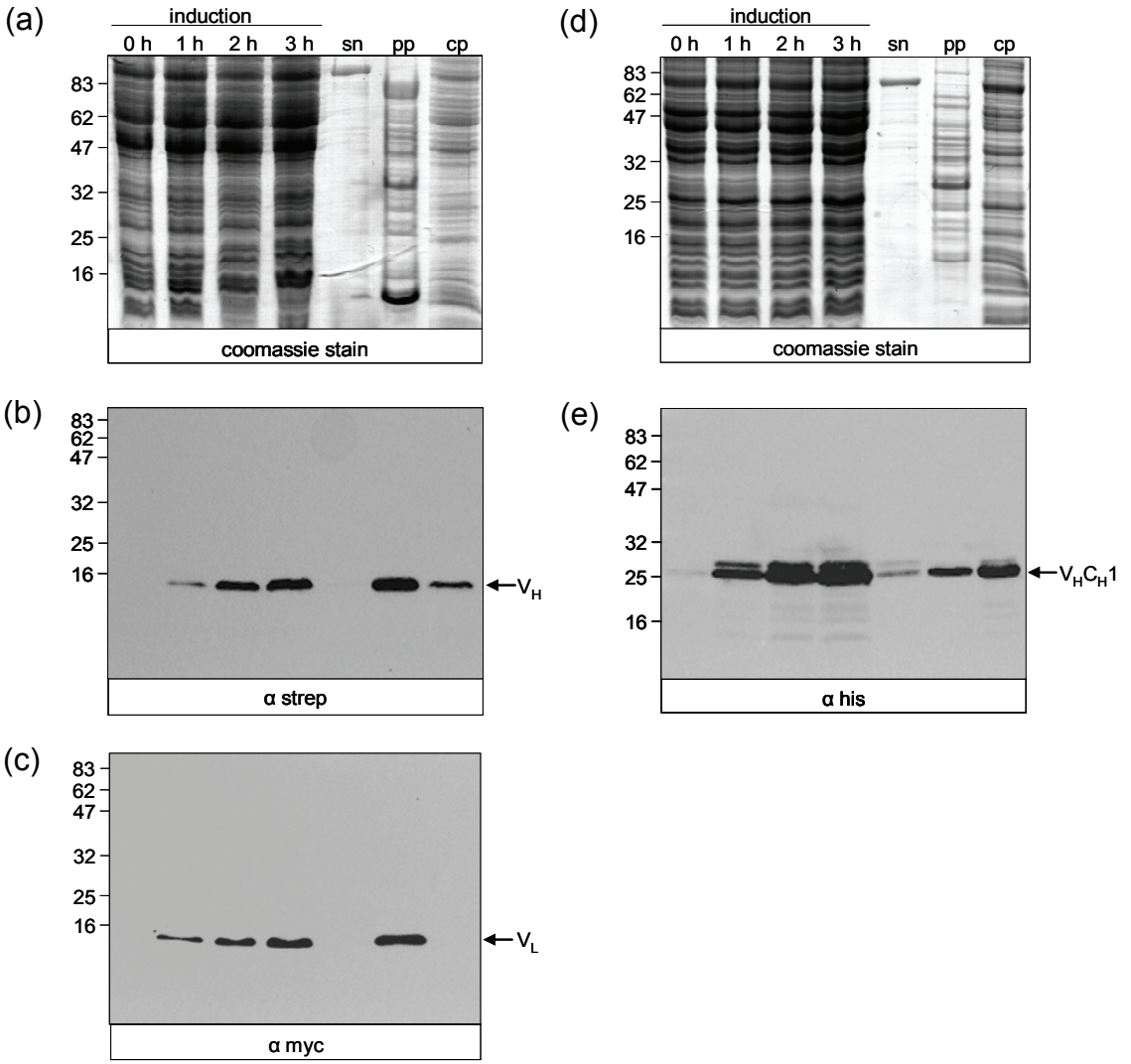

Figure 6-2. Expression of recombinant antibodies. *E. coli* were transformed with the expression vectors pASK68 (Fv) or pASK85 (Fab). Expression was induced with IPTG (pASK68) or AHT (pASK85) for 3 h. Aliquots of the bacterial cell lysates (0, 1, 2, 3 h), the supernatant after harvesting (sn), the periplasmic fraction (pp, 1/25 aliquot), and the cytoplasmic fraction (cp) were analyzed by reducing Tricine-SDS-PAGE ((a), 16%, expression of Fv; (d), 12%, expression of Fab). The V_H (b) and V_L (c) chains of the Fv fragment were detected with tag-specific antibodies at 14.4 kDa and 13.8 kDa, respectively. The heavy chain (V_HC_H1) of the Fab fragment at 25 kDa (e). Molecular mass standard in kDa.

The recombinant antibody fragments were initially purified *via* the C-terminal Strep-tag of the Fv-V_H chain and the C-terminal His_6-tag of the Fab-V_HC_H1 chain. However, the Fv fragment displayed a tendency to dimerize, leading to reduced affinity to its epitope. Therefore, the recombinant antibody fragments were purified by affinity chromatography employing the peptide CWAVQPADAPE (epitope underlined). The Fv fragment was purified to

homogeneity in a single affinity chromatography step as shown by silver-staining of an SDS-PAGE and immunoblotting using a Streptactin-HRP conjugate (Figure 6-3 (a)). By contrast, the purity as well as the total amount of purified Fab fragment was considerably lower than for the Fv fragment (Figure 6-3 (b)). The Fab fragment was however clearly detectable by immunoblotting using an Fab-specific antibody (Figure 6-3 (b)). Heterodimer assembly of the purified Fab fragment was confirmed by SDS-PAGE under oxidizing conditions. The Fab fragment has an apparent molecular mass of 50 kDa due to the intermolecular disulfide bridge at the C-termini of the constant regions (between C_H1 and C_L) (Figure 6-3 (c)). The yields of purified Fv and Fab fragments were 100 µg and 20 µg per liter of *E. coli* culture, respectively. Comparable amounts of the Fab fragment were purified also by IMAC. Correct folding and monodispersity of the purified Fv fragment was demonstrated by analytical size exclusion chromatography (Figure 6-3 (d)). The Fv fragment appears as a single peak with a molecular mass of 28 kDa. A proteolytic Fab fragment (50 kDa), which was generated by papain digestion of mAb148.3, eluted shortly before the Fv fragment and was used as an internal standard (Figure 6-3 (d)). The proteolytic Fab fragment appears as a monomeric peak with an additional sub-fraction corresponding to an $(Fab)_2$ fragment as described for other antibodies (Better *et al.,* 1988).

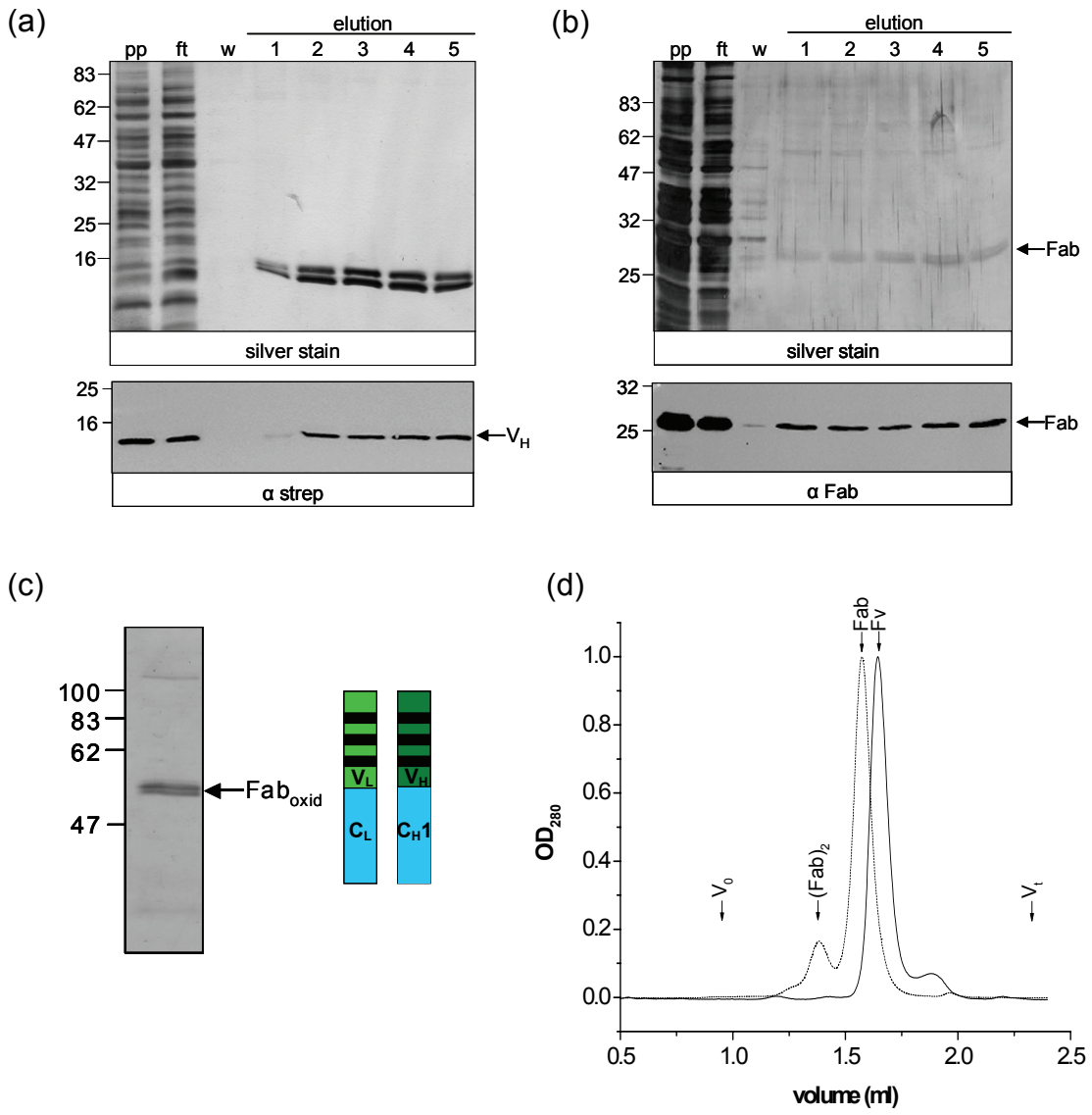

Figure 6-3. Affinity purification of recombinant antibody fragments. Fv and Fab fragments were affinity-purified *via* the epitope peptide CYWAMVQAPADAPE of TAP1. Aliquots of the periplasmic fraction (pp), the flow through (ft), the washing step (w), and the elution fractions (1-5) were analyzed. (a) Purification profile of the Fv fragment analyzed by Tricine-SDS-PAGE (16%, silver-stained). The V_H chain was detected with a Streptactin-HRP conjugate. (b) Purification of the Fab fragment was monitored by Tricine-SDS-PAGE (12%, silver-stained). The Fab fragment was detected with a Fab-specific antibody. (c) Heterodimer assembly of the purified Fab fragment (200 ng) analyzed by Tricine-SDS-PAGE (12%, silver-stained) under non-reducing conditions. Molecular mass standard in kDa. (d) The affinity-purified Fv and proteolytic Fab fragments were separated by size exclusion chromatography (Superdex 200 PC3.2/30). Proteins (0.3 mg total protein) were monitored at 280 nm. The void volume (V_0 = 0.85 mL) and the total volume (V_t = 2.3 mL) are indicated by arrows in the chromatogram.

6.1.3. Cloning, expression and purification of scFv and Fab fragments of mAb148.3 from insect cells

Eukaryotic expression systems have been widely used for the expression of recombinant antibodies (Verma *et al.,* 1998). Since the periplasmic expression of the Fv and Fab fragment resulted in an over all low expression and purification yield, the genes of the recombinant antibody fragments were subcloned into pFastBac1 and pFastBacDual for production and secretion of scFv and Fab fragments, respectively, in insect cells. Briefly, a secretion signal sequence (pro-melittin sequence from honeybee) was introduced into the pFastBac1 and pFastBacDual. The V_HC_H1 and V_LC_L antibody chain genes were cloned in the pFastBacDual for expression and secretion of the Fab fragment. For the expression of the scFv fragment the V_H and V_L chain genes were amplified and linked *via* a $(SG_4)_3$ linker following ligation in pFastBac1.

After generation of recombinant baculoviruses by using the Bac-to-Bac System (Invitrogen) a *Sf*9 shaking culture was infected with 10% (v/v) of the respective virus. Supernatants were collected after 72-96 h of infection and dialyzed extensively against buffer containing 20 mM Tris/HCl, pH 8.0, 150 mM NaCl at 4°C. Purification of His_6-tagged scFv and Fab fragments was performed with either nickel-nitrilotriacetic acid (Ni-NTA) or epitope-coupled affinity chromatography employing the peptide CYWAMVQAPADAPE (epitope underlined). Both scFv and Fab fragments were purified to homogeneity by a single affinity chromatography step (Figure 6-4 (a) and (b)) with a molecular weight of approximately 25 kDa for the V_HC_H1 and V_LC_L, respectively, and 28 kDa for the scFv due to the $(G_4S)_3$ linker bridging the V_H and V_L chain. The heterodimer assembly of the Fab fragment was analyzed by SDS-PAGE (coomassie-stained) under reducing and oxidizing conditions (Figure 6-4 (a)). Here, the Fab fragment had an apparent molecular mass of 50 kDa due to the intermolecular disulfide bridge at the C-termini of the constant regions (between C_H1 and C_L). Analytical size exclusion chromatography demonstrated monomeric scFv and Fab fragments after a single-step purification (Figure 6-4 (c)).

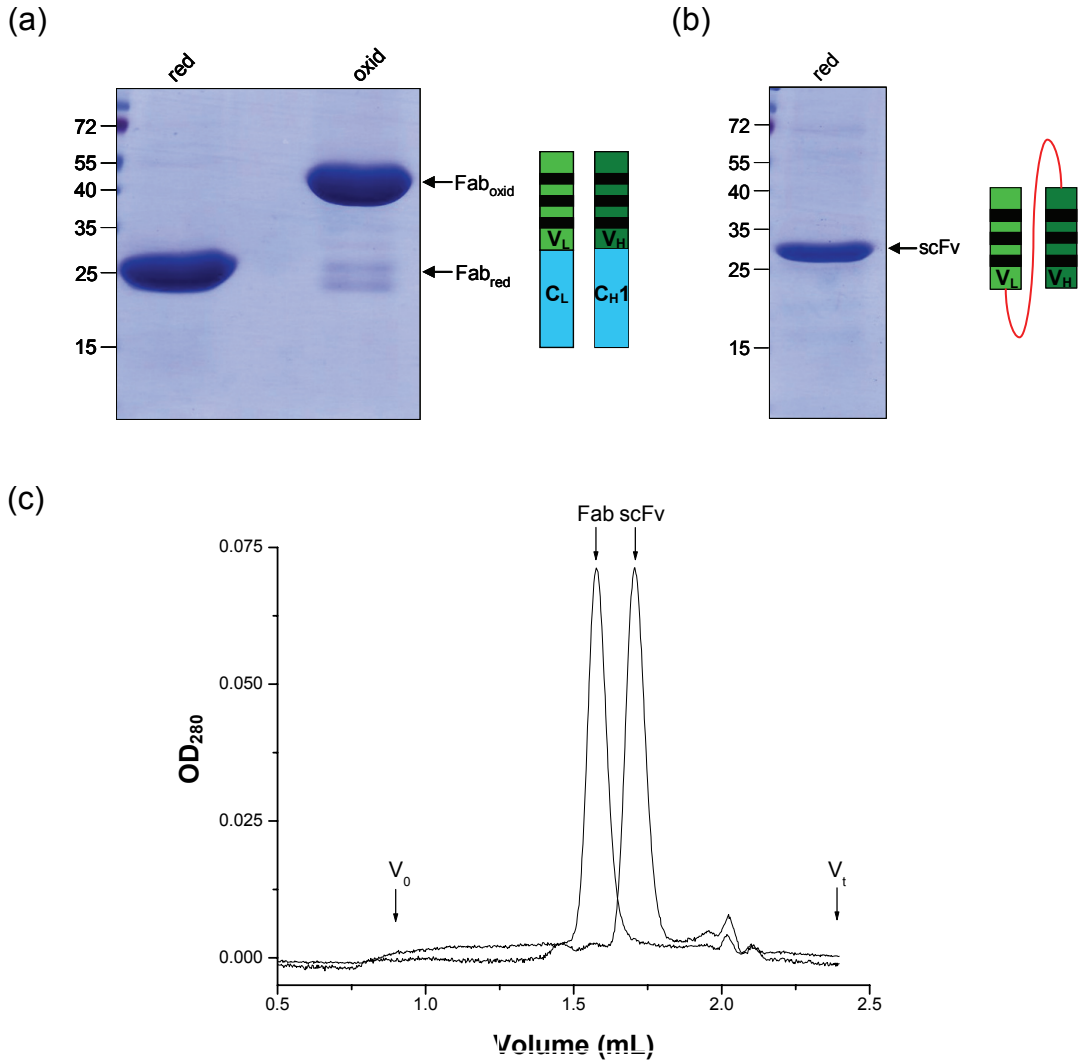

Figure 6-4. Affinity purification of scFv and Fab fragments secreted from insect cells. scFv and Fab fragments were affinity-purified *via* the epitope peptide CYWAMVQAPADAPE of TAP1 and the elution fraction was analyzed by SDS-PAGE (12%, coomassie-stained). (a) 2 µg Fab fragment were analyzed under reducing (with β-mercaptoethanol, red) or non-reducing (without β-mercaptoethanol, oxid) conditions to prove proper heterodimer assembly. (b) The purity of the purified scFv fragment (1 µg) was estimated by SDS-PAGE (12%, coomassie-stained) under reducing conditions (red). (c) The affinity-purified scFv and Fab fragments were separated by size exclusion chromatography (Superdex 200 PC3.2/30) monitoring proteins (20 µg) at 280 nm. The void volume (V_0=0.85 mL) and the total volume (V_t=2.3 mL) are indicated by arrows in the chromatogram. Molecular mass standard in kDa.

6.1.4. Recombinant antibody fragments bind with nanomolar affinity to the TAP1 epitope

The binding affinity of the recombinant antibody fragments was analyzed by ELISA using the NBD of TAP1 as antigen (Müller *et al.,* 1994). The equilibrium binding constants (K_D) for the monovalent recombinant Fv (31.8±2.7 nM) and the Fab fragment (39.5±2.7 nM) are very similar (Figure 6-5 (a) and (b)), however they differed drastically by two orders of magnitude from the K_D value of the mAb148.3 (0.42±0.04 nM) (Figure 6-6. (d)). To investigate whether this difference is based on avidity effects of the bivalent IgG molecules, I generated proteolytic Fab fragments by papain cleavage of the mAb148.3. The resulting Fab fragments were purified on Protein G Sepharose and analyzed by SDS-PAGE under oxidizing conditions and immunoblotting using Fab- and Fc-specific antibodies (Figure 6-6 (a) and (b)). In addition to the monovalent Fab fragment a small amount of the bivalent $(Fab)_2$ fragment was detected with the Fab-specific antibody. The proteolytic Fab fragment displays a K_D value of 14.8±0.8 nM (Figure 6-6 (c)), demonstrating that the K_D values of the isolated paratopes of the bivalent mAb148.3 for binding to the TAP1-NBD are comparable with those of the recombinant Fv and Fab fragments.

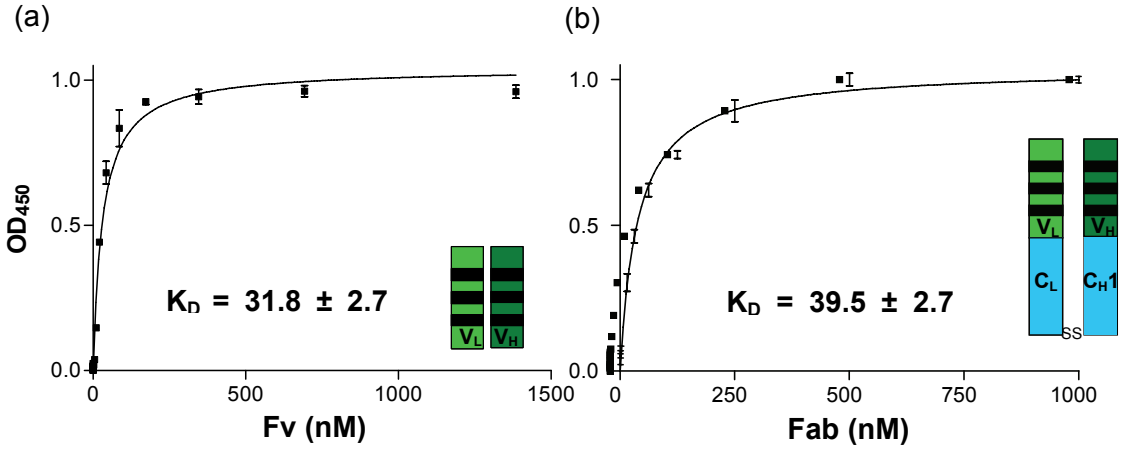

Figure 6-5. Affinity binding constants of the recombinant antibodies. ELISA plates were coated with purified TAP1-NBD (10 µg/mL) and probed with various concentrations of the affinity-purified Fv (a) and Fab fragments (b). The experimental data were fitted to a 1:1 Langmuir binding model.

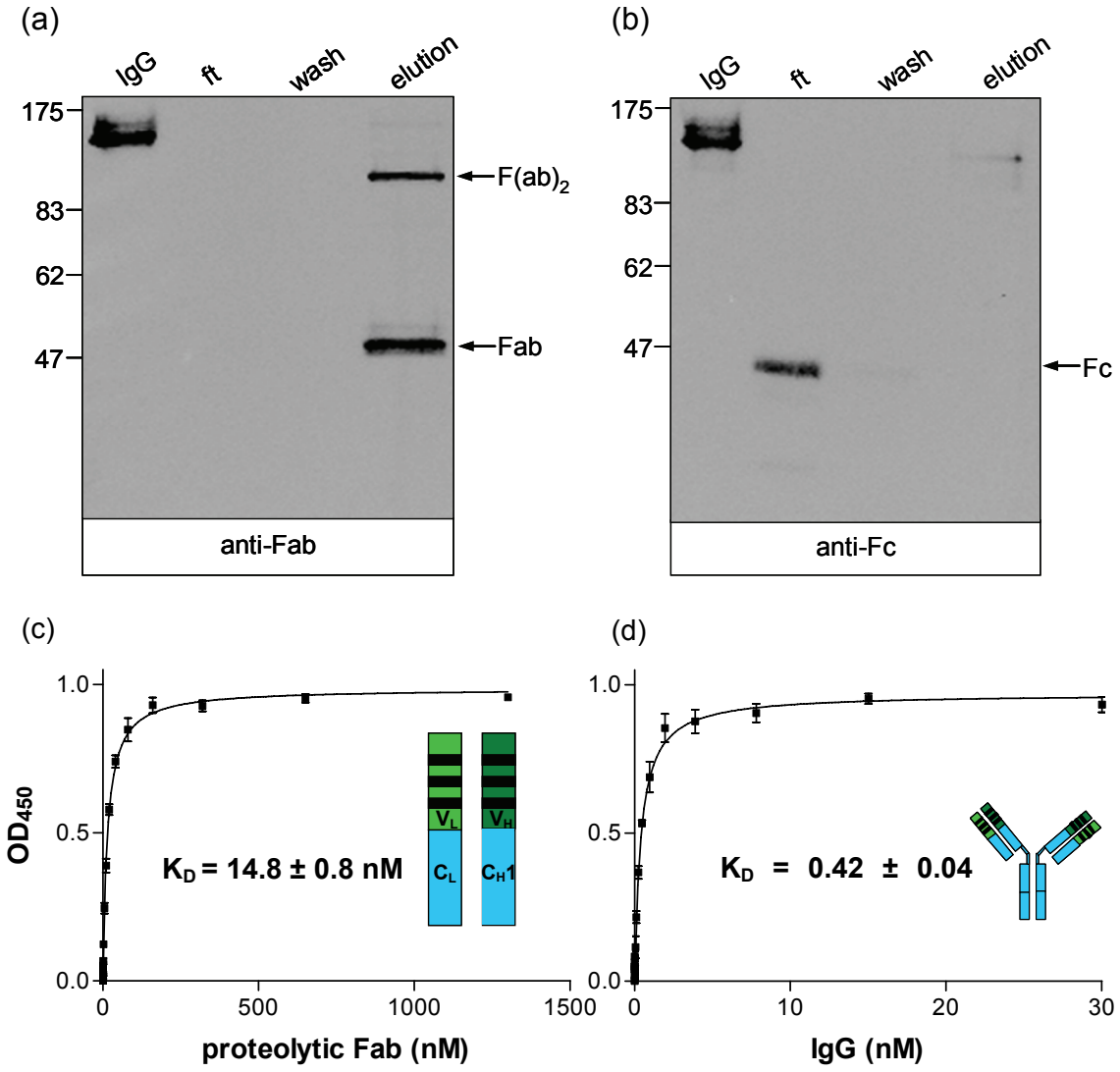

Figure 6-6. Affinity binding constant of the proteolytic Fab fragment. After papain cleavage, the proteolytic Fab fragment was affinity-purified on Protein G Sepharose and analyzed by non-reducing SDS-PAGE (10%). The Fab (a) and Fc fragments (b) were detected with specific antibodies. The binding constants of the proteolytic Fab fragment (c) and the mAb148.3 (d) for the NBD of TAP1 were determined by ELISA. The experimental data were fitted to a 1:1 Langmuir binding model. Molecular mass standard in kDa.

The association and dissociation kinetics of the Fv fragment were analyzed by surface plasmon resonance (SPR) spectroscopy using the epitope peptide CYWAMVQAPADAPE immobilized on a CM5 biosensor chip (Figure 6-7 (a)). Rate constants and equilibrium binding constants were determined based on a standard model for 1:1 interaction and are summarized in Table 6-1.

Table 6-1. Association and dissociation rate constants at 4°C.

Fv (nM)	k_a ($10^4 \times M^{-1} \times s^{-1}$)	k_d ($10^{-3} \times s^{-1}$)	$K_{D, kin}$ (nM)
15.6	12.76	1.40	11.00
31.3	8.12	1.42	17.50
62.5	8.27	1.43	17.30
125.0	8.33	1.45	17.40

The association rate constant derived from the various concentrations (arithmetic mean) of Fv fragments was determined to $k_a = (8.57 \pm 0.31) \times 10^4\ M^{-1}s^{-1}$ (4°C). The dissociation rate constant was $k_d = (1.43 \pm 0.06) \times 10^{-3}\ s^{-1}$ (4°C). Diffusion limitation and multivalency effects (crowding at the sensor interface) could be excluded by investigating the rate constants at different flow rates as well as at different concentrations of the immoblized epitope peptide. The K_D (arithmetic mean) derived from these rate constants was 16.80 (± 0.69) nM. The K_D value calculated from the resonance units at equilibrium binding of the Fv fragment to the surface (R_{eq}) is 32.1 (± 1.10) nM (Figure 6-7 (b)). The R_{eq} value deduced from binding experiments at 25°C is 35.4 (± 2.20) nM. These results prove the self-consistency of the data and confirm the nanomolar affinity of the recombinant antibody fragments for TAP1 as determined by ELISA.

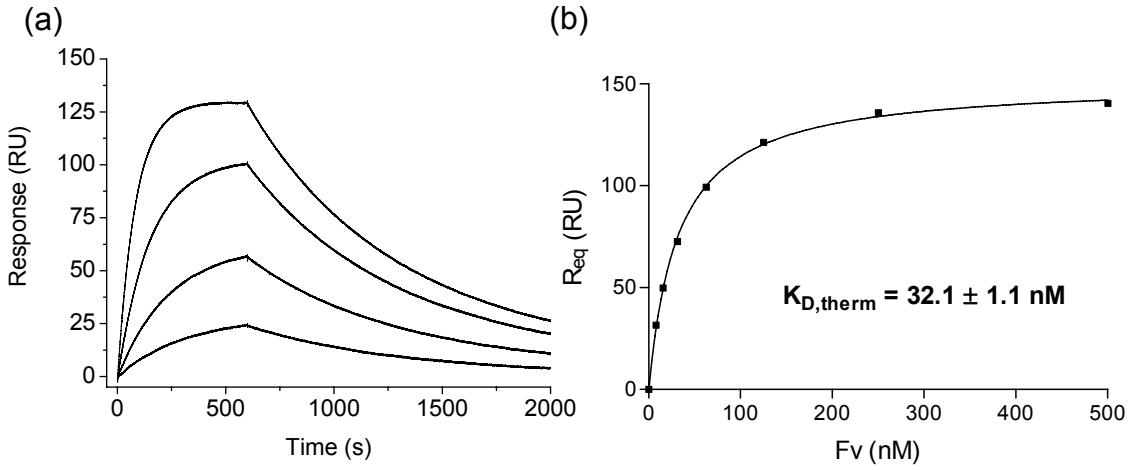

Figure 6-7. Determination of the affinity binding constant of the Fv fragment by surface plasmon resonance (SPR). (a) The binding kinetics of the Fv fragment to the epitope peptide CYWAMVQAPADAPE were analyzed with concentrations of 15.6 nM, 31.2 nM, 62.5 nM and 125 nM at 4°C. (b) Determination of the thermodynamic K_D value calculated from the plasmon shifts at equilibrium binding of the Fv fragment to the surface (R_{eq}). Rate constants and equilibrium binding constants were determined based on a standard model for a 1:1 interaction.

The kinetic rate constants of Fv148.3 for binding to the epitope peptide CYWAMVQAPADAPE immobilized on a CM5 biosensor chip were also compared at several temperatures between 5 and 25°C (Figure 6-8). Both, k_a and k_d of Fv148.3 increased with the temperature. However, the k_d increases moderately between 5 and 20°C and rises suddenly at 25°C. The reason for this difference may lie in the reduced stability of the Fv fragment at higher temperature. Since both, the k_a and k_d rate constants increased with the temperature, the corresponding binding constant of the Fv148.3 for epitope peptide CYWAMVQAPADAPE decreased (Figure 6-9). The fact that the temperature dependence on the binding constant decreases as the temperature rises, is an indication for an exothermic reaction. This temperature-dependent decrease in binding affinity of the Fv148.3 to the epitope peptide may have several reasons: (1) increase in temperature may result in rearrangement of the paratope, subsequently leading to a decrease in affinity, and (2) elevated temperatures may affect the functionality of the Fv fragment, since both V_H and V_L are non-covalently associated and may fall apart.

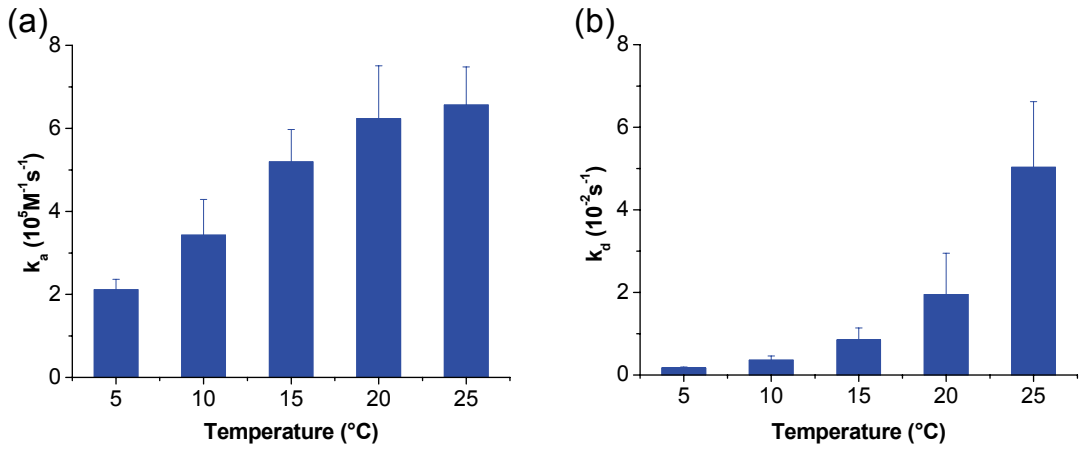

Figure 6-8. The kinetic rate constants for the Fv148.3 monitored at several temperatures. The association (a) and dissociation (b) rate constants of Fv148.3, for binding to the epitope peptide CYWAMVQAPADAPE immobilized on a CM5 biosensor chip, were analyzed at several temperatures between 5 and 25°C.

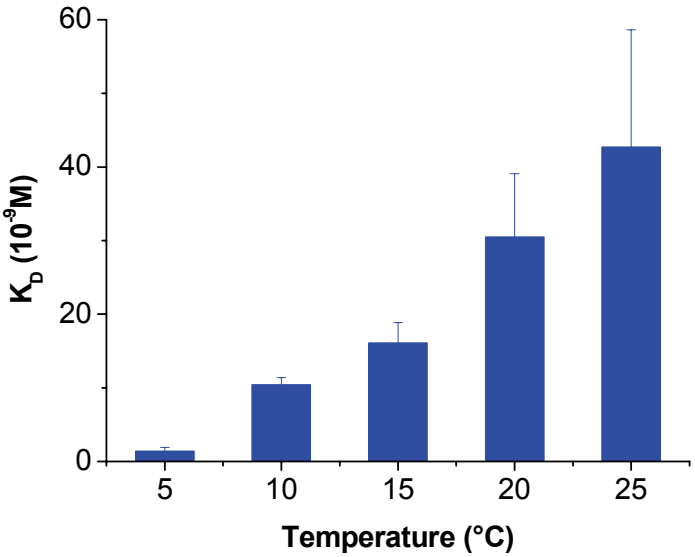

Figure 6-9. Affinity binding constants determined by kinetic measurements for Fv148.3 observed at several temperatures.

The association and dissociation rate constants measured at temperatures between 5 and 25°C allowed determining thermodynamic characteristics such as the enthalpy and the entropy changes of the reaction. The graphical representations carried out are summarized in Figure 6-9, Figure 6-10, and

Figure 6-11. The results obtained from graphical representations are summarized in Table 6-2.

To investigate the temperature effect on the interaction between the Fv148.3 and the epitope peptide, precisely the effect of temperature on the binding constant, the van't Hoff equation was used. Under certain conditions the binding constant is linked to the standard Gibbs free energy change of the interaction (ΔG^0) as stated in the van't Hoff equation:

$$\Delta G^0 = -RT \times \ln(K_D)^{-1} = RT \times \ln K_D$$

with

ΔG^0	standard free energy change
R	universal gas constant
T	absolute temperature (K)
K_D	equilibrium dissociation constant

Substitution of the following expression with the van't Hoff equation

$$\Delta G^0 = \Delta H^0 - T\Delta S^0$$

and rearranging gives finally

$$\ln K_D = \frac{\Delta H^0}{RT} - \frac{\Delta S^0}{R}$$

with

ΔH^0	standard enthalpy change
ΔS^0	standard entropy change

In case of $\Delta H^0 < 0$, corresponding to an exothermic reaction, the entire term on the right of the equation is negative and as shown in Figure 6-10, the equilibrium constant of an exothermic reaction decreases with an increase in temperature.

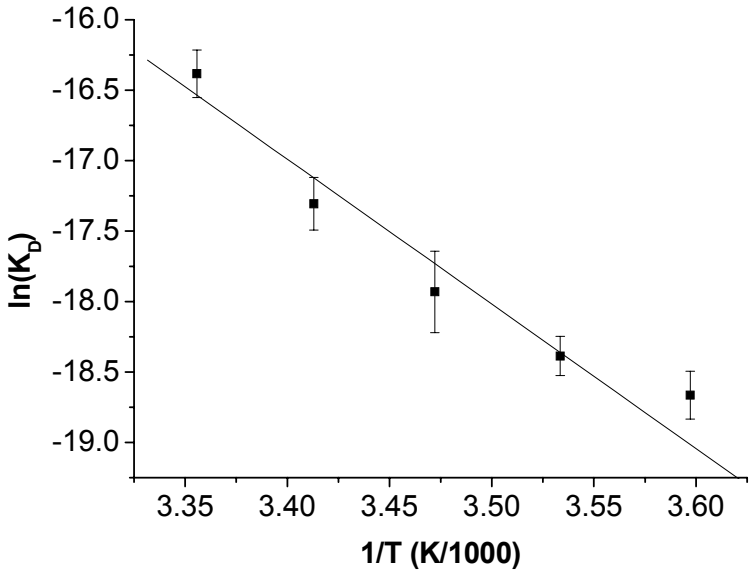

Figure 6-10. Van't Hoff presentation of lnK_D as a function of the inverse of the temperature.

The linear regression of lnK_D as a function of the inverse of the temperature gives a slope of -9,304 (± 1,300) and an intercept value of 15 (± 5), with a correlation coefficient (R) of -0.97. The slope is defined as $\Delta H^0/R$ and the intercept of the y-axis as $\Delta S^0/R$.

The increase of the association and dissociation rate constants with the temperature is explained by the Arrhenius and the Eyring equations. Both the Arrhenius and the Eyring equation describe a temperature dependence of the reaction rates. The linear regression for lnk_a and lnk_d as a function of the temperature gave a slope of -4,781 (± 842) with R = -0.96 and an intercept of -14,084 (± 480) with R = -0.99, respectively. The slopes allowed to calculate the energy of activation (ΔE_a) by implementing the Arrhenius equation:

$$\ln k = -\frac{\Delta E_a}{RT} + \ln A$$

With $-\Delta E_a/R$ defined as the slope and lnA as the intercept of the linear regression. A high activation energy (ΔE) corresponds to a reaction rate that is very sensitive to temperature (the Arrhenius plot has a steep slope). On the contrary, Arrhenius plot with a shallow slope, suggesting a small activation energy, indicates a reaction rate that varies slightly with the temperature. In this case, the corresponding activation energy ($E_{a,d}$; Table 6-2) indicates that the

dissociation rate constant of the Fv148.3 from the epitope peptide is more dependent on the changes in temperature than the association rate constant.

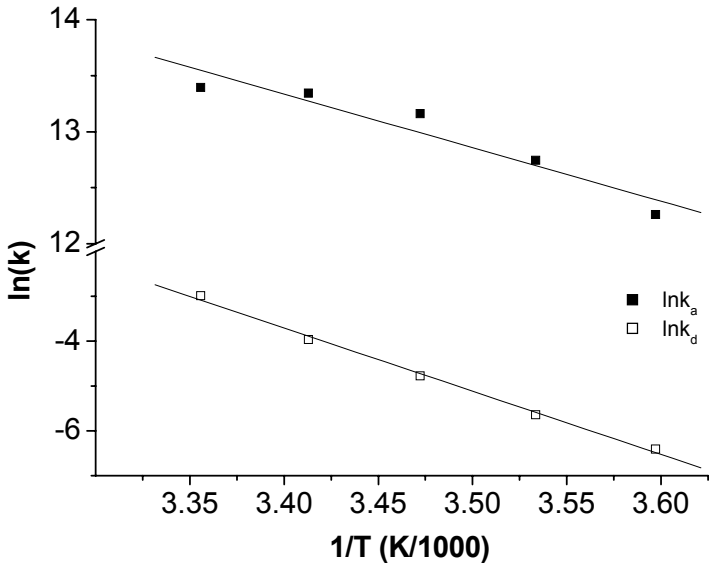

Figure 6-11. Temperature dependence demonstrated by the Arrhenius plot: lnk_a and lnk_d as a function of the inverse of the temperature.

The Eyring equation is based on the transition state model which implies that the reaction includes an unsteady intermediate state on the reaction pathway. The kinetic rates are dependent on the variation of enthalpy and entropy of association and dissociation of the activated complex:

$$\ln\left(\frac{k_a}{T}\right) = \ln\left(\frac{k_B}{\hbar}\right) + \frac{\Delta S_a^*}{R} - \frac{\Delta H_a^*}{RT}$$

$$\ln\left(\frac{k_d}{T}\right) = \ln\left(\frac{k_B}{\hbar}\right) + \frac{\Delta S_d^*}{R} - \frac{\Delta H_d^*}{RT}$$

with

ΔH^* enthalpy change of the activated complex

ΔS^* entropy change of the activated complex

$\hbar$ Planck's constant (6.6262×10^{-34} J × s)

k_B Boltzmann's constant (1.3806×10^{-23} J × K^{-1})

Thus the thermodynamic transition state constants for the forward and backward reactions can be obtained from plots of $\ln(k_a/T)$ and $\ln(k_d/T)$ respectively against 1/T. The linear regression of $\ln(k_a/T)$ and $\ln(k_d/T)$ as a function of the inverse of the temperature gives for k_a a slope of -4,378 (± 810) and an intercept value of 23 (± 3), with a correlation coefficient of -0.95, and for k_d a slope equal to -13,416 (± 531), an intercept value of 36 (± 2) with a correlation coefficient of -0.99. The change of enthalpy of the activated complex (ΔH^*) is given by the slope ($-\Delta H/R$), whereas the entropy of the activated complex (ΔS^*) is calculated from the intercept value ($\ln(k_B/\hbar)+(\Delta S^*/R)$).

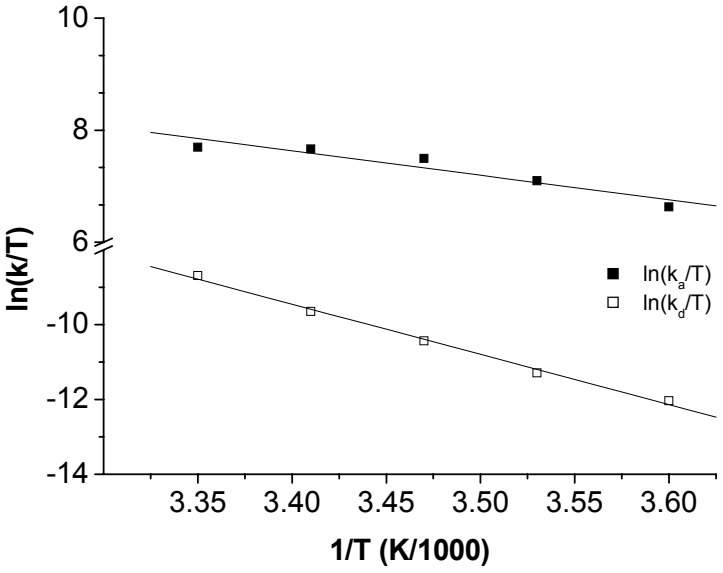

Figure 6-12. Temperature dependence demonstrated by the Eyring plot: $\ln(k_a/T)$ and $\ln(k_d/T)$ as a function of the inverse of the temperature.

The differences between the association (k_a) and dissociation (k_d) values of the entropy and enthalpy of the activated complex give the changes of the entropy and enthalpy of the reactions:

$$\Delta H^0 = \Delta H_a^* - \Delta H_d^*$$

$$\Delta S^0 = \Delta S_a^* - \Delta S_d^*$$

Table 6-2. Summary of the thermodynamical data of the interaction of the Fv fragment and the epitope peptide CYWAMVQAPADAPE.

	Fv148.3
ΔH^0 (kJ / mol)	-77.4 (± 0.2)
ΔS^0 (J × (K × mol)$^{-1}$)	-121.3 (± 37.4)
ΔG^0 (kJ / mol)	-41.2 (± 0.2)
$\Delta E_{a;a}$ (kJ / mol)	39.7 (± 7.0)
$\Delta E_{a;d}$ (kJ / mol)	117.1 (± 4.0)
ΔH^*_a (kJ / mol)	36.4 (± 6.7)
ΔH^*_d (kJ / mol)	111.5 (± 4.4)
ΔS^*_a (J × (K × mol)$^{-1}$)	-10.3 (± 2.8)
ΔS^*_d (J × (K × mol)$^{-1}$)	103.1 (± 1.8)

In conclusion, moving from free Fv148.3 fragment to the transition state is enthalpically opposed yet entropically favored, whereas going from the transition state of the bound Fv148.3 fragment to the epitope peptide is favored both enthalpically and entropically. The transition state thermodynamics of Fv148.3 fragment binding to the epitope peptide is largely entropy-driven since $-T\times\Delta S^0$ is higher than ΔH^0: 36.1 (kJ / mol) > -77.4 (kJ / mol) at 298 K. This is consistent with the significant hydrophobic character of the Fv148.3 paratope. The enthalpic barrier to binding may result from the stripping of water from partial and full charges on the Fv148.3 fragment paratope as well es the epitope peptide (Baker & Murphy, 1998). As the transition state settles into the bound state, some favorable enthalpy is regained as paratope-epitope hydrogen bonds and salt bridges are formed (Gabdoulline & Wade, 2002). If one assumes the interface at the transition state is partially dehydrated, then entropically, formation of the transition state from the unbound components again reflects the hydrophobic effect as waters are released. Forming the bound state from the transition state requires release of further water, giving rise to additional entropy. Entropy also plays a significant role in influencing the kinetics of the paratope-epitope reaction. It is also evident from Table 6-2 how the entropy component of the transition state thermodynamics simultaneously reduces the activation barrier for binding ($\Delta E_{a;a}$) and increases the barrier for dissociation ($\Delta E_{a;d}$). This demonstrates an entropic component of the paratope-epitope interaction by which tight paratope-epitope binding and slow dissociation are achieved.

6.1.5. Fv binding to the C-terminus of TAP1 arrests the TAP complex in a peptide transport incompetent state

It was recently shown that the NBDs of TAP1 and TAP2 have non-equivalent C-terminal tails, which may account for functional differences in ATP binding and hydrolysis at both NBDs (Bouabe & Knittler, 2003). Moreover, the C-terminus of the dimeric HlyB-NBD, the closest homologue of a dimer NBD structure, is involved in stabilization of the dimer interface (Zaitseva *et al.,* 2005). Based on this information I speculated that the Fv fragment modulates peptide translocation into the ER lumen by binding to the C-terminus of TAP1. I performed transport inhibition studies in semipermeabilized cells after pre-incubation with graded amounts of recombinant antibodies. Strikingly, the Fv fragment inhibits TAP-dependent peptide transport in a concentration dependent manner (Figure 6-13). The inhibitory effect is fully reversible in the presence of a 1000-fold molar excess of the 5mer epitope (Ac-ADAPE-OH), demonstrating that the translocation arrest is specifically linked to the C-terminus of TAP1. Since the 5mer peptide is too short and is also blocked at its N-terminus, it cannot be recognized and transported by TAP (Uebel *et al.,* 1997). In the presence of 10 µM of mAb148.3, peptide transport was blocked to a similar extent when compared to the Fv fragment. By contrast, the same amount of the TAP2-specific mAb435.3 did not inhibit peptide transport. The epitope of the mAb435.3 is localized within a sequence stretch C-terminal of the TMD of TAP2 (^{469}KFQDVSFAYPNR^{480}) as determined by epitope mapping. These findings argue against simple steric hinderance by the Fv fragment or the mAb148.3. In the absence of either ATP or in the presence of the TAP-specific inhibitor ICP47 (10 µM with ATP), peptide transport was reduced to background level.

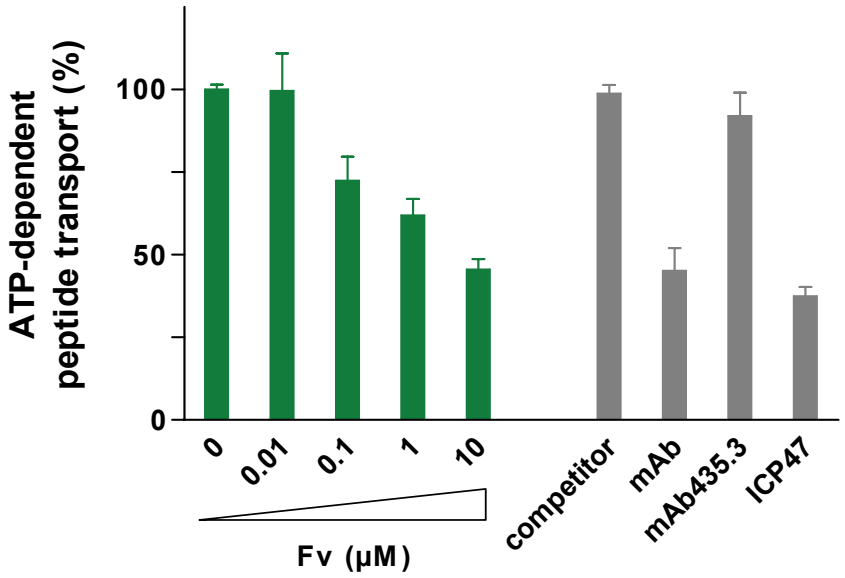

Figure 6-13. Inhibition of intracellular peptide transport in semipermeabilized cells. Transport assays were performed in semipermeabilized cells with fluorescein-labeled peptide (500 nM of RRYQNSTC$^{(F)}$L) for 3 min at 32°C in the presence of ATP (10 mM). For inhibition studies the samples were pre-incubated with either ICP47 (10 µM), Fv fragment (10 µM) together with the competitor peptide Ac-ADAPE-OH (10 mM), different concentrations of Fv fragment (0.01-10 µM), mAb148.3 (10 µM) or mAb435.3 (10 µM). After cell lysis, N-core glycosylated (transported) peptides were bound to Concanavalin A-Sepharose and quantified after specific elution. Background transport activity was determined by replacing ATP with apyrase (one unit). Data represent the arithmetic mean of triplicate measurements after subtraction of background transport activity.

6.1.6. The TAP complex is stabilized by antibody fragments

Since the C-terminal tails of TAP1 and TAP2 control nucleotide interaction (Bouabe & Knittler, 2003), I investigated whether binding of the Fv fragment to the C-terminus of the TAP1-NBD influences the ATP-binding properties of TAP. However, ATP-agarose binding experiments in the absence and presence of 10 µM of Fv fragment revealed that ATP binding to the heterodimeric TAP complex as well as TAP1 alone was not altered by the recombinant antibodies (Figure 6-14 (a)). Furthermore, peptide binding experiments at non-saturating conditions revealed no effect of the Fv fragment on peptide binding by TAP (Figure 6-14 (b)).

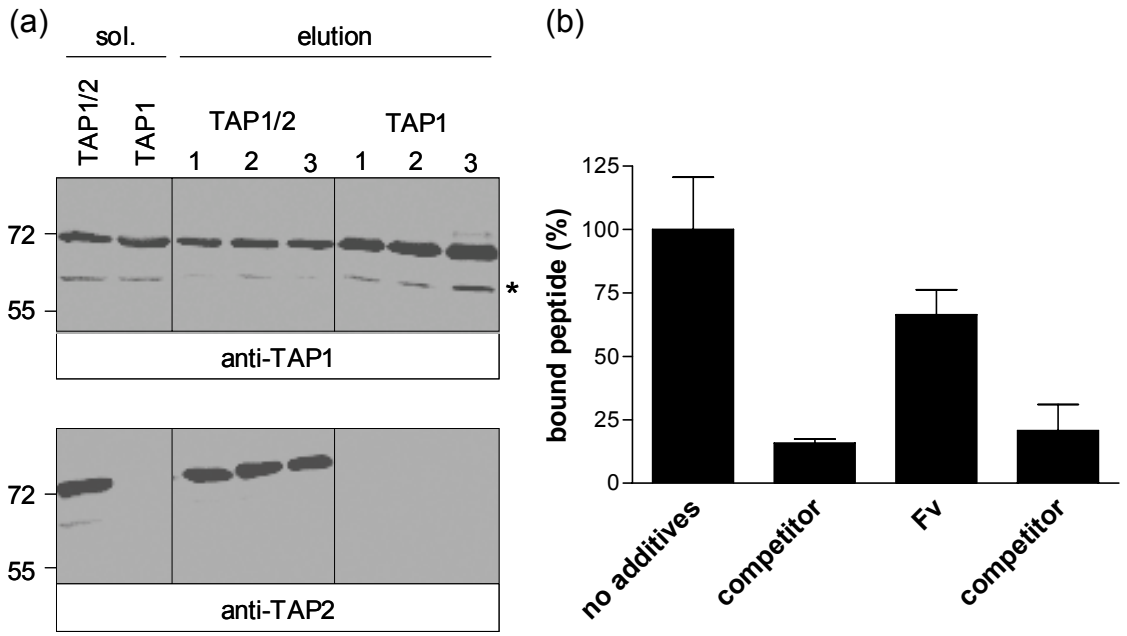

Figure 6-14. ATP and peptide binding to TAP in the presence of recombinant antibodies. (a) Microsomes containing either the heterodimeric TAP1/2 complex or the TAP1-subunit alone (both 3.75 mg total protein) were solubilized with digitonin (1%) and split into three vials (250 µL each). One of the samples was pre-incubated in the presence of Fv fragment. TAP was bound to C8-coupled ATP-Agarose (Sigma) and washed with buffer (one sample with buffer supplemented with Fv fragment (10 µM)). TAP was specifically eluted with 50 µL of Mg-ATP (5 mM) and analyzed by SDS-PAGE (solubilisate, 5 µL/lane; eluate, 10 µL/lane) and subsequent immunoblotting. Solubilizate (sol.), sample without Fv (1), sample pre-incubated with Fv (2), sample washed with Fv (3), minor degradation product of TAP1 (*). Molecular mass standard in kDa. (b) Peptide binding to the TAP complex at half-maximal peptide concentrations. TAP-containing Raji microsomes (25 µg protein) were pre-incubated with 10 µM of Fv fragment or without additives for 15 min at 4°C. Peptide binding was performed with 250 nM of radiolabeled peptide R9LQK for 20 min at 4°C. TAP-associated peptides were quantified by γ-counting. Data represent the arithmetic mean of triplicate measurements.

Peptides and ATP bind independently from each other to TAP (Androlewicz *et al.,* 1993; Uebel *et al.,* 1995; van Endert *et al.,* 1994). Moreover, the heterodimeric TAP complex is highly unstable in the absence of ATP or ADP (van Endert *et al.,* 1999). Based on these data I speculated that the Fv fragment could compensate for the absence of nucleotides. TAP-containing microsomes were preincubated in the absence of ATP and in the presence of either ATP (3 mM) or Fv fragment (5 µM) for up to 120 min at 27°C and subjected to peptide binding experiments (at 4°C) with the radiolabeled peptide

RR(^{125}I)YQKSTEL at saturation concentration (1 µM). Interestingly, the Fv fragment could stabilize TAP to a similar extent as ATP (Figure 6-15). Even after 2 h 80% of the peptide-binding capacity of TAP was maintained. By contrast, in the absence of ATP and stabilizing Fv fragment the amount of peptide-receptive TAP decreased in a time-dependent manner with only 10% of bound peptide after 2 h. The decrease of peptide binding directly reflects the loss of peptide transport function as previously shown (van Endert *et al.,* 1999). Importantly, the amount of peptides bound to the TAP complex in the presence and absence of the Fv fragment was comparable not only at saturating but also at half-maximal (non-saturating) peptide concentrations (Figure 6-14 (b)).

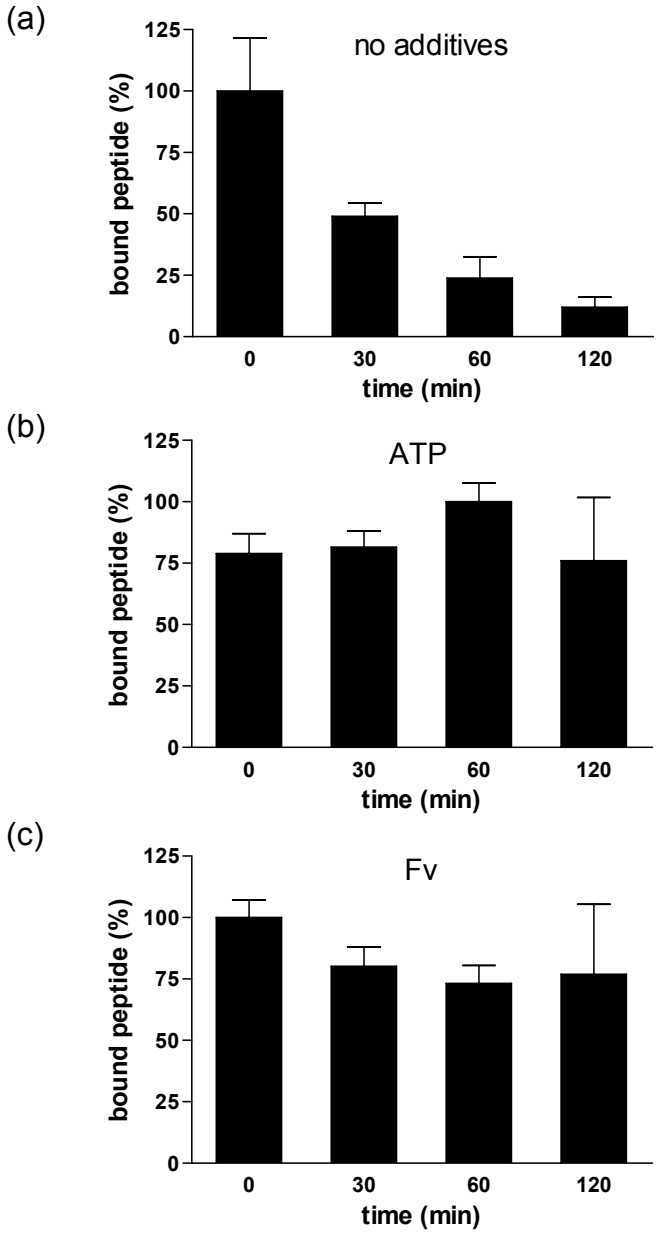

Figure 6-15. Stabilization of the TAP complex. TAP-containing microsomes (15 µg total protein) were preincubated with 3 mM of ATP or 5 µM of Fv fragment for the indicated periods at 27°C. Peptide binding was performed with 1 µM of radiolabeled peptide for 15 min at 4°C. TAP-associated peptides were quantified by γ-counting. Measurements without ATP and Fv fragment (a), in the presence of ATP (b), and in the presence of Fv fragment but without ATP (c). Data represent the mean of triplicate measurements and were normalized to the peptide-binding data of TAP without additives (0 min).

Since in peptide-binding experiments the recombinant antibody fragments displayed a stabilizing effect on the TAP complex with regard to peptide-binding (Figure 6-15), I also investigated the kinetics of substrate release by the TAP complex in the presence of the recombinant antibodies. Here, I used fluorescence polarization to analyze the kinetics of peptide association and dissociation in real time in the presence and absence of the recombinant antibody fragments. Interaction of the fluorescein-labeled peptide with the peptide-binding pocket of the TAP complex results in fluorescence quenching. This phenomenon is based on the characteristics of fluorescein, which is sensitive to polarity or pH changes of the surrounding (Neumann *et al.,* 1999). The fluorescence quenching is caused by a structural rearrangement of the TAP-peptide complex moving a proton donor group in close proximity to the fluorophore (Neumann *et al.,* 1999). Here, I analyzed the fluorescence quenching during the process of substrate binding and dissociation in the presence or absence of the Fab148.3 fragment. The addition of the affinity-purified TAP complex to the buffer containing the fluorescein-labeled peptide resulted in a decrease of the fluorescence signal reaching equilibrium within 8 min (Figure 6-16). A 100-fold molar excess of non-labeled peptide (competitor) resulted in the release of the bound fluorescein-labeled peptide. A time-dependent increase of the fluorescence signal approaching the initial fluorescence intensity was observed (Figure 6-16). All experiments were performed in the absence of ATP to exclude the possibility that the change of the fluorescence signal is due to ATP-dependent substrate transport instead of the formation and dissociation of the TAP-peptide complex. After pre-incubating the TAP complex with the Fab148.3 fragment, and adding the preformed complex to the buffer containing the fluorescein-labeled peptide a double decrease in the fluorescence signal was observed comparing to the decrease without the Fab fragment (Figure 6-16). Equilibrium was reached within 500 s and after addition of 100-fold molar excess of non-labeled peptide initial fluorescence intensity was restored. However, in the presence of the Fab fragment the fluorescence recovery was delayed indicating again that the recombinant antibody fragment stabilizes the TAP complex by inhibiting the dissociation of the TAP-peptide complex (Figure 6-16).

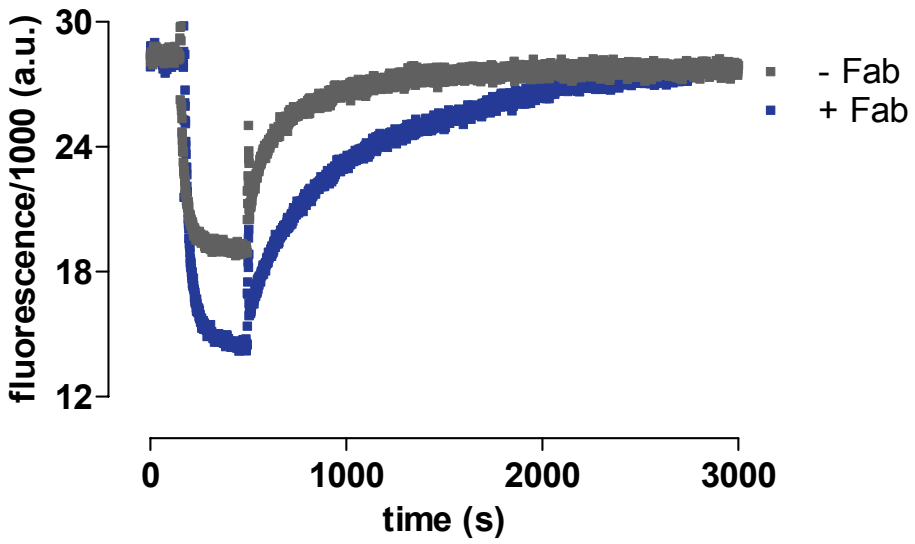

Figure 6-16. Fluorescence quenching of peptide bound to TAP. Time-dependent change of fluorescence emission was analyzed during the binding and dissociation of fluorescein-labeled peptide to TAP in the presence or absence of the Fab148.3 fragment. The fluorescence emission ($\lambda_{ex/em}$=470/515 nm) was monitored with 80 nM of fluorescein-labeled peptide (C4F) in 170 µL of HBS buffer at 10°C. After reaching a stable fluorescence emission signal, 30 µL of both, purified TAP1/TAP2 heterodimer or purified TAP1/TAP2 heterodimer preincubated with 10 µM Fab148.3 fragment, were injected into the cuvette. When binding reached equilibrium, as indicated by a stable fluorescent emission signal, a 100-fold molar excess of non-labeled peptide (RRYQKSTEL) was added to compete for the bound fluorescent peptide.

6.1.7. Purification of the peptide-loading complex from a human B-lymphoblastoid cell line (Raji)

In order to circumvent destruction by cytotoxic T cells of the adaptive immune system viruses in particular have evolved manifold strategies to interfere with the MHC class I antigen presentation pathway (Loch *et al.,* 2008, Lehner *et al.,* 2003). Especially, shortly after infection, when antigenic peptides are presented at low frequency, time as well as efficiency in selection of those antigenic peptides for the recognition of the infected cell by the immune system plays a critical role. Thus MHC class I molecules being loaded with high-affinity peptides, depend on the optimal peptide supply by the PLC. Current evidence suggests that MHC class I molecules loaded with suboptimal peptides are later edited by the peptide-exchange mechanism provided by tapasin and ERp57

(Wearsch & Cresswell, 2007). But the detailed molecular mechanism of peptide-binding and -editing is still under debate and needs further investigation of the PLC with respect to its function and structural subunits composition.

Antibody fragments are widely used for the purification and crystallization of macromolecular protein complexes. Since the mAb148.3 allowed for the identification and isolation of the macromolecular PLC composed of TAP1, TAP2, tapasin, MHC class I heavy chain, β_2-microglobulin, calreticulin, and ERp57 (Bangia, *et al.,* 2005; Ortmann *et al.,* 1997), I used the genetically engineered Fv and Fab fragments to purify the endogenous PLC from a human lymphoblastoid Raji cell line. The aim was to identify novel components of the PLC that could provide insight into the precise molecular mechanism of optimal peptide loading as well as peptide editing but also to get a more detailed view into the structural composition of the PLC. In contrast to the purification of the PLC with mAb148.3, where the PLC was eluted with a low pH buffer, the application of the recombinant antibody fragments, generated here, harboring C-terminal affinity-tags, allows for an elegant purification technique with regard to the mild elution conditions. I isolated the TAP complexes from digitonin-solubilized microsomes of Raji cells and purified the Fab-TAP complexes via the C-terminal histidine-tag of the Fab fragment. The elution fraction was concentrated on StrataClean beads (Stratagene) and visualized on SDS-PAGE (coomassie-stained) (Figure 6-17 (a)). Subsequent analysis of the protein bands by MALDI mass spectrometry verified specific association of calreticulin (60 kDa), ERp57/PDI (57 kDa), tapasin (48 kDa), human lymphocyte antigen (HLA) class I heavy chain (44 kDa) with TAP1 (72 kDa) and TAP2 (70 kDa). Notably, β_2m (12 kDa) was missing, probably due to the non-covalent association with the class I heavy chain it was lost during the purification procedure. The MALDI-MS results are summerized in Table 6-3. The analysis of the 58 kDa protein band revealed that this band was a mixture of ERp57 and a novel factor, protein disulfide isomerase (PDI). PDI, a member of the protein disulfide isomerase family, is an enzyme in the endoplasmic reticulum of eukaryotes or periplasmic space of prokaryotes and mediates proper protein folding by acting on disulfide-bond oxidation, reduction, and isomerization. Unfortunately, shortly after our discovery Ahn and colleagues (Park *et al.,* 2006) published the newly identified PDI as a novel factor of the PLC, describing its

editing function in the redox regulation of the MHC class I molecules facilitating selection of high-affnity peptides. They hypothesize that editing of the MHC class I peptide repertoire involves a rapid thiol disulfide exchange between PDI and the MHC class I α_2 disulfide as well as a competition between peptides of various affinities for MHC class I binding. A prerequisite for peptide transfer to MHC class I peptide cleft by PDI, is the oxidation of the α_2 disulfide bond of MHC class I molecules in the PLC. Binding of a high-affinity peptide to the MHC class I molecule stops the competition of peptides and induces a conformational change resulting in the release of the MHC class I-peptide from the PLC.

An insight into the structural organization of the *in vivo* PLC composition would contribute greatly to the understanding of this macromolecular machinery. Single particle analysis (SPR) enables the analysis of quaternary structure and oligomerization state of protein complexes even with very low protein concentrations as already shown for TAP1/TAP2 (Velarde *et al.,* 2001). Here, Figure 6-17 (b) shows for the first time electron micrographs of negatively-stained digitonin-solubilized endogenous PLC complexes obtained from a human lymphoblastoid Raji cell line. Unfortunately, the particles differed in their size, which made further analysis of the particles impossible. The reason for the heterogeneous population of the single particles may lie in the transient nature of the PLC, consequently leading to instability and further dissociation of single components during the purification procedure. The optimization of the purification procedure, for instance in the presence of cross-linkers to stabilize the complex, is still in progress.

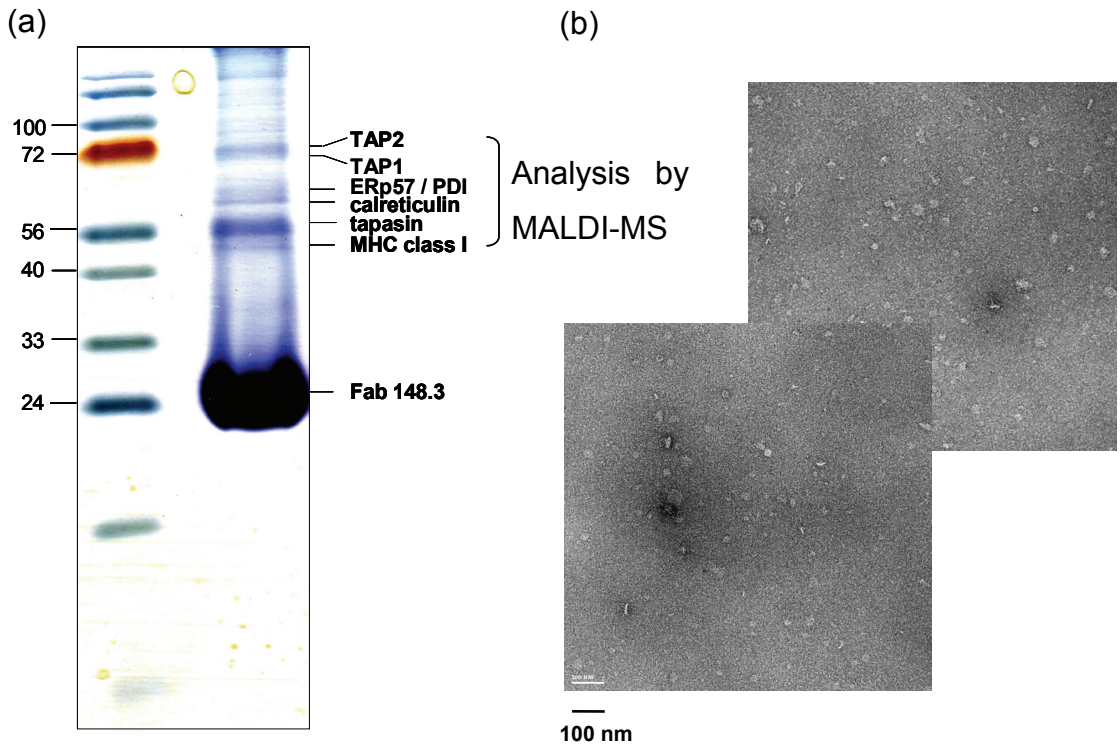

Figure 6-17. Composition of the purified peptide-loading complex from Raji cells. Microsomes (5 mg/mL total protein) prepared from 10^{10} Raji cells were solubilized with 2% digitonin. The PLC was co-purified via TAP1-specific Fab fragment affinity-coupled on Ni-NTA beads. The elution fraction was concentrated on StrataClean beads (Stratagene) and subjected to SDS-PAGE (coomassie-stained). Molecular mass standard in kDa. (b) Single particle electron microscopy of digitonin-solubilized PLC particles. Electron micrographs of the negatively stained PLC elution fraction, with the protein density appearing white, were kindly provided by Dr. David Parcej (Institute of Biochemistry, Goethe-University).

Table 6-3. Identification of the PLC components after separation on SDS-PAGE and analysis by MALDI-MS. Additional information about the databank acquisition number, the score (derived from ions scores as a non-probabilistic basis for ranking protein hits with a value of >70 being significant), number of identified peptides, the molecular weight and the isoelectric point (pI).

Protein	Databank acquisition number	Score	Number of identified peptides	Molecular weight (Da)	pI
TAP2	gi|62087486	100	18	76186	8.2
TAP1	gi|549042	86	16	81427	6.9
PDI	gi|21361657	163	23	57146	6.0
ERp57	gi|2245365	148	22	57143	6.2
calreticulin	gi|5031873	85	15	57798	6.3
tapasin	gi|57209901	46	9	47938	6.7
MHC class I	gi|27657357	79	12	36508	5.3

6.2. Tapasin and MHC class I molecules: Intrinsic modulators of the antigen peptide transporter TAP

The macromolecular PLC displays an elaborated machinery of the immune system involved in the presentation of antigenic peptides to effector cells for rapid interference in case of an infection. However, the transient nature of the macromolecular PLC makes it difficult to look at single interactions *in vivo*. However, without structural information about the *in vivo* composition of the PLC, it is impossible to draw mechanistic conclusions. To date, little is known about the dynamic interaction within the PLC, including the reorganization of the PLC after formation of stabile MHC I-peptide complexes and their disassembly from the PLC ready to leave for the cell surface. And how does tapasin, the supposed peptide editor, come into play? Thus it is indispensable to establish an *in vitro* platform for the investigation of individual interactions using recombinant proteins. To investigate the dynamic interaction between tapasin and MHC class I molecules *in vitro*, it is necessary to work with monodispersely purified and active proteins. This part of the work aims at establishing the expression, purification, as well as functional characterization of soluble tapasin and soluble MHC class I B44 alleles in insect cells.

6.2.1. Expression and purification of soluble tapasin in insect cells

The cloning of the soluble tapasin in pFastBac1 was done by Stefan Ammer, Institute of Biochemistry, Goethe-University Frankfurt (PhD thesis). Tapasin lacking the cytosolic and the transmembrane domains (amino acids 1-384) was PCR-amplified introducing a His_6-tag (3'-end) and the restriction sites BamH I (5'-end) and Hind III (3'-end), which were subsequently used for cloning into pFastBacI (Figure 6-18 (a)). For biochemical characterization, theoretical parameters of the tapasin variant are summarized in Table 6-4.

Table 6-4. Theoretical protein profile of tapasin (based on calculations with the ProtParam at www.expasy.ch).

	Molecular weight (kDa)	pI	Extinction coefficient ($M^{-1}cm^{-1}$) (at 280 nm and pH 6.5)
$tapasin_{(1-384)}$	41.9	6.65	66,920

Soluble tapasin was expressed in *Tn*5 cells for 72 h at 27°C. Since the cytosolic ER retention signal is deleted in the soluble tapasin, it is secreted into the medium. The recombinant tapasin with an apparent molecular mass of 42 kDa was detected after dialyzing the supernatant as shown by SDS-PAGE and immunoblotting with tag-specific antibodies (Figure 6-18 (b)). Tapasin was purified by immobilized metal affinity chromatography (IMAC) using the C-terminal His_6-tag (Figure 6-18 (b)). Here, tapasin was purified to homogeneity in a single affinity chromatography step as shown by SDS-PAGE (coomassie-stained) (Figure 6-18 (c)), yielding 100-200 µg of tapasin per liter of *Tn*5 culture. Correct folding and monodispersity of the purified tapasin was demonstrated by size exclusion chromatography (Figure 4-18 (d)). Tapasin eluted in a symmetric peak at a retention volume expected for the monomer. Bovine serum albumin with a molecular mass of 66 kDa was used as an internal standard. An aliquot of the elution fraction was also subjected to reducing and oxidizing SDS-PAGE (coomassie-stained) verifying minor differences in the running behaviour due to the intramolecular disulfide bridges (C_7-C_{71}, C_{292}-C_{362}) (Figure 6-18 (e)).

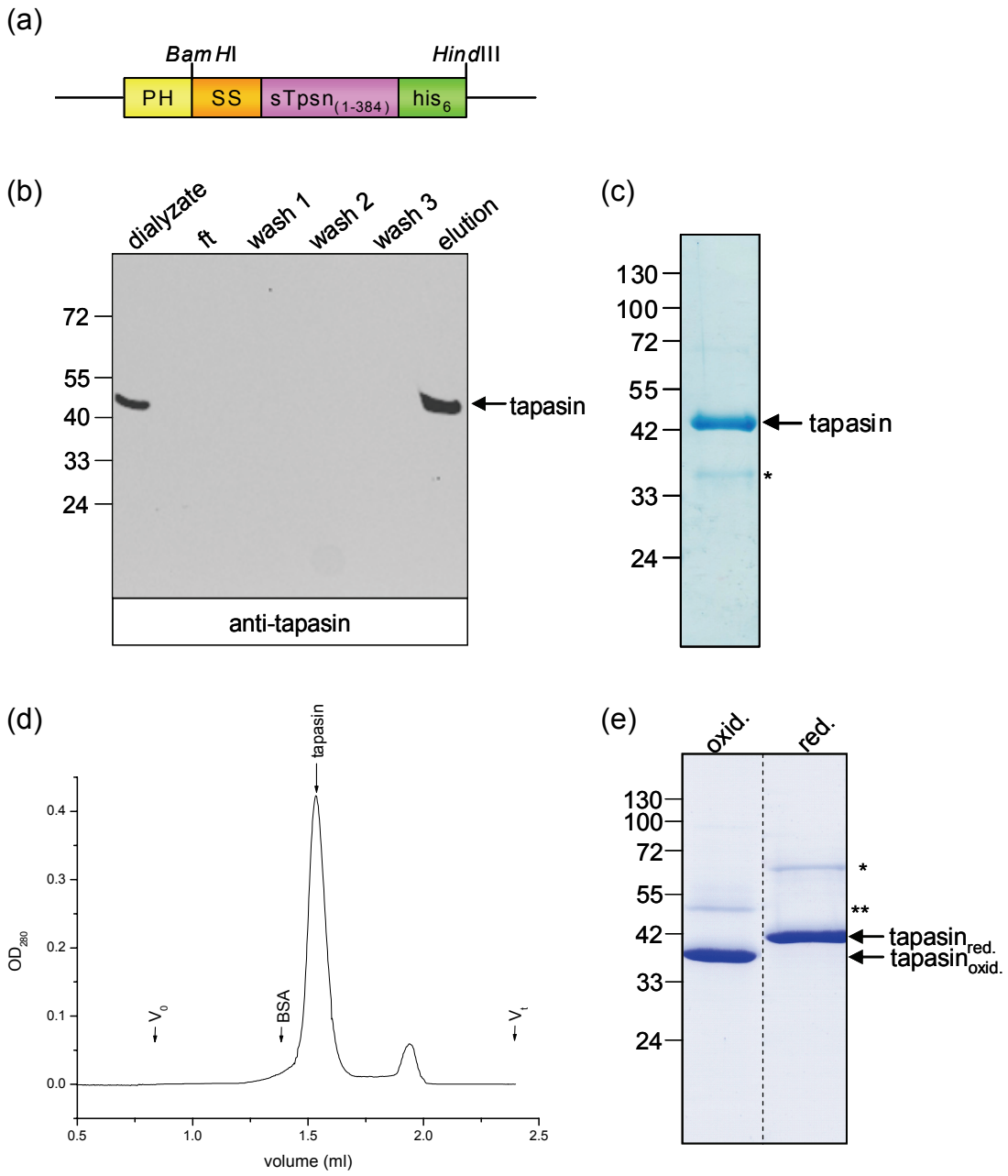

Figure 6-18. Purification of soluble tapasin from *Tn*5 insect cells. (a) Schematic representation of the soluble tapasin gene cassette in the pFB1 plasmid. (b) 72 h post infection cells were harvested and the supernatant was dialyzed against 20 mM Tris/HCl (pH 8.0), 200 mM NaCl, changing the buffer at least three times every 8-10 h. Aliquots of the dialyzed supernatant (dialyzate), the flow through (ft), the washing steps (wash 1, wash 2, wash 3) and the elution fraction (elution) were analyzed by 12% SDS-PAGE and detected with a tapasin-specific antibody. (c) 1 µg of purified tapasin after concentration with an ultrafiltration device (Amicon, Millipore) analyzed on a SDS-PAGE (12%, coomassie-stained). (d) The affinity-purified tapasin (150 µg) was analyzed by size exclusion chromatography (Superdex 200 PC3.2/30) by monitoring at 280 nm. The void volume (V_0 = 0.85), the total volume (V_t = 2.3 mL) and calibration standard bovine serum albumin (BSA, 66 kDa) are indicated by arrows in the graph.

(e) 1 µg of purified tapasin were subjected to SDS-PAGE (12%, coomassie-stained) under reducing (red.) and oxidizing (oxid.) conditions. Molecular mass standard in kDa. Minor impurities after purification (*), (**).

6.2.2. Expression of single chain MHC class I conjugates in insect cells

Human leukocyte antigen (HLA) -B4402 and -B4405 (amino acids 1-276) MHC class I alleles lacking their transmembrane domains were linked N-terminally to β_2m *via* an $(SG_4)_3$ linker resulting in soluble single chain B4402-β_2m (scB4402-β_2m) and soluble single chain B4405-β_2m (scB4405-β_2m) conjugates (Figure 6-19 (b)). A C-terminal TEV-cleavage site and a His_6-tag alone or in combination with an N-terminal Strep-tag were introduced (Figure 6-19 (a)). For biochemical characterization the theoretical parameters were retrieved from the amino acid composition and are summarized in Table 6-5.

Table 6-5. Theoretical protein profile of scB4402-β_2m and scB4405-β_2m (based on calculations with the ProtParam at www.expasy.ch.).

	Molecular weight (kDa)	pI	Extinction coefficient ($M^{-1}cm^{-1}$) (at 280 nm and pH 6.5)
scB4402-β_2m	47.4	5.47	87,780
scB4405-β_2m	47.4	5.53	89,270

To analyze the expression level of the conjugates, 0.5 x 10^6 insect cells from P_2 virus amplification of scB4402-β_2m and scB4405-β_2m were subjected to SDS-PAGE following imunoblotting (Figure 6-19 (c)). Both scB4402-β_2m and scB4405-β_2m were equally well expressed as detected by tag-specific antibodies.

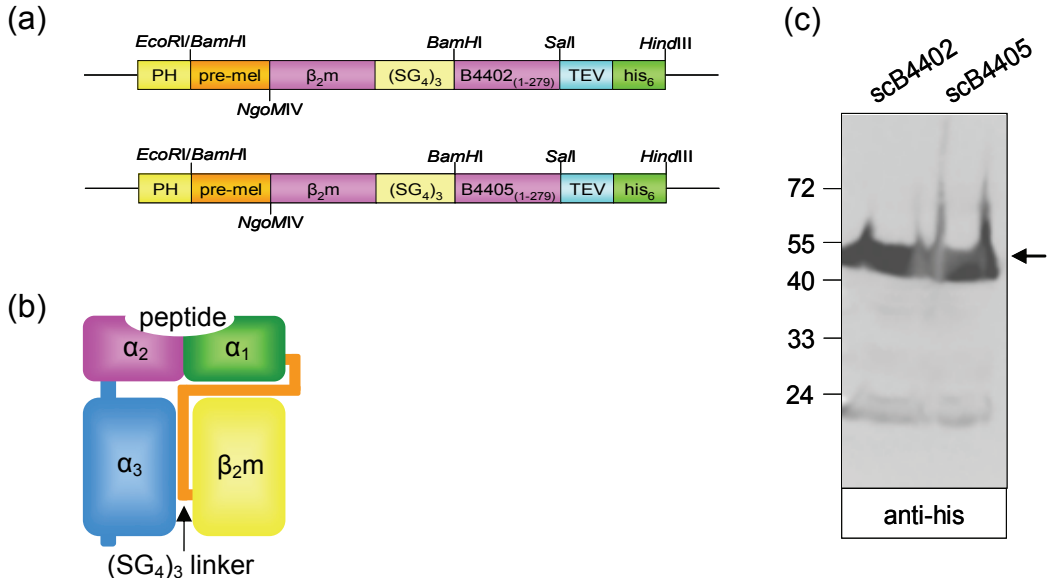

Figure 6-19. Expression of soluble MHC class I in insect cells. (a) Schematic representation of the soluble single chain MHC class I B4402 and B4405 expression cassette in pFastBac1. The cassette includes the polyhedrin promoter region (yellow), a newly introduced pro-melittin signal sequence (orange), the soluble B4402 (pink) and B4405 (pink) as well as β_2m (pink) connected by a $(SG_4)_3$ linker (light yellow), a TEV cleavage site (blue), a His_6-tag (green) at the 3'-end and a N-terminal strepII-tag (green) at the 5'-end. (b) Schematic representation of the single chain MHC class I conjugate. (c) Expression profile of scB4402-β_2m and scB4405-β_2m. 5×10^5 *Sf*9 cells from P_2 virus amplification were analyzed by reducing SDS-PAGE (12%). The scB44 conjugates were detected with a histidine-tag specific antibody as demonstrated by the arrow. Molecular mass standard in kDa.

6.2.3. Purification of scB4405-β_2m expressed in *Tn*5 insect cells

For large scale expression, *Tn*5 insect cells were infected with 10% of the total culture volume with the respective baculovirus. 72 h - 96 h post infection, cells were harvested and culture supernatants dialyzed, changing buffer at least 3 times every 8 – 12 h. Dialyzed supernatant was applied on a Ni-NTA resin, washed and eluted finally with 200 mM histidine. The scB4405-β_2m conjugate, with an apparent molecular mass of 49 kDa, was detected by SDS-PAGE and immunoblotting with an MHC class I-specific antibody (Figure 6-20 (a)). The scB4405-β_2m conjugate was purified to homogeneity in a single affinity chromatography step as shown by SDS-PAGE (coomassie-stained) (Figure 6-20 (b)) with a yield of 100-200 µg per liter of *Tn*5 culture. When subjected to oxidizing SDS-PAGE analysis the oxidized scB4405-β_2m conjugate

migrated faster than the fully reduced conjugate (Figure 4-18 (c)). The higher migration rates of the oxidized protein suggest the presence of several intramolecular disulfide bonds. Size exclusion chromatography revealed a monodisperse peak for scB4405-β_2m running at approximately 49 kDa with a minor dimer peak immediately after purification eluting shortly before the monomer (Figure 6-20 (d) black line). Storage of the scB4405-β_2m conjugate for two weeks at 4°C lead to increase of the dimer peak, eluting shortly before the monomer, as shown by the dashed line (Figure 6-20 (d)).

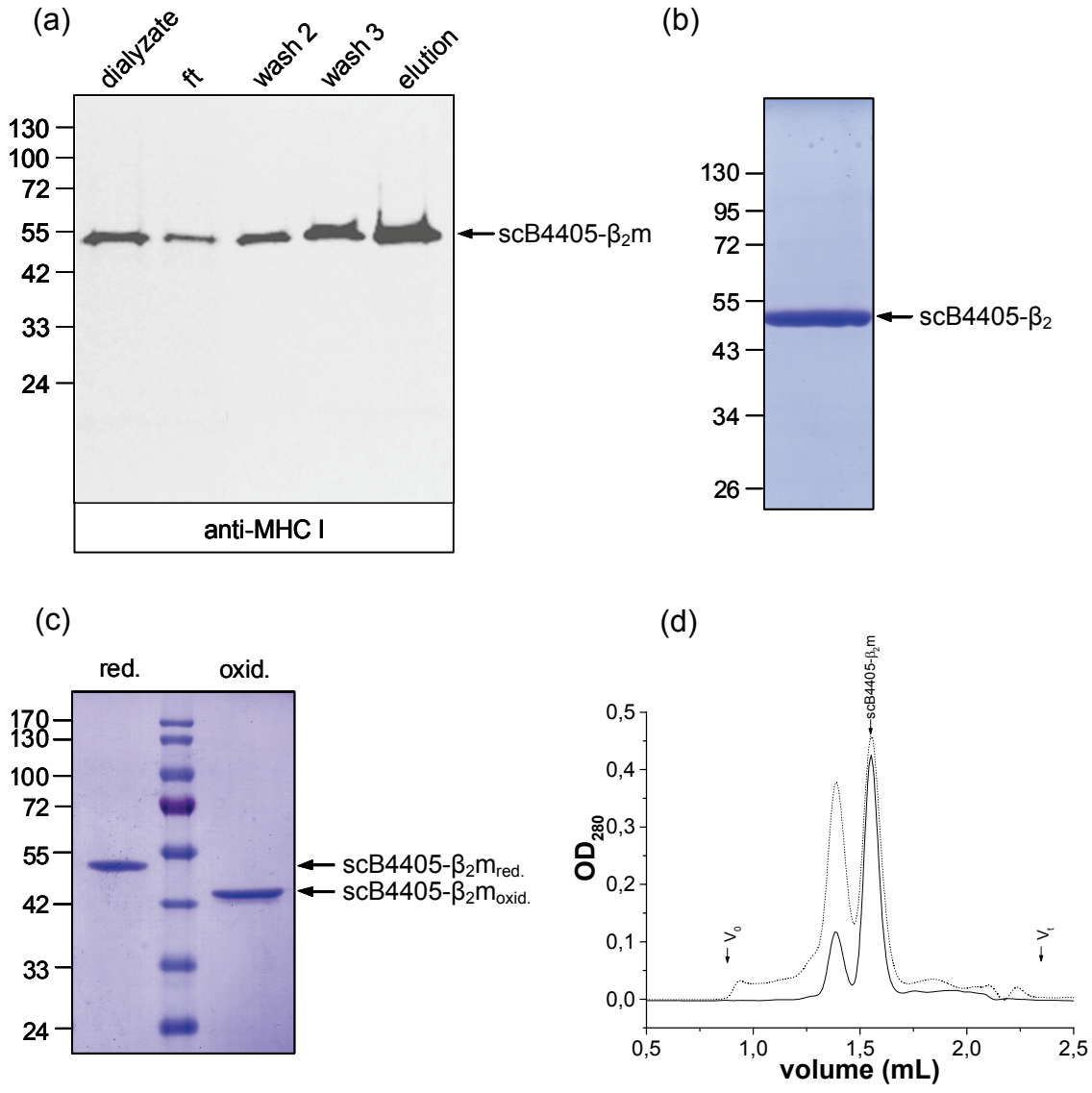

Figure 6-20. Purification of soluble single chain B4405-β_2m from *Tn*5 insect cells. 72 h post infection cells were harvested and the supernatant was dialyzed against 20 mM Tris/HCl (pH 8.0), 200 mM NaCl, changing the buffer at least three times every 8-10 h. Aliquots of the

dialyzed supernatant (dialyzate), the flow through (ft), the washing steps (wash 2, wash 3) and the elution fraction (elution) were analyzed. (a) Purification profile of scB4405-β_2m analyzed by 12% SDS-PAGE and detected with an MHC class I-specific antibody. (b) 1 µg of purified scB4405-β_2m after concentration with an ultrafiltration device (Amicon, Millipore) analyzed by SDS-PAGE (12%, coomassie-stained). (c) 1 µg of purified scB4405-β_2m were subjected to SDS-PAGE (12%, coomassie-stained) under reducing (red.) and oxidizing (oxid.) conditions. (d) The affinity-purified scB4405-β_2m (100 µg) was analyzed immediately after affinity-purification (black line) and after storage for two weeks at 4°C (250 µg, dashed line) by size exclusion chromatography (Superdex 200 PC3.2/30) by monitoring at 280 nm. The void volume (V_0 = 0.85 mL), the total volume (V_t = 2.3 mL) are indicated by arrows in the chromatogram. Molecular mass standard in kDa.

6.2.4. Purification of scB4402-β_2m expressed in *Tn*5 insect cells

The scB4402-β_2m conjugate was also produced in *Tn*5 cells infected with 10% of the total culture volume with the respective baculovirus. The expression as well as the affinity purification was performed analogous to scB4405-β_2m (for details see 6.2.3). The scB4402-β_2m conjugate with an apparent molecular mass of 49 kDa was detected with an MHC class I-specific antibody by reducing and oxidizing SDS-PAGE and immunoblotting (Figure 6-21 (a)). The oxidized state of the conjugate showed the same migration behaviour as the scB4405-β_2m conjugate, confirming proper folding (Figure 6-21 (a), oxid. lane). In comparison to the scB4405-β_2m conjugate purification, the secretion of the scB4402-β_2m conjugate into the media was drastically decreased together with the purity and the yield of approximately 20 µg per liter *Tn*5 culture. Size exclusion chromatography of the elution fraction revealed several peaks, which were subsequently analyzed by reducing SDS-PAGE (coomassie-stained) and immunoblotting with an MHC class I-specific antibody. The scB4402-β_2m was however clearly detectable in the fraction A8-B2 by immunoblotting (Figure 6-21 (b)).

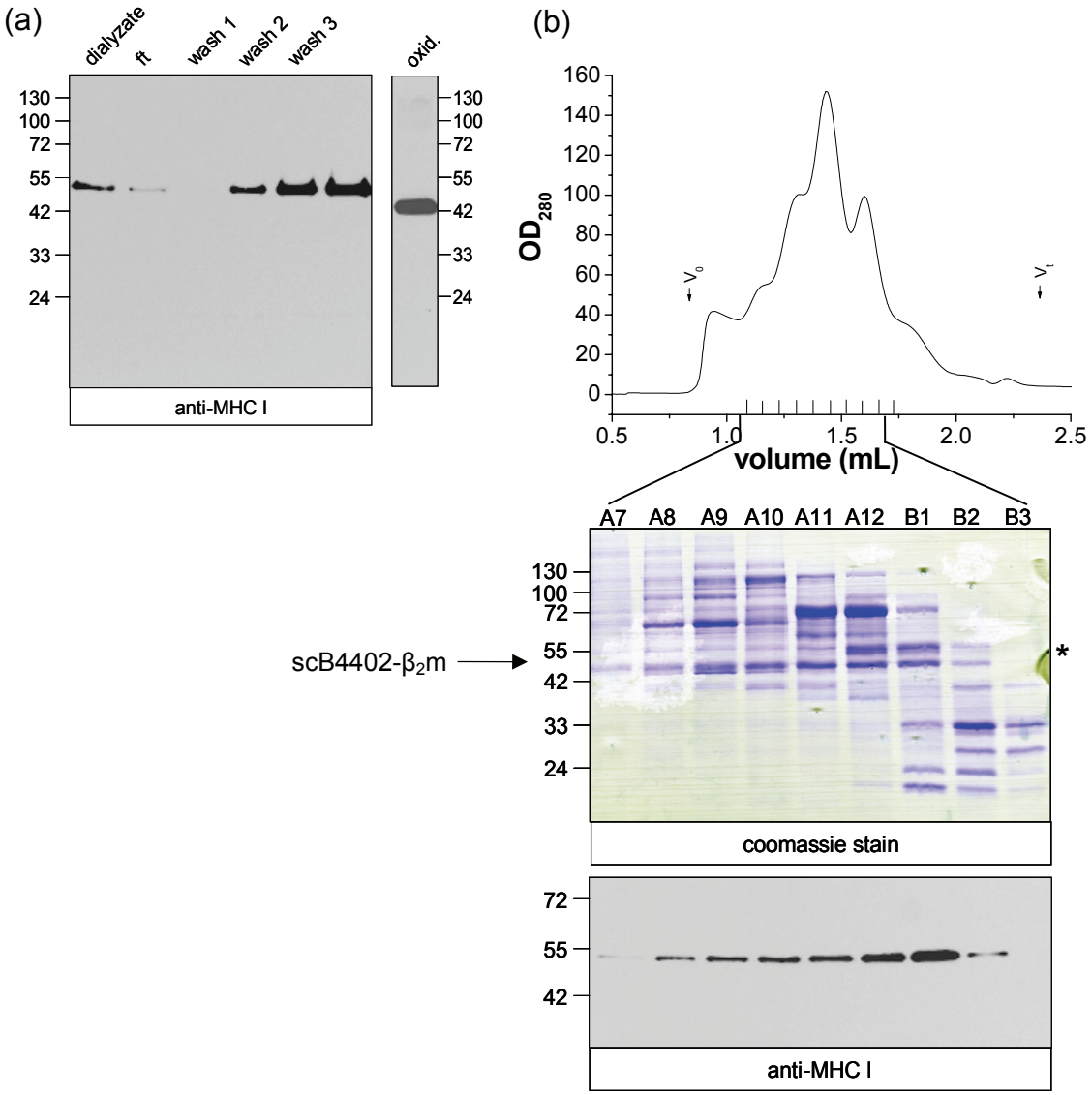

Figure 6-21. Purification of soluble single chain B4402-β$_2$m from *Tn5* insect cells. 72 h post infection cells were harvested and the supernatant was dialyzed against 20 mM Tris/HCl (pH 8.0), 200 mM NaCl, changing the buffer at least three times every 8-10 h. Aliquots of the dialyzed supernatant (dialyzate), the flow through (ft), the washing steps (wash 2, wash 3) and the elution fraction (elution) were analyzed. (a) Purification profile of scB4402-β$_2$m analyzed by reducing SDS-PAGE (12%) and detected with a MHC class I-specific antibody. An aliquot of the elution fraction was also submerged to oxidizing SDS-PAGE (12%) and immunoblotting. (b) The affinity-purified scB4402-β$_2$m (*, 200 µg) was analyzed by size exclusion chromatography (Superdex 200 PC3.2/30) by monitoring at 280 nm. The void volume (V_0 = 0.85 mL), the total volume (V_t = 2.3 mL) are indicated by arrows in the graph. Aliquots of the fractions were subjected to reducing SDS-PAGE (12%, coomasie-stained) and scB4402-β$_2$m was detected with an MHC class I-specific antibody. Molecular mass standard in kDa.

6.2.4.1. Peptide-binding to recombinant HLA-B44

The analysis of peptide-binding by the recombinant scB4405-β_2m and scB4402-β_2m conjugates was performed to analyse their functionality. First, the pH sensitivity of peptide-binding by the conjugates was investigated. For this purpose the naturally occurring ligand peptide DP$\alpha_{46\text{-}54}$ ($_{46}$EEFGRAFSF$_{54}$) was chosen. This peptide, derived from HLA-DP and shared by HLA-B4402 and -B4405 molecules, has been isolated from immunoaffinity purified HLA-B44 complexes and identified by MALDI-TOF MS (MacDonald *et al.,* 2002). This peptide was subsequently used as a matrix for the synthesis of cysteine variants (EEFGCAFSF, EEFGRCFSF, EEFGRACSF and EEFGRAFCF), which were used for fluorescein-labeling (see chapter 5.4.17). Peptide-binding by scB4405-β_2m was first investigated at pH 8.0 and pH 6.5. Here, I confirmed that peptide-deficient scB4405-β_2m expressed in insect cells as recombinant conjugates bind peptides efficiently and that peptide binding is pH dependent with a preference for basic pH (pH 8.0 was preferred compared to pH 6.5). A decrease of about 40% in peptide binding was observed at pH 6.5. Specificity of peptide binding was demonstrated by adding an excess of the non-labeled peptide as competitor (Figure 6-22).

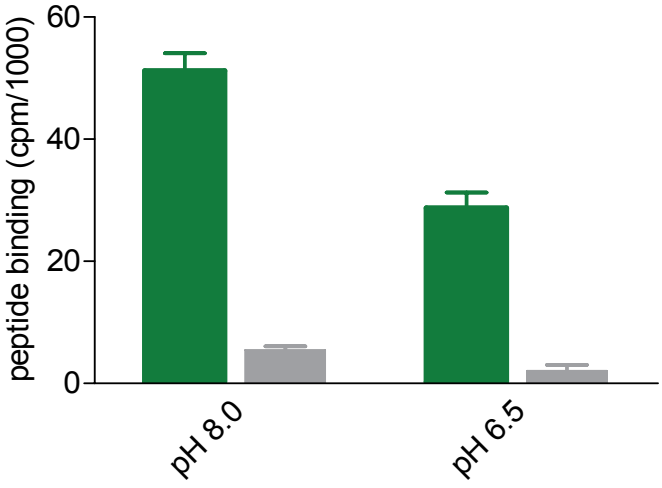

Figure 6-22. pH sensitivity of peptide binding by scB4405-β_2m. Purified scB4405-β_2m (1 µM) was pH-shocked with 0.1 M citric acid (pH 2.5) for 2 min on ice and neutralized with 1 M Tris/HCl (pH 9.0). Subsequently, buffer exchange was performed on Micro-Spin columns (Biorad) with 20 mM HEPES, pH 8.0 or pH 6.5, supplemented with 140 mM NaCl. Peptide binding was performed with 500 nM of the fluorescein-labeled peptide EEFG**C**$^{(F)}$AFSF for 12 h at 16°C (green bars). Subsequently, free peptide was removed and buffer was exchanged again to

20 mM HEPES (pH 7.5), 140 mM NaCl. The specificity of peptide binding was determined by adding a 100-fold excess of the peptide EEFGRAFSF as competitor (grey bars). Data represent the arithmetic mean of triplicate measurements.

Since the purity as well as the overall yield of scB4402-β_2m differed drastically from scB4405-β_2m, it was important to show whether the purified, peptide-deficient scB4402-β_2m conjugate is active in peptide-binding (Figure 6-23 (a)). Here, the elution fraction as well as the 20 mM washing step from the purification step (named 20 mM eluate), was analyzed, showing specific peptide binding when compared to the sample incubated additionally with a 100-fold excess of non-labeled peptide (Figure 6-23 (a)). Comparing the effective peptide binding of scB4402-β_2m and scB4405-β_2m at equal protein amount I could show that scB4402-β_2m has roughly 95% reduced peptide binding activity.

(a)

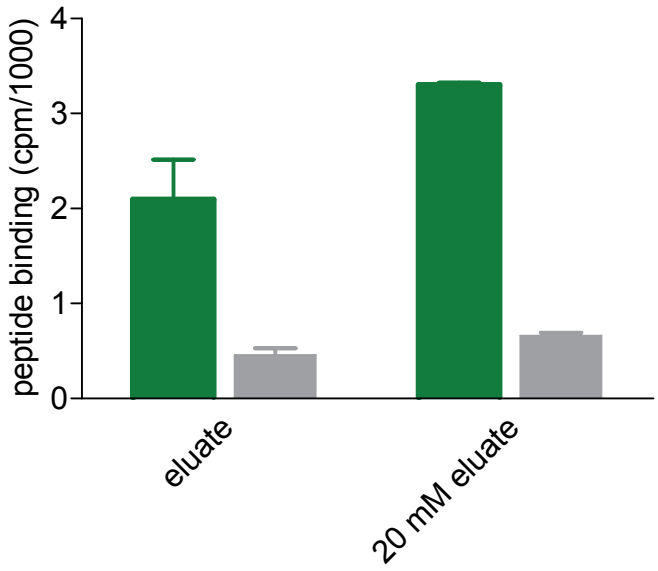

(b)

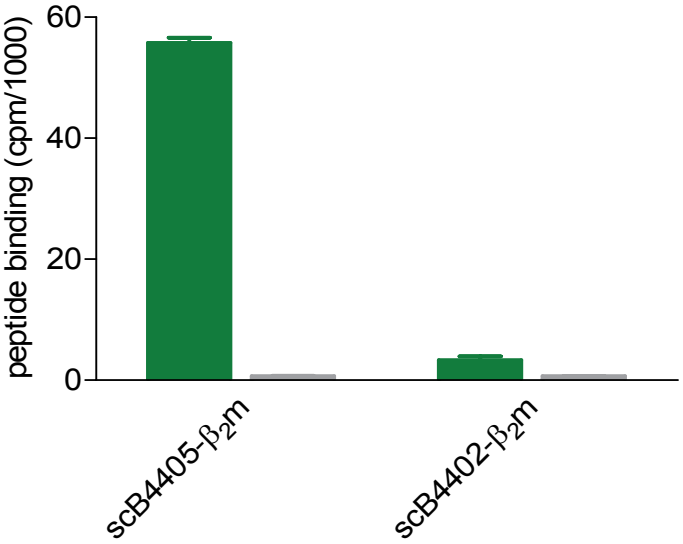

Figure 6-23. Peptide-binding to scB4405-β_2m and scB4402-β_2m. (a) 1 µM of purified scB4402-β_2m molecules, from the elution with 200 mM histidine (eluat) and from the elution with 20 mM histidine (20 mM eluate) were pH-shocked with 0.1 M citric acid (pH 2.5) for 2 min on ice and neutralized with 1 M Tris/HCl (pH 9.0). Peptide-deficient MHC I complexes were isolated on Micro-Spin columns (Biorad). Peptide-binding was performed with 500 nM of the fluorescein-labeled peptide EEFG**C**$^{(F)}$AFSF for 12 h at 16°C (black bars). The specificity of peptide-binding was determined by adding a 100-fold excess of the peptide EEFGRAFSF as competitor (grey bars). (b) Peptide-binding of 1 µM purified scB4405-β_2m in comparison to 1 µM scB4402-β_2m, as described in (a). Data represent the mean of triplicate measurements.

6.2.4.2. Monitoring MHC class I-peptide interactions in solution

To examine the kinetics of peptide association with peptide-deficient scB4405-β_2m conjugates, the binding of four fluorescein-labeled peptides derived from the naturally occurring ligand peptide DP$\alpha_{46\text{-}54}$ ($_{46}$EEFGRAFSF$_{54}$) was monitored by fluorescence anisotropy at 20°C (Figure 4-24). The scB4405-β_2m conjugates were pH-shocked and immediately mixed with the appropriate peptide prior to measurement. The obtained anisotropy profiles were collected for 12 h and data up to 30 min reaching saturation were fitted to monophasic kinetics. All anisotropy profiles followed first-order kinetics and are summarized in Table 6-6.

Table 6-6. Association kinetics of the natural ligand peptide DP$\alpha_{46\text{-}54}$ EEFGRAFSF to scB4405-β_2m

Peptides	Amplitude [x 10^{-4}]	τ [s]	k_a [10^5 $M^{-1}s^{-1}$]
EEFGRAF$C^{(F)}$F	0.09 (±2.4)	672 (±98)	0.75 (±0.02)
EEFGRA$C^{(F)}$SF	0.04 (±3.3)	1157 (±126)	0.43 (±0.04)
EEFGR$C^{(F)}$FSF	0.11 (±5.5)	300 (±27)	1.67 (±0.06)
EEFG$C^{(F)}$AFSF	0.12 (±3.6)	458 (±76)	1.10 (±0.04)

$C^{(F)}$ denotes fluorescein-labeled cysteine; time constant (τ) defined as 1/k_{obs}.

The association rate constants (k_a) of the recombinant scB4405-β_2m conjugates were found to be between 0.43×10^5 $M^{-1}s^{-1}$ and 1.67×10^5 $M^{-1}s^{-1}$ at 20°C (Table 6-6) with an amplitude ranging between 0.04 and 0.12, and are comparable to published fluorescence polarization data of MHC class I-peptide interactions in solution (Chen & Bouvier, 2007; Binz *et al.,* 2003; Dédier *et al.,* 2001). Changes in the amplitude reflect the flexibility of the fluorophore: the mobile the fluorophore the less prominent are the changes in anisotropy. Here, the fluorescein-labeled peptide, which induced a change of 0.12 in anisotropy, represents a rigid fluorophore coupled to the cysteine which is deeply anchored in the peptide-binding groove. On the contrary, an amplitude of 0.04, reflects a very flexible fluorophore coupled to a cysteine, which is not directly involved in the interaction with the peptide-binding groove. These results demonstrate the functionality of the generated recombinant scB4405-β_2m conjugate. Interestingly, anisotropy measurements performed with refolded recombinant MHC class I-β_2m heterodimer by Gakamsky and colleagues

revealed that peptide binding to as well as peptide dissociation from the MHC class I molecule are both biphasic processes (Gakamsky *et al.,* 2000). Binz and colleagues claim that peptide binding is a two-step process limited by the conformational rearrangement in the heavy chain/β_2m heterodimer. They also propose two pathways to explain the biphasic peptide dissociation: (I) peptide dissociates and leaves the heavy chain/β_2m heterodimer and (II) β_2m dissociates first from the MHC class I-β_2m-peptide complex, followed by the peptide (Binz *et al.,* 2003). In my case, the recombinant HLA-B44 heavy chain molecule is linked via a $(SG_4)_3$ linker with β_2m, preventing the dissociation of β_2m and allowing measurements of monophasic peptide association and dissociation kinetics. For scB4405-β_2m conjugates, which were not pH-shocked, the increase in anisotropy was less prominent, than for pH-shocked scB4405-β_2m conjugates, proving the fact that the recombinant complexes must be loaded with suboptimal peptides, when secreted in insect cells (Figure 6-24 (b)). The anisotropy profiles were specific as demonstrated by adding a 100-fold excess of the non-labeled competitor peptide EEFGRAFSF (Figure 6-24 (c), competition), which reduced the anisotropy signal to background level corresponding to the anisotropy observed with the free fluorescein-labeled peptide in buffer (Figure 6-24 (c), peptide + buffer).

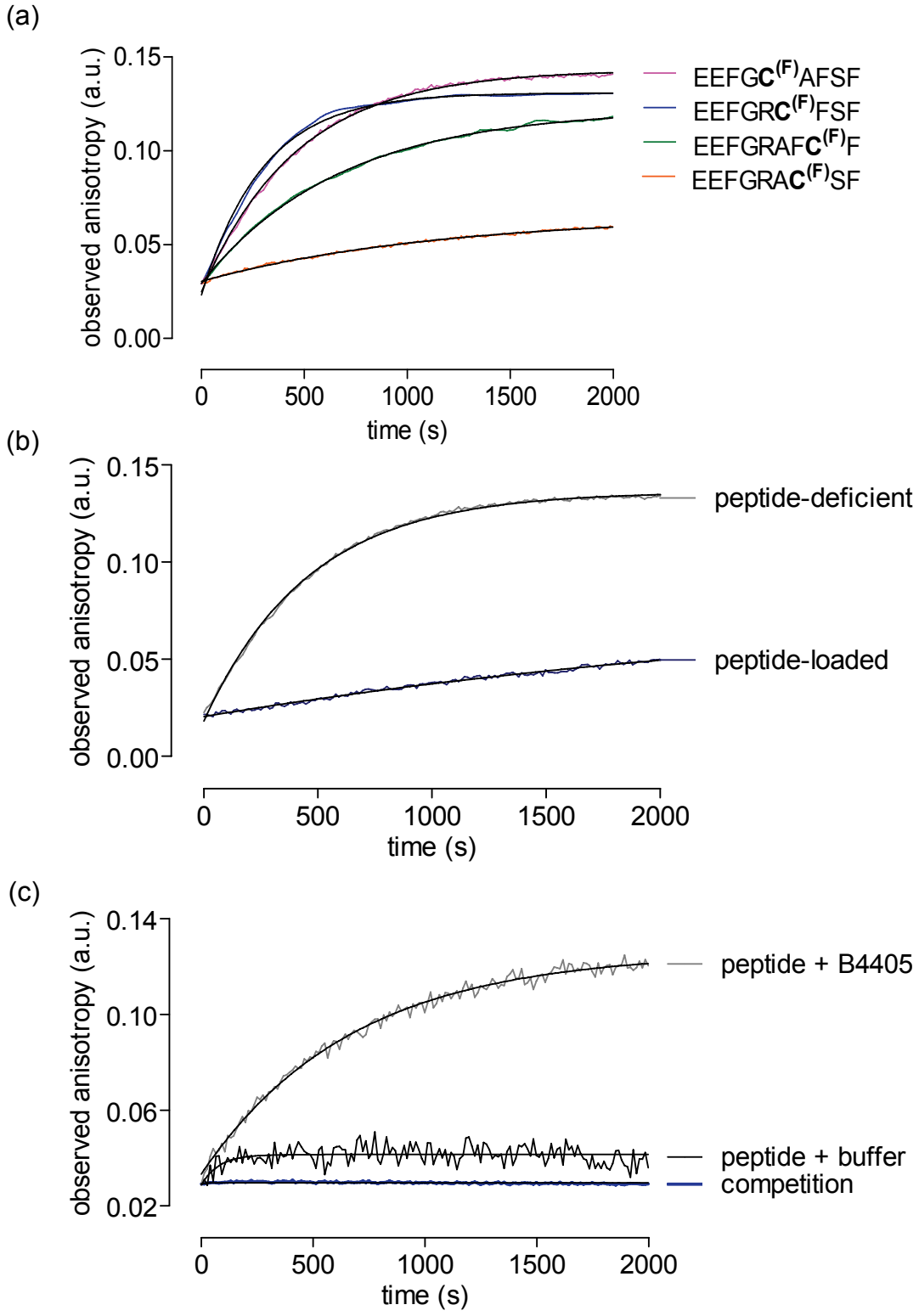

Figure 6-24. Kinetics of peptide association onto peptide-deficient scB4405-β_2m molecules. (a) 20 nM of fluorescein-labeled peptide EEFGRAF**C**$^{(F)}$F, EEFGRA**C**$^{(F)}$SF, EEFGR**C**$^{(F)}$FSF or EEFG**C**$^{(F)}$AFSF, were mixed with 1 µM of the peptide-deficient scB4405-β_2m molecules in 20 mM HEPES, 150 mM NaCl (pH 7.5). The time course of the reaction was monitored at 20°C. (b) EEFGRAF**C**$^{(F)}$F (20 nM) without (grey) or with (blue) EEFGRAFSF competitor peptide (1 µM) were mixed with 400 nM of peptide-deficient scB4405-β_2m molecules (400 nM) in 20 mM

HEPES, 150 mM NaCl (pH 7.5). The time course of the association was monitored at 20°C. (c) EEFGRAF**C**$^{(F)}$F (20 nM) was mixed with peptide-deficient scB4405-β_2m molecules (400 nM) (grey) or together with the competitor peptide EEFGRAFSF (400 nM) (blue), EEFGRAF**C**$^{(F)}$F (20 nM) alone in 20 mM HEPES, 150 mM NaCl (pH 7.5) (black). For (a), (b) and (c) data were collected for 12 h, data up to 2000 s were fitted to monophasic kinetics. Excitation and emission wavelengths were 470 and 515 nm, respectively.

Since the MHC class I-peptide complex is very stable in regard to its half-life, the dissociation kinetics were obtained by measuring one single anisotropy profile for up to 50 h. To examine the kinetics of peptide dissociation from scB4405-β_2m, the decay curves of two peptides, EEFGRAF**C**$^{(F)}$F and EEFG**C**$^{(F)}$AFSF, were monitored by fluorescence anisotropy (Figure 6-25). The decay curves followed simple first-order kinetics and are summarized in Table 6-7. For the EEFGRAF**C**$^{(F)}$F peptide a dissociation half-life (τ) of 4.5 h was determined, when data were collected for up to 14 h. The dissociation half-life changed to 17.5 h when the decay was monitored for 50 h. The corresponding amplitudes of 0.007 and 0.014, and the dissociation rate constants (k_d) of 6.16×10^{-5} s^{-1} and 1.59×10^{-5} s^{-1}, respectively, were determined by fitting to simple first-order kinetics. The EEFG**C**$^{(F)}$AFSF peptide displayed similar dissociation kinetics with a dissociation half-life of 6.8 h, an amplitude of 0.01 and a k_d of 4.08×10^{-5} s^{-1}.

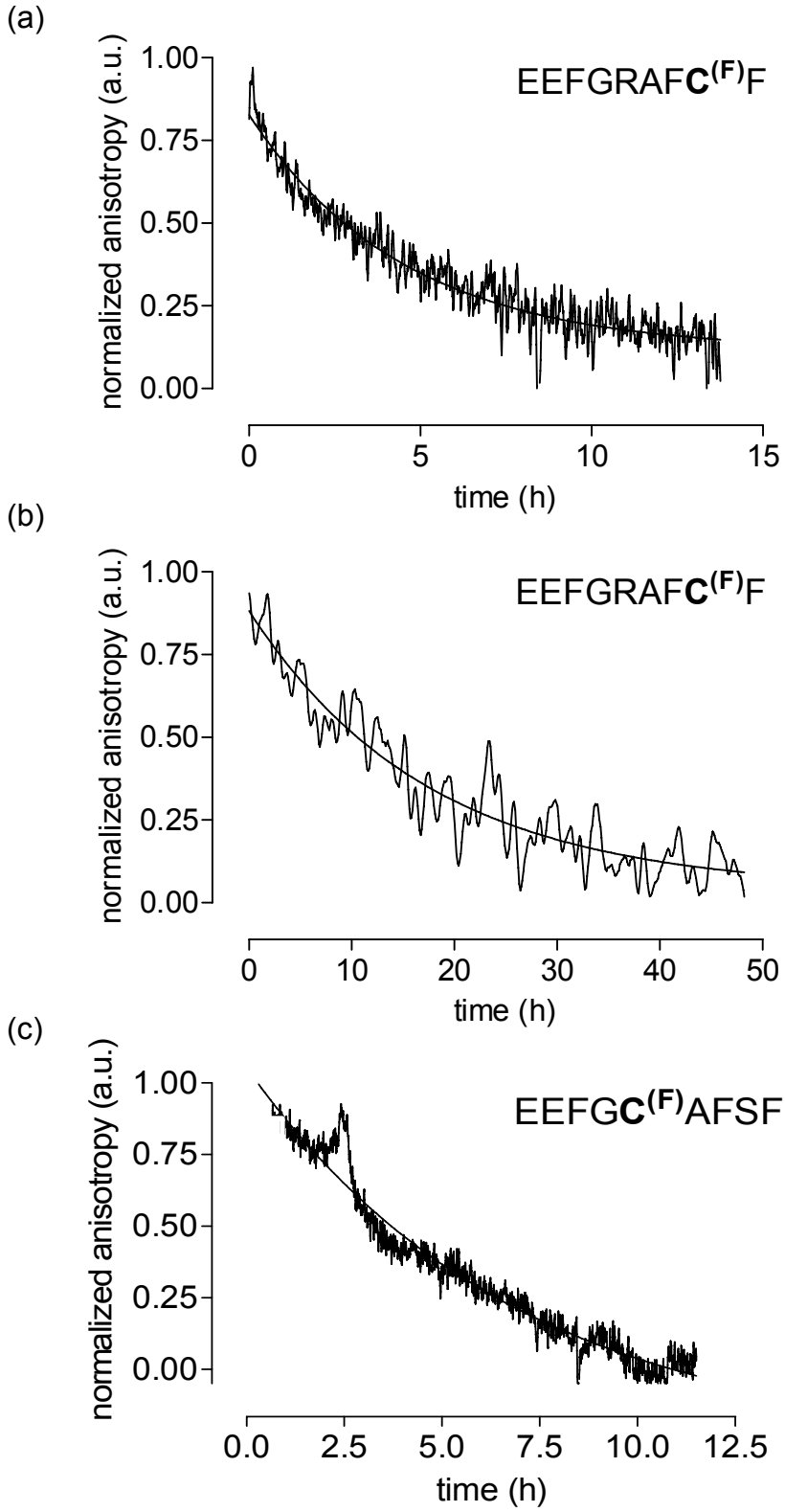

Figure 6-25. Kinetics of peptide dissociation from scB4405-β_2m. (a), (b) scB4405-β_2m (400 nM) loaded with the peptide EEFGRAFC$^{(F)}$F was added to a 10-mm cuvette containing 20 mM HEPES, 150 mM NaCl (pH 7.5). Peptide dissociation was monitored at 20°C. Excitation and emission wavelengths were monitored at 470 and 515 nm, respectively. Data points were

collected for 14 h. (b) Same set-up as in (a). Data points were collected for 50 h. (c) scB4405-β_2m (400 nM) loaded with EEFGC$^{(F)}$AFSF was added to a 10-mm cuvette containing 20 mM HEPES, 150 mM NaCl (pH 7.5). Peptide dissociation was monitored at 20°C for 12 h.

Table 6-7. Dissociation kinetics of the natural ligand peptide DP$\alpha_{46\text{-}54}$ EEFGRAFSF from scB4405-β_2m.

Peptide	Amplitude [x 10^{-4}]	τ [h]	k_d [$10^{-5}s^{-1}$]
EEFGRAFC$^{(F)}$F	0.007 (±1.3)	4.5 (±1.2)	6.16 (±0.30)
EEFGRAFC$^{(F)}$F (50 h)	0.014 (±2.2)	17.5 (±3.4)	1.59 (±0.08)
EEFGC$^{(F)}$AFSF	0.01 (±3.6)	6.8 (±0.9)	4.08 (±0.08)

C$^{(F)}$ denotes fluorescein-labeled cysteine; time constant (τ) defined as 1/k_d.

6.2.5. SPR interaction analysis of soluble tapasin and recombinant HLA-B44

To date, the dynamic assembly and disassembly of MHC class I molecules within the PLC was investigated solely *in vivo* using cell-based methods. In order to quantitatively investigate differences between individual MHC class I molecules with respect to peptide loading and its association and dissociation kinetics as well as the interaction with single proteins of the PLC, for instance tapasin, an *in vitro* assay was required. Although the peptide repertoire as well as subtype-specific folding properties and the related dependency upon the PLC were investigated, dynamic properties of MHC class I molecules have so far received comparatively little attention. Here, an *in vitro* platform was established for measuring MHC class I-tapasin interactions on solid-supported biosensors using the SPR technology. To investigate the interaction between soluble tapasin and the scB44-β_2m conjugates, a commercially available streptavidin-functionalized Biacore SA sensor chip (Biacore) was used. The Biacore SA chip was further functionalized to the multivalent chelator trisnitrilotriacetic acid biotin conjugated (^{BT}tris-NTA, Figure 6-26 (a)) (Reichel *et al.,* 2007), which allows a reversible biotinylation of histidine-tagged proteins (Figure 6-26 (b)). Subsequently, histidine-tagged tapasin was successfully immobilized at roughly 250 RUs (Figure 6-26 (c)) and the stability of the immobilization was monitored for 600 s at constant flow of HBS buffer. Due to the His_6-tag of tapasin, drifting of about 100 RUs over 800 s was

observed. The weak interactive loss of surface could not be reversed by blocking the surface after tapasin immobilization, neither with maltose-binding protein (MBP) having a His_6-tag nor with MBP bearing a His_{10}-tag (data not shown).

For probing the scB4405-β_2m conjugate on the tapasin-immobilized sensor chip, the His_6-tag at the C-terminus of the conjugate was successfully cleaved off by TEV protease (Figure 6-26 (a)). Immunoblotting against heavy chain MHC class I molecules revealed the presence of the conjugate before and after cleavage but absence of the His_6-tag after TEV protease treatment. The conjugate lacking the histidine-tag was applied for 30 s with a flow rate of 30 µL/min on the tapasin-immobilized sensor chip, displaying concentration-dependent association and dissociation rate constants (Figure 6-26 (b)).

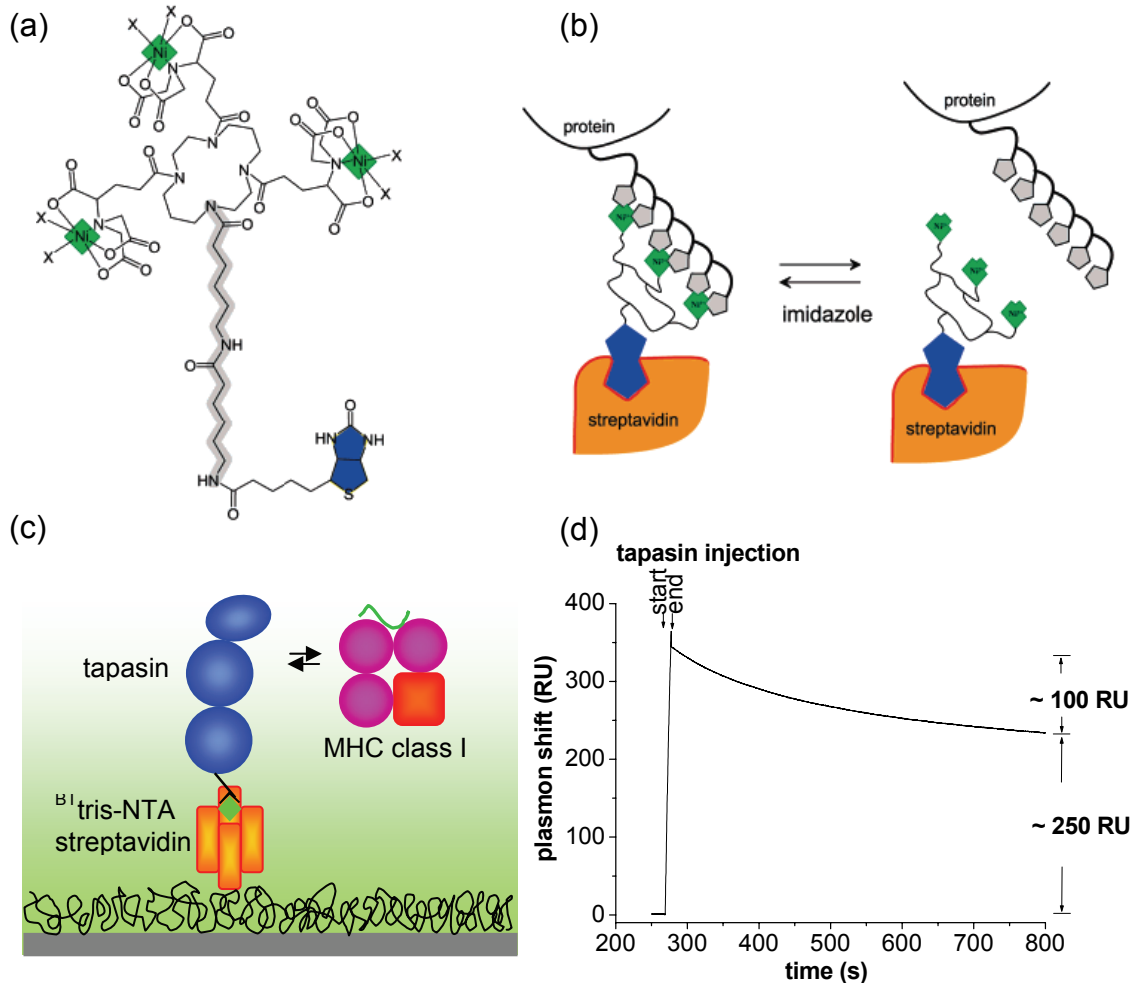

Figure 6-26. Principle of functionalization of the Biacore SA sensor chip with ^{BT}tris-NTA. (a) Chemical structure of ^{BT}tris-NTA loaded with Ni^{2+} ions. (b) Principle of the reversible biotinylation of histidine-tagged proteins according to Piehler and colleagues (Reichel *et al.,* 2007). (c) Schematic representation of the SPR setup for the investigation of the MHC class I-tapasin interaction. (d) After functionalizing the Biacore SA chip with 100 nM ^{BT}tris-NTA (flow rate 10 µL/min for 60 s), 100 nM tapasin with a C-terminal His_6-tag (flow rate of 10 µL/min for 60 s) was immobilized. The stability of immobilization was monitored for 800 s.

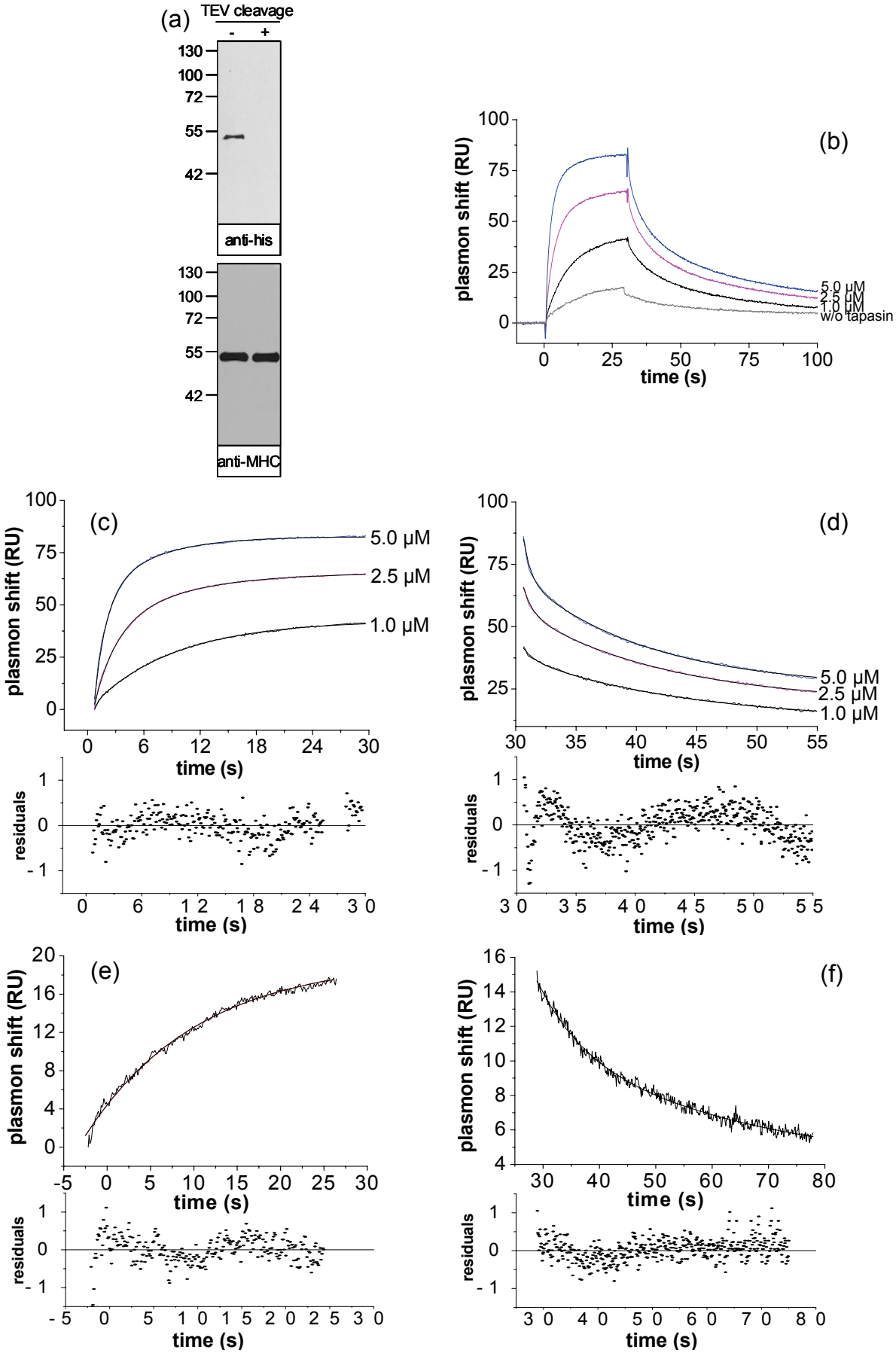
(a)
TEV cleavage
-
+
130
100
72
55
42
anti-his
130
100
72
55
42
anti-MHC
(b)
plasmon shift (RU)
time (s)
5.0 µM
2.5 µM
1.0 µM
w/o tapasin
(c)
plasmon shift (RU)
time (s)
5.0 µM
2.5 µM
1.0 µM
residuals
(d)
plasmon shift (RU)
time (s)
5.0 µM
2.5 µM
1.0 µM
residuals
(e)
plasmon shift (RU)
time (s)
residuals
(f)
plasmon shift (RU)
time (s)
residuals

Figure 6-27. Binding of scB4405-β_2m to immobilized tapasin. (a) Detection of the scB4405-β_2m conjugate (200 ng) by reducing SDS-PAGE and subsequent immunoblotting before (-) and after (+) TEV cleavage. (b) Binding of the scB4405-β_2m conjugate after TEV cleavage to the immobilized tapasin at various concentrations (1.0, 2.5 and 5.0 µM) and binding of the scB4405-β_2m conjugate (2.5 µM) after TEV cleavage to ^{BT}tris-NTA functionalized Biacore SA sensor chip without immobilized tapasin (w/o tapasin). (c) Fit and residuals for the association of the scB4405-β_2m conjugate shown in (b). (d) Fit and residuals for the dissociation of the scB4405-β_2m conjugate shown in (b). (e) Fit and residuals for the association of the scB4405-β_2m conjugate to ^{BT}tris-NTA functionalized Biacore SA sensor chip without tapasin shown in (b). (f) Fit and residuals for the dissociation of the scB4405-β_2m conjugate from ^{BT}tris-NTA functionalized Biacore SA sensor chip without tapasin shown in (b).

The association and dissociation curves for probing immobilized tapasin with scB4405-β_2m conjugate are summarized in Table 6-8. In detail, the association curves were fitted to a mono-exponential equation with k_a values of $(4.93 \pm 1.16) \times 10^4$ M^{-1} s^{-1} for 1 µM, $(6.59 \pm 1.50) \times 10^4$ M^{-1} s^{-1} for 2.5 µM and $(6.17 \pm 1.83) \times 10^4$ M^{-1} s^{-1} for 5.0 µM of the scB4405-β_2m conjugate. The dissociation curves were fitted to a bi-exponential equation with slow and fast k_d values of $(0.73 \pm 0.02) \times 10^{-1}$ s^{-1} and $(11.22 \pm 1.11) \times 10^{-1}$ s^{-1} for 1 µM, of $(0.85 \pm 0.01) \times 10^{-1}$ s^{-1} and $(13.24 \pm 0.63) \times 10^{-1}$ s^{-1} for 2.5 µM and of $(0.96 \pm 0.01) \times 10^{-1}$ s^{-1} and $(16.88 \pm 0.70) \times 10^{-1}$ s^{-1} for 5.0 µM of the scB4405-β_2m conjugate. Since the SPR technique allows a quantification of chemical association rates of up to 10^5-10^6 M^{-1} s^{-1} and dissociation rates of between 10^{-5} and 10^{-1} s^{-1}, the fast k_d value of 10^{-1} s^{-1} is very error prone. The dissociation phase deviated significantly from a single exponential decay, indicating rebinding (Figure 6-27 (d) and (f)). It can not be ruled out that the biphasic behaviour is also associated with the tapasin loss (drift) from the surface. The scB4405-β_2m conjugate interacted also with the ^{BT}tris-NTA functionalized SA surface in the absence of tapasin, yielding a response of about 12 RUs (Figure 6-27 (b), w/o tapasin). A divalent cation mediated non-specific interaction via a histidine cluster within the conjugate could not be ruled out, since both association and dissociation phases deviated strongly from the monoexponential model (Figure 6-27 (e) and (f)) with a k_a value of $(0.95 \pm 0.02) \times 10^4$ $M^{-1}s^{-1}$ and k_d value of $0.53 \times 10^{-1}s^{-1}$. Mass transfer limitations could be excluded by different immobilization levels of tapasin as well as different flow rates of the scB4405-β_2m conjugate over the immobilized tapasin.

In conclusion, the scB4405-β_2m conjugate showed a concentration-dependent interaction with immobilized tapasin. Unfortunately, biphasic dissociation kinetics did not allow a kinetically meaningful evaluation of the obtained data.

Table 6-8. Association and dissociation rate constants for the scB4405-β_2m-tapasin interaction.

scB4405-β_2m (µM)	k_a ($10^4 M^{-1}s^{-1}$)	k_d ($10^{-1}s^{-1}$)	
		slow	fast
1.0	4.93 (± 1.16)	0.73 (± 0.02)	11.22 (± 1.11)
2.5	6.59 (± 1.50)	0.85 (± 0.01)	13.24 (± 0.63)
5.0	6.17 (± 1.83)	0.96 (± 0.01)	16.88 (± 0.70)

6.2.6. SPR interaction analysis of tapasin and recombinant HLA-B27

Analogous to the SPR interaction analysis of tapasin and the scB4405-β_2m conjugate produced in insect cells, refolded soluble HLA-B2705 and HLA-B2709 alleles were probed for interaction with tapasin. The HLA-B2705 and HLA-B2709 produced in *E. coli* and refolded in the presence of a high-affinity peptide and β_2m were kindly provided by Rolf Misselwitz (Charité, Berlin). Likewise the HLA-B4405 and HLA-B4402 alleles, the HLA-B2705 and HLA-B2709 too, display distinct characteristics in regard to tapasin. The HLA-B27 is strongly associated to spondyloarthropathies, particularly ankylosing spondylitis (AS) (Khan, 2002; Ramos & Lopez de Castro, 2002). Interestingly, not all of the HLA-B27 subtypes are associated to AS. The difference between AS associated and non-associated HLA-B27 subtypes is determined mainly by very few amino acids, which predominantly affect peptide-binding properties of the MHC class I molecule. The HLA-B2709 allele is very weakly associated to AS, whereas the HLA-B2705 is tightly associated with the disease. Both alleles differ only in one amino acid at position 116: in B2709 we find His116 and in B2705 Asp116 (D'Amato *et al.,* 1995). These amino acids at position 116 are located within the peptide binding cleft at the floor of the F pocket. Furthermore, both alleles display different dependencies on tapasin: HLA-B2709 shows tapasin dependency for peptide presentation on the cell surface, whereas HLA-B2705 is tapasin-independent in regard to the presentation of peptides on the cell surface.

The interactions of tapasin with the HLA-B27 alleles were probed on the Biacore SA chip functionalized to the ^{BT}tris-NTA, which allows a reversible biotinylation of histidine-tagged proteins (for details see 6.2.5). Subsequently, histidine-tagged tapasin was successfully immobilized at roughly 40 RUs (Figure 6-28 (a)) and stability of the immobilization was monitored for 400 s at constant flow of HBS buffer. Following immobilization of tapasin, peptide-loaded and peptide-deficient HLA-B2709 and HLA-B2705 were probed, respectively, for interaction (Figure 6-28). The peptide-deficient HLA-B27 molecules were generated as described in chapter 5.4.18. As a result, binding of the tapasin-dependent HLA-B2709 to the immobilized tapasin was only detectable in its peptide-deficient state (Figure 6-28 (a) black curve) whereas peptide-proficient molecules showed no interaction (Figure 6-28 (a), blue curve). This interaction was specific for the immobilized tapasin as confirmed by control experiments without tapasin on the surface (data not shown). Further, there was no measurable interaction of the tapasin-independent HLA-B2705 and tapasin neither in peptide-deficient nor -proficient state at 5 µM of HLA-B2705 (Figure 6-28 (b)). Since it was not possible to determine R_{eq} from titration curves at various protein concentrations due to low concentrations of HLA-B2709, it was not possible to calculate a K_D value. Instead, the association and dissociation curves were fitted to a biphasic exponential equation which could also be a characteristic for changes in the refractive index. A slow and a fast k_a value of (1.15 ± 0.7) × 10^4 M^{-1} s^{-1} and (1.52 ± 0.9) × 10^5 M^{-1} s^{-1} as well as a slow and a fast k_d value of 0.13 ± 0.07 s^{-1} and 1.60 ± 1.00 s^{-1}, respectively, were determined. Also here, since the SPR technique allows a quantification of chemical association rates of up to 10^5-10^6 M^{-1} s^{-1} and dissociation rates of between 10^{-5} and 10^{-1} s^{-1}, the fast k_d value of 1.60 ± 1.00 s^{-1} is error prone. It could not be excluded that the biphasic behaviour was due to the dissociation of the immobilized tapasin from the surface.

B2709 (µM)	k_a ($10^4 M^{-1}s^{-1}$)		k_d ($10^{-1}s^{-1}$)	
	slow	fast	slow	fast
5.0	1.15 (±0.7)	15.20 (±0.9)	0.13 (± 0.07)	1.60 (± 1.0)

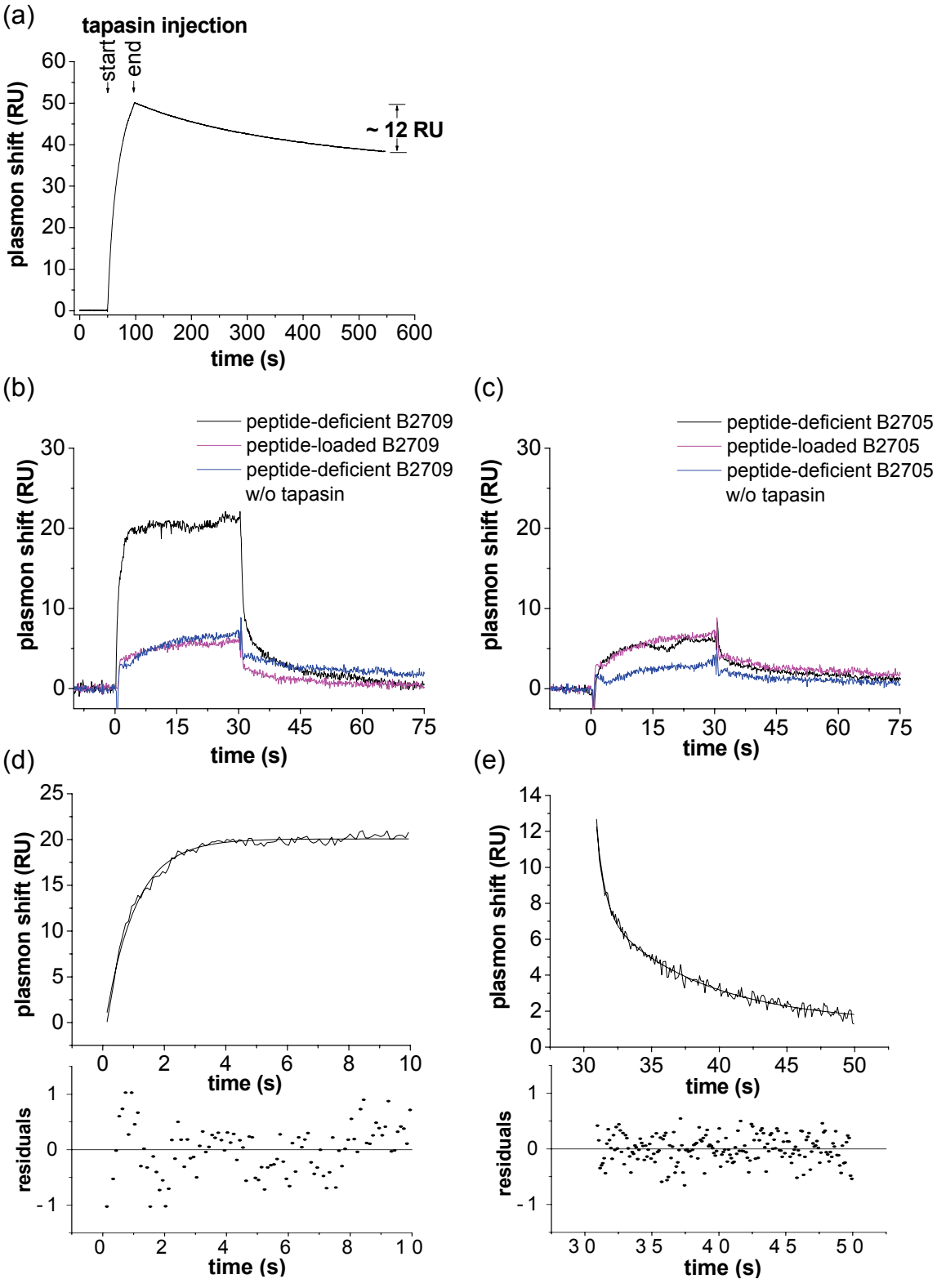

Figure 6-28. Binding of HLA-B2709 and HLA-B2705 to immobilized tapasin on a functionalized ^{BT}tris-NTA sensor chip. (a) The BIAcore SA chip was functionalized with 100 nM ^{BT}tris-NTA, with a flow rate of 10 µL/min for 60 s, following immobilization of 50 nM tapasin with a C-terminal His_6-tag with a flow rate of 10 µL/min for 60 s. Stability of the tapasin immobilization was monitored for 400 s. Binding of peptide-deficient (black) and peptide-proficient (blue)

HLA-B2709 (5 µM; (b)) and HLA-B2705 (5 µM; (c)) to immobilized tapasin or to ^{BT}tris-NTA functionalized Biacore SA sensor chip without immobilized tapasin (peptide-deficient B2709 w/o tapasin, peptide-deficient B2705 w/o tapasin ((b), (c), magenta). (d) Fit and residuals of the association of the peptide-deficient B2709 to the tapasin-immobilized ^{BT}tris-NTA functionalized sensor chip. (e) Fit and residuals of the dissociation of the peptide-deficient B2709 from the tapasin-immobilized ^{BT}tris-NTA functionalized sensor chip.

7.2.7. Influence of tapasin on the peptide dissociation from HLA-B44

The analysis of the MHC class I-tapasin interaction by SPR spectroscopy revealed difficulties in quantification due to transient, low affinity interaction, and consequently limitation in protein amount. Additionally, surface-exposed clusters of two histidines within the heavy chain MHC class I molecules contributed to non-specific interaction with the ^{BT}tris-NTA chelator groups. Thus the influence of tapasin on peptide dissociation from the scB4405-β_2m conjugate was monitored in real-time by simultaneous total internal reflection fluorescence spectroscopy (TIRFS) and reflectance interferometry (RIf) detection (Gavutis *et al.,* 2005) on lipid bilayers fused to a glass substrate to ensure lateral mobility, in cooperation with Dirk Paterok und Jacob Piehler (Institute of Biochemistry, Goethe University). The proper formation and thickness of the bilayer was monitored by RIf system before conditioning (imidazole, EDTA, Ni^{2+}). Here, the scB4405-β_2m conjugate loaded with fluorescein-labeled peptide (EEFG**C**^{F}AFSF) was immobilized via the C-terminal His_6-tag on a chelatorlipid mimicking the anchoring by the transmembrane domain, and the stability of immobilization was monitored for about 350 s before tapasin was injected. After 300 s non-labeled high affinity peptide (EEFGRAFSF) was injected and the peptide dissociation was monitored in the TIRFs channel (Figure 6-29).

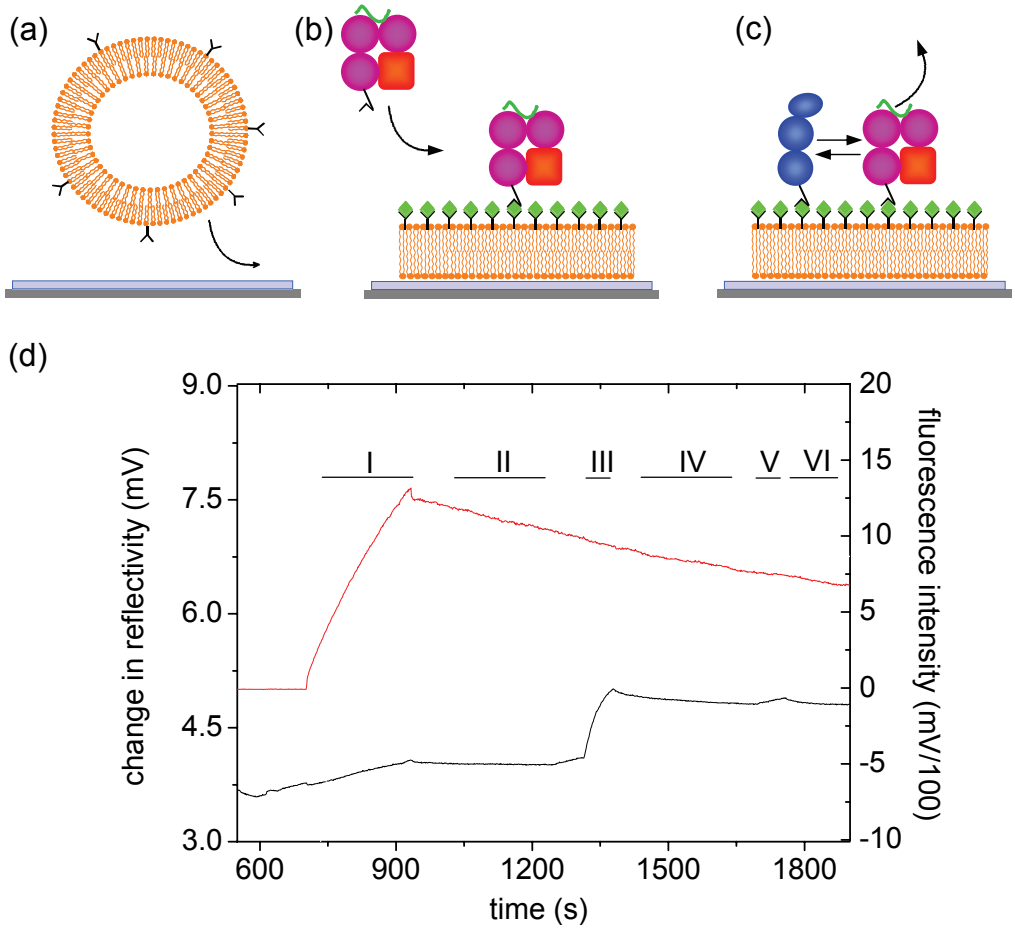

Figure 6-29. Influence of tapasin on peptide exchange by the scB4405-β_2m conjugate. (a) Schematic model of a co-immobilization experiment consisting of the generation of a fluid lipid bilayer by fusing unilaminar vesicles to the surface, (b) after immobilization of MHC class I molecules loaded with fluorescein-labeled peptide, (c) tapasin is probed. (d) Interference signal (black) and fluorescence signal (red) during immobilization of scB4405-β_2m (I, 150 nM), stability of immobilization (II), tapasin injection (III, 500 nM), buffer flow after tapasin injection (IV), EEFGRAFSF peptide injection (V, 100 µM), buffer flow after EEFGRAFSF peptide injection (VI).

Table 6-9. Dissociation kinetics of the fluorescence signal

	k_d ($10^{-4}s^{-1}$)	τ [h]
II	6.42 (±0.31)	0.43 (±0.21)
III	8.23 (±0.26)	0.33 (±0.13)
IV	6.32 (±0.38)	0.44 (±0.15)
V	4.63 (±0.41)	0.60 (±0.20)
VI	6.78 (±0.60)	0.41 (±0.19)

In the simultaneous TIRFS-RIfs system fluorescence-labeled as well as label-free detection of interacting molecules is advantageous in comparison to the

SPR spectroscopy, where interaction of proteins is solely based on mass changes on the sensor surface. Here, the role of tapasin, as peptide editor, on the fluorescein-labeled peptide loaded onto the scB4405-β_2m conjugate was further investigated. Unfortunately, no significant differences in the peptide dissociation rates were observed, neither during or after tapasin injection nor during or after non-labeled peptide was injected as depicted from the fluorescence signal (red curve) shown in Figure 6-29. The k_d values derived from fitting the fluorescence signal to a mono-exponential decay are summarized in Table 6-9 and are 10-fold faster than the peptide dissociation kinetics obtained by anisotropy measurements. It is reasonable that a tapasin-dependent MHC class I allele is needed to further investigate the peptide-editing role of tapasin. Unfortunately, the tapasin-dependent scB4402-β_2m I generated, was not secreted properly and therefore not available for further tapasin interaction studies. Furthermore, recombinant and refolded HLA-B27 molecules are tag-less and were also not available for probing with tapasin. Recently, Wearsch and colleagues reported in a cell-free system, that recombinant soluble tapasin was ineffective in recruiting MHC class I molecules and facilitating peptide binding. However, they showed, that recombinant tapasin-ERp57 conjugates accomplished not only both of the above mentioned functions but also were capable to edit the repertoire of bound peptides to increase their affinity (Wearsch & Cresswell, 2007). The investigation of peptide dissociation kinetics in the presence of the tapasin-ERp57 conjugate, instead of tapasin alone, may shed light on the dynamics of reassembly of the subcomplex.

7. Discussion

7.1. Recombinant antibodies as extrinsic modulators of the antigen peptide transporter TAP

The major and rather unexpected finding of this systematic study is that the peptide transport of human TAP can be inhibited by antibodies that specifically recognize a discrete linear epitope comprised of the very last five C-terminal amino acid residues of TAP1 (^{744}ADAPE^{748}). In addition, these antibodies strongly stabilize the heterodimeric TAP complex against rapid thermal inactivation in the absence of ATP. Since no other region within TAP was recognized by the antibodies both effects are exclusively linked to the C-terminus of TAP1.

7.1.1. Expression, purification and characterization of the recombinant antibodies

Here, I generated recombinant Fv, scFv and Fab fragments by genetic engineering from hybridoma cells expressing the mAb148.3. First, the recombinant antibody fragments were heterologously expressed in *E. coli*. Both the Fv and Fab fragments from *E. coli*, were purified to homogeneity and monodispersity as demonstrated by SDS-PAGE, immunoblotting, and size exclusion chromatography (Figure 6-3). However the low yield, especially of the Fab fragment, supported the decision to choose an alternative strategy, and switch to *Sf*9 insect cells as expression host. As for other eukaryotic expression systems, insect cells provide their own eukaryotic chaperones mediating correct folding in the endoplasmatic reticulum (ER) as well as posttranslational modification similar to those found in mammalian cells. In this work a novel expression strategy for recombinant antibodies in insect cells was successfully established. The combination of the advantages of genetic engineering in baculovirus together with the processing machinery of the *Sf*9 secretion pathway provided an efficient expression system for recombinant antibodies.

The expression vectors pFastBac 1 and pFastBacDual were modified by inserting a leader peptide from the pro-melittin gene of honeybee for secretion of the recombinant proteins. The scFv as well as the Fab fragments were expressed and secreted into the insect cell medium. They were subsequently purified to homogeneity and monodispersity as demonstrated by SDS-PAGE, immunoblotting, and size exclusion chromatography (Figure 6-4). Moreover, successful formation of disulfide bonds in the immunoglobulin domains was confirmed by oxidizing SDS-PAGE (Figure 6-4 (a)). The yield of 2-4 mg/L cell culture was an increase by a factor of 10-20 for the scFv and by a factor of 100-200 for the Fab fragment compared to expression in the periplasm of *E. coli*.

7.1.2. Characterization of the antigen-antibody interaction

Based on kinetic and thermodynamic analysis, the epitope-paratope interaction was characterized in detail and compared with the parental antibody demonstrating nanomolar affinity of the monovalent antibody fragments for TAP1. The equilibrium binding constants of the recombinant antibodies as well as of the mAb148.3 were determined by ELISA (Figure 6-5; Figure 6-6) and SPR using the isolated NBD and the C-terminal epitope peptide CYWAMVQAPADAPE of TAP1, respectively, as antigen (Figure 6-7). The K_D values for the monovalent recombinant Fv and Fab fragments are very similar. Moreover, the K_D of the monovalent proteolytic Fab fragment of the mAb148.3 for the NBD of TAP1 is in the same range as for the recombinant antibody fragments.

7.1.3. Dissection of the inhibition mechanism

Surprisingly, the recombinant Fv fragment inhibits TAP-dependent peptide translocation into the ER similar to viral factors such as ICP47 of herpes simplex virus or US6 of human cytomegalovirus. Transport inhibition of the monovalent Fv fragment and the intact mAb148.3 was equally efficient (Figure 6-13). This observation demonstrates that inhibition results from a direct interaction of the paratopes with the C-terminus of TAP1 and not from steric effects caused by the

Fc regions of the intact antibodies or cross-linking of adjacent TAP heterodimers because of the bivalent interactions of the mAb148.3. To elucidate the inhibition mechanism I considered interference with ATP or peptide binding to the TAP complex. However, I could not detect an adverse effect on ATP or peptide binding in the presence of the Fv fragment, illustrating that the overall integrity of the heterodimeric TAP complex is maintained (Figure 6-14). Strikingly, the recombinant antibody fragments stabilize the TAP complex similar to ATP. The peptide-binding capacity of TAP was maintained over 2 h, whereas only 10% of remaining TAP activity was observed in the absence of Fv fragment (Figure 6-15). Moreover, the presence of antibody fragments decelerated peptide dissociation kinetics from the purified TAP complex, inhibiting the dissociation of the TAP complex (Figure 6-16). These results are reminiscent of observations made during characterization of the recently identified TAP-specific viral inhibitor UL49.5 from bovine herpesvirus 1 (BHV-1). This protein employs two mechanisms to inhibit peptide translocation: (I) arrest of the transporter in a functionally incompetent conformation and (II) induction of proteasomal degredation of components of the peptide-loading complex (Koppers-Lalic *et al.,* 2005). However, this effect could be explained by either protection from proteolytic degradation or stabilization of the TAP complex.

By binding to the C-terminus of TAP1, the antibodies presented in my study, arrest TAP in a transport-incompetent state. Several lines of argumentation have to be considered: The X-ray crystal structure of the isolated NBD of human TAP1 bound to ADP-Mg^{2+} was solved at a resolution of 2.5 Å (Gaudet *et al.,* 2001). However, the structure of the last six C-terminal amino acid residues, which contain the epitope of the mAb148.3, was not resolved, indicating high flexibility of this region in the ADP-bound monomeric state of the NBD. Based on truncation studies and chimeras of rat TAP1 and TAP2, Knittler and colleagues could show that the C-terminal tails of TAP1 and TAP2 are non-equivalent (Bouabe *et al.,* 2003). It became also evident that the control of nucleotide interaction in the NBD of TAP1 is more complex than in the NBD of TAP2. Although nucleotide binding to the NBDs can be modulated by both C-terminal tails, the exchange of ADP to ATP within the NBD of TAP1 is restricted to the intrinsic C-terminal tail. Interestingly, the C-terminal tail of the NBD of TAP1 can force the NBD of TAP2 to adapt the same ATP binding

properties as the NBD of TAP1, and the transporter containing two C-terminal tails of TAP1 has a remaining peptide transport activity of only 30% when compared to wild-type TAP (Bouabe *et al.,* 2003). More recently, it was suggested that the so-called α6/β10-loops close to the C-termini of TAP1 and TAP2 determine the non-synonymous nucleotide binding of the two NBDs (Ehses *et al.,* 2005). However there is no indication from structural or biochemical studies that the α6/β10-loop region makes direct contact with bound ATP or ADP, suggesting that the α6/β10-loops contribute to the regulation of nucleotide binding in a conformational rather than a sequence-specific manner.

The recombinant antibody fragments generated here did not affect ATP binding to TAP. However, peptide translocation was significantly inhibited. Considering the potential importance of the α6/β10-loop, the distance between this region and the epitope of the antibodies at the C-terminus of TAP1 might be too large to fully disturb the intramolecular cross-talk within the NBD of TAP1. Inhibition of peptide transport was highly specific, since the mAb435.3 directed against TAP2 showed absolutely no effect on peptide transport even at a concentration of 10 µM. If the affinity of mAb435.3 were to be 1,000-fold lower than that of mAb148.3 I would still have expected to see an effect on peptide transport. Furthermore, the fact that mAb435.3 is widely used in co-immunoprecipitation studies of TAP and the peptide-loading complex, demonstrates that the native conformation of TAP2 is recognized with a reasonable affinity. Notably, the TAP-specific viral inhibitor ICP47, which displays a similar equilibrium binding constant (50 nM, Beinert *et al.,* 1997) to the Fv fragment (32 nM), inhibits peptide translocation to a similar extent (75%) when used at a concentration of 10 µM.

It is commonly accepted that ATP binding to the NBDs of ABC-transporters induces the formation of a composite dimer, which in turn is required for productive ATP hydrolysis (Jones *et al.,* 2004). Several sequence motifs of both NBD monomers contribute to dimer formation, most importantly the Walker A motif and the C-loop (Zaitseva *et al.,* 2005, Smith *et al.,* 2002, Chen *et al.,* 2003). The crystal structure of the HlyB-NBD dimer bound to ATP-Mg^{2+} provides evidence that also the C-terminus of the NBDs contributes

to the dimer interface (Zaitseva *et al.,* 2005). This suggests one possible explanation of the data presented here, namely that the antibody-mediated inhibition of the TAP-dependent peptide transport is due to interference with the formation of a stable dimer interface between the NBDs of TAP1 and TAP2. Notably, alignment of HlyB and TAP1 shows little conservation of the C-terminal 20 residues. However, of the few dimeric NBD structures of ABC transporters available, HlyB is the closest relative to TAP. At this stage, therefore, I can only suggest a direct contribution of the C-terminus of TAP1 to the dimer interface. In order to provide strong experimental proof we have to rely on high-resolution 3D structures of a TAP heterodimer, which are not available yet.

Within the current study, a detailed analysis of the inhibition mechanism of TAP-dependent peptide transport is provided (peptide binding, ATP binding). The only open issue is whether TAP is inhibited by steric hindrance of the recombinant antibody fragments or by neutralizing a possible direct functional role of the C-terminus of TAP1. Therefore, studies with the isolated NBDs would be required. However, nobody in the field has so far managed to form a non-artificial heterodimer of the NBDs of TAP1 and TAP2 in solution. Finally, even if available, it remains questionable whether the isolated NBD dimer represents a valid model system for the TAP heterodimer within the ER membrane.

In conclusion, the recombinant antibody fragments generated here proved useful to analyze the functional importance of the very last amino acid residues at the C-terminus of TAP1. Moreover, the antibodies represent valuable tools to modulate TAP function and might prove useful in the structural analysis and 3D-crystallization of the TAP complex.

7.2. Tapasin and MHC class I molecules: Intrinsic modulators of the antigen peptide transporter TAP

The presentation of endogenous peptides by major histocompatibility complex (MHC) class I molecules to cytotoxic T-lymphocytes ($CD8^+$) on the surface of nucleated cells is a prerequisite for eliminating infected or malignantly transformed cells (Lehner *et al.,* 2004, Yewdell & Haeryfar, 2005). The highly regulated process of high-affinity loading of an optimized pool of peptides onto MHC class I involves the interplay of specialized proteins including the lectin chaperones calnexin and calreticulin, the class I-specific accessory molecule tapasin, the thiol-disulfide oxidoreductase ERp57, the protein disulfide isomerase (PDI), and the heterodimeric peptide transporter TAP1/2 within the endoplasmic reticulum (ER) (Paulsson & Wang, 2004, Antoniou *et al.,* 2003; Ahn *et al.,* 2006). To dissect this elaborate pathway and to develop a mechanistic understanding of peptide loading and peptide selectivity, including the necessary interplay of other components of the PLC, an *in vitro* assay is indespensable. The prerequisite for performing functional *in vitro*-based assays is the establishment of an efficient expression and purification system for the recombinant proteins. In the current study, I report for the first time human MHC class I molecules engineered as single chain MHC class I-β_2m complexes including a honeybee secretion signal sequence for the secretion in insect cells. Moderate yields of purified functional MHC class I scB44-β_2m conjugates as well as tapasin were achieved. Furthermore, a peptide-binding assay as well as a homogenous assay to monitor MHC class I-peptide assembly in solution was established to verify functionality of the recombinant MHC class I molecules. Last but not least, an *in vitro* platform for probing MHC class I-tapasin interactions on biosensors was developed. Two recombinant MHC class I alleles, HLA-B27 and HLA-B44, as well as tapasin were probed for interaction by SPR and TIRF spectroscopy.

7.2.1. Expression, purification, and characterization of single chain B44 conjugates

The choice of an expression system for heterologous expression of human proteins very often demands a compromise between yield and functionality. The heterologous expression of recombinant proteins in *E. coli*, the working horse for recombinant protein production, is very often associated with high expression yields but mostly the proteins are insoluble and therefore inactive. Hence, elaborate refolding methods have to be established. Besides the tedious refolding process bacteria lack also the post-translational modification machinery, often needed for protein-protein interactions, which is present in eukaryotic organisms (Sambrook *et al.,* 1998). Here, the insect cell expression system was applied, which is widely used to produce high quantities of post-translationally modified human soluble as well as transmembrane proteins. Selecting the insect cells as hosts for the production of human recombinant MHC class I molecules, the functionality of the recombinant proteins was a major criterion, which was addressed. Hence, for the biochemical and the biophysical characterization it was necessary that the heterologously expressed recombinant MHC class I molecules could be loaded with defined peptides, designed here. Additionally a fluorescence-based peptide-binding assay was necessary to verify the functionality of the recombinant MHC class I molecules as well as a fluorescence polarization-based assay to directly monitor the kinetics of peptide-binding to the recombinant MHC class I molecules.

Here, I successfully expressed HLA-B4402 and HLA-B4405 fused to β_2m via a $(SG_4)_3$ linker, resulting in single chain conjugates. The leader peptide from the pro-melittin gene of the honeybee was employed for secretion of the recombinant MHC class I conjugates (Figure 6-19). The scB4405-β_2m conjugate was purified to homogeneity in a single step purification yielding 100-200 µg/L cell culture. Size exclusion chromatography revealed a monodisperse protein peak running at approximately 49 kDa (Figure 6-20). Peptide binding and anisotropy measurements verified the functionality of the scB4405-β_2m conjugate, thus demonstrating insect cells as the appropriate expression host (Figure 6-22; 6-23; 6-24; 6-25). Kinetic studies of scB4405-β_2m-peptide complexes carried out with variants of the naturally occurring ligand peptide

EEFGRAFSF (with introduced cysteines at various positions (position 5-8)), revealed no significant changes in the association and dissociation rate constants (Figure 6-24; 6-25). Thus by substituting define amino acids in the ligand peptide EEFGRAFSF to cysteines and subsequent fluorescein-labeling, I did not succeed in generating short-lived peptide for suboptimal loading of the scB44-β_2m conjugates for direct comparison with optimal loaded molecules. The association and dissociation rate constants ($10^5 \times M^{-1}s^{-1}$ and $10^{-5} \times s^{-1}$) of the scB4405-β_2m conjugate are comparable to those published ones (Chen *et al.,* 2007). However, the obtained dissociation rate constant may be error prone due to the stability of the complex and consequently the slow dissociation rate constant as well as the experimental setup monitoring the dissociation for up to 50 h. The scB4402-β_2m conjugate was also successfully expressed (Figure 6-19 (c)) but the secretion into the medium was drastically decreased with the immediate consequence that it was very difficult to purify. The purified scB4402-β_2m conjugate, as shown by coomassie-stained SDS-PAGE and verified by immunoblotting, represented only a minor portion of the abundant proteins in the eluate (Figure 6-21). Furthermore, in the size exclusion chromatography the scB4402-β_2m conjugate was distributed over several fractions, as detected by immunoblotting, indicating polydisperse behaviour of the protein. This is indicative for misfolded, unstable, or unfolded proteins. However, unfolded scB4402-β_2m conjugate would not display different running behaviour under reducing and oxidizing conditions as detected by immunoblotting (Figure 6-21, oxid. lane). When testing for functionality it was clearly demonstrated that it showed peptide-binding activity, however representing only 10% of the scB4405-β_2m conjugate activity (Figure 6-23). Taking into account the fact that both molecules display great differences in their purity may reflect the difference in peptide-binding activity. Since both proteins, scB4405-β_2m and scB4402-β_2m, differ only in one amino acid it is very surprising how drastically this might affect the secretion, thus providing an insight into the intrinsic instability and therefore sequestration within the ER. It is known, that single MHC class I alleles differ in their selectivity of peptide loading depending on tapasin. While some HLA-alloforms are barely presented on the cell surface of tapasin$^{-/-}$-cells, others show only minor differences in comparison to tapasin$^{-/-}$-cells transfected with tapasin (Greenwood *et al.,* 1994,

Ortmann *et al.,* 1997, Peh *et al.,* 1998, Lewis *et al.,* 1998, Barnden *et al.,* 2000). A direct comparison showed that HLA-B2705 and HLA-A202, tapasin-independent alleles, are present at the cell surface of .220-cells, a tapasin deficient cell line. By contrast, the expression of HLA-B4402, highly tapasin-dependent allele, was drastically impaired in those cells. The HLA-B8 allele presented an average dependency on tapasin (Peh *et al.,* 1998). Based on these results the original hypothesis was that some HLA-alloforms, for instance HLA-B2705, were loaded with high affinity peptides in the absence of tapasin and that individual MHC class I molecules were affected differently by the tapasin editing function. Further investigation of HLA-B2705 in the presence and absence of tapasin revealed major differences in loaded peptides. It was observed that HLA-B2705 loaded with a viral peptide was presented to cytotoxic T cells in the absence of tapasin within a time-lag. In tapasin$^{-/-}$-cells the HLA-B2705 molecules were prone to thermally induced instability as well as shortened half-life on the cell surface. In addition, they were loaded with a different peptide repertoire as in tapasin positive cells (Purcell *et al.,* 2000, Purcell *et al.,* 2001, Tan *et al.,* 2002). Consequently, the peptide loading of HLA-B2705 was subject to quality control by tapasin. However, the HLA-B2705 is also peptide stabilized in the absence of tapasin albeit to a lesser extent. This was one of the criteria why besides the HLA-B4402 and HLA-B4405, also HLA-B2705 and HLA-B2709 were chosen to directly probe the interaction of tapasin and MHC class I molecules.

Besides the peptide supply, further factors must influence the tapasin-independent maturation. It is conceivable that a high intrinsic stability of an MHC class I allele promotes maturation. Also, a differential retention impact retains certain MHC class I alleles in the ER. In the absence of peptides the interaction of the HC with β_2m determines the stability and probably also the export of MHC class I molecules from the ER (Neefjes & Ploegh, 1998, Shields *et al.,* 1999). One can speculate whether the weak scB4402-β_2m conjugate secretion in insect cells is due to the loss of bound peptide on the way to the cell surface, resulting in HC/β_2m unfolding. It is important to mention that in tapasin-deficient cells the ER export of HLA-B4402 is very weak when compared to tapasin-proficient cells (Tan *et al.,* 2001). This supports the assumption that the HLA-B44 allele has a decreased intrinsic stability in the ER,

than for instance the HLA-B27 allele, leading to a decrease ER export. Alleles such as HLA-B2705 and HLA-B4405 show reduced tapasin dependencies (Peh *et al.,* 1998, Williams *et al.,* 2002, Park *et al.,* 2003, Zernich *et al.,* 2004), implying that these alleles can mature through a pathway that bypasses equilibria at which tapasin can associate either with the peptide-deficient, open (active) conformation or with the peptide-filled, closed conformation. This in turn implies that the open forms of HLA-B2705 and HLA-B4405 molecules possess a binding cleft that is intrinsically more stable relative to the more tapasin-dependent alleles. An increased stability could be achieved, for example, by engineering a peptide-binding cleft displaying a more intrinsic conformational maturity. As a consequence, it is expected that the open forms of peptide-deficient HLA-B2705 and HLA-B4405 molecules show more specificity in the initial capture of peptides relative to tapasin-dependent alleles, which I suggested above to be more permissive in their initial selection of peptides. In other words, it is possible that allele-specific tapasin dependencies may be rooted by differences in intrinsic conformational maturity and maybe also by differences in peptide association kinetics. The question arises whether it is possible that peptide-binding to the highly tapasin-dependent alleles, including the scB4402-β_2m conjugate, does not take place at all or is slowed down in the absence of tapasin. Although this remains to be examined experimentally, a role for MHC residues 114 and 116 (Williams *et al.,* 2002, Park *et al.,* 2003, Zernich *et al.,* 2004) may be considered to influence the intrinsic conformational maturity of the class I binding cleft.

The question remains how to improve the secretion of scB4402-β_2m? Co-expression with soluble tapasin did not solve the problem (data not shown), which was also confirmed by the work of Everett and Edidin, who showed that tapasin increases the efficiency of MHC class I assembly but did not affect MHC class I stability at the cell surface (Everett & Edidin, 2007). Though, one would expect an increased retention of scB4402-β_2m in the ER. Another idea would be to co-express scB4402-β_2m together with a tapasin-ERp57 conjugate (Wearsch & Cresswell, 2007). Here again, in case the appropriate peptide is the missing link, I would still lack a high affinity peptide needed for loading and secretion since insect cells lack TAP expression, the supplier of the needed peptide pool. The simultaneous expression of scB4402-β_2m, tapasin/ERp57 and

TAP together with the appropriate peptide is a very tedious task to perform, since all three viruses have to infect one cell at the same time. One would have to analyze single expression pattern of all three proteins and quantify their expression pattern at the same level. This could be solved using the MultiBac system where up to five separate genes are cloned for insect cell expression and expressed simultaneously. Furthermore, the expression of the ligand peptide itself, as a mini-gene construct, is another possibility but will not solve the problem if the tapasin-dependent HLA-B4402 displays slower peptide association kinetics and is dependent on other components of the PLC. Flutter and colleagues demonstrated that covalently linked HLA-B4402 heavy chain to β_2m (B44-β_2m) is efficiently expressed inside as well as on the surface of human cells (Flutter *et al.,* 2007). However, the linked B44-β_2m molecule is not expressed on the surface of a murine fibroblast, although it is expressed inside the cell. The authors showed that the lack of appearance on the surface is not due to degradation of unloaded B44-β_2m molecules, since provision of HLA-B4402 binding peptide could not rescue impaired surface expression. Furthermore, they showed that co-expression with human tapasin does not rescue the cell surface expression either. But since human A2-β_2m, a tapasin independent allele, was successfully expressed on the cell surface of these murine fibroblasts, it is obviously an allele-specific phenomenon to be further investigated.

7.2.2. MHC-tapasin interaction

So far, the function of tapasin was characterized almost entirely by *in-vivo* studies. These experiments are primarily based on the analysis of tapasin$^{-/-}$-cells, mutagenesis, and co-immunoprecipitation studies. Only recently, Chen and Bouvier examined for the first time interactions in a soluble tapasin / HLA-B0801 complex to gain mechanistic insights into the functions of tapasin. By fusing the ER-luminal domains of tapasin and HLA-B0801 heavy chain at their C-termini to Jun and Fos peptides, respectively, they increased the intrinsic affinity of both proteins, succeeding in detecting interaction in solution by anisotropy measurements. Furthermore, they suggest that tapasin influences presentation of antigenic peptides by excluding peptides from the

repertoire that are unable to conformationally disengage tapasin from class I molecules (Chen & Bouvier, 2007).

Within the current PhD-thesis, I investigated the MHC class I-tapasin interaction for the first time on solid-supported surfaces using SPR as well as RIfs-TIRF spectroscopy. To investigate association and dissociation kinetics of the MHC class I-tapasin interaction, a commercially available streptavidin-coated sensor chip was used. This biosensor was further functionalized to the ^{BT}tris-NTA, which allows a reversible biotinylation of histidine-tagged proteins (Figure 6-26). The setup used here, allowed an immobilization of soluble tapasin via the C-terminal His_6-tag for subsequent probing with the recombinant MHC class I molecules. Generating recombinant proteins for biochemical and biophysical analysis always bears the risk that the introduced modifications, for instance in case of tapasin the deletion of the transmembrane domain and the introduction of an affinity-tag, of rendering the recombinant protein non-functional and unstable. This is the reason why modifications regarding the protein structure should always be as non-invasive as possible. Here, for the recombinant tapasin a hexa- instead of a His_{10}-tag was chosen. In the following interaction analysis however, the immobilization via the His_6-tag of tapasin, turned out to be the achilles' heel of the system. Due to the C-terminal His_6-tag and the decrease affinity towards the tris-NTA moieties on the sensor surface compared with His_{10}-tag (Lata *et al.,* 2005), tapasin drifted from the ^{BT}tris-NTA functionalized SA sensor surface over time, making it impossible for quantitative analysis. Blocking the tapasin-immobilized surface additionally with MBP, bearing a His_{10}- or a His_6-tag, did not eliminate background binding. On the contrary, tapasin, or tapasin together with MBP, were drifiting from the surface. This can be explained by the fact that the His_{10}-tag of MBP of course competes for the His_6-tag of tapasin for binding sites. Due to the drifting effects the obtained dissociation curves for scB4405-β_2m were fitted best to biphasic kinetic, which make a qualitative evaluation in regard to actual rate constants impossible. After tapasin immobilization, first the scB4405-β_2m conjugate, lacking the C-terminal His_6-tag, was probed at different concentrations. From anisotropy measurements it became evident, that the purified scB4405-β_2m conjugate was already loaded with a peptide, which could be competed out with the high-affinity ligand peptide EEFGRAFSF (Figure 6-24 (b)). This loaded

peptide may represent a suboptimal peptide, allowing the interaction with tapasin (Figure 6-27 (b)). The observed interaction of scB4405-β_2m-tapasin was concentration-dependent and tapasin specific (Figure 6-27 (b)) but followed a biphasic dissociation kinetic. Consequently, leaking of the surface affected the obtained dissociation curves for the scB4405-β_2m conjugate, which made a qualitative evaluation in regard to the actual rate constants impossible. Since an increase of the flow rate as well as different levels of tapasin immobilization did not automatically change the association and dissociation kinetics, the biphasic behaviour may reflect the leaking of the surface. Even a more prominent drawback for the applied measurements of the MHC class I-tapasin interaction is the low protein amount relative to the transient low-affinity interaction. Transient, low-affinity interactions can be calculated from the equilibrium values derived from the kinetic data at different concentrations. Here, concentrations at least up to 10-100-fold higher than 5 µM should have been applied, which represent protein amounts not achievable with the shaking cultures of insect cells. The recombinant HLA-B27 molecules were also probed for interaction with tapasin. Peptide-loaded as well as peptide-deficient tapasin-independent HLA-B2705 and the tapasin-dependent HLA-B2709 were probed on the tapasin-immobilized sensor surface (Figure 6-28). In contrast to the tapasin-independent scB4405-β_2m conjugate produced in insect cells and loaded with a sub-optimal peptide as stated above, the HLA-B2705 produced in *E. coli* and refolded in the presence of a high-affinity ligand peptide, showed neither a peptide-proficient nor a peptide-deficient tapasin-specific interaction (Figure 6-28 (c)). Since the refolded heavy chain-β_2m molecules disintergrate in the absence of a ligand peptide, it is obvious that the pH shock, used to generate peptide-deficient MHC class I molecules, resulted in non-functional HLA-B27. However, tapasin-dependent HLA-B2709 displayed tapasin-specific interaction in the peptide-deficient state (Figure 6-28 (b)). Thus it cannot be ruled out, that the obtained plasmon shift is rather due to changes in refractive index, than to protein-protein interaction. As already mentioned for the scB4405-β_2m conjugate, the association and dissociation rate constants followed biphasic kinetics. Low-affinity interaction resulting in the limited protein amount available hindered concentration-dependent analysis.

Because the transient, low-affinity interaction of the MHC class I-tapasin complex and the low protein amounts available, the SPR measurements proved not to be the optimal method for evaluating these interactions. The TIRF-RIfs system was applied instead. The advantage to the SPR technology lies in the immobilization of proteins on chelated lipid bilayer surface, allowing for lateral mobility of the immobilized proteins. Another advantage to the mass-sensitive channel is the simultaneous monitoring of the fluorescence-labeled probe in the fluorescence channel. Here, the scB4405-β_2m conjugate loaded with the fluorescein-labeled peptide as well as tapasin were immobilized on the chelated lipid bilayer via their C-terminal histidine-tags. Stable immobilization of both proteins was observed (Figure 6-29). Since the MHC class I-peptide association is slow as shown by the anisotropy measurements (Figure 6-24), only the tapasin editing function on the peptide dissociation kinetics was investigated. Unfortunately, immobilization of tapasin did not affect peptide dissociation kinetics. As already mentioned above the HLA-B4405 is rather a tapasin-independent allele which may not necessarily be edited by tapasin when already loaded with a high affinity peptide. To my knowledge there is no endogenous suboptimal ligand peptide known for the HLA-B44 allele, which could be used for the investigation of the tapasin influence on peptide kinetics. However, the high-affinity peptide used here could be further modified by scanning the N-terminal amino acids (position 1 to 4) for a low-affinity interaction with the MHC class I peptide-binding cleft. Also, a tapasin-dependent MHC class I allele is important to further investigate the peptide-editing role of tapasin.

Conclusively, the recombinant MHC class I molecules generated here, proved useful to analyze MHC class I-tapasin interaction as well as further interactions within the macromolecular PLC. Here, I presented for the first time an *in vitro* platform based on the SPR technology for measuring protein-protein interactions within the PLC. The heavily discussed question, whether or not tapasin serves as peptide-editor on preloaded MHC class I molecules, still remains open. Only biochemical data exist, supporting tapasin's editing function. Here, I applied the TIRF-RIfs system, immobilizing tapasin and pre-loaded MHC class I molecules for the first time on chelated lipid bilayer to

ensure lateral mobility of the immobilized proteins, and to further investigate tapasin's function in detail.

8. Abbreviations

ABC	ATP-binding cassette
ADCC	antibody dependent cellular cytotoxicity
ADP	adenosine 5’-diphosphate
AHT	anhydrotetracycline
Amp	ampicillin
APC	antigen presenting cell
APS	ammonium persulfate
ATP	adenosine 5’-triphosphate
Bap	B cell associated protein
BiP	immunoglobulin binding protein
bp	base pair(s)
BSA	bovine serum albumin
CCL2	chemotactic protein
CDC	complement-dependent cytotoxicity
cDNA	complementary DNA
CDR	complementarity determing region
CLIP	class II-associated invariant chain peptide
Con A	Concanavalin A
COP	coat protein complex
CPM	counts per minute
CTP	cytidine 5’-triphosphate
DMF	dimethylformamide
DMSO	dimethyl sulfoxide
DNA	deoxyribonucleic acid
DTT	1,4-dithiothreitol
dNTP	deoxynucleotide triphosphate

dsFv	disulfide-stabilized Fv fragment
E. coli	*Escherichia coli*
ECL	enhanced chemiluminescence
EDTA	ethylene diamine tetraacetic acid
ELISA	enzyme-linked immunosorbent assay
ER	endoplasmic reticulum
Fc	fragment crystallizable
Fv	fragment variable
Fab	fragment antigen binding
g	gravity
GM-CSF	granulocyte and macrophage colony-stimulating factor
GTP	guanosine 5'-triphosphate
HABA	(2-(4-hydroxyphenylazo)benzoic acid
HBS	HEPES buffered saline
HC	heavy chain
HLA	human leukocyte antigen
hsFv	helix-stabilized Fv fragment
IDA	iodo-diacetic acid
IFN	interferon
IL	interleukin
IgG	immunglobulin G
IMAC	immobilized metal affinity chromatography
IPTG	isopropyl β-D-thiogalactopyranoside
k_a	association rate constant
kDa	kilo Dalton
K_D	dissociation constant
k_d	dissociation rate constant
L	liter

LB	lysogeny broth
mAb	monoclonal antibody
MBP	maltose-binding protein
MHC	major histocompatibility complex
min	minute
mRNA	messenger RNA
NBD	nucleotide-binding domain
Ni-NTA	nickel nitrilotriacetic acid
NO	nitric oxide
OD	optical density
PAGE	polyacrylamide gel electrophoresis
PBS	phosphate buffered saline
PCR	polymerase chain reaction
pI	isoelectric point
PI-Mix	protease inhibitor mix
Rif(s)	reflectance interference spectroscopy
RNA	ribonucleic acid
RNase	ribonuclease
rpm	rounds per minute
RT	room temperature
RT-PCR	reverse transcription polymerase chain reaction
s	second
scFv	single chain Fv fragment
SDS	sodium dodecyl sulfate
SEC	size exclusion chromatography
*Sf*9	*Spodoptera frugiperda* 9
Sm	streptomycin
SOPC	stearoyl-oleoyl phosphatidylcholine

SPR	surface plasmon resonance
T. ni	*Trichoplusia ni*
TAE	Tris-acetate-EDTA buffer
TAP	transporter associated with antigen processing
TAPBP	TAP binding protein
Taq	*Thermophilus aquaticus*
TBS	Tris-buffered saline
TEMED	N,N,N',N'-tetramethylethylenediamine
TIRFS	total internal reflection fluorescence spectroscopy
TMD	transmembrane domain
TMH	transmembrane helix
Tris	2-amino-2-hydroxymethyl-propane-1,3-diol
TY	tryptone yeast
U	unit
V	Volt
v/v	volume per volume
w/v	weight per volume
WT	wild type
X-Gal	5-bromo-4-chloro-3-indolyl-β-D-galactopyranoside

9. References

Abele, R. & Tampé, R. (1999) Function of the transport complex TAP in cellular immune recognition. *Biochim Biophys Acta*, **1461**, 405-19.

Abele, R. & Tampé, R. (2004) The ABCs of immunology: Structure and function of TAP, the transporter associated with antigen processing. *Physiology (Bethesda)*, **19**, 216-24.

Abele, R. & Tampé, R. (2006) Modulation of the antigen transport machinery TAP by friends and enemies. *FEBS Lett*, **580**, 1156-63.

Ackerman, A.L., Kyritsis, C., Tampé, R. & Cresswell, P. (2005) Access of soluble antigens to the endoplasmic reticulum can explain cross-presentation by dendritic cells. *Nat Immunol*, **6**, 107-13.

Ammer, S., (2003) Funktionale Expression des ER-Chaperons Tapasin und Charakterisierung der Interaktion von Tapasin mit MHC-Klasse I-Molekülen *in vitro*. Doktorarbeit, *Institut für Biochemie*, Goethe-Universität, Frankfurt am Main.

Androlewicz, M.J., Anderson, K.S. & Cresswell, P. (1993) Evidence that transporters associated with antigen processing translocate a major histocompatibility complex class I-binding peptide into the endoplasmic reticulum in an ATP-dependent manner. *Proc Natl Acad Sci U S A*, **90**, 9130-4.

Androlewicz, M.J., Ortmann, B., Van Endert, P.M., Spies, T. & Cresswell, P. (1994) Characteristics of peptide and major histocompatibility complex class I/beta 2-microglobulin binding to the transporters associated with antigen processing (TAP1 and TAP2). *Proc Natl Acad Sci U S A*, **91**, 12716-20.

Antoniou, A.N. & Powis, S.J. (2003) Characterization of the ERp57-tapasin complex by rapid cellular acidification and thiol modification. *Antioxid Redox Signal*, **5**, 375-9.

Antoniou, A.N., Powis, S.J. & Elliott, T. (2003) Assembly and export of MHC class I peptide ligands. *Curr Opin Immunol*, **15**, 75-81.

Antoniou, A.N., Santos, S.G., Campbell, E.C., Lynch, S., Arosa, F.A. & Powis, S.J. (2007) ERp57 interacts with conserved cysteine residues in the MHC class I peptide-binding groove. *FEBS Lett*, **581**, 1988-92.

Attaya, M., Jameson, S., Martinez, C.K., Hermel, E., Aldrich, C., Forman, J., Lindahl, K.F., Bevan, M.J. & Monaco, J.J. (1992) Ham-2 corrects the class I antigen-processing defect in rma-s cells. *Nature*, **355**, 647-9.

Baas, E.J., Van Santen, H.M., Kleijmeer, M.J., Geuze, H.J., Peters, P.J. & Ploegh, H.L. (1992) Peptide-induced stabilization and intracellular localization of empty HLA class I complexes. *J Exp Med*, **176**, 147-56.

Baker, B.M. & Murphy, K.P. (1998) Prediction of binding energetics from structure using empirical parameterization. *Methods Enzymol*, **295**, 294-315.

Balow, J.P., Weissman, J.D. & Kearse, K.P. (1995) Unique expression of major histocompatibility complex class I proteins in the absence of glucose trimming and calnexin association. *J Biol Chem*, **270**, 29025-9.

Bangia, N. & Cresswell, P. (2005) Stoichiometric tapasin interactions in the catalysis of major histocompatibility complex class I molecule assembly. *Immunology*, **114**, 346-53.

Bangia, N., Lehner, P.J., Hughes, E.A., Surman, M. & Cresswell, P. (1999) The N-terminal region of tapasin is required to stabilize the MHC class I loading complex. *Eur J Immunol*, **29**, 1858-70.

Barnden, M.J., Purcell, A.W., Gorman, J.J. & Mccluskey, J. (2000) Tapasin-mediated retention and optimization of peptide ligands during the assembly of class I molecules. *J Immunol*, **165**, 322-30.

Beinert, D., Neumann, L., Uebel, S. & Tampé, R. (1997) Structure of the viral TAP-inhibitor ICP47 induced by membrane association. *Biochemistry*, **36**, 4694-700.

Beissbarth, T., Sun, J., Kavathas, P.B. & Ortmann, B. (2000) Increased efficiency of folding and peptide loading of mutant MHC class I molecules. *Eur J Immunol*, **30**, 1203-13.

Bergeron, J.J., Brenner, M.B., Thomas, D.Y. & Williams, D.B. (1994) Calnexin: A membrane-bound chaperone of the endoplasmic reticulum. *Trends Biochem Sci*, **19**, 124-8.

Better, M., Chang, C.P., Robinson, R.R. & Horwitz, A.H. (1988) Escherichia coli secretion of an active chimeric antibody fragment. *Science*, **240**, 1041-3.

Binz, A.K., Rodriguez, R.C., Biddison, W.E. & Baker, B.M. (2003) Thermodynamic and kinetic analysis of a peptide-class I MHC interaction highlights the noncovalent nature and conformational dynamics of the class I heterotrimer. *Biochemistry*, **42**, 4954-61.

Bjorkman, P.J., Saper, M.A., Samraoui, B., Bennett, W.S., Strominger, J.L. & Wiley, D.C. (1987) Structure of the human class I histocompatibility antigen, HLA-A2. *Nature*, **329**, 506-12.

Bouabe, H. & Knittler, M.R. (2003) The distinct nucleotide binding states of the transporter associated with antigen processing (TAP) are regulated by the nonhomologous C-terminal tails of TAP1 and TAP2. *Eur J Biochem*, **270**, 4531-46.

Bouvier, M. (2003) Accessory proteins and the assembly of human class I MHC molecules: A molecular and structural perspective. *Mol Immunol*, **39**, 697-706.

Brocke, P., Armandola, E., Garbi, N. & Hämmerling, G.J. (2003) Downmodulation of antigen presentation by H2-O in B cell lines and primary B lymphocytes. *Eur J Immunol*, **33**, 411-21.

Brocke, P., Garbi, N., Momburg, F. & Hämmerling, G.J. (2002) HLA-DM, HLA-DO and tapasin: Functional similarities and differences. *Curr Opin Immunol*, **14**, 22-9.

Burgdorf, S., Schölz, C., Kautz, A., Tampé, R. & Kurts, C. (2008) Spatial and mechanistic separation of cross-presentation and endogenous antigen presentation. *Nat Immunol*, **9**, 558-66.

Carreno, B.M., Schreiber, K.L., Mckean, D.J., Stroynowski, I. & Hansen, T.H. (1995) Aglycosylated and phosphatidylinositol-anchored MHC class I molecules are associated with calnexin. Evidence implicating the class I-connecting peptide segment in calnexin association. *J Immunol*, **154**, 5173-80.

Chambers, J.E., Jessop, C.E. & Bulleid, N.J. (2008) Formation of a major histocompatibility complex class I tapasin disulfide indicates a change in spatial organization of the peptide-loading complex during assembly. *J Biol Chem*, **283**, 1862-9.

Chang, S.C., Momburg, F., Bhutani, N. & Goldberg, A.L. (2005) The ER aminopeptidase, ERAP1, trims precursors to lengths of MHC class I peptides by a "molecular ruler" Mechanism. *Proc Natl Acad Sci U S A*, **102**, 17107-12.

Chen, M., Abele, R. & Tampé, R. (2003) Peptides induce ATP hydrolysis at both subunits of the transporter associated with antigen processing. *J Biol Chem*, **278**, 29686-92.

Chen, M., Abele, R. & Tampé, R. (2004) Functional non-equivalence of ATP-binding cassette signature motifs in the transporter associated with antigen processing (TAP). *J Biol Chem*, **279**, 46073-81.

Chen, M. & Bouvier, M. (2007) Analysis of interactions in a tapasin/class I complex provides a mechanism for peptide selection. *EMBO J*, **26**, 1681-90.

Click, E.M., Anderson, K.S., Androlewicz, M.J., Wei, M.L. & Cresswell, P. (1992) Transport and expression of class I MHC glycoproteins in an antigen-processing mutant cell line. *Cold Spring Harb Symp Quant Biol*, **57**, 571-7.

Cooper, N.R. (1985) The classical complement pathway: Activation and regulation of the first complement component. *Adv Immunol*, **37**, 151-216.

Cresswell, P., Ackerman, A.L., Giodini, A., Peaper, D.R. & Wearsch, P.A. (2005) Mechanisms of MHC class I-restricted antigen processing and cross-presentation. *Immunol Rev*, **207**, 145-57.

Cresswell, P., Arunachalam, B., Bangia, N., Dick, T., Diedrich, G., Hughes, E. & Maric, M. (1999) Thiol oxidation and reduction in MHC-restricted antigen processing and presentation. *Immunol Res*, **19**, 191-200.

Cresswell, P., Bangia, N., Dick, T. & Diedrich, G. (1999) The nature of the MHC class I peptide loading complex. *Immunol Rev*, **172**, 21-8.

D'amato, M., Fiorillo, M.T., Carcassi, C., Mathieu, A., Zuccarelli, A., Bitti, P.P., Tosi, R. & Sorrentino, R. (1995) Relevance of residue 116 of HLA-B27 in determining susceptibility to ankylosing spondylitis. *Eur J Immunol*, **25**, 3199-201.

D'amato, M., Fiorillo, M.T., Galeazzi, M., Martinetti, M., Amoroso, A. & Sorrentino, R. (1995) Frequency of the new HLA-B*2709 allele in ankylosing spondylitis patients and healthy individuals. *Dis Markers*, **12**, 215-7.

Dedier, S., Reinelt, S., Rion, S., Folkers, G. & Rognan, D. (2001) Use of fluorescence polarization to monitor MHC-peptide interactions in solution. *J Immunol Methods*, **255**, 57-66.

Demars, R., Rudersdorf, R., Chang, C., Petersen, J., Strandtmann, J., Korn, N., Sidwell, B. & Orr, H.T. (1985) Mutations that impair a posttranscriptional step in expression of HLA-A and -B antigens. *Proc Natl Acad Sci U S A*, **82**, 8183-7.

Demars, R. & Spies, T. (1992) New genes in the MHC that encode proteins for antigen processing. *Trends Cell Biol*, **2**, 81-6.

Dibrino, M., Parker, K.C., Margulies, D.H., Shiloach, J., Turner, R.V., Biddison, W.E. & Coligan, J.E. (1995) Identification of the peptide binding motif for HLA-B44, one of the most common HLA-B alleles in the caucasian population. *Biochemistry*, **34**, 10130-8.

Dick, T.P., Bangia, N., Peaper, D.R. & Cresswell, P. (2002) Disulfide bond isomerization and the assembly of MHC class I-peptide complexes. *Immunity*, **16**, 87-98.

Dustin, M.L. (2003) Coordination of T cell activation and migration through formation of the immunological synapse. *Ann N Y Acad Sci*, **987**, 51-9.

Ehses, S., Leonhardt, R.M., Hansen, G. & Knittler, M.R. (2005) Functional role of C-terminal sequence elements in the transporter associated with antigen processing. *J Immunol*, **174**, 328-39.

Ellgaard, L. & Helenius, A. (2003) Quality control in the endoplasmic reticulum. *Nat Rev Mol Cell Biol*, **4**, 181-91.

Ellgaard, L. & Ruddock, L.W. (2005) The human protein disulphide isomerase family: Substrate interactions and functional properties. *EMBO Rep*, **6**, 28-32.

Elliott, T. (1997) How does TAP associate with MHC class I molecules? *Immunol Today*, **18**, 375-9.

Everett, M.W. & Edidin, M. (2007) Tapasin increases efficiency of MHC I assembly in the endoplasmic reticulum but does not affect MHC I stability at the cell surface. *J Immunol*, **179**, 7646-52.

Farmery, M.R., Allen, S., Allen, A.J. & Bulleid, N.J. (2000) The role of ERp57 in disulfide bond formation during the assembly of major histocompatibility complex class I in a synchronized semipermeabilized cell translation system. *J Biol Chem*, **275**, 14933-8.

Flutter, B., Fu, H.M., Wedderburn, L. & Gao, B. (2007) An extra molecule in addition to human tapasin is required for surface expression of beta2m linked HLA-B4402 on murine cell. *Mol Immunol*, **44**, 3528-36.

Frickel, E.M., Riek, R., Jelesarov, I., Helenius, A., Wuthrich, K. & Ellgaard, L. (2002) TROSY-NMR reveals interaction between ERp57 and the tip of the calreticulin P-domain. *Proc Natl Acad Sci U S A*, **99**, 1954-9.

Früh, K., Ahn, K., Djaballah, H., Sempe, P., Van Endert, P.M., Tampé, R., Peterson, P.A. & Yang, Y. (1995) A viral inhibitor of peptide transporters for antigen presentation. *Nature*, **375**, 415-8.

Gabdoulline, R.R. & Wade, R.C. (2002) Biomolecular diffusional association. *Curr Opin Struct Biol*, **12**, 204-13.

Gakamsky, D.M., Davis, D.M., Strominger, J.L. & Pecht, I. (2000) Assembly and dissociation of human leukocyte antigen (HLA)-A2 studied by real-time fluorescence resonance energy transfer. *Biochemistry*, **39**, 11163-9.

Gao, B., Adhikari, R., Howarth, M., Nakamura, K., Gold, M.C., Hill, A.B., Knee, R., Michalak, M. & Elliott, T. (2002) Assembly and antigen-presenting function of MHC class I molecules in cells lacking the ER chaperone calreticulin. *Immunity*, **16**, 99-109.

Garbi, N., Hämmerling, G. & Tanaka, S. (2007) Interaction of ERp57 and tapasin in the generation of MHC class I-peptide complexes. *Curr Opin Immunol*, **19**, 99-105.

Garbi, N., Tan, P., Diehl, A.D., Chambers, B.J., Ljunggren, H.G., Momburg, F. & Hämmerling, G.J. (2000) Impaired immune responses and altered peptide repertoire in tapasin-deficient mice. *Nat Immunol*, **1**, 234-8.

Garbi, N., Tan, P., Momburg, F. & Hämmerling, G.J. (2001) Role of tapasin in MHC class I antigen presentation in vivo. *Adv Exp Med Biol*, **495**, 71-8.

Garbi, N., Tanaka, S., Momburg, F. & Hämmerling, G.J. (2006) Impaired assembly of the major histocompatibility complex class I peptide-loading complex in mice deficient in the oxidoreductase ERp57. *Nat Immunol*, **7**, 93-102.

Garbi, N., Tanaka, S., Van Den Broek, M., Momburg, F. & Hämmerling, G.J. (2005) Accessory molecules in the assembly of major histocompatibility complex class I/peptide complexes: How essential are they for $CD8^+$ T-cell immune responses? *Immunol Rev*, **207**, 77-88.

Garbi, N., Tiwari, N., Momburg, F. & Hämmerling, G.J. (2003) A major role for tapasin as a stabilizer of the TAP peptide transporter and consequences for MHC class I expression. *Eur J Immunol*, **33**, 264-73.

Gavutis, M., Lata, S., Lamken, P., Müller, P. & Piehler, J. (2005) Lateral ligand-receptor interactions on membranes probed by simultaneous fluorescence-interference detection. *Biophys J*, **88**, 4289-302.

Gething, M.J. & Sambrook, J. (1992) Protein folding in the cell. *Nature*, **355**, 33-45.

Gorbulev, S., Abele, R. & Tampé, R. (2001) Allosteric crosstalk between peptide-binding, transport, and ATP hydrolysis of the ABC transporter TAP. *Proc Natl Acad Sci U S A*, **98**, 3732-7.

Grandea, A.G., 3rd, Golovina, T.N., Hamilton, S.E., Sriram, V., Spies, T., Brutkiewicz, R.R., Harty, J.T., Eisenlohr, L.C. & Van Kaer, L. (2000) Impaired assembly yet normal trafficking of MHC class I molecules in tapasin mutant mice. *Immunity*, **13**, 213-22.

Grandea, A.G., 3rd, Lehner, P.J., Cresswell, P. & Spies, T. (1997) Regulation of MHC class I heterodimer stability and interaction with TAP by tapasin. *Immunogenetics*, **46**, 477-83.

Greenwood, R., Shimizu, Y., Sekhon, G.S. & Demars, R. (1994) Novel allele-specific, post-translational reduction in HLA class I surface expression in a mutant human B cell line. *J Immunol*, **153**, 5525-36.

Gromme, M., Van Der Valk, R., Sliedregt, K., Vernie, L., Liskamp, R., Hammerling, G., Koopmann, J.O., Momburg, F. & Neefjes, J. (1997) The rational design of TAP inhibitors using peptide substrate modifications and peptidomimetics. *Eur J Immunol*, **27**, 898-904.

Hammond, C., Braakman, I. & Helenius, A. (1994) Role of N-linked oligosaccharide recognition, glucose trimming, and calnexin in glycoprotein folding and quality control. *Proc Natl Acad Sci U S A*, **91**, 913-7.

Harris, M.R., Lybarger, L., Myers, N.B., Hilbert, C., Solheim, J.C., Hansen, T.H. & Yu, Y.Y. (2001) Interactions of HLA-B27 with the peptide loading complex as revealed by heavy chain mutations. *Int Immunol*, **13**, 1275-82.

Harris, M.R., Lybarger, L., Yu, Y.Y., Myers, N.B. & Hansen, T.H. (2001) Association of ERp57 with mouse MHC class I molecules is tapasin dependent and mimics that of calreticulin and not calnexin. *J Immunol*, **166**, 6686-92.

Hebert, D.N., Garman, S.C. & Molinari, M. (2005) The glycan code of the endoplasmic reticulum: Asparagine-linked carbohydrates as protein maturation and quality-control tags. *Trends Cell Biol*, **15**, 364-70.

Heintke, S., Chen, M., Ritz, U., Lankat-Buttgereit, B., Koch, J., Abele, R., Seliger, B. & Tampé, R. (2003) Functional cysteine-less subunits of the transporter associated with antigen processing (TAP1 and TAP2) by de novo gene assembly. *FEBS Lett*, **533**, 42-6.

Helenius, A. & Aebi, M. (2001) Intracellular functions of N-linked glycans. *Science*, **291**, 2364-9.

Helenius, A. & Aebi, M. (2004) Roles of N-linked glycans in the endoplasmic reticulum. *Annu Rev Biochem*, **73**, 1019-49.

Herberg, J.A., Sgouros, J., Jones, T., Copeman, J., Humphray, S.J., Sheer, D., Cresswell, P., Beck, S. & Trowsdale, J. (1998) Genomic analysis of the tapasin gene, located close to the TAP loci in the MHC. *Eur J Immunol*, **28**, 459-67.

Herget, M., Oancea, G., Schrodt, S., Karas, M., Tampé, R. & Abele, R. (2007) Mechanism of substrate sensing and signal transmission within an ABC transporter: Use of a trojan horse strategy. *J Biol Chem*, **282**, 3871-80.

Hill, A.B., Barnett, B.C., Mcmichael, A.J. & Mcgeoch, D.J. (1994) HLA class I molecules are not transported to the cell surface in cells infected with herpes simplex virus types 1 and 2. *J Immunol*, **152**, 2736-41.

Hopfner, K.P., Karcher, A., Shin, D.S., Craig, L., Arthur, L.M., Carney, J.P. & Tainer, J.A. (2000) Structural biology of Rad50 ATPase: ATP-driven conformational control in DNA double-strand break repair and the ABC-ATPase superfamily. *Cell*, **101**, 789-800.

Horwitz, A.H., Chang, C.P., Better, M., Hellstrom, K.E. & Robinson, R.R. (1988) Secretion of functional antibody and Fab fragment from yeast cells. *Proc Natl Acad Sci U S A*, **85**, 8678-82.

Hosken, N.A. & Bevan, M.J. (1992) An endogenous antigenic peptide bypasses the class I antigen presentation defect in RMA-S. *J Exp Med*, **175**, 719-29.

Hosokawa, N., Wada, I., Hasegawa, K., Yorihuzi, T., Tremblay, L.O., Herscovics, A. & Nagata, K. (2001) A novel ER alpha-mannosidase-like protein accelerates ER-associated degradation. *EMBO Rep*, **2**, 415-22.

Howarth, M., Williams, A., Tolstrup, A.B. & Elliott, T. (2004) Tapasin enhances MHC class I peptide presentation according to peptide half-life. *Proc Natl Acad Sci U S A*, **101**, 11737-42.

Hung, L.W., Wang, I.X., Nikaido, K., Liu, P.Q., Ames, G.F. & Kim, S.H. (1998) Crystal structure of the ATP-binding subunit of an ABC transporter. *Nature*, **396**, 703-7.

Hunte, C. & Müncke, C. (2004) Application of antibody-fragments as crystallization enhancers. *Molecular biology in medicinal chemistry*. Dingermann, T., Steinhilber, D., Folkers, C. (eds.), WILEY-VCH, Weinheim, Germany.

Hunter, W.M. & Greenwood, F.C. (1964) A radio-immunoelectrophoretic assay for human growth hormone. *Biochem J*, **91**, 43-56.

Jakob, C.A., Bodmer, D., Spirig, U., Battig, P., Marcil, A., Dignard, D., Bergeron, J.J., Thomas, D.Y. & Aebi, M. (2001) Htm1p, a mannosidase-like protein, is involved in glycoprotein degradation in yeast. *EMBO Rep*, **2**, 423-30.

Janas, E., Hofacker, M., Chen, M., Gompf, S., Van Der Does, C. & Tampé, R. (2003) The ATP hydrolysis cycle of the nucleotide-binding domain of the mitochondrial ATP-binding cassette transporter Mdl1p. *J Biol Chem*, **278**, 26862-9.

Jessop, C.E., Chakravarthi, S., Garbi, N., Hämmerling, G.J., Lovell, S. & Bulleid, N.J. (2007) ERp57 is essential for efficient folding of glycoproteins sharing common structural domains. *EMBO J*, **26**, 28-40.

Kabat, E.A., Wu, T.T., Reid-Miller, M., Perry, H. M. & Gottesmann, K. (1987) *Sequences of proteins of immunological interest*. Public Health Science, National Institutes of Health, Bethesda, Maryland, USA.

Kapoor, M., Srinivas, H., Kandiah, E., Gemma, E., Ellgaard, L., Oscarson, S., Helenius, A. & Surolia, A. (2003) Interactions of substrate with calreticulin, an endoplasmic reticulum chaperone. *J Biol Chem*, **278**, 6194-200.

Karttunen, J.T., Lehner, P.J., Gupta, S.S., Hewitt, E.W. & Cresswell, P. (2001) Distinct functions and cooperative interaction of the subunits of the transporter associated with antigen processing (TAP). *Proc Natl Acad Sci U S A*, **98**, 7431-6.

Kelly, A., Powis, S.H., Kerr, L.A., Mockridge, I., Elliott, T., Bastin, J., Uchanska-Ziegler, B., Ziegler, A., Trowsdale, J. & Townsend, A. (1992) Assembly and function of the two ABC transporter proteins encoded in the human major histocompatibility complex. *Nature*, **355**, 641-4.

Khan, M.A. (2002) Update on spondyloarthropathies. *Ann Intern Med*, **136**, 896-907.

Kienast, A., Preuss, M., Winkler, M. & Dick, T.P. (2007) Redox regulation of peptide receptivity of major histocompatibility complex class I molecules by ERp57 and tapasin. *Nat Immunol*, **8**, 864-72.

Kleijmeer, M.J., Kelly, A., Geuze, H.J., Slot, J.W., Townsend, A. & Trowsdale, J. (1992) Location of MHC-encoded transporters in the endoplasmic reticulum and *cis*-Golgi. *Nature*, **357**, 342-4.

Kleymann, G., Ostermeier, C., Ludwig, B., Skerra, A. & Michel, H. (1995) Engineered Fv fragments as a tool for the one-step purification of integral multisubunit membrane protein complexes. *Biotechnology (N Y)*, **13**, 155-60.

Knittler, M.R., Alberts, P., Deverson, E.V. & Howard, J.C. (1999) Nucleotide binding by TAP mediates association with peptide and release of assembled MHC class I molecules. *Curr Biol*, **9**, 999-1008.

Koch, J., Guntrum, R., Heintke, S., Kyritsis, C. & Tampé, R. (2004) Functional dissection of the transmembrane domains of the transporter associated with antigen processing (TAP). *J Biol Chem*, **279**, 10142-7.

Koch, J., Guntrum, R. & Tampé, R. (2005) Exploring the minimal functional unit of the transporter associated with antigen processing. *FEBS Lett*, **579**, 4413-6.

Koch, J., Guntrum, R. & Tampé, R. (2006) The first N-terminal transmembrane helix of each subunit of the antigenic peptide transporter TAP is essential for independent tapasin binding. *FEBS Lett*, **580**, 4091-6.

Koch, J. & Tampé, R. (2006) The macromolecular peptide-loading complex in MHC class I-dependent antigen presentation. *Cell Mol Life Sci*, **63**, 653-62.

Koopmann, J.O., Post, M., Neefjes, J.J., Hämmerling, G.J. & Momburg, F. (1996) Translocation of long peptides by transporters associated with antigen processing (TAP). *Eur J Immunol*, **26**, 1720-8.

Koppers-Lalic, D., Reits, E.A., Ressing, M.E., Lipinska, A.D., Abele, R., Koch, J., Marcondes Rezende, M., Admiraal, P., Van Leeuwen, D., Bienkowska-Szewczyk, K., Mettenleiter, T.C., Rijsewijk, F.A., Tampé, R., Neefjes, J. & Wiertz, E.J. (2005) Varicelloviruses avoid T cell recognition by UL49.5-mediated inactivation of the transporter associated with antigen processing. *Proc Natl Acad Sci U S A*, **102**, 5144-9.

Koppers-Lalic, D., Verweij, M.C., Lipinska, A.D., Wang, Y., Quinten, E., Reits, E.A., Koch, J., Loch, S., Rezende, M.M., Daus, F., Bienkowska-Szewczyk, K., Osterrieder, N., Mettenleiter, T.C., Heemskerk, M.H., Tampé, R., Neefjes, J.J., Chowdhury, S.I., Ressing, M.E., Rijsewijk, F.A. & Wiertz, E.J. (2008) Varicellovirus UL 49.5 proteins differentially affect the function of the transporter associated with antigen processing, TAP. *PLoS Pathog*, **4**, e1000080.

Kyritsis, C., Gorbulev, S., Hutschenreiter, S., Pawlitschko, K., Abele, R. & Tampé, R. (2001) Molecular mechanism and structural aspects of transporter associated with antigen processing inhibition by the cytomegalovirus protein US6. *J Biol Chem*, **276**, 48031-9.

Lage, H., Perlitz, C., Abele, R., Tampé, R., Dietel, M., Schadendorf, D. & Sinha, P. (2001) Enhanced expression of human ABC-transporter TAP is associated with cellular resistance to mitoxantrone. *FEBS Lett*, **503**, 179-84.

Lanier, L.L., Phillips, J.H., Hackett, J., Jr., Tutt, M. & Kumar, V. (1986) Natural killer cells: Definition of a cell type rather than a function. *J Immunol*, **137**, 2735-9.

Lapinski, P.E., Neubig, R.R. & Raghavan, M. (2001) Walker A lysine mutations of TAP1 and TAP2 interfere with peptide translocation but not peptide binding. *J Biol Chem*, **276**, 7526-33.

Lata, S., Reichel, A., Brock, R., Tampé, R. & Piehler, J. (2005) High-affinity adaptors for switchable recognition of histidine-tagged proteins. *J Am Chem Soc*, **127**, 10205-15.

Lauvau, G., Gubler, B., Cohen, H., Daniel, S., Caillat-Zucman, S. & Van Endert, P.M. (1999) Tapasin enhances assembly of transporters associated with antigen processing-dependent and -independent peptides with HLA-A2 and HLA-B27 expressed in insect cells. *J Biol Chem*, **274**, 31349-58.

Lauvau, G., Kakimi, K., Niedermann, G., Ostankovitch, M., Yotnda, P., Firat, H., Chisari, F.V. & Van Endert, P.M. (1999) Human transporters associated with antigen processing (TAPs) select epitope precursor peptides for processing in the endoplasmic reticulum and presentation to T cells. *J Exp Med*, **190**, 1227-40.

Leach, M.R., Cohen-Doyle, M.F., Thomas, D.Y. & Williams, D.B. (2002) Localization of the lectin, ERp57 binding, and polypeptide binding sites of calnexin and calreticulin. *J Biol Chem*, **277**, 29686-97.

Leach, M.R. & Williams, D.B. (2004) Lectin-deficient calnexin is capable of binding class I histocompatibility molecules in vivo and preventing their degradation. *J Biol Chem*, **279**, 9072-9.

Lehner, P.J. (2003) The calculus of immunity: Quantitating antigen processing. *Immunity*, **18**, 315-7.

Lehner, P.J., Surman, M.J. & Cresswell, P. (1998) Soluble tapasin restores MHC class I expression and function in the tapasin-negative cell line .220. *Immunity*, **8**, 221-31.

Lewis, J.W. & Elliott, T. (1998) Evidence for successive peptide binding and quality control stages during MHC class I assembly. *Curr Biol*, **8**, 717-20.

Lewis, J.W., Sewell, A., Price, D. & Elliott, T. (1998) HLA-A*0201 presents TAP-dependent peptide epitopes to cytotoxic T lymphocytes in the absence of tapasin. *Eur J Immunol*, **28**, 3214-20.

Li, S., Sjogren, H.O., Hellman, U., Pettersson, R.F. & Wang, P. (1997) Cloning and functional characterization of a subunit of the transporter associated with antigen processing. *Proc Natl Acad Sci U S A*, **94**, 8708-13.

Liu, Y.J., Zhang, J., Lane, P.J., Chan, E.Y. & Maclennan, I.C. (1991) Sites of specific B cell activation in primary and secondary responses to T cell-dependent and T cell-independent antigens. *Eur J Immunol*, **21**, 2951-62.

Lobigs, M., Chelvanayagam, G. & Mullbacher, A. (2000) Proteolytic processing of peptides in the lumen of the endoplasmic reticulum for antigen presentation by major histocompatibility class I. *Eur J Immunol*, **30**, 1496-506.

Loch, S., Klauschies, F., Schölz, C., Verweij, M.C., Wiertz, E.J., Koch, J. & Tampé, R. (2008) Signaling of a varicelloviral factor across the endoplasmic reticulum membrane induces destruction of the peptide-loading complex and immune evasion. *J Biol Chem*, **283**, 13428-36.

Loch, S. & Tampé, R. (2005) Viral evasion of the MHC class I antigen-processing machinery. *Pflugers Arch*, **451**, 409-17.

Lundberg, K.S., Shoemaker, D.D., Adams, M.W., Short, J.M., Sorge, J.A. & Mathur, E.J. (1991) High-fidelity amplification using a thermostable DNA polymerase isolated from pyrococcus furiosus. *Gene*, **108**, 1-6.

Macdonald, W., Williams, D.S., Clements, C.S., Gorman, J.J., Kjer-Nielsen, L., Brooks, A.G., Mccluskey, J., Rossjohn, J. & Purcell, A.W. (2002) Identification of a dominant self-ligand bound to three HLA B44 alleles and the preliminary crystallographic analysis of recombinant forms of each complex. *FEBS Lett*, **527**, 27-32.

Madden, D.R. (1995) The three-dimensional structure of peptide-MHC complexes. *Annu Rev Immunol*, **13**, 587-622.

Mandel, B. (1976) Neutralization of poliovirus: A hypothesis to explain the mechanism and the one-hit character of the neutralization reaction. *Virology*, **69**, 500-10.

Mccluskey, J., Rossjohn, J. & Purcell, A.W. (2004) TAP genes and immunity. *Curr Opin Immunol*, **16**, 651-9.

Medana, I.M., Gallimore, A., Oxenius, A., Martinic, M.M., Wekerle, H. & Neumann, H. (2000) MHC class I-restricted killing of neurons by virus-specific $CD8^+$ T lymphocytes is effected through the Fas/FasL, but not the perforin pathway. *Eur J Immunol*, **30**, 3623-33.

Meyer, T.H., Van Endert, P.M., Uebel, S., Ehring, B. & Tampé, R. (1994) Functional expression and purification of the ABC transporter complex associated with antigen processing (TAP) in insect cells. *FEBS Lett*, **351**, 443-7.

Momburg, F., Neefjes, J.J. & Hämmerling, G.J. (1994) Peptide selection by MHC-encoded TAP transporters. *Curr Opin Immunol*, **6**, 32-7.

Momburg, F., Roelse, J., Hämmerling, G.J. & Neefjes, J.J. (1994) Peptide size selection by the major histocompatibility complex-encoded peptide transporter. *J Exp Med*, **179**, 1613-23.

Momburg, F., Roelse, J., Neefjes, J. & Hämmerling, G.J. (1994) Peptide transporters and antigen processing. *Behring Inst Mitt*, 26-36.

Morrice, N.A. & Powis, S.J. (1998) A role for the thiol-dependent reductase ERp57 in the assembly of MHC class I molecules. *Curr Biol*, **8**, 713-6.

Müller, K.M., Ebensperger, C. & Tampé, R. (1994) Nucleotide binding to the hydrophilic C-terminal domain of the transporter associated with antigen processing (TAP). *J Biol Chem*, **269**, 14032-7.

Mullis, K., Faloona, F., Scharf, S., Saiki, R., Horn, G. & Erlich, H. (1986) Specific enzymatic amplification of DNA in vitro: The polymerase chain reaction. *Cold Spring Harb Symp Quant Biol*, **51 Pt 1**, 263-73.

Neefjes, J.J. & Ploegh, H.L. (1988) Allele and locus-specific differences in cell surface expression and the association of HLA class I heavy chain with beta 2-microglobulin: Differential effects of inhibition of glycosylation on class I subunit association. *Eur J Immunol*, **18**, 801-10.

Neisig, A., Roelse, J., Sijts, A.J., Ossendorp, F., Feltkamp, M.C., Kast, W.M., Melief, C.J. & Neefjes, J.J. (1995) Major differences in transporter associated with antigen presentation (TAP)-dependent translocation of MHC class I-presentable peptides and the effect of flanking sequences. *J Immunol*, **154**, 1273-9.

Neisig, A., Wubbolts, R., Zang, X., Melief, C. & Neefjes, J. (1996) Allele-specific differences in the interaction of MHC class I molecules with transporters associated with antigen processing. *J Immunol*, **156**, 3196-206.

Neumann, L., Abele, R. & Tampé, R. (2002) Thermodynamics of peptide binding to the transporter associated with antigen processing (TAP). *J Mol Biol*, **324**, 965-73.

Neumann, L. & Tampé, R. (1999) Kinetic analysis of peptide binding to the TAP transport complex: Evidence for structural rearrangements induced by substrate binding. *J Mol Biol*, **294**, 1203-13.

Nijenhuis, M. & Hämmerling, G.J. (1996) Multiple regions of the transporter associated with antigen processing (TAP) contribute to its peptide binding site. *J Immunol*, **157**, 5467-77.

Oliver, J.D., Roderick, H.L., Llewellyn, D.H. & High, S. (1999) ERp57 functions as a subunit of specific complexes formed with the ER lectins calreticulin and calnexin. *Mol Biol Cell*, **10**, 2573-82.

Ortmann, B., Copeman, J., Lehner, P.J., Sadasivan, B., Herberg, J.A., Grandea, A.G., Riddell, S.R., Tampé, R., Spies, T., Trowsdale, J. & Cresswell, P. (1997) A critical role for tapasin in the assembly and function of multimeric MHC class I-TAP complexes. *Science*, **277**, 1306-9.

Pamer, E. & Cresswell, P. (1998) Mechanisms of MHC class I-restricted antigen processing. *Annu Rev Immunol*, **16**, 323-58.

Paquet, M.E., Cohen-Doyle, M., Shore, G.C. & Williams, D.B. (2004) Bap29/31 influences the intracellular traffic of MHC class I molecules. *J Immunol*, **172**, 7548-55.

Park, B., Lee, S., Kim, E. & Ahn, K. (2003) A single polymorphic residue within the peptide-binding cleft of MHC class I molecules determines spectrum of tapasin dependence. *J Immunol*, **170**, 961-8.

Park, B., Lee, S., Kim, E., Cho, K., Riddell, S.R., Cho, S. & Ahn, K. (2006) Redox regulation facilitates optimal peptide selection by MHC class I during antigen processing. *Cell*, **127**, 369-82.

Paulsson, K. & Wang, P. (2003) Chaperones and folding of MHC class I molecules in the endoplasmic reticulum. *Biochim Biophys Acta*, **1641**, 1-12.

Paulsson, K.M., Kleijmeer, M.J., Griffith, J., Jevon, M., Chen, S., Anderson, P.O., Sjogren, H.O., Li, S. & Wang, P. (2002) Association of tapasin and COPI provides a mechanism for the retrograde transport of major histocompatibility complex (MHC) class I molecules from the Golgi complex to the endoplasmic reticulum. *J Biol Chem*, **277**, 18266-71.

Paulsson, K.M. & Wang, P. (2004) Quality control of MHC class I maturation. *FASEB J*, **18**, 31-8.

Peaper, D.R., Wearsch, P.A. & Cresswell, P. (2005) Tapasin and ERp57 form a stable disulfide-linked dimer within the MHC class I peptide-loading complex. *EMBO J*, **24**, 3613-23.

Peh, C.A., Burrows, S.R., Barnden, M., Khanna, R., Cresswell, P., Moss, D.J. & Mccluskey, J. (1998) HLA-B27-restricted antigen presentation in the absence of tapasin reveals polymorphism in mechanisms of HLA class I peptide loading. *Immunity*, **8**, 531-42.

Peh, C.A., Burrows, S.R., Barnden, M., Khanna, R., Cresswell, P., Moss, D.J. & Mccluskey, J. (1998) HLA-B27-restricted antigen presentation in the absence of tapasin reveals polymorphism in mechanisms of HLA class I peptide loading. *Immunity*, **8**, 531-42.

Plewnia, G., (2003) Generierung und Charakterisierung rekombinanter Antikörper gegen den humanen Peptidtransporter TAP. Diplomarbeit. *Institut für Biochemie*, Goethe-Universität, Frankfurt am Main.

Plewnia, G., Schulze, K., Hunte, C., Tampe, R. & Koch, J. (2007) Modulation of the antigenic peptide transporter TAP by recombinant antibodies binding to the last five residues of TAP1. *J Mol Biol*, **369**, 95-107.

Pollock, S., Kozlov, G., Pelletier, M.F., Trempe, J.F., Jansen, G., Sitnikov, D., Bergeron, J.J., Gehring, K., Ekiel, I. & Thomas, D.Y. (2004) Specific interaction of ERp57 and calnexin determined by NMR spectroscopy and an ER two-hybrid system. *EMBO J*, **23**, 1020-9.

Powis, S.H. & Trowsdale, J. (1991) HLA and disease. *Br J Clin Pract*, **45**, 116-20.

Powis, S.J., Young, L.L., Joly, E., Barker, P.J., Richardson, L., Brandt, R.P., Melief, C.J., Howard, J.C. & Butcher, G.W. (1996) The rat CIM effect: TAP allele-dependent changes in a class I MHC anchor motif and evidence against C-terminal trimming of peptides in the ER. *Immunity*, **4**, 159-65.

Purcell, A.W. (2000) The peptide-loading complex and ligand selection during the assembly of HLA class I molecules. *Mol Immunol*, **37**, 483-92.

Purcell, A.W., Gorman, J.J., Garcia-Peydro, M., Paradela, A., Burrows, S.R., Talbo, G.H., Laham, N., Peh, C.A., Reynolds, E.C., Lopez De Castro, J.A. & Mccluskey, J. (2001) Quantitative and qualitative influences of tapasin on the class I peptide repertoire. *J Immunol*, **166**, 1016-27.

Rammensee, H.G., Falk, K. & Rotzschke, O. (1993) MHC molecules as peptide receptors. *Curr Opin Immunol*, **5**, 35-44.

Rammensee, H.G., Rotzschke, O. & Falk, K. (1993) MHC class I-restricted antigen processing-lessons from natural ligands. *Chem Immunol*, **57**, 113-33.

Ramos, M. & Lopez De Castro, J.A. (2002) HLA-B27 and the pathogenesis of spondyloarthritis. *Tissue Antigens*, **60**, 191-205.

Reichel, A., Schaible, D., Al Furoukh, N., Cohen, M., Schreiber, G. & Piehler, J. (2007) Noncovalent, site-specific biotinylation of histidine-tagged proteins. *Anal Chem*, **79**, 8590-600.

Ritz, U., Momburg, F., Pircher, H.P., Strand, D., Huber, C. & Seliger, B. (2001) Identification of sequences in the human peptide transporter subunit TAP1 required for transporter associated with antigen processing (TAP) function. *Int Immunol*, **13**, 31-41.

Ritz, U. & Seliger, B. (2001) The transporter associated with antigen processing (TAP): Structural integrity, expression, function, and its clinical relevance. *Mol Med*, **7**, 149-58.

Rocha, N. & Neefjes, J. (2008) MHC class II molecules on the move for successful antigen presentation. *EMBO J*, **27**, 1-5.

Rufer, E., Leonhardt, R.M. & Knittler, M.R. (2007) Molecular architecture of the TAP-associated MHC class I peptide-loading complex. *J Immunol*, **179**, 5717-27.

Sadasivan, B., Lehner, P.J., Ortmann, B., Spies, T. & Cresswell, P. (1996) Roles for calreticulin and a novel glycoprotein, tapasin, in the interaction of MHC class I molecules with TAP. *Immunity*, **5**, 103-14.

Sadasivan, B.K., Cariappa, A., Waneck, G.L. & Cresswell, P. (1995) Assembly, peptide loading, and transport of MHC class I molecules in a calnexin-negative cell line. *Cold Spring Harb Symp Quant Biol*, **60**, 267-75.

Saiki, R.K., Scharf, S., Faloona, F., Mullis, K.B., Horn, G.T., Erlich, H.A. & Arnheim, N. (1985) Enzymatic amplification of beta-globin genomic sequences and restriction site analysis for diagnosis of sickle cell anemia. *Science*, **230**, 1350-4.

Santos, S.G., Campbell, E.C., Lynch, S., Wong, V., Antoniou, A.N. & Powis, S.J. (2007) Major histocompatibility complex class I-ERp57-tapasin interactions within the peptide-loading complex. *J Biol Chem*, **282**, 17587-93.

Saric, T., Chang, S.C., Hattori, A., York, I.A., Markant, S., Rock, K.L., Tsujimoto, M. & Goldberg, A.L. (2002) An IFN-gamma-induced aminopeptidase in the ER, ERAP1, trims precursors to MHC class I-presented peptides. *Nat Immunol*, **3**, 1169-76.

Schagger, H. & Von Jagow, G. (1987) Tricine-sodium dodecyl sulfate-polyacrylamide gel electrophoresis for the separation of proteins in the range from 1 to 100 kda. *Anal Biochem*, **166**, 368-79.

Schmidt, T.G. & Skerra, A. (1993) The random peptide library-assisted engineering of a C-terminal affinity peptide, useful for the detection and purification of a functional Ig Fv fragment. *Protein Eng*, **6**, 109-22.

Schoenhals, G.J., Krishna, R.M., Grandea, A.G., 3rd, Spies, T., Peterson, P.A., Yang, Y. & Fruh, K. (1999) Retention of empty MHC class I molecules by tapasin is essential to reconstitute antigen presentation in invertebrate cells. *EMBO J*, **18**, 743-53.

Schölz, C. & Tampé, R. (2005) The intracellular antigen transport machinery TAP in adaptive immunity and virus escape mechanisms. *J Bioenerg Biomembr*, **37**, 509-15.

Schrag, J.D., Bergeron, J.J., Li, Y., Borisova, S., Hahn, M., Thomas, D.Y. & Cygler, M. (2001) The structure of calnexin, an ER chaperone involved in quality control of protein folding. *Mol Cell*, **8**, 633-44.

Schrodt, S., Koch, J. & Tampé, R. (2006) Membrane topology of the transporter associated with antigen processing (TAP1) within an assembled functional peptide-loading complex. *J Biol Chem*, **281**, 6455-62.

Schumacher, T.N., Kantesaria, D.V., Heemels, M.T., Ashton-Rickardt, P.G., Shepherd, J.C., Fruh, K., Yang, Y., Peterson, P.A., Tonegawa, S. & Ploegh, H.L. (1994) Peptide length and sequence specificity of the mouse TAP1/TAP2 translocator. *J Exp Med*, **179**, 533-40.

Scott, J.E. & Dawson, J.R. (1995) MHC class I expression and transport in a calnexin-deficient cell line. *J Immunol*, **155**, 143-8.

Seliger, B., Ritz, U., Abele, R., Bock, M., Tampé, R., Sutter, G., Drexler, I., Huber, C. & Ferrone, S. (2001) Immune escape of melanoma: First evidence of structural alterations in two distinct components of the MHC class I antigen processing pathway. *Cancer Res*, **61**, 8647-50. (a)

Seliger, B., Schreiber, K., Delp, K., Meissner, M., Hammers, S., Reichert, T., Pawlischko, K., Tampé, R. & Huber, C. (2001) Downregulation of the constitutive tapasin expression in human tumor cells of distinct origin and its transcriptional upregulation by cytokines. *Tissue Antigens*, **57**, 39-45. (b)

Seliger, B., Wollscheid, U., Momburg, F., Blankenstein, T. & Huber, C. (2001) Characterization of the major histocompatibility complex class I deficiencies in B16 melanoma cells. *Cancer Res*, **61**, 1095-9. (c)

Serwold, T., Gaw, S. & Shastri, N. (2001) ER aminopeptidases generate a unique pool of peptides for MHC class I molecules. *Nat Immunol*, **2**, 644-51.

Serwold, T., Gonzalez, F., Kim, J., Jacob, R. & Shastri, N. (2002) ERAAP customizes peptides for MHC class I molecules in the endoplasmic reticulum. *Nature*, **419**, 480-3.

Shields, M.J., Hodgson, W. & Ribaudo, R.K. (1999) Differential association of beta2-microglobulin mutants with MHC class I heavy chains and structural analysis demonstrate allele-specific interactions. *Mol Immunol*, **36**, 561-73.

Shields, M.J., Kubota, R., Hodgson, W., Jacobson, S., Biddison, W.E. & Ribaudo, R.K. (1998) The effect of human beta2-microglobulin on major histocompatibility complex I peptide loading and the engineering of a high affinity variant. Implications for peptide-based vaccines. *J Biol Chem*, **273**, 28010-8.

Shyamala, V., Baichwal, V., Beall, E. & Ames, G.F. (1991) Structure-function analysis of the histidine permease and comparison with cystic fibrosis mutations. *J Biol Chem*, **266**, 18714-9.

Skerra, A. & Plückthun, A. (1988) Assembly of a functional immunoglobulin Fv fragment in Escherichia coli. *Science*, **240**, 1038-41.

Smith, P.C., Karpowich, N., Millen, L., Moody, J.E., Rosen, J., Thomas, P.J. & Hunt, J.F. (2002) ATP binding to the motor domain from an ABC transporter drives formation of a nucleotide sandwich dimer. *Mol Cell*, **10**, 139-49.

Solda, T., Garbi, N., Hämmerling, G.J. & Molinari, M. (2006) Consequences of ERp57 deletion on oxidative folding of obligate and facultative clients of the calnexin cycle. *J Biol Chem*, **281**, 6219-26.

Spies, T., Cerundolo, V., Colonna, M., Cresswell, P., Townsend, A. & Demars, R. (1992) Presentation of viral antigen by MHC class I molecules is dependent on a putative peptide transporter heterodimer. *Nature*, **355**, 644-6.

Spies, T. & Demars, R. (1991) Restored expression of major histocompatibility class I molecules by gene transfer of a putative peptide transporter. *Nature*, **351**, 323-4.

Spiliotis, E.T., Manley, H., Osorio, M., Zuniga, M.C. & Edidin, M. (2000) Selective export of MHC class I molecules from the ER after their dissociation from TAP. *Immunity*, **13**, 841-51.

Sugawara, S., Abo, T. & Kumagai, K. (1987) A simple method to eliminate the antigenicity of surface class I MHC molecules from the membrane of viable cells by acid treatment at pH 3. *J Immunol Methods*, **100**, 83-90.

Suh, W.K., Derby, M.A., Cohen-Doyle, M.F., Schoenhals, G.J., Fruh, K., Berzofsky, J.A. & Williams, D.B. (1999) Interaction of murine MHC class I molecules with tapasin and TAP enhances peptide loading and involves the heavy chain alpha3 domain. *J Immunol*, **162**, 1530-40.

Tan, P., Kropshofer, H., Mandelboim, O., Bulbuc, N., Hämmerling, G.J. & Momburg, F. (2002) Recruitment of MHC class I molecules by tapasin into the transporter associated with antigen processing-associated complex is essential for optimal peptide loading. *J Immunol*, **168**, 1950-60.

Tanioka, T., Hattori, A., Masuda, S., Nomura, Y., Nakayama, H., Mizutani, S. & Tsujimoto, M. (2003) Human leukocyte-derived arginine aminopeptidase. The third member of the oxytocinase subfamily of aminopeptidases. *J Biol Chem*, **278**, 32275-83.

Tomazin, R., Hill, A.B., Jugovic, P., York, I., Van Endert, P., Ploegh, H.L., Andrews, D.W. & Johnson, D.C. (1996) Stable binding of the herpes simplex virus ICP47 protein to the peptide binding site of TAP. *EMBO J*, **15**, 3256-66.

Trowsdale, J., Ragoussis, J. & Campbell, R.D. (1991) Map of the human MHC. *Immunol Today*, **12**, 443-6.

Tseng, S.Y. & Dustin, M.L. (2002) T-cell activation: A multidimensional signaling network. *Curr Opin Cell Biol*, **14**, 575-80.

Turnquist, H.R., Kohlgraf, K.G., Mcilhaney, M.M., Mosley, R.L., Hollingsworth, M.A. & Solheim, J.C. (2004) Tapasin decreases immune responsiveness to a model tumor antigen. *J Clin Immunol*, **24**, 462-70.

Turnquist, H.R., Petersen, J.L., Vargas, S.E., Mcilhaney, M.M., Bedows, E., Mayer, W.E., Grandea, A.G., 3rd, Van Kaer, L. & Solheim, J.C. (2004) The Ig-like domain of tapasin influences intermolecular interactions. *J Immunol*, **172**, 2976-84.

Turnquist, H.R., Vargas, S.E., Reber, A.J., Mcilhaney, M.M., Li, S., Wang, P., Sanderson, S.D., Gubler, B., Van Endert, P. & Solheim, J.C. (2001) A region of tapasin that affects I(d) binding and assembly. *J Immunol*, **167**, 4443-9.

Uebel, S., Kraas, W., Kienle, S., Wiesmuller, K.H., Jung, G. & Tampé, R. (1997) Recognition principle of the TAP transporter disclosed by combinatorial peptide libraries. *Proc Natl Acad Sci U S A*, **94**, 8976-81.

Uebel, S., Meyer, T.H., Kraas, W., Kienle, S., Jung, G., Wiesmuller, K.H. & Tampé, R. (1995) Requirements for peptide binding to the human transporter associated with antigen processing revealed by peptide scans and complex peptide libraries. *J Biol Chem*, **270**, 18512-6.

Uebel, S., Plantinga, T., Weber, P.J., Beck-Sickinger, A.G. & Tampé, R. (1997) Peptide binding and photo-crosslinking to detergent solubilized and to reconstituted transporter associated with antigen processing (TAP). *FEBS Lett*, **416**, 359-63.

Underhill, D.M., Bassetti, M., Rudensky, A. & Aderem, A. (1999) Dynamic interactions of macrophages with T cells during antigen presentation. *J Exp Med*, **190**, 1909-14.

Urlinger, S., Kuchler, K., Meyer, T.H., Uebel, S. & Tampé, R. (1997) Intracellular location, complex formation, and function of the transporter associated with antigen processing in yeast. *Eur J Biochem*, **245**, 266-72.

Van Der Burg, S.H., Klein, M.R., Van De Velde, C.J., Kast, W.M., Miedema, F. & Melief, C.J. (1995) Induction of a primary human cytotoxic T-lymphocyte response against a novel conserved epitope in a functional sequence of HIV-1 reverse transcriptase. *AIDS*, **9**, 121-7.

Van Endert, P.M. (1999) Genes regulating MHC class I processing of antigen. *Curr Opin Immunol*, **11**, 82-8.

Van Endert, P.M. (1999) Role of nucleotides and peptide substrate for stability and functional state of the human ABC family transporters associated with antigen processing. *J Biol Chem*, **274**, 14632-8.

Van Endert, P.M., Liblau, R.S., Patel, S.D., Fugger, L., Lopez, T., Pociot, F., Nerup, J. & Mcdevitt, H.O. (1994) Major histocompatibility complex-encoded antigen processing gene polymorphism in IDDM. *Diabetes*, **43**, 110-7.

Van Endert, P.M., Tampé, R., Meyer, T.H., Tisch, R., Bach, J.F. & Mcdevitt, H.O. (1994) A sequential model for peptide binding and transport by the transporters associated with antigen processing. *Immunity*, **1**, 491-500.

Van Kaer, L., Ashton-Rickardt, P.G., Ploegh, H.L. & Tonegawa, S. (1992) TAP1 mutant mice are deficient in antigen presentation, surface class I molecules, and CD4-8$^+$ T cells. *Cell*, **71**, 1205-14.

Velarde, G., Ford, R.C., Rosenberg, M.F. & Powis, S.J. (2001) Three-dimensional structure of transporter associated with antigen processing (TAP) obtained by single particle image analysis. *J Biol Chem*, **276**, 46054-63.

Verma, R., Boleti, E. & George, A.J. (1998) Antibody engineering: Comparison of bacterial, yeast, insect and mammalian expression systems. *J Immunol Methods*, **216**, 165-81.

Wearsch, P.A. & Cresswell, P. (2007) Selective loading of high-affinity peptides onto major histocompatibility complex class I molecules by the tapasin-ERp57 heterodimer. *Nat Immunol*, **8**, 873-81.

Wei, M.L. & Cresswell, P. (1992) HLA-A2 molecules in an antigen-processing mutant cell contain signal sequence-derived peptides. *Nature*, **356**, 443-6.

Williams, A.P., Peh, C.A., Purcell, A.W., Mccluskey, J. & Elliott, T. (2002) Optimization of the MHC class I peptide cargo is dependent on tapasin. *Immunity*, **16**, 509-20.

Wright, C.A., Kozik, P., Zacharias, M. & Springer, S. (2004) Tapasin and other chaperones: Models of the MHC class I loading complex. *Biol Chem*, **385**, 763-78.

York, I.A., Chang, S.C., Saric, T., Keys, J.A., Favreau, J.M., Goldberg, A.L. & Rock, K.L. (2002) The ER aminopeptidase ERAP1 enhances or limits antigen presentation by trimming epitopes to 8-9 residues. *Nat Immunol*, **3**, 1177-84.

York, I.A., Roop, C., Andrews, D.W., Riddell, S.R., Graham, F.L. & Johnson, D.C. (1994) A cytosolic herpes simplex virus protein inhibits antigen presentation to $CD8^+$ T lymphocytes. *Cell*, **77**, 525-35.

Yu, Y.Y., Turnquist, H.R., Myers, N.B., Balendiran, G.K., Hansen, T.H. & Solheim, J.C. (1999) An extensive region of an MHC class I alpha 2 domain loop influences interaction with the assembly complex. *J Immunol*, **163**, 4427-33.

Zacharias, M. & Springer, S. (2004) Conformational flexibility of the MHC class I alpha1-alpha2 domain in peptide bound and free states: A molecular dynamics simulation study. *Biophys J*, **87**, 2203-14.

Zaitseva, J., Jenewein, S., Jumpertz, T., Holland, I.B. & Schmitt, L. (2005) H662 is the linchpin of ATP hydrolysis in the nucleotide-binding domain of the ABC transporter HlyB. *EMBO J*, **24**, 1901-10.

Zaitseva, J., Jenewein, S., Oswald, C., Jumpertz, T., Holland, I.B. & Schmitt, L. (2005) A molecular understanding of the catalytic cycle of the nucleotide-binding domain of the ABC transporter HlyB. *Biochem Soc Trans*, **33**, 990-5.

Zarling, A.L., Luckey, C.J., Marto, J.A., White, F.M., Brame, C.J., Evans, A.M., Lehner, P.J., Cresswell, P., Shabanowitz, J., Hunt, D.F. & Engelhard, V.H. (2003) Tapasin is a facilitator, not an editor, of class I MHC peptide binding. *J Immunol*, **171**, 5287-95.

Zernich, D., Purcell, A.W., Macdonald, W.A., Kjer-Nielsen, L., Ely, L.K., Laham, N., Crockford, T., Mifsud, N.A., Bharadwaj, M., Chang, L., Tait, B.D., Holdsworth, R., Brooks, A.G., Bottomley, S.P., Beddoe, T., Peh, C.A., Rossjohn, J. & Mccluskey, J. (2004) Natural HLA class I polymorphism controls the pathway of antigen presentation and susceptibility to viral evasion. *J Exp Med*, **200**, 13-24.

Zhang, C., Anderson, A. & Delisi, C. (1998) Structural principles that govern the peptide-binding motifs of class I MHC molecules. *J Mol Biol*, **281**, 929-47.

Zhang, Q. & Salter, R.D. (1998) Distinct patterns of folding and interactions with calnexin and calreticulin in human class I MHC proteins with altered N-glycosylation. *J Immunol*, **160**, 831-7.

Zhang, Q., Tector, M. & Salter, R.D. (1995) Calnexin recognizes carbohydrate and protein determinants of class I major histocompatibility complex molecules. *J Biol Chem*, **270**, 3944-8.

Zhang, Y., Baig, E. & Williams, D.B. (2006) Functions of ERp57 in the folding and assembly of major histocompatibility complex class I molecules. *J Biol Chem*, **281**, 14622-31.

10. Appendix

Sequence of the XbaI-HindIII fragment of pASK68-F_v148.3

```
TCTAGATAACGAGGGCAAAAAATGAAAAAGACAGCTATCGCGATTGCAGTGGCACTGGCT
                      M  K  K  T  A  I  A  I  A  V  A  L  A
GGTTTCGCTACCGTAGCGCAGGCCGAAGTTAAACTGCAGGAGACTGGTGGAGGATTGGTG
  G  F  A  T  V  A  Q  A  E  V  K  L  Q  E  T  G  G  G  L  V
CAGCCTAAAGGGTCATTGCAACTCTCATGTGCAGCCTCTGGATTCACCTTCAATACCATT
  Q  P  K  G  S  L  Q  L  S  C  A  A  S  G  F  T  F  N  T  I
GCCATGAACTGGGTCCGCCAGGCTCCAGGAAAGGGTTTGGAATGGGTTGCTCGCATAAGA
  A  M  N  W  V  R  Q  A  P  G  K  G  L  E  W  V  A  R  I  R
AGTAAAAGTAATAATTATGCAGCGTATTATGCCGATTCAGTGAAAGACAGGTTCACCATC
  S  K  S  N  N  Y  A  A  Y  Y  A  D  S  V  K  D  R  F  T  I
TCCAGAGATGATTCACAAAGCATCCTCTATCTGCAAATGAACAACTTGAAAACTGAGGAC
  S  R  D  D  S  Q  S  I  L  Y  L  Q  M  N  N  L  K  T  E  D
ACTGCCATGTATTACTGTGTGAGGGGTGCTTACGAGGGGGGTGCTATGGACTACTGGGGT
  T  A  M  Y  Y  C  V  R  G  A  Y  E  G  G  A  M  D  Y  W  G
CAAGGAACCTCGGTCACCGTCTCCTCAGCGTGGAGGCATCCACAGTTCGGAGGCTAATAA
  Q  G  T  S  V  T  V  S  S  A  W  R  H  P  Q  F  G  G
CCATGGAGAAAATAAAGTGAAACAAAGCACTATTGCACTGGCACTCTTACCGTTACTGTT
                   M  K  Q  S  T  I  A  L  A  L  L  P  L  L
TACCCCTGTGACAAAAGCCGACATCGAGCTCACTCAGGCTGCACCCTCTGTCTCTGTCAA
F  T  P  V  T  K  A  D  I  E  L  T  Q  A  A  P  S  V  S  V
TCCTGGAGAGTCAGTATCCATCTCCTGCAGGTCTAGTAGGAGTCTCCTGCATATTAATGG
N  P  G  E  S  V  S  I  S  C  R  S  S  R  S  L  L  H  I  N
CAACACTTTCTTATATTGGTTCCTACAGAGGCCAGGCCAGTCTCCTCAGCTCCTGATATA
G  N  T  F  L  Y  W  F  L  Q  R  P  G  Q  S  P  Q  L  L  I
TCGGATGTCCAACCTTGCCTCAGGAGTCCCAGACAGGTTCAGTGGCAGTGGGTCAGGAAT
Y  R  M  S  N  L  A  S  G  V  P  D  R  F  S  G  S  G  S  G
TGCTTTCACACTGAGAATCAGTAGAGTGGAGGCTGAGGATGTGGGTGTTTATTACTGTAT
I  A  F  T  L  R  I  S  R  V  E  A  E  D  V  G  V  Y  Y  C
GCAACATCTAGAATATCCGCTCACGTTCGGTGCTGGGACCAAGCTCGAGATCAAACGGGA
M  Q  H  L  E  Y  P  L  T  F  G  A  G  T  K  L  E  I  K  R
ACAAAAACTCATCTCAGAAGAGGATCTGAATTAATAATGATCTAAGCTT
E  Q  K  L  I  S  E  E  D  L  N
```

Sequence of the XbaI-HindIII fragment of pASK85-F_{ab}148.3

```
TCTAGATAACGAGGGCAAAAAATGAAAAAGACAGCTATCGCGATTGCAGTGGCACTGGCT
                      M  K  K  T  A  I  A  I  A  V  A  L  A
GGTTTCGCTACCGTAGCGCAGGCCGAAGTTAAACTGCAGGAGACTGGTGGAGGATTGGTG
  G  F  A  T  V  A  Q  A  E  V  K  L  Q  E  T  G  G  G  L  V
CAGCCTAAAGGGTCATTGCAACTCTCATGTGCAGCCTCTGGATTCACCTTCAATACCATT
  Q  P  K  G  S  L  Q  L  S  C  A  A  S  G  F  T  F  N  T  I
GCCATGAACTGGGTCCGCCAGGCTCCAGGAAAGGGTTTGGAATGGGTTGCTCGCATAAGA
  A  M  N  W  V  R  Q  A  P  G  K  G  L  E  W  V  A  R  I  R
AGTAAAAGTAATAATTATGCAGCGTATTATGCCGATTCAGTGAAAGACAGGTTCACCATC
  S  K  S  N  N  Y  A  A  Y  Y  A  D  S  V  K  D  R  F  T  I
TCCAGAGATGATTCACAAAGCATCCTCTATCTGCAAATGAACAACTTGAAAACTGAGGAC
  S  R  D  D  S  Q  S  I  L  Y  L  Q  M  N  N  L  K  T  E  D
ACTGCCATGTATTACTGTGTGAGGGGTGCTTACGAGGGGGGTGCTATGGACTACTGGGGT
  T  A  M  Y  Y  C  V  R  G  A  Y  E  G  G  A  M  D  Y  W  G
CAAGGAACCTCGGTCACCGTCTCCTCAGCAAAGACCACTCCTCCGTCTGTTTACCCTCTG
  Q  G  T  S  V  T  V  S  S  A  K  T  T  P  P  S  V  Y  P  L
GCTCCTGGTTCTGCGGCTCAGACTAACTCTATGGTGACTCTGGGATGCCTGGTCAAGGGC
  A  P  G  S  A  A  Q  T  N  S  M  V  T  L  G  C  L  V  K  G
TATTTCCCTGAGCCAGTGACAGTGACCTGGAACTCTGGATCCCTGTCCAGCGGTGTGCAC
  Y  F  P  E  P  V  T  V  T  W  N  S  G  S  L  S  S  G  V  H
ACCTTCCCAGCTGTCCTGCAATCTGACCTCTACACTCTGAGCAGCTCAGTGACTGTCCCC
  T  F  P  A  V  L  Q  S  D  L  Y  T  L  S  S  S  V  T  V  P
TCCAGCACCTGGCCCAGCGAGACCGTCACCTGCAACGTTGCCCACCCGGCTTCTAGCACC
  S  S  T  W  P  S  E  T  V  T  C  N  V  A  H  P  A  S  S  T
AAAGTTGACAAGAAAATCGTACCGCGCGACTGCCATCACCACCATCACCATTAATAACCA
  K  V  D  K  K  I  V  P  R  D  C  H  H  H  H  H  H
TGGAGAAAATAAAGTGAAACAAAGCACTATTGCACTGGCACTCTTACCGTTACTGTTTAC
                M  K  Q  S  T  I  A  L  A  L  L  P  L  L  F
CCCTGTGACAAAAGCCGACATCGAGCTCACTCAGGCTGCACCCTCTGTCTCTGTCAATCC
T  P  V  T  K  A  D  I  E  L  T  Q  A  A  P  S  V  S  V  N
TGGAGAGTCAGTATCCATCTCCTGCAGGTCTAGTAGGAGTCTCCTGCATATTAATGGCAA
P  G  E  S  V  S  I  S  C  R  S  S  R  S  L  L  H  I  N  G
CACTTTCTTATATTGGTTCCTACAGAGGCCAGGCCAGTCTCCTCAGCTCCTGATATATCG
N  T  F  L  Y  W  F  L  Q  R  P  G  Q  S  P  Q  L  L  I  Y
GATGTCCAACCTTGCCTCAGGAGTCCCAGACAGGTTCAGTGGCAGTGGGTCAGGAATTGC
R  M  S  N  L  A  S  G  V  P  D  R  F  S  G  S  G  S  G  I
TTTCACACTGAGAATCAGTAGAGTGGAGGCTGAGGATGTGGGTGTTTATTACTGTATGCA
A  F  T  L  R  I  S  R  V  E  A  E  D  V  G  V  Y  Y  C  M
ACATCTAGAATATCCGCTCACGTTCGGTGCTGGGACCAAGCTCGAGCTGAAGCGCGCTGA
```

```
Q  H  L  E  Y  P  L  T  F  G  A  G  T  K  L  E  L  K  R  A
TGCTGCACCGACTGTATCCATCTTCCCACCATCCAGTGAGCAGTTAACATCTGGAGGTGC
D  A  A  P  T  V  S  I  F  P  P  S  S  E  Q  L  T  S  G  G
CTCAGTCGTGTGCTTCTTGAACAACTTCTACCCCAAAGACATCAATGTCAAGTGGAAGAT
A  S  V  V  C  F  L  N  N  F  Y  P  K  D  I  N  V  K  W  K
TGATGGCAGTGAACGACAAAATGGCGTCCTGAACAGTTGGACTGATCAGGACAGCAAAGA
I  D  G  S  E  R  Q  N  G  V  L  N  S  W  T  D  Q  D  S  K
CAGCACCTACAGCATGAGCAGCACCCTCACGTTGACCAAGGACGAGTATGAACGACATAA
D  S  T  Y  S  M  S  S  T  L  T  L  T  K  D  E  Y  E  R  H
CAGCTATACCTGTGAGGCCACTCACAAGACATCAACTTCACCCATTGTCAAGAGCTTCAA
N  S  Y  T  C  E  A  T  H  K  T  S  T  S  P  I  V  K  S  F
CAGGAATGAGTGTTAGAGACAAAGGTCCTGATGCTGCTGATAGCAGGTAAGCTT
N  R  N  E  C
```

Sequence of the EcoRI-HindIII fragment of pFastBac$_1$-scF$_v$148

```
GAATTCCCCGGGGGATCCTCTAGAAACTCCTAAAAAACCGCCACCATGAAATTCTTAGTC
                                                  M  K  F  L  V

AACGTTGCCCTTGTCTTTATGGTCGTATACATTTCTTACATCTATGCCGGCGACATCGAG
 N  V  A  L  V  F  M  V  V  Y  I  S  Y  I  Y  A  G  D  I  E

CTCACTCAGGCTGCACCCTCTGTCTCTGTCAATCCTGGAGAGTCAGTATCCATCTCCTGC
 L  T  Q  A  A  P  S  V  S  V  N  P  G  E  S  V  S  I  S  C

AGGTCTAGTAGGAGTCTCCTGCATATTAATGGCAACACTTTCTTATATTGGTTCCTACAG
 R  S  S  R  S  L  L  H  I  N  G  N  T  F  L  Y  W  F  L  Q

AGGCCAGGCCAGTCTCCTCAGCTCCTGATATATCGGATGTCCAACCTTGCCTCAGGAGTC
 R  P  G  Q  S  P  Q  L  L  I  Y  R  M  S  N  L  A  S  G  V

CCAGACAGGTTCAGTGGCAGTGGGTCAGGAATTGCTTTCACACTGAGAATCAGTAGAGTG
 P  D  R  F  S  G  S  G  S  G  I  A  F  T  L  R  I  S  R  V

GAGGCTGAGGATGTGGGTGTTTATTACTGTATGCAACATCTAGAATATCCGCTCACGTTC
 E  A  E  D  V  G  V  Y  Y  C  M  Q  H  L  E  Y  P  L  T  F

GGTGCTGGGACCAAGCTCGAGATCAAACGGGGTGGCGGTGGCTCTGGTGGCGGCGGTTCT
 G  A  G  T  K  L  E  I  K  R  G  G  G  G  S  G  G  G  G  S

GGCGGTGGCGGTTCTGCCGGCGAAGTTAAACTGCAGGAGACTGGTGGAGGATTGGTGCAG
 G  G  G  G  S  A  G  E  V  K  L  Q  E  T  G  G  G  L  V  Q

CCTAAAGGGTCATTGCAACTCTCATGTGCAGCCTCTGGATTCACCTTCAATACCATTGCC
 P  K  G  S  L  Q  L  S  C  A  A  S  G  F  T  F  N  T  I  A

ATGAACTGGGTCCGCCAGGCTCCAGGAAAGGGTTTGGAATGGGTTGCTCGCATAAGAAGT
 M  N  W  V  R  Q  A  P  G  K  G  L  E  W  V  A  R  I  R  S

AAAAGTAATAATTATGCAGCGTATTATGCCGATTCAGTGAAAGACAGGTTCACCATCTCC
 K  S  N  N  Y  A  A  Y  Y  A  D  S  V  K  D  R  F  T  I  S

AGAGATGATTCACAAAGCATCCTCTATCTGCAAATGAACAACTTGAAAACTGAGGACACT
 R  D  D  S  Q  S  I  L  Y  L  Q  M  N  N  L  K  T  E  D  T

GCCATGTATTACTGTGTGAGGGGTGCTTACGAGGGGGGTGCTATGGACTACTGGGGTCAA
 A  M  Y  Y  C  V  R  G  A  Y  E  G  G  A  M  D  Y  W  G  Q

GGAACCTCGGTCACCGTCTCCTCACACCATCACCATCACCATTAATGACCATGGAAGCTT
 G  T  S  V  T  V  S  S  H  H  H  H  H  H  -
```

Sequence of the BamHI-HindIII fragment (V_LC_L) of pFastBacDual-F_{ab}148.3

```
GGATCCTCTAGAAACTCCTAAAAAACCGCCACCATGAAATTCTTAGTCAACGTTGCCCTT
                                    M  K  F  L  V  N  V  A  L

GTCTTTATGGTCGTATACATTTCTTACATCTATGCCGGCGACATCGAGCTCACTCAGGCT
 V  F  M  V  V  Y  I  S  Y  I  Y  A  G  D  I  E  L  T  Q  A

GCACCCTCTGTCTCTGTCAATCCTGGAGAGTCAGTATCCATCTCCTGCAGGTCTAGTAGG
 A  P  S  V  S  V  N  P  G  E  S  V  S  I  S  C  R  S  S  R

AGTCTCCTGCATATTAATGGCAACACTTTCTTATATTGGTTCCTACAGAGGCCAGGCCAG
 S  L  L  H  I  N  G  N  T  F  L  Y  W  F  L  Q  R  P  G  Q

TCTCCTCAGCTCCTGATATATCGGATGTCCAACCTTGCCTCAGGAGTCCCAGACAGGTTC
 S  P  Q  L  L  I  Y  R  M  S  N  L  A  S  G  V  P  D  R  F

AGTGGCAGTGGGTCAGGAATTGCTTTCACACTGAGAATCAGTAGAGTGGAGGCTGAGGAT
 S  G  S  G  S  G  I  A  F  T  L  R  I  S  R  V  E  A  E  D

GTGGGTGTTTATTACTGTATGCAACATCTAGAATATCCGCTCACGTTCGGTGCTGGGACC
 V  G  V  Y  Y  C  M  Q  H  L  E  Y  P  L  T  F  G  A  G  T

AAGCTCGAGCTGAAGCGCGCTGATGCTGCACCGACTGTATCCATCTTCCCACCATCCAGT
 K  L  E  L  K  R  A  D  A  A  P  T  V  S  I  F  P  P  S  S

GAGCAGTTAACATCTGGAGGTGCCTCAGTCGTGTGCTTCTTGAACAACTTCTACCCCAAA
 E  Q  L  T  S  G  G  A  S  V  V  C  F  L  N  N  F  Y  P  K

GACATCAATGTCAAGTGGAAGATTGATGGCAGTGAACGACAAAATGGCGTCCTGAACAGT
 D  I  N  V  K  W  K  I  D  G  S  E  R  Q  N  G  V  L  N  S

TGGACTGATCAGGACAGCAAAGACAGCACCTACAGCATGAGCAGCACCCTCACGTTGACC
 W  T  D  Q  D  S  K  D  S  T  Y  S  M  S  S  T  L  T  L  T

AAGGACGAGTATGAACGACATAACAGCTATACCTGTGAGGCCACTCACAAGACATCAACT
 K  D  E  Y  E  R  H  N  S  Y  T  C  E  A  T  H  K  T  S  T

TCACCCATTGTCAAGAGCTTCAACAGGAATGAGTGTTAGAGACAAAGGTCCTGATGCTGC
 S  P  I  V  K  S  F  N  R  N  E  C  -

TGATAGCAGGTAAGCTT
```

Sequence of the XmaI-NcoI fragment (V_HC_H) of pFastBacDual-F_{ab}148.3

```
CCCGGGGGATCCTCTAGAAACTCCTAAAAAACCGCCACCATGAAATTCTTAGTCAACGTT
                                        M  K  F  L  V  N  V

GCCCTTGTCTTTATGGTCGTATACATTTCTTACATCTATGCCGGCGAAGTTAAACTGCAG
 A  L  V  F  M  V  V  Y  I  S  Y  I  Y  A  G  E  V  K  L  Q

GAGACTGGTGGAGGATTGGTGCAGCCTAAAGGGTCATTGCAACTCTCATGTGCAGCCTCT
 E  T  G  G  G  L  V  Q  P  K  G  S  L  Q  L  S  C  A  A  S

GGATTCACCTTCAATACCATTGCCATGAACTGGGTCCGCCAGGCTCCAGGAAAGGGTTTG
 G  F  T  F  N  T  I  A  M  N  W  V  R  Q  A  P  G  K  G  L

GAATGGGTTGCTCGCATAAGAAGTAAAAGTAATAATTATGCAGCGTATTATGCCGATTCA
 E  W  V  A  R  I  R  S  K  S  N  N  Y  A  A  Y  Y  A  D  S

GTGAAAGACAGGTTCACCATCTCCAGAGATGATTCACAAAGCATCCTCTATCTGCAAATG
 V  K  D  R  F  T  I  S  R  D  D  S  Q  S  I  L  Y  L  Q  M

AACAACTTGAAAACTGAGGACACTGCCATGTATTACTGTGTGAGGGGTGCTTACGAGGGG
 N  N  L  K  T  E  D  T  A  M  Y  Y  C  V  R  G  A  Y  E  G

GGTGCTATGGACTACTGGGGTCAAGGAACCTCGGTCACCGTCTCCTCAGCAAAGACCACT
 G  A  M  D  Y  W  G  Q  G  T  S  V  T  V  S  S  A  K  T  T

CCTCCGTCTGTTTACCCTCTGGCTCCTGGTTCTGCGGCTCAGACTAACTCTATGGTGACT
 P  P  S  V  Y  P  L  A  P  G  S  A  A  Q  T  N  S  M  V  T

CTGGGATGCCTGGTCAAGGGCTATTTCCCTGAGCCAGTGACAGTGACCTGGAACTCTGGA
 L  G  C  L  V  K  G  Y  F  P  E  P  V  T  V  T  W  N  S  G

TCCCTGTCCAGCGGTGTGCACACCTTCCCAGCTGTCCTGCAATCTGACCTCTACACTCTG
 S  L  S  S  G  V  H  T  F  P  A  V  L  Q  S  D  L  Y  T  L

AGCAGCTCAGTGACTGTCCCCTCCAGCACCTGGCCCAGCGAGACCGTCACCTGCAACGTT
   S  S  S  V  T  V  P  S  S  T  W  P  S  E  T  V  T  C  N  V

GCCCACCCGGCTTCTAGCACCAAAGTTGACAAGAAAATCGTACCGCGCGACTGCCATCAC
   A  H  P  A  S  S  T  K  V  D  K  K  I  V  P  R  D  C  H  H

CACCATCACCATTAATAACCATGG
 H  H  H  H  -
```

Sequence of the EcoRI-HindIII fragment of pFastBac$_1$-scMHC-B4402

```
GGAATTCAAAGGCCTACGTCGACGAGCTCACTAGTCGCGGCCGCTTTCGAATCTAGAAAC
TCCTAAAAAACCGCCACCATGAAATTCTTAGTCAACGTTGCCCTTGTCTTTATGGTCGTA
                  M  K  F  L  V  N  V  A  L  V  F  M  V  V
TACATTTCTTACATCTATGCCGGCATCCAGCGTACTCCAAAGATTCAGGTTTACTCACGT
 Y  I  S  Y  I  Y  A  G  I  Q  R  T  P  K  I  Q  V  Y  S  R
CATCCAGCAGAGAATGGAAAGTCAAATTTCCTGAATTGCTATGTGTCTGGGTTTCATCCA
 H  P  A  E  N  G  K  S  N  F  L  N  C  Y  V  S  G  F  H  P
TCCGACATTGAAGTTGACTTACTGAAGAATGGAGAGAGAATTGAAAAAGTGGAGCATTCA
 S  D  I  E  V  D  L  L  K  N  G  E  R  I  E  K  V  E  H  S
GACTTGTCTTTCAGCAAGGACTGGTCTTTCTATCTCTTGTACTACACTGAATTCACCCCC
 D  L  S  F  S  K  D  W  S  F  Y  L  L  Y  Y  T  E  F  T  P
ACTGAAAAAGATGAGTATGCCTGCCGTGTGAACCATGTGACTTTGTCACAGCCCAAGATA
 T  E  K  D  E  Y  A  C  R  V  N  H  V  T  L  S  Q  P  K  I
GTTAAGTGGGATCGAGACATGGGTGGCGGAGGTAGTGGTGGCGGTGGCTCCGGTGGTGGC
 V  K  W  D  R  D  M  G  G  G  G  S  G  G  G  G  S  G  G  G
GGATCCGGCTCCCACTCCATGAGGTATTTCTACACCGCCATGTCCCGGCCCGGCCGCGGG
 G  S  G  S  H  S  M  R  Y  F  Y  T  A  M  S  R  P  G  R  G
GAGCCCCGCTTCATCACCGTGGGCTACGTGGACGACACGCTGTTCGTGAGGTTCGACAGC
 E  P  R  F  I  T  V  G  Y  V  D  D  T  L  F  V  R  F  D  S
GACGCCACGAGTCCGAGGAAGGAGCCGCGGGCGCCATGGATAGAGCAGGAGGGGCCGGAG
 D  A  T  S  P  R  K  E  P  R  A  P  W  I  E  Q  E  G  P  E
TATTGGGACCGGGAGACACAGATCTCCAAGACCAACACACAGACTTACCGAGAGAACCTG
 Y  W  D  R  E  T  Q  I  S  K  T  N  T  Q  T  Y  R  E  N  L
CGCACCGCGCTCCGCTACTACAACCAGAGCGAGGCCGGGTCTCACATCATCCAGAGGATG
 R  T  A  L  R  Y  Y  N  Q  S  E  A  G  S  H  I  I  Q  R  M
TACGGCTGCGACGTGGGGCCGGACGGGCGCCTCCTCCGCGGGTATGACCAGGACGCCTAC
 Y  G  C  D  V  G  P  D  G  R  L  L  R  G  Y  D  Q  D  A  Y
GACGGCAAGGATTACATCGCCCTGAACGAGGACCTGAGCTCCTGGACCGCGGCGGACACC
 D  G  K  D  Y  I  A  L  N  E  D  L  S  S  W  T  A  A  D  T
GCGGCTCAGATCACCCAGCGCAAGTGGGAGGCGGCCCGTGTGGCGGAGCAGGACAGAGCC
 A  A  Q  I  T  Q  R  K  W  E  A  A  R  V  A  E  Q  D  R  A
TACCTGGAGGGCCTGTGCGTGGAGTCGCTCCGCAGATACCTGGAGAACGGGAAGGAGACA
 Y  L  E  G  L  C  V  E  S  L  R  R  Y  L  E  N  G  K  E  T
CTGCAGCGCGCGGACCCCCCAAAGACACATGTGACCCACCACCCCATCTCTGACCATGAG
 L  Q  R  A  D  P  P  K  T  H  V  T  H  H  P  I  S  D  H  E
```

GTCACCCTGAGGTGCTGGGCCCTGGGCTTCTACCCTGCGGAGATCACACTGACCTGGCAG

V T L R C W A L G F Y P A E I T L T W Q

CGGGATGGCGAGGACCAAACTCAGGACACCGAGCTTGTGGAGACCAGACCAGCAGGAGAT

R D G E D Q T Q D T E L V E T R P A G D

AGAACCTTCCAGAAGTGGGCAGCTGTGGTGGTGCCTTCTGGAGAAGAGCAGAGATACACA

R T F Q K W A A V V V P S G E E Q R Y T

TGCCATGTACAGCATGAGGGGCTGCCGAAGCCCCTCACCCTGAGATGGGAGCCGGTCGAC

C H V Q H E G L P K P L T L R W E P V D

GAGAACCTGTACTTCCAGTCTCATCACCATCACCATCACTAATGAAAGCTT

E N L Y F Q S H H H H H H -

Danksagung

Mein besonderer Dank gilt Prof. Dr. Robert Tampé für das spannende wissenschaftliche Umfeld, die Möglichkeit in seinem Arbeitskreis meine Promotionsarbeit anfertigen zu dürfen, die hervorragende Betreuung sowie seine stete Diskussionsbereitschaft.

Prof. Dr. Bernd Ludwig danke ich für die Übernahme des Zweitgutachtens dieser Arbeit.

Ein ganz besonderes Dankeschön gilt PD Dr. Joachim Koch für die ausgezeichnete Betreuung, sowie seine stete Hilfs- und Diskussionsbereitschaft insbesondere während des Schreibens der Publikation sowie dieser Arbeit.

PD Dr. Carola Hunte gilt mein herzlicher Dank für die Einführung in die Thematik der monoklonalen und rekombinanten Antikörper, sowie für die stete Hilfs- und Diskussionsbereitschaft.

Ferner danke ich auch PD Dr. Rupert Abele für die Einführung in die Fluoreszenzspektroskopie sowie viele Anregungen während meiner gesamten Promotionszeit.

Dr. Rolf Misselwitz (Charité Berlin) danke ich für die Bereitstellung von HLA-B2705 und HLA-B2709.

Dirk Paterok danke ich für die Einführung in die „biophysikalische Unterwelt“, seine Unterstützung und Mitwirkung an den TIRFS-Messungen, insbesondere für die Herstellung der Chelator-Lipide. Annett Reichel danke ich sehr für die Bereitstellung von ^{BT}tris-NTA und MBP. Prof. Dr. Jakob Piehler danke ich für die Diskussionen und die Anregungen insbesondere bezüglich der TIRFS-Messungen.

Mein herzlicher Dank geht auch an Eckhard Linker für die Unterstützung in der Zellkultur.

Özlem Demirel und Nina Kreißig sowie allen früheren und jetzigen Kollegen im Labor 1.23 danke ich ganz besonders für die angenehme und hilfsbereite Arbeitsatmosphäre! Der gesamten TAP-Gruppe danke ich ebenfalls für das angenehme Arbeitsklima und die stete Hilfsbereitschaft. Nicht zuletzt möchte ich mich bei allen Kollegen des Instituts für Biochemie für die fachlichen und fachübergreifenden Diskussionen bedanken.

Ruta Almedom, Stefanie Dinkelacker, Meike Herget, Christine Oswald, Chiara Presenti, Katrin Schulze möchte ich für die gemeinsame Promotionszeit, die resultierenden Freundschaften und die unvergeßlichen Kochabende danken!

Ein ganz besonderer Dank geht an Meike Herget für die Bereitstellung des gereinigten TAP-Komplexes, für die tolle gemeinsame Promotionszeit, vielen motivierenden Gespräche und nicht zuletzt die gemeinsame Zeit außerhalb des Frankfurter-Labors.

Robert and Christine Ingram thank you for your everlasting motivation and support!

Auch meiner Familie und Klaus Hoffmeier danke ich herzlich für ihre liebevolle und grenzenlose Unterstützung und Motivation während meiner Studien- und Promotionszeit.

Veröffentlichung

Teile der vorliegenden Arbeit wurden veröffentlicht in

Plewnia, G., Schulze, K., Hunte, C., Tampe, R. & Koch, J. (2007) Modulation of the antigenic peptide transporter TAP by recombinant antibodies binding to the last five residues of TAP1. *J Mol Biol*, **369**, 95-107.

Lebenslauf

Persönliche Daten

Gabriele Plewnia
geboren am 17.07.1977 in Kreuzburg, ledig, deutsch

Berufliche Tätigkeiten

Wissenschaftliche Mitarbeiterin & Promotion 01/2005 – dato
Dissertation: *Extrinsic and intrinsic modulators of the Transporter Associated with Antigen Presentation (TAP)* bei Prof. Dr. Robert Tampé
Institut für Biochemie, Goethe – Universität, Frankfurt

Stipendiatin & Promotion 12/2003 – 12/2004
Institut für Biochemie & Center for Membrane Proteomics (CMP)
Goethe – Universität, Frankfurt

Studentische Mitarbeiterin 10/2003 – 12/2003
Institut für Biochemie, Goethe – Universität, Frankfurt

Hochschulbildung

Diplomarbeit 12/2002 – 09/2003
Diplom: *Generierung und Charakterisierung rekombinanter Antikörper gegen den humanen Peptidtransporter TAP* bei Prof. Dr. Robert Tampé
Institut für Biochemie, Goethe – Universität, Frankfurt

Studium Biologie 10/1998 – 11/2002
Hauptfächer: Biochemie, Mikrobiologie und Zellbiologie
Goethe – Universität, Frankfurt

Schulbildung

Gymnasium 09/1991 – 06/1998
Friedrich List – Schule, Reutlingen

Realschule 09/1988 – 07/1991
Hermann Hesse – Schule, Reutlingen

Grundschule 09/1984 – 07/1988
Kreuzburg, Polen

Erklärung

Hiermit erkläre ich, dass ich die vorliegende Arbeit in allen Teilen selbständig und nur unter Zuhilfenahme der angegebenen Quellen und Literatur verfasst habe.

Frankfurt am Main, den .....

(Gabriele Plewnia)